

Illinois Institute of Technology

Chicago, Illinois 60616



**Department of Civil Engineering
Armour College of Engineering**

Geotechnical Series 77-201

**FOUNDATION RESPONSE TO SOIL
TRANSMITTED LOADS**

by

Satya N. Varadhi

Surendra K. Saxena

Eben Vey

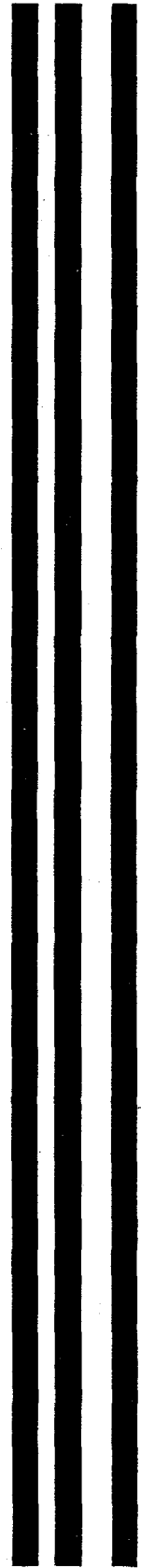
December 1977

Prepared for

NATIONAL SCIENCE FOUNDATION

Research Grant GK-41903

REPRODUCED BY
**NATIONAL TECHNICAL
INFORMATION SERVICE**
U. S. DEPARTMENT OF COMMERCE
SPRINGFIELD, VA. 22161





BIBLIOGRAPHIC DATA SHEET		1. Report No.	2.	3. Recipient's Accession No. B279055	
4. Title and Subtitle				5. Report Date Dec 77	
FOUNDATION RESPONSE TO SOIL TRANSMITTED LOADS				6.	
7. Author(s) S. N. Varadhi, S. K. Saxena and E. Vey				8. Performing Organization Rept. No. Geotech series 77-201	
9. Performing Organization Name and Address Illinois Institute of Technology Department of Civil Engineering Armour College of Engineering Chicago, Ill 60616				10. Project/Task/Work Unit No.	
				11. Contract/Grant No. GK-41903	
12. Sponsoring Organization Name and Address National Science Foundation Washington, D C				13. Type of Report & Period Covered	
				14.	
15. Supplementary Notes					
16. Abstracts <p>This research deals with effects on foundation response produced by stress waves propagating from underlying soils. A circular footing was located at the surface and at different depths of burial and a transient load was applied to the footings through the underlying soils. Stress-time and strain-time histories were recorded through embedded gages. These records were correlated with acceleration-time records of the input load and foundation response to provide a comprehensive picture of stresses and strains in a soil mass subjected to earthquake type loading. The investigation also includes some static and dynamic experiments, conducted using a thin layer of compressible material buried at depths of one radius below the footing.</p>					
17. Key Words and Document Analysis. 17a. Descriptors <p>Foundation Response, Earthquake Type Loads, Passive Isolators, Stress Reduction, Subgrade Modulus.</p>					
17b. Identifiers/Open Ended Terms					
17c. COSATI Field/Group					
18. Availability Statement HSP Approval Ods 09/23/78 Releasable to the public thru NTIS				19. Security Class (This Report) UNCLASSIFIED	
				20. Security Class (This Page) UNCLASSIFIED	
				22. Price PCA 10 MF A01	

ATTENTION

AS NOTED IN THE NTIS ANNOUNCEMENT,
PORTIONS OF THIS REPORT ARE NOT LEGIBLE.
HOWEVER, IT IS THE BEST REPRODUCTION
AVAILABLE FROM THE COPY SENT TO NTIS.

Geotechnical Series 77 - 201

FOUNDATION RESPONSE TO SOIL
TRANSMITTED LOADS

by

Satya N. Varadhi
Surendra K. Saxena
Eben Vey

A Report on Research Sponsored

by

National Science Foundation

Grant No. GK-41903

Illinois Institute of Technology
Department of Civil Engineering
Armour College of Engineering

December 1977

Please read instructions on reverse carefully before completing this form.

1. INSTITUTION AND ADDRESS Illinois Institute of Tech, Civil Engineering Dept. Chicago, Illinois 60616		2. NSF PROGRAM Civil and Environmental Technology		3. PRINCIPAL INVESTIGATOR(S) Eben Vey Surendra K. Saxena	
4. AWARD NUMBER ENG73-03922A02		5. DURATION (MOS) 24		6. AWARD PERIOD from to Dec, '78	
7. AWARD ACCOUNT NUMBER GK-41903					

8. PROJECT TITLE

Foundation Response to Soil Transmitted Loads

9. SUMMARY (ATTACH LIST OF PUBLICATIONS TO FORM)

This research deals with effects on foundation response produced by stress waves propagating from the underlying soils. In this research the circular footings were located at the surface and at different depths of burial and a transient load was applied to the footings through the underlying soils. Measurements were made of stress-time and strain-time histories using embedded gages throughout the soil mass. These records were correlated with acceleration-time records of the input load and the foundation response to provide a comprehensive picture of stresses and strains in a soil mass subjected to an earthquake type loading. The data obtained also evaluates to what extent these stresses and strains are influenced by the foundation and the distribution of pressures in the soil beneath it. In the cases studied, it was noticed that the influence of the mass of the footing on the stress distribution is negligible at a depth more than two footing diameters below the footing. It was also noticed that the stress intensities in the vicinity of the footing increases as the distance from the transient load source decreases. The investigation also includes some experiments, static and dynamic, conducted using a thin layer of compressible material buried at depth of one radius below the footing. Data from these tests has been analyzed to 1) obtain a relationship between the percentage reduction in deceleration of the footing and the subgrade modulus of the compressible material, 2) obtain a relationship between the percentage reduction of the vertical stress in the vicinity of the footing and the subgrade modulus of the compressible material, and 3) obtain a relationship between the percentage reduction in deceleration of the footing and percentage reduction in the factor of safety against the bearing capacity failure based on allowable settlement.

9. SIGNATURE OF PRINCIPAL INVESTIGATOR/ PROJECT DIRECTOR <i>Surendra K. Saxena</i>	TYPED OR PRINTED NAME Surendra K. Saxena	DATE 12/30/77
--	---	------------------



ACKNOWLEDGEMENTS

This report is part of a series devoted to the problem of foundation response to soil transmitted loads. The research program was supported by National Science Foundation under grant GK-41903 awarded to the Illinois Institute of Technology.

TABLE OF CONTENTS

	Page
ACKNOWLEDGEMENTS	iii
LIST OF TABLES	v
LIST OF FIGURES	vi
LIST OF SYMBOLS	xv
CHAPTER	
I. INTRODUCTION	1
II. REVIEW OF LITERATURE	4
Footing Behavior Under Dynamic Loads	4
Recent Soil Dynamics Research at IIT	15
The Isolation Studies	22
III. PURPOSE AND SCOPE OF INVESTIGATION	27
IV. TEST APPARATUS AND EXPERIMENTAL PROCEDURES.	31
Test Apparatus.	31
Embedded Gages.	39
Instrumentation	51
Experimental Procedures	56
V. PRESENTATION AND ANALYSIS OF RESULTS	67
Footing Response.	67
Stress-Wave Propagation	78
Depth of Burial	126
Footing Isolation	139
VI. CONCLUSIONS	175
APPENDICES	
A. SOIL PROPERTIES	180
B. WAVE PROPAGATION VELOCITIES AND SOIL MODULI	184
C. STRESS-DEFORMATION RELATIONSHIP FOR COMPRESSIBLE MATERIALS	188
BIBLIOGRAPHY	194

LIST OF TABLES

Table		Page
1.	Sensitivity Values of Piezoresistive Stress Gages Under Hydrostatic Conditions	42
2.	Sensitivity Values of Piezoresistive Stress Gages in Confined Specimens of the Soil	44

LIST OF FIGURES

Figure		Page
1.	A General View of the Experimental Apparatus	32
2.	Bottom Movable Steel Plate Mounted on Three Hydro-Line Cylinders	33
3.	Various Size Footings Used in This Study	34
4.	Schematic Diagram of Transient Loading System	35
5.	A View of the Loading System	37
6.	Apparatus for Statically Loaded Footing	38
7.	Piezoresistive Soil Stress Gage	40
8.	Schematic Diagram of Water Chamber for Gage Calibration	41
9.	Typical Calibration Curve for Piezoresistive Gage Under Hydrostatic Conditions	43
10.	Typical Calibration Curve for Piezoresistive Gage Embedded in Sand	45
11.	IITRI Coil Strain Gage	47
12.	Calibration of Strain Gage (1 in. dia. coils) (Displacement vs Gage Output)	48
13.	Calibration of Strain Gage (1 in. dia. coils) (Strain vs Gage Output)	49
14.	Calibration of Strain Gage (3/4 in. dia. coils) (Displacement vs Gage Output)	50
15.	Instrumentation Setup	52
16.	Schematic Diagram of Electrical Circuit for the Soil-Strain Gage Unit	54
17.	Data Recording System (Magnetic Tape Recorder Model 5600B, Honeywell).	55
18.	Data Printing Equipment (Visicorder Oscillograph Model 1508B, Honeywell).	57
19.	Raining Device for Placement of 20-40 Ottawa Sand	58

LIST OF FIGURES (Cont'd.)

Figure		Page
20.	Location of Stress and Strain Measurements . . .	60
21.	A Typical Gage Array of the Embedded Gages . . .	61
22.	Schematic Diagram of Placement Methods for Strain Gages	62
23.	Footing Before Being Subjected to Transient Load	64
24.	Schematic Diagram of Footing Apparatus	69
25.	Acceleration-Time Traces for the Bottom Movable Steel Plate and a Footing (6 in. dia. circular).	70
26.	Velocity vs Time Relationship for a Surface Footing (6 in. dia. circular).	73
27.	Displacement vs Time Relationship for a Surface Footing (6 in. dia. circular).	74
28.	Acceleration, Displacement-Time Traces for a Footing (6 in. dia. circular).	75
29.	Acceleration-Time Traces for the Bottom Movable Steel Plate and a Footing (3 in. dia. circular).	76
30.	Acceleration-Time Traces for the Bottom Movable Steel Plate and a Footing (3 in. by 3 in. square)	77
31.	Deceleration of Surface Footing vs Weight of Footing	79
32.	Vertical Stress-Time Traces on Axis of Symmetry at $Z = 1/2$ in.; 6 in.; 12 in. (6 in. dia. circular footing).	81
33.	Vertical Stress-Time Trace at $R = 0$ in.; $Z =$ $1-1/2$ in. (6 in. dia. circular footing).	82
34.	Vertical Stress-Time Traces on Axis of Symmetry at $Z = 2$ in.; 4 in. (6 in. dia. circular footing)	83

LIST OF FIGURES (Cont'd.)

Figure		Page
35.	Vertical Stress-Time Traces on Axis of Symmetry at Z = 3 in.; 9 in. (6 in. dia. circular footing)	84
36.	Attenuation of Peak Vertical Stress on Axis of Symmetry for a 6 in. dia. Circular Footing ($\sigma_c = 0.55$ psi)	85
37.	Vertical Stress-Time Trace at R = 0 in.; Z = 1/2 in. (3 in. dia. circular footing)	87
38.	Vertical Stress-Time Trace at R = 0 in.; Z = 1 in. (3 in. dia. circular footing).	88
39.	Vertical Stress-Time Trace at R = 0 in.; Z = 1-1/2 in. (3 in. dia. circular footing).	89
40.	Vertical Stress-Time Traces on Axis of Symmetry at Z = 6 in.; 12 in. (3 in. dia. circular footing)	90
41.	Vertical Stress-Time Trace at R = 0 in.; Z = 9 in. (3 in. dia. circular footing)	91
42.	Attenuation of Peak Vertical Stress on Axis of Symmetry for a 3 in. dia. Circular Footing ($\sigma_c = 0.88$ psi).	92
43.	Vertical Stress-Time Traces on Axis of Symmetry at Z = 1/2 in.; 1-1/2 in. (3 in. by 3 in. square footing)	93
44.	Vertical Stress-Time Traces on Axis of Symmetry at Z = 1 in.; 6 in.; 12 in. (3 in. by 3 in. square footing)	94
45.	Attenuation of Peak Vertical Stress on Axis of Symmetry for a 3 in. by 3 in. Square Footing ($\sigma_c = 0.20$ psi)	95
46.	Stress at Any Point from Circular Bearing Area (Boussinesque's Stress Distribution Theory).	97
47.	Peak Vertical Stress Distribution With Depth Under Transient Loads (without any footing on the surface)	98

LIST OF FIGURES (Cont'd.)

Figure		Page
48.	Vertical Stress-Time Traces at 6 in. Depth and at R = 0 in.; 6 in.; 12 in. (6 in. dia. circular footing)	101
49.	Vertical Stress-Time Traces at 3 in. Depth and at R = 0 in.; 6 in.; 12 in. (6 in. dia. circular footing)	102
50.	Vertical Stress-Time Traces at 1-1/2 in. Depth and at R = 0 in.; 6 in.; 12 in. (6 in. dia. circular footing).	103
51.	Attenuation of Peak Vertical Stress vs Offset from Axis of Symmetry for a 6 in. dia. Circular Footing ($\sigma_c = 0.55$ psi)	104
52.	Vertical Stress-Time Traces at 6 in. Depth and at R = 0 in.; 3 in.; 6 in. (3 in. dia. circular footing).	105
53.	Vertical Stress-Time Traces at 6 in. Depth and at R = 9 in.; 12 in. (3 in. dia. circular footing)	106
54.	Vertical Stress-Time Traces at 3 in. Depth and at R = 0 in.; 6 in.; 12 in. (3 in. dia. circular footing)	107
55.	Vertical Stress-Time Traces at 1-1/2 in. Depth and at R = 0 in.; 6 in. (3 in. dia. circular footing)	108
56.	Vertical Stress-Time Trace at R = 12 in.; Z = 1-1/2 in. (3 in. dia. circular footing)	109
57.	Vertical Stress-Time Trace at R = 0 in.; Z = 1/2 in. (3 in. circular footing)	110
58.	Vertical Stress-Time Traces at 1/2 in. Depth and at R = 6 in.; 12 in. (3 in. dia. circular footing)	111
59.	Attenuation of Peak Vertical Stress vs Offset from Axis of Symmetry for a 3 in. dia. Circular Footing ($\sigma_c = 0.88$ psi)	112

LIST OF FIGURES (Cont'd.)

Figure		Page
60.	Vertical Stress-Time Traces at 6 in. Depth and at R = 0 in.; 6 in.; 12 in (3 in. by 3 in. square footing)	113
61.	Vertical Stress-Time Traces at 3 in. Depth and at R = 0 in.; 6 in.; 12 in. (3 in. by 3 in. square footing)	114
62.	Vertical Stress-Time Traces at 1-1/2 in. Depth and at R = 0 in.; 6 in.; 12 in. (3 in. by 3 in. square footing)	115
63.	Vertical Stress-Time Traces at 1/2 in. Depth and at R = 0 in.; 6 in.; 12 in. (3 in. by 3 in. square footing)	116
64.	Attenuation of Peak Vertical Stress vs Offset from Axis of Symmetry for a 3 in. by 3 in. Square Footing ($\sigma_c = 0.20$ psi)	117
65.	Strain-Time Trace at R = 0 in.; Z = 2 in. (6 in. dia. circular footing)	119
66.	Strain-Time Traces on Axis of Symmetry at Z = 3 in.; 4 in. (6 in. dia. circular footing).	120
67.	Vertical Strain Distribution With Depth on Axis of Symmetry for 6 in. dia. Circular Footing	122
68.	Vertical Strain Distribution vs Offset from Axis of Symmetry for a 6 in. dia. Circular Footing	123
69.	Modulus vs Strain Relationship at Z/r = 1/2; R/r = 2 (Test No. TA-61)	124
70.	Modulus vs Strain Relationship at Z/r = 1; R/r = 1 (Test No. TA-111)	125
71.	Vertical Stress-Time Traces on Axis of Symmetry at Various Depths for a 6 in. dia. Circular Footing With 2 in. Surcharge	127
72.	Vertical Stress-Time Traces on Axis of Symmetry at Various Depths for a 6 in. dia. Circular Footing on the Surface of a Soil Media	128

LIST OF FIGURES (Cont'd.)

Figure		Page
73.	Vertical Stress-Time Traces on Axis of Symmetry at Various Depths for a 6 in. dia. Circular Footing Buried at 2 in. Depth . . .	129
74.	Vertical Stress-Time Traces on Axis of Symmetry at Various Depths for a 6 in. dia. Circular Footing Buried at 4 in. Depth . . .	130
75.	Vertical Stress-Time Traces on Axis of Symmetry at Various Depths for a 6 in. dia. Circular Footing Buried at 6 in. Depth . . .	131
76.	Attenuation of Peak Vertical Stress With Depth on Axis of Symmetry for a 6 in. dia. Circular Footing at Different Depths of Burial	132
77.	Acceleration-Time Trace for a 6 in. dia. Circular Footing on the Surface of a Soil Media in the Vessel	134
78.	Acceleration-Time Trace for a 6 in. dia. Circular Footing Buried at 2 in. Depth . . .	135
79.	Acceleration-Time Trace for a 6 in. dia. Circular Footing Buried at 4 in. Depth . . .	136
80.	Acceleration-Time Trace for a 6 in. dia. Circular Footing Buried at 6 in. Depth . . .	137
81.	Deceleration of Footing vs Footing Depth from the Surface of the Soil Media for a 6 in. dia. Circular Footing.	138
82.	Stress vs Deformation for Compressible Materials M_1, M_2, M_3	140
83.	Stress vs Deformation for Compressible Materials M_4, M_5	141
84.	Acceleration-Time Trace for a 6 in. dia. Circular Footing on the Surface Without Any Compressible Material in the Soil Media. . .	143
85.	A Compressible Material M_1 Placed in Position at a Depth $Z/r = 1$ Before Being Buried in the Sand	144

LIST OF FIGURES (Cont'd.)

Figure		Page
86.	Acceleration-Time Trace for a 6 in. dia. Circular Footing With a Compressible Material M_1 Buried at $R/r = 0$; $Z/r = 1$. . .	145
87.	Acceleration-Time Trace for a 6 in. dia. Circular Footing With a Compressible Material M_2 Buried at $R/r = 0$; $Z/r = 1$. . .	146
88.	Acceleration-Time Trace for a 6 in. dia. Circular Footing With a Compressible Material M_3 Buried at $R/r = 0$; $Z/r = 1$. . .	147
89.	Acceleration-Time Trace for a 6 in. dia. Circular Footing With a Compressible Material M_4 Buried at $R/r = 0$; $Z/r = 1$. . .	148
90.	Acceleration-Time Trace for a 6 in. dia. Circular Footing With a Compressible Material M_5 Buried at $R/r = 0$; $Z/r = 1$. . .	149
91.	Deceleration Reduction vs Subgrade Modulus of Compressible Material	150
92.	Deceleration Reduction vs Log of Subgrade Modulus of Compressible Material	151
93.	Stress-Time Trace at $R = 0$ in.; $Z = 1-1/2$ in. (6 in. dia. circular footing on the surface)	153
94.	Stress-Time Trace at $R/r = 0$; $Z/r = 1/2$ With a Compressible Material M_1 Buried at $R/r = 0$; $Z/r = 1$ (6 in. dia. circular footing on the surface).	154
95.	Stress-Time Trace at $R/r = 0$; $Z/r = 1/2$ With a Compressible Material M_2 Buried at $R/r = 0$; $Z/r = 1$ (6 in. dia. circular footing on the surface).	155
96.	Stress-Time Trace at $R/r = 0$; $Z/r = 1/2$ With a Compressible Material M_3 Buried at $R/r = 0$; $Z/r = 1$ (6 in. dia. circular footing on the surface)	156
97.	Stress-Time Trace at $R/r = 0$; $Z/r = 1/2$ With a Compressible Material M_4 Buried at $R/r = 0$; $Z/r = 1$ (6 in. dia. circular footing on the surface)	157

LIST OF FIGURES (Cont'd.)

Figure		Page
98.	Stress-Time Trace at $R/r = 0$; $Z/r = 1/2$ With a Compressible Material M_5 Buried at $R/r = 0$; $Z/r = 1$ (6 in. dia. circular footing on the surface)	158
99.	Peak Vertical Stress Reduction vs Subgrade Modulus of Compressible Material.	160
100.	Peak Vertical Stress Reduction vs Log of Subgrade Modulus of Compressible Material	161
101.	A View of the Apparatus for Statically Loaded Footing	163
102.	Footing Pressure vs Settlement (under static conditions)	165
103.	Ultimate Load Criterion Based on Log Load-Log Settlement Plot (De Beer's Method)	166
104.	Footing Pressure vs Settlement With a Compressible Material M_1 Buried at $R/r = 0$; $Z/r = 1$	167
105.	Footing Pressure vs Settlement with a Compressible Material M_2 Buried at $R/r = 0$; $Z/r = 1$	168
106.	Footing Pressure vs Settlement With a Compressible Material M_3 Buried at $R/r = 0$; $Z/r = 1$	169
107.	Footing Pressure vs Settlement With a Compressible Material M_4 Buried at $R/r = 0$; $Z/r = 1$	170
108.	Footing Pressure vs Settlement With A Compressible Material M_5 Buried at $R/r = 0$; $Z/r = 1$	171
109.	Deceleration Reduction vs Factor of Safety Reduction (factor of safety based on 0.18 in. allowable settlement)	173
110.	Deceleration Reduction vs Factor of Safety Reduction (factor of safety based on 0.10 in. allowable settlement)	174

LIST OF FIGURES (Cont'd.)

Figure		Page
111.	Grain Size Distribution of Ottawa Sand	182
112.	Relative Density vs Specimen Density for Dry Ottawa Sand (20-40 Mesh)	183
113.	Vertical Stress Arrival Time vs Depth	187
114.	Stress vs Deformation Relationship for Compressible Material No. 1 (loading and unloading conditions).	189
115.	Stress vs Deformation Relationship for Compressible Material No. 2 (loading and unloading conditions).	190
116.	Stress vs Deformation Relationship for Compressible Material No. 3 (loading and unloading conditions).	191
117.	Stress vs Deformation Relationship for Compressible Material No. 4 (loading and unloading conditions).	192
118.	Stress vs Deformation Relationship for Compressible Material No. 5 (loading and unloading conditions).	193

LIST OF SYMBOLS

AContact area of the footing
A_1, A_2, A_3 and A_4Constants
A_BAcceleration of the bottom movable steel plate
A_TAcceleration of the footing
aDeceleration of footing
BOne half width of footing
DDiameter of the footing
D_fFooting depth from surface
DRRelative density
C_DDilatational wave velocity
CSCoil spacing
EModulus of elasticity (Young's modulus)
E_cConstrained modulus
$F.S.$Factor of safety
K_cSubgrade modulus of the compressible material
GSpecific gravity of sand
νPoisson's ratio
ρMass density
γDry density of soil
γ_{max}Maximum dry density
γ_{min}Minimum dry density
gAcceleration due to Earth's gravity
RRadial cylindrical coordinate from axis of symmetry
R_aPercentage reduction of the deceleration of the footing

LIST OF SYMBOLS (Cont'd.)

R_s	Percentage reduction of the vertical stress
R_F	Percentage reduction of the Factor of Safety (based on allowable settlement)
r	Radius of the footing
S	Settlement of the footing
S_a	Allowable settlement of the footing
St	Sensitivity
Q	Static load applied on the footing
Z	Vertical cylindrical coordinate below surface
σ_c	Static contact pressure
σ_z	Vertical stress
σ_2	Stress gage number 2
σ_3	Stress gage number 3
σ_4	Stress gage number 4
ϵ	Strain at any arbitrary point
ϵ_z	Vertical strain at depth Z
ϵ_2	Strain gage number 2
ϵ_3	Strain gage number 3
ϵ_4	Strain gage number 4
M_1	Material designation number 1
M_2	Material designation number 2
M_3	Material designation number 3
M_4	Material designation number 4
M_5	Material designation number 5



CHAPTER I

INTRODUCTION

This thesis deals with effects on foundation response produced by stress waves propagating from the underlying soils.

The research described in this thesis is a part of the research program which began at the Illinois Institute of Technology and the IIT Research Institute in 1960 to study the transient stress-strain properties of soil by means of embedded stress gages and strain gages. The previous research was concerned with one-dimensional, two-dimensional and three-dimensional stress and strain through soil media under transient loads applied through a foundation at the surface.

In the design of structures which lie within earthquake regions, designers have been mainly concerned with lateral forces and very little attention has been given to forces in the vertical direction. But during the San Fernando earthquake in Los Angeles^{18*}, Southern California, in February, 1971, vertical loads resulting from the earthquake-initiated motions in the vertical direction, produced sufficiently large forces in first-floor columns of some buildings to collapse the entire structure. Seed⁵⁷ has pointed out that the main lessons to be learned from recent

*Numerical superscripts refer to references in the bibliography at the end of the thesis.

earthquakes are the dangers resulting from inadequate considerations of site conditions for structure.

As discussed and recommended by Varadhi⁷¹ this study forms an extension of the work where vertical loads were transmitted to small size footings enclosed in a 10 in. diameter vessel. In this study, however, a 3 ft. diameter vessel was used in which a 24 in. thick layer of 20-40 Ottawa sand was used as a soil mass beneath the footing. Two circular footings, 6 in. and 3 in. diameter, and a square footing of 3 in. size, having different contact pressures, were used. Vertical loads were transmitted to the foundation from mechanically-induced ground motions by means of three hydro-line cylinders.

The behavior of surface footings as well as buried footings was investigated in this study. Measurements were made of vertical acceleration and displacement-time records by mounting accelerometers on the footing. Stress-time and strain-time relations using embedded gages were made at various locations throughout the soil layer, with special emphasis to the area in the vicinity of the footing.

Experiments were also conducted using a thin layer of compressible material buried at a depth of one radius below the footing. Four sponge materials and a rubber material, having different compressible characteristics, were used in the investigation. These compressible materials were used as damping materials which absorbed some of the compressional waves travelling towards the bottom of the footing. This

technique of screening the waves (generated at a distance away from the footing) was defined by Woods⁸² as Passive Isolation. A series of five tests were conducted, each time using one of the different compressible materials. The foundation response (acceleration-time), and the vertical stress in the vicinity of the footing were recorded under dynamic load conditions.

The above test series was repeated for static load conditions where static loads were applied to the soil through the footing to estimate the bearing capacity of the footing (surface footing only).

CHAPTER II

REVIEW OF LITERATURE

This review is separated into three studies: first, the footing behavior under dynamic loads is studied; second, the recent soil dynamics research at IIT is studied; and, finally, the isolation studies are covered.

Footing Behavior Under Dynamic Loads

Detailed review of literature concerning the behavior of foundations under dynamic loads was done by Selig⁵⁸. A brief description of the review is presented herein. Lamb³⁶ was the first to derive a relationship between the vertical harmonic force, applied at a point on the surface of an isotropic, homogeneous, semi-infinite, elastic medium, and the displacement. In Germany, the German research society for soil mechanics, DEGEBO (Deutsche, Gesellschaft fur Bodenmechanik) and the University of Gottingen, together, carried out the empirical investigations^{39,40,41}. A simple mass-spring analogy was chosen as the mathematical model to represent the system. This mass included the mass of the vibrator and the foundation, but the experiments showed that the portion of the soil beneath the foundation should also be included in the mass. The system consisted of a foundation and the vibrator supported by a massless, linear spring with a dash-pot. Barkan^{3,4} performed a series of similar, but independent, foundation tests in Russia at VIOS, the institute of engineering foundation research. From his tests

he concluded, among other things, that the spring constant was not a constant but varied with the contact area of the foundation. Furthermore, he concluded that it varied with the frequency or rate at which the load was applied and removed. In 1936, Reissner⁵³ derived a solution for a system of vertical, periodic forces distributed over a circular area on the surface of an elastic body. He assumed that the dynamic soil pressure developed was uniform. The resonance frequency and amplitude of oscillation of the vibrator-soil system were determined as functions of radius of loaded area, static weight of the vibrator, weight and frequency of the vibrating mass, and the modulus of elasticity, Poisson's ratio and density of the soil. Crockett and Hammond^{12,13} suggested a refinement of the mass-spring analogy, in which the mass of the vibrating soil be distributed as weight for the spring rather than lumped with mass of foundation and vibrator. Vibration-compaction experiments on sand were carried out at the California Institute of Technology⁹. Based on these experiments an empirical natural frequency formula was derived, which included the following soil properties: soil density, soil shearing modulus, weight of foundation and vibrator, dynamic force and radius of the foundation.

Eastwood¹⁷ has carried out a considerable number of experiments to obtain a quantitative information about the effect of the various parameters on the natural frequency of the foundations and the effect of vibrations on the bearing

capacity and settlement of foundations.

Quinlan⁵⁰ used three types of load distributions (uniform, parabolic and a load for a rigid base) and derived a solution for vibration of circular and long rectangular vibrators assuming various contact pressures. He has shown a method for determining the phase angle, natural frequency and the amplitude of vibration. An analytical investigation was conducted by Sung⁶⁵ to determine the effect of the amplitude of oscillation on the resonant frequency.

Slade⁶⁴ has suggested that different models determined principally by the energy level of the vibration, must be used to represent soil. At low energy levels, the soil may be approximately represented as elastic. Since the displacements in the soil are principally irreversable, at medium-energy levels the soil is considered as nonelastic. At high-energy levels, the characteristics of the soil change significantly. Winterkorn⁸⁰ called this state of soil at high-energy levels, as a macrometric liquid. When the surface of a soil medium is subjected to dynamic loads, similar to those imparted by a vibrator, there will be several zones in the soil each with a different energy state. The highest state is in the vicinity of the vibrating footing, and it decreases as the distance from the vibrating footing increases. Because of the difference in the nature of the soil in these different energy states, Slade feels that one cannot describe the entire soil medium by a single model; instead, a discontinuous model must be used to represent the

actual conditions. Slade suggested: 1) a coupling-region consisting of a spring and a dashpot in place of the high and medium regions; and, 2) a mass which transmits a concentrated force to the low-energy region. This low-energy region is treated as an elastic region and the solution presented by Lamb³⁶ is used to determine motion of the soil.

Arnold, Bycroft and Warburton² determined the forced vibrations of a rigid body resting on a homogeneous, isotropic, elastic medium of infinite surface area and of constant depth, which may be finite or infinite. Four modes of vibration of a mass on a circular base were considered: 1) vertical translation; 2) torsion; 3) horizontal translation; and, 4) rocking. Arnold checked his theory experimentally using an electromagnetic vibrator on a rubber medium and concluded that the results agreed favorably with the theoretical predictions.

Richart⁵⁵ outlined Sung's work and presented extensive curves which may be used for analysis and design of foundations under dynamic loads. He assumed the foundation to be rigid.

Triandafilidis⁶⁷ solved analytically the dynamic problem for a very simplified, rigid, plastic material. He found that the footing response is greatly influenced by the inertia of the participating soil mass. In case of dynamic problems, the inertia forces play an important role, therefore, the participating soil mass in the motion is of paramount importance.

Cox, et al.,¹¹ analyzed the dynamic response of a smooth circular punch on the surface of a semi-infinite, rigid and plastic medium by numerical techniques. In their analysis, they assumed the soil to be rigid and plastic obeying the Mohr-Coulomb yield criterion.

Carroll⁸ studied the behavior of square, rigid footings resting on the surface of a clay medium (Buckshot Clay) subjected to static and impulsive vertical loadings, both experimentally and analytically. Load was applied to the clay layer through the footing. The purpose of his investigation was to establish relations between applied transient foundation loads and the resulting foundation motions. Measurements consisted of recording the vertical displacement and reaction load of the footing when subjected to known input load.

From the results of his investigation Carroll categorized the dynamic load-displacement behavior of the footing in to three inertial regimes: 1) three-dimensional static in which inertial forces exert only a minor influence on footing response and a three-dimensional static analysis should give reliable results; 2) three-dimensional dynamic in which the footing response should be considered as a three-dimensional problem; and, 3) one-dimensional dynamic in which one-dimensional wave theory, with appropriate dynamic stress-strain curves, should reliably predict footing response.

Hadala²³, Jackson and Hadala³⁰ at Waterways Experiment Station used the principles of similitude in the analysis of

dynamically loaded square footings on clay. Three non-dimensional relationships were developed to predict the maximum displacement and the time of its occurrence. The first relationship was between the resistance parameter and the displacement parameter. The second relation was that of a strength parameter to the displacement parameter. The third relationship included the strength and inertia parameters.

In 1965, Whitman⁷⁸ reviewed the theoretical work on foundation vibrations and compared the results with some field tests. He concluded that, if the soil properties-especially the shear modulus and Poisson's ratio-can be estimated more accurately, the theoretical and experimental results would have a better correlation.

Richart and Whitman⁵⁶ expanded Whitman's⁷⁸ review work to include other modes of vibration. From their study of model footing tests, they concluded that the theory assuming the soil media as elastic and semi-infinite, gives good approximation of the amplitudes of motion, when the vertical oscillations produce a linear acceleration of the footing of less than 0.5g.

Lysmer and Richart⁴² developed a method for analysis of the vertical mode of vibration of a rigid circular footing resting on the surface of an elastic half-space. Their solution included all ranges of frequencies for steady state vibration. From the results of their study it was shown that all vertically loaded footing-soil systems were strongly

damped because of wave propagation into the subsoil. Therefore, it was suggested that the material damping could be neglected in practical calculations. It was also shown that the damping ratio decreased with increasing mass ratio of the system.

Drnevich and Hall¹⁵ conducted transient loading tests on a foot diameter, relatively rigid footing resting on the surface of a bed of sand. Two types of load pulses were applied to the footing. The magnitude of the loads was such that the response of the footing was essentially elastic. The mass of the footing was also varied to produce different footing response characteristics. From the analysis of their test results, it was concluded that the theoretical approach developed by Lysmer leads to reasonable predictions of the "elastic" dynamic response of the footing.

Experimental and analytical investigations on the behavior of small boy footings were conducted by Hadala and Jackson²⁴. They have found that the static preloads of less than 30% of static bearing capacity, do not influence either the change in maximum footing displacement or the change in time to maximum displacement. Although the preload-induced static settlements were negligible, it was possible that the preload-induced field beneath the footing, influenced the magnitude of the dynamic displacements.

Rao and Höeg⁵¹ developed a numerical procedure for predicting the dynamic response of strip footings on saturated clayey soils. The soil was assumed to be linearly

elastic-perfectly plastic, yielding according to Tresca's criterion and flowing plastically according to the normality rule of plasticity. They used a discrete lumped parameter mathematical model replacing the clay continuum. The effect of various variables on the peak displacement of the footing was studied. They concluded that the peak displacement is very sensitive to: 1) pulse duration; 2) applied load pulse; and, 3) soil properties like, soil modulus and Poisson's ratio, but is not sensitive to the density and pressure distribution under the footing.

Larkin³⁸ used perfectly smooth strip and circular footings resting on a cohesionless soil to obtain the bearing capacities. He obtained the bearing capacities of very shallow footings by integration of the equations of plastic equilibrium of soils. It was found that the footing was very sensitive to depth of burial. In the case of circular footing located at the surface, an increase in depth of about 0.09 to 0.13 of the footing diameter is sufficient to increase the bearing capacity 100%. This indicated that the small footing settlements which accompany the loading up to the point of failure, significantly increase the actual bearing capacity of footings.

Orrje⁴⁹ developed a new method to evaluate the deformation and strength properties of cohesionless soils. Both laboratory and field tests were conducted on four different soils. Behavior of these soils was investigated by measuring the retardation of free falling weight when it

strikes the soil surface. Static plate loading tests were also conducted on the same soil material for comparison purposes.

The load-deformation curves, the failure loads and the equivalent moduli of elasticity from the dynamic and static loading tests were compared at various relative densities of the soil materials. He also investigated the failure modes of the dynamic static loading tests. From the analysis of the test results Orrje concluded that: 1) the shape of load-settlement curves obtained from the dynamic loading tests with a free falling weight agreed well with the load-settlement curves for the static plate loading tests; 2) the dynamic failure load and the dynamic equivalent moduli of elasticity increased with increasing height of free fall; 3) the dynamic failure load increased with increasing plate diameter; 4) the failure load also increased with increasing mass of the falling weight and the equivalent modulus of elasticity was approximately independent of the mass of the falling weight; 5) the footing response was sensitive to any changes in the dry unit weight of the sand (The maximum retardation increased approximately linearly with increasing dry unit weight of the sand. The dynamic and static failure loads also increased linearly with increasing dry unit weight.); and, 6) in the dynamic tests with retardations between 1g and 6g, the failure mode differed from that of the static tests.

He also concluded that the depth to which the loading

tests affected the underlying soil corresponded to approximately 1.5 plate diameters.

Rhines⁵⁴ proposed a new foundation model for punch-shear failure in soils. An infinitely long rigid footing resting on an elastic-perfectly plastic soil was considered in their analysis. The foundation model consisted of two elastic spring layers interconnected by an elastic shear layer.

The important characteristics of the foundation response included: 1) yielding began at and was confined to, points in the foundation layer directly under the edges of the punch; 2) the load-deflection curve was bilinear and the peak corresponded to the onset of yielding in the shear layer; and, 3) once yielding occurred, the maximum contact pressure was less than it would have been had the foundation, under the same load, remained elastic.

Duns¹⁶ numerically examined the dynamic behavior of a rigid circular footing on a linear-elastic isotropic half-space by means of the finite element method. For the reflection, an equivalent viscous damping was used at the footing. Results showed a good agreement with the analytical methods. The calculation of the vertical footing acceleration for unsteady (shock) excitation by means of a Δt -method was confirmed by the results of measurements obtained in a similar test.

Skormin⁶³ conducted some bearing tests using a circular plate 60 cm. in diameter resting on the surface of a sand layer three meters thick. The contact pressure at the base

of the plate and the normal stresses in the subgrade were measured at different loading increments. From the investigation it was found that the stress under the foundation was concentrated more than that suggested by the theory of semi-infinite elastic solids.

Naik⁴⁸ proposed a method to find displacements and stresses within a foundation on a semi-infinite mass under dynamic loads. The soil was assumed to be a semi-infinite, homogeneous, isotropic, elastic solid and the foundation was treated as a plate supported on the soil. The finite element method was used to calculate the soil reaction beneath a foundation subjected to a dynamic load. He then used Lamb's study of 1904 to describe the foundation displacement. With the method proposed in his study, the natural frequency of vibration for a foundation of any shape can be easily computed. Some of his conclusions were that the displacement, due to one or more foundations, at any location on the surface of the semi-infinite mass can be computed by the method described in the study. The natural frequency of a given foundation-soil system can be easily computed. For this foundation-soil system, the displacement gradient between the mid-section and the edge of the foundation decreases as the loaded area increases.

Medearis⁴⁷ of Kenneth Medearis Associates (KMA), Ft. Collins, Colorado, prepared a report for the ASCE Research Council on Performance of Structures. KMA has investigated the response characteristics of fullscale structures to the

transient, earthquake-like ground motions resulted from an underground nuclear detonation. They used the Plowshare Project (of U.S. AEC) to study the dynamic response of actual structures.

Project Rio Blanco was the third Plowshare natural gas-stimulation experiment to be conducted in the United States. It involved the detonation of 3-30 kiloton nuclear devices more than a mile below ground level in Rio Blanco County, Western Colorado on May 17, 1973. Five Rio Blanco area structures were selected for instrumentation and analysis. These structures were located between 4 and 40 miles from the detonation point, and experienced peak accelerations of 0.003-1.0g's. All these structures were previously analyzed by KMA. Seismic recorders were installed at the base of and on each of these structures to monitor their responses to the detonation ground motions. The structures were subsequently reanalyzed and the theoretical and recorded responses compared.

The results of their study indicated a good correlation between the recorded responses and those obtained using modern, computer-oriented, structural dynamics models and analysis.

It was also indicated that the Uniform Building Code seismic recommendations are inadequate with regard to both low-rise and high-rise construction. It was suggested to revise the Uniform Building Code seismic recommendations.

Recent Soil Dynamics Research at IIT

One-dimensional Studies. The stress wave propagation

study at IIT began in 1960. In this study, a series of experiments were conducted in which long horizontal columns of sand and clay were subjected at one end to a shock loading^{61,75}. Stress gages were buried along the length of the specimen and information was obtained on wave velocity, peak stress attenuation and reflected stresses. This study also included the development of an embedded soil stress gage⁶⁰. A piezoelectric crystal was used as the sensing element for this gage. The gage possessed the advantages of high frequency response and high sensitivity.

Gage Development. Concurrently with the program outlined above, a program of gage development was conducted to develop a soil strain gage that would minimize interface of the gage with free soil movement⁶⁸. This gage consists of two sets of two mechanically uncoupled thin coil disks and associated electronic circuitry. The principle of operation is that of a null balance differential transformer, i.e., each set of coils represents transformer primary and secondary windings and are so arranged in the circuitry that the resulting signal is the difference of the individual coil outputs. In operation, one set of coils is embedded in the soil as the strain sensing element while the other is positioned externally at a known spacing to serve as a reference. The gage is well adapted for use in soil as the sensing elements are mechanically uncoupled.

Januskevicius and Vey³¹ performed a series of experiments to evaluate the performance of strain gage and the

previously mentioned stress gage in soil. In these experiments, the gages were used to measure stresses and strains in triaxial specimens of sand under both slow and rapid rates of loading. Evaluation of the results led to two important conclusions relative to the reliability of the gages to record true free field stresses and strains:

- (1) The stress gage must be calibrated in soil. Moreover in any stress gage measurement the modular ratio of the soil to the gage must lie within determined limits of the ratio at which the gage was calibrated.
- (2) The strain gage output can be related to the true strain up to 6 percent strain if the strain is due to volume decrease. Where strains occur without a change in volume or if the volume increases during deformation, the presence of the gage begins to have an appreciable effect on the deformation at about 3 percent strain.

Later, a series of one-dimensional wave propagation experiments were conducted in which the gages were employed to measure stress-strain relations in the soil^{74,26}. Stress gages and strain gages were embedded at intervals along the length of long columns of soil (both sand and clay). The soil columns were loaded at one end by a shock wave with a peak stress in the range of 5-300 psi and the gages used to measure stress-time and strain-time as the stress wave

traversed the specimen. Stress-strain curves were constructed by interpolating between gage locations. In a subsequent study soil specimens were subjected to shock waves up to 1100 psi peak stress.

Further studies to eliminate certain undesirable features of the piezoelectric gage such as the adverse effects of moisture and the gage's inability to sense quasi-static loads led to the development of a piezoresistive gage⁶². A number of gage concepts were evaluated and it was determined that the deflecting diaphragm type gage was most satisfactory, provided the deflection was kept sufficiently small. A prototype gage was constructed which used a piezoresistive element on a deflecting diaphragm as the sensing element. The principle factors considered⁵⁹ in the gage design include:

- (1) application, i.e., free field or against structures
- (2) frequency response
- (3) geometry
- (4) relative stiffness of the gage and the soil
- (5) density of gage relative to soil
- (6) nature of sensing element, and
- (7) the placement of the gage in soil.

Depending upon a particular application, gages must be selected or designed (if not available in the market). If there are any major variations in environmental conditions, such as temperature and moisture, they must be controlled.

For measurement of stress under transient loading conditions, frequency response of the gage must be considered. The geometry of the gage is also an important factor to be considered. Small size gages for laboratory experiments and larger size gages for stress measurements in the field are generally used.

Most important factor to be considered in evaluation of the response is the difference between the stiffness of the gage and the soil. By burying the stress gage into the soil, some soil is displaced. The stiffness of the gage is entirely different from that of the soil. Therefore, this will cause a redistribution of stresses around and in the vicinity of the gage and produce a higher or lower stress reading, depending upon whether the gage has a greater or small stiffness than the soil. It has been found that the thickness-to-diameter ratio of the gage is also an important factor which effects the magnitude of the redistribution of stresses. It is generally accepted that this ratio should be as small as possible. A typical value^{28,29} of this ratio is 0.2.

The density of a gage is another important factor to be considered in dynamic measurements. For instance, if the density of the gage is higher than that of the soil replaced by the gage, the free motion in the soil is interfered. As a result, the gage inertia produces a stress which either increases or decreases the stress in free soil conditions. This effect becomes more significant at higher rates of loading. By selecting a proper gage material, one which weighs same as the soil replaced by the gage, density matching can be achieved.

Most of the gages are constructed using a flexible diaphragm supported at the perimeter of the gage by a rigid ring. The deflection of the diaphragm is sensed by piezoresistive strain gage bonded to the diaphragm. Due to the less rigid diaphragm and more rigid case, the soil arches the stress onto the gage perimeter causing a higher than free-field value on the perimeter (ring) and a lower than free-field value on the diaphragm.

Selig⁵⁹ in his review suggested that the gage design must also take into consideration the methods of placement. Gage placement method and calibration procedures are discussed in detail in Chapter IV of this thesis.

Footings on Sand. The experimental programs using surface applied time dependent loads were undertaken to measure the behavior of sand beneath a rigid circular footing^{76,77}. Two types of loads were applied to the footing; an impulsive-type dynamic load and a quasi-static load. Embedded soil stress gages and soil strain gages were employed to obtain the complete stress-strain-time relationship in the soil at various depths below the surface on the centerline of the loaded area. Data was also obtained off the centerline. Stress-time and strain-time measurements were obtained at the same or symmetrical locations.

These studies led to the following conclusions:

- (1) The soil response to the impacting load exhibited both elastic and plastic characteristics. During the initial

loading phase plastic behavior was noted primarily in the stress measurements.

Plastic behavior was subsequently noted in the displacement and strain measurements as the inertia effects decreased.

- (2) The attenuation of the peak vertical stress with depth on the axis of symmetry was essentially spatial as predicted from the theory of elasticity even though the peak surface pressure was considerably greater than the bearing capacity of the soil. The absence of evidence of attenuation due to inelastic effects was ascribed to the significant inertia forces acting during the initial loading phase.
- (3) An initial decrease in volume was followed by a volume increase as yielding occurred for tests on both medium and dense Ottawa sand.
- (4) Relating to a foundation subjected to an impulsive load, the experimental data indicated that the problem may be divided into three inertial regions----one-dimensional dynamic, three-dimensional dynamic, and three-dimensional static----depending on the size of the footing, the rise time of the load pulse, and the soil stiffness.

Footings on Clay. An experimental program similar to that conducted for sand was also carried out for clay (EPK Clay)³⁷. In addition to the experimental work a computer program was developed⁶ to predict wave developments in clay using an axisymmetric model, and assuming the clay to be an elastic-perfectly plastic material subjected to a known impulsive loading applied through a circular footing at the surface. A finite difference technique was used to integrate the differential equations of motion. In order to get comparative results, assuming the elastic-plastic behavior of clay, several trial values were given to the modulus of elasticity, Poisson's ratio, and the yield limit in simple shear using three types of boundaries-rigid and flexible, for various sizes of footings.

A study of the computed stresses and strains in the soil as a function of time indicated the sensitivity of the results to changes in individual soil parameters and a comparison of the theoretical values with those from the experiments yielded approximate values of the parameters for the clay. The latter were well within the limits of what had been previously reported for clay with similar properties.

The Isolation Studies

The isolation technique has been applied to the earthquake problem to reduce the effect of transient loadings on the structure. In 1935, Green²¹ proposed that buildings be constructed with a flexible first story.

Barkan⁵ reviewed many applications of trenches and sheet

pile barriers in isolation problems and presented some empirical rules for design.

Matsushita and Izumi⁴⁴ proposed a double basement design which incorporates a flexible first story.

Woods⁸² conducted some field tests to evaluate the effectiveness of open trenches in reducing the amplitude of vertical ground motion. He used annular trenches surrounding the source of vibration to reduce the disturbance of the adjacent ground, and defined this isolation as 'active' isolation (isolation at the source). He defined 'passive' isolation as employing some barriers (straight trenches) at remote points from the source of vibrations but near a site, to reduce the amplitude of vibration. From the active isolation tests, he concluded that a maximum depth of 0.6 wavelengths was required for a trench to satisfy the amplitude reduction criteria of 0.25. Circular trenches were effective in reducing motions outside the trench to some distance (≈ 10 wavelengths) away. From the passive isolation tests, he concluded that larger trenches were required at greater distances from the source to accomplish a given amplitude reduction. He also concluded that sheet-wall barriers were not as effective as open trenches in screening surface waves.

Matsushita and Izumi⁴⁵ conducted fundamental studies on the 'Earthquake Free Mechanisms' to decrease earthquake forces applied to the buildings. They defined 'Earthquake Free Mechanism' as the mechanism to be installed in a structure,

to decrease the input earthquake energy. The effective application of the mechanisms and the media is to install them near the boundary between the structure and the soil since the earthquake forces are fed to the structures through the boundary. They proposed a concept of isolating buildings with rollers which would cause the building to rise when displaced laterally. The four types of mechanisms satisfying the necessary conditions were: 1) Bearing Mechanism; 2) Column and Rod Mechanism; 3) Wall and Brace Mechanism; and, 4) Boundary Mechanism. The 'bearing mechanism' consisted of using bearings including ball bearings. The 'column and rod mechanism' consisted of flexible but strong columns and rods. The 'wall and brace mechanism' produced 'restoring force-deflection' relations against lateral displacement. And the 'boundary mechanism' provided shock absorbing materials at the boundary between the structure and the ground. Mechanisms shown in their study were designed for about and less than twenty storied R.C. buildings built on good ground.

From the results of earthquake response calculations and recorded data they concluded that the acceleration at the top of the building of medium height was three times the input acceleration at the base and, in case of structures with 'Earthquake Free Mechanism', the acceleration values at the top of the building were small. Some of the calculated results showed more than a 50% decrease of input earthquake forces.

Gupta and Chandrasekaran²² considered an absorber system

having both linear and elasto-plastic restoring force characteristics and viscous type of damping in their analysis. They considered a parent system represented by a mathematical model of idealized single degree of freedom. Some of their conclusions were that the response reduction factor (β) decreased as the mass ratio (μ_a : the ratio of sum of masses of all absorbers to that of the parent system mass) was increased. The response of the parent system was increased as the damping of absorbers was increased. The response of absorbers themselves decreased with the increase in numbers.

Wirsching and Yao⁸¹ studied some techniques for improving the safety of seismic structures. In particular, the effect of passive motion reducing device on seismic structures was investigated. They used a Monte Carlo technique for analog simulations of the random earthquake and corresponding response processes. The seismic response of a single-story system having a nonlinear isolator was studied. They also considered the same nonlinear isolator with 5 and 10 story models.

From the results of the single-story tests, two general conclusions were drawn. They found that it is desirable to have significant damping in the isolator (perfect isolation occurs when the isolator stiffness approaches zero). And the isolator must maintain sufficient stiffness to prevent excessive displacement of a structure in a strong wind.

They also conducted two test series with the absorber (using the optimum value of damping) in the system of the

five and ten story models. From the analysis of the results, they concluded that: 1) a considerable reduction in structural response could be realized with the isolator; 2) there was little dispersion in the peak response data with the isolator in the system; and, 3) the absorber, used with the isolator, caused an increase in the response. They also reported that the use of the absorbers did not help the isolated system because the top floor motion was relatively small and little energy was absorbed.

Finally, on the basis of safety considerations and without regard to the cost, they concluded that the design modifications were ranked in the order of their efficiency as: 1) the isolator system; 2) the isolator-absorber system; 3) the absorber-damper system; 4) the absorber system; and, 5) the damper system. The ranking was based on only limited studies of each of the systems.

CHAPTER III

PURPOSE AND SCOPE OF INVESTIGATION

Based upon the review presented in Chapter II the present state of knowledge in the area of footing response under dynamic loads may be summarized briefly as follows.

Earlier theoretical investigations were based on the assumption that soil behaved like an homogeneous, isotropic and a linear elastic material. But the general behavior of soil is nonhomogeneous, anisotropic, inelastic and nonlinear. However, for small strains the behavior may be considered as that of a linear elastic material. Some recent⁵¹ studies also included complex constitutive relations into the analysis, in which soil was assumed as linearly elastic-perfectly plastic material.

All of the studies to date, both analytical and experimental, have dealt with stress-time and strain-time measurements throughout the soil mass under the effect of a surface applied time-dependent load. Measurements were made in the soil as a function of direction and distance from the foundation applied load. In these studies the foundation was initially in motion and the soil was at rest.

The February 9, 1971 San Fernando earthquake in California demonstrated that ground accelerations can occur in excess of those previously considered in the design of dams¹⁰. It is recognized, of course, that in most earthquakes, horizontal loads are more damaging to structures and actual foundation-soil structure interaction results

from loads that are inclined. These inclined loads could be resolved into two components vertical and horizontal and considered independently. Of the two, only the vertical component involves the support of the structure under both static and dynamic loads. If the foundation is designed with a safety factor of 2 or 3 for example, as is normally the case, against bearing failure by shear in the soil under static load, the capacity of the soil to transmit superimposed vertical dynamic loads before yielding, is likely to be far in excess of the strength of the columns or piers. In the San Fernando earthquake in Los Angeles¹⁸ the failure in the columns of bridges and buildings was caused by the motions transmitted to the foundation soil from the base rock which propagated upward through the soil to the structure. They were found to be quite severe in localized areas with accelerations estimated near the 1.0g level.

Examples of other than natural occurring phenomena that transient vertical dynamic loads to structure are underground explosions, large drop hammer forges, demolition operations, pile driving and even heavy truck traffic for some soil conditions, e.g., soft saturated clays underlying a thin dessicated surface stratum. Design of foundations, considering possible structural failure due to vertical dynamic loads, has received much less attention than has the effects of horizontal loads. In many of these cases it is possible to establish the input load spectrum with reasonable accuracy. The problem lies in evaluating the soil trans-

missibility and the soil-foundation interaction that one also needs for an evaluation of the force-deflection response of the structure.

Thus, it is evident that a need for a basic understanding of this phenomenon exists. To accomplish this, an experimental program was undertaken in which the foundation was situated at the surface and at different depths of burial, and vertical transient loads were applied to the foundation through the underlying soil. Therefore, in this study the foundation was initially at rest and the soil at the interface between the soil and the foundation was in motion. In the previous studies, the foundation was initially in motion and the soil was at rest, thus inertia effects in the present study were reversed. Initial stress conditions in the soil mass were also varied by varying the foundation size and mass.

Measurements were made of stress-time and strain-time histories using embedded gages throughout the soil mass and particularly in the vicinity of the foundation. From the results of the test data an attempt was made to obtain a comprehensive picture of stresses and strains in a soil mass, and to evaluate the extent of the influence of foundation and distribution of pressures in the soil beneath it, on the stresses and strains. Measurement of acceleration-time histories were also made. These records were integrated to provide velocity-time and displacement-time relations for the foundation.

In addition, the study included some efforts to reduce

the effect of input transient loads on the foundation response. This was accomplished by providing a layer of compressible material at a depth of one radius. The measurements included the acceleration-time histories and subgrade modulus of the compressible material at the static contact pressure level. An attempt was also made to establish a relation between the reduction factor of the footing response and the reduction of the safety factor against bearing capacity failure based on an allowable settlement.

CHAPTER IV

TEST APPARATUS AND EXPERIMENTAL PROCEDURES

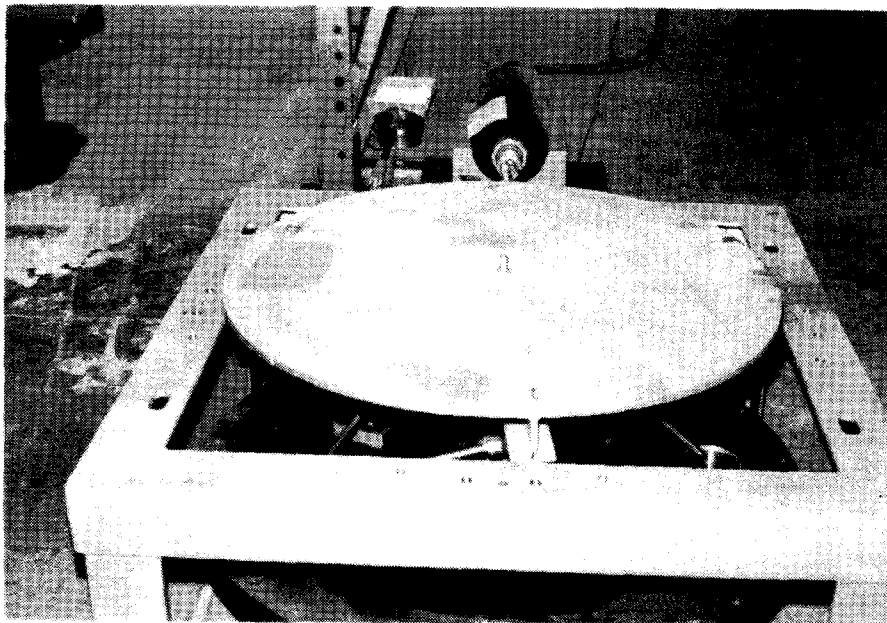
Test Apparatus

A general view of the experimental apparatus used in this study is shown in Fig. 1. A pressure vessel 3 ft. dia. by 3 ft. deep with both ends open was used. A movable steel plate 1/2 in. thick, supported by three I-sections welded (to improve the rigidity of the plate) to the plate at 120° apart, as shown in Fig. 2, was positioned at the bottom inside the vessel. The vertical movements of this plate were maintained vertically by three hydro-line cylinders. A 24 in. thick layer of dry Ottawa sand was used as a soil media beneath the footing. The properties of this sand are given in Appendix A. Rigid footings, circular and square shapes 6 in. dia., 3 in. dia. and 3 in. by 3 in., as shown in Fig. 3, were used. Ground motions induced mechanically using a loading apparatus specially designed for this purpose were transmitted to these footings through the underlying layer of sand bed by moving the bottom plate. The behavior of surface as well as buried footings was studied.

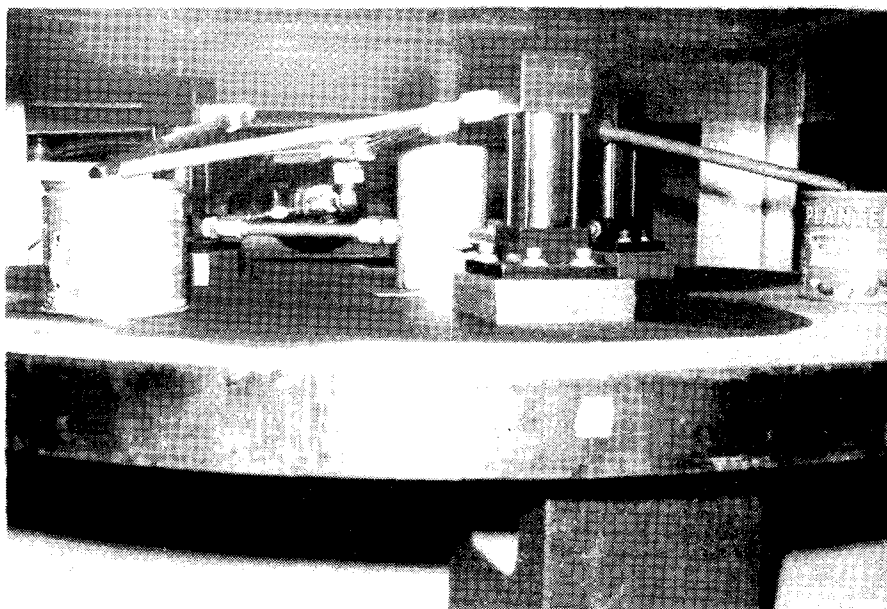
A schematic diagram of the loading apparatus is shown in Fig. 4. As shown, the apparatus consisted of a nitrogen cylinder, accumulator, solenoid-dump valve, flow control valve, relief valve, distribution chamber, three hydro-line cylinders, oil storage and oil dump. Oil under pressure in the system was released to the hydro-line cylinders and hence the transient loads to the bottom movable plate attached to



Figure 1. A General View of the Experimental Apparatus



a) Top View



b) Bottom View

Figure 2. Bottom Movable Steel Plate Mounted on Three Hydro-Line Cylinders

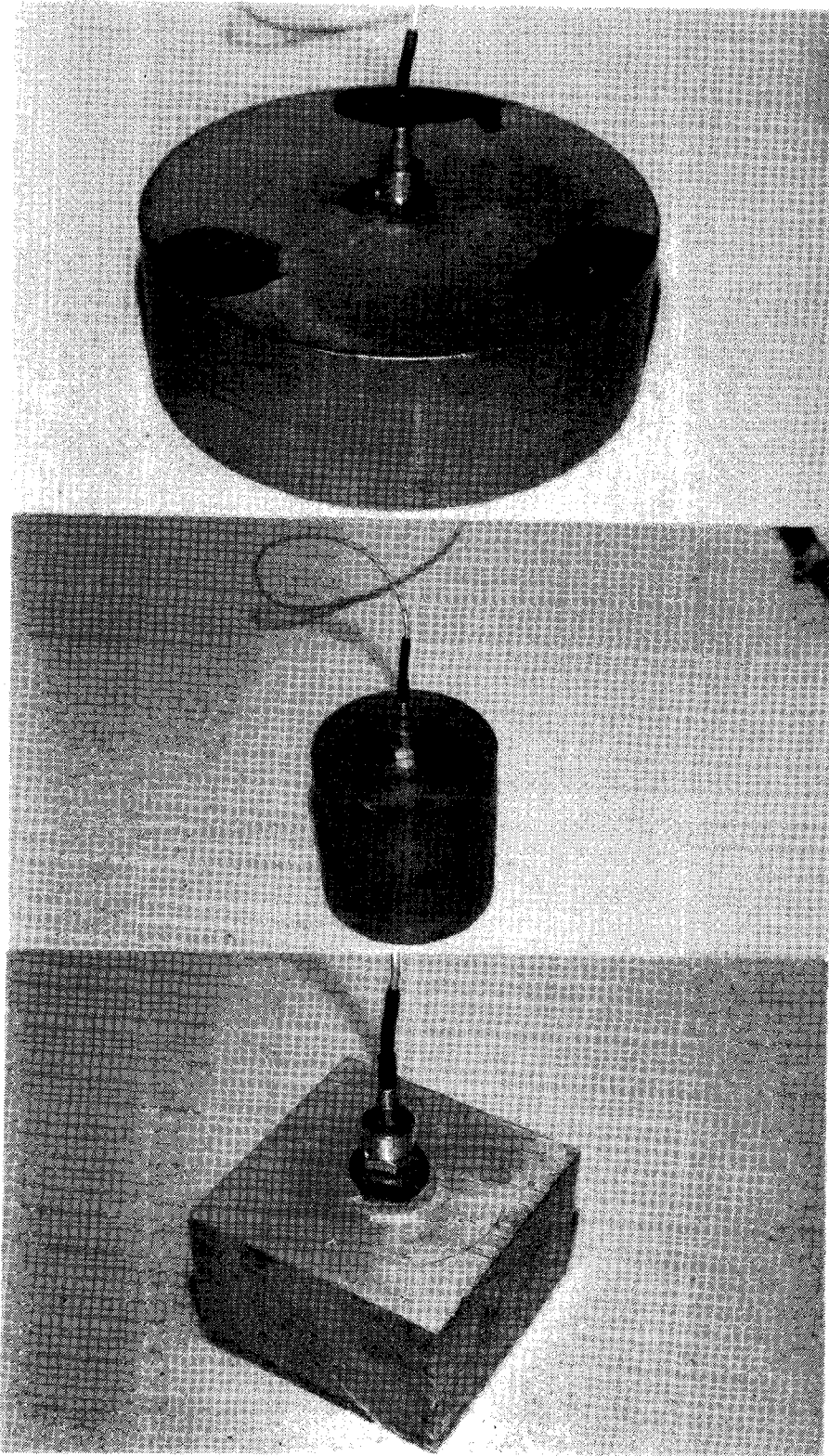


Figure 3. Various Size Footings Used in This Study

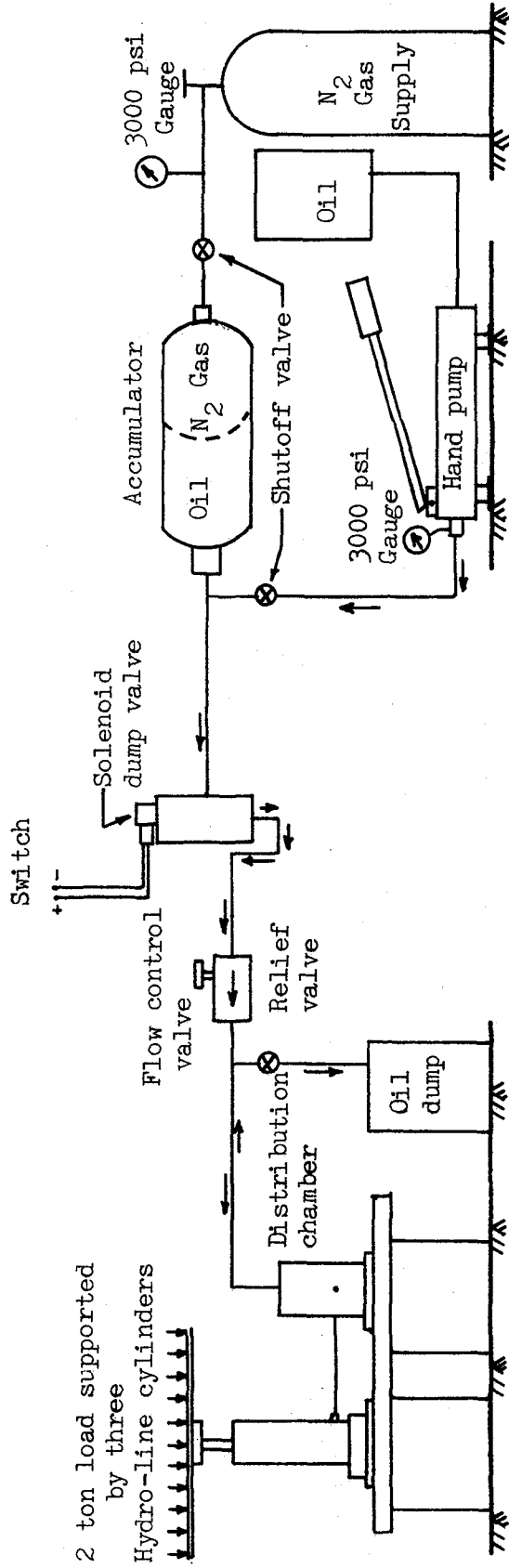


Figure 4. Schematic Diagram of Transient Loading System

the cylinders. A view of this system is shown in Fig. 5.

Embedded stress gages and strain gages were positioned at various locations throughout the soil layer and in the vicinity of the footing as the sand was being placed in the vessel. Two accelerometers (High Resonance Frequency, Shock Accelerometer Model 2225, ENDEVCO Dynamic Instrument Division), one on the bottom movable plate of the vessel and the other one on the top of the footing, and a DCDT were used to record the acceleration-time and displacement-time relationships.

Stress-time and strain-time histories in the vicinity of the footing were recorded by using the embedded gages. For this purpose a 14-Channel magnetic tape recorder (Magnetic Tape Recorder, Model 5600B, Honeywell) and a visicorder (Model 1508B, Honeywell) were used. A bank of four oscilloscopes (Dual Beam Oscilloscopes Type 502, Tektronix Inc.) were also used to record the response (for some tests) of the gages and accelerometers, and traces recorded on a polaroid film simultaneously, for comparison purposes. An internal triggering system was used in the first oscilloscope of this bank and the remaining oscilloscopes were simultaneously triggered by means of a trigger wire.

A series of static load-displacement tests were also conducted for a 6 in. dia. surface footing. These tests were conducted in the same vessel as the dynamic tests, using the apparatus shown in Fig. 6. The load was applied to the footing at a constant strain rate through a gear box arrangement. The footing pressure was measured by means of

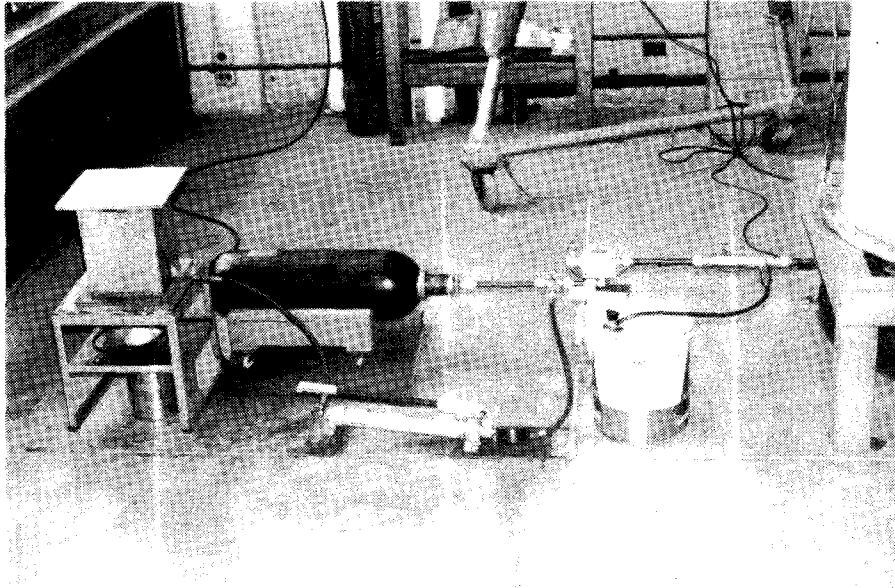


Figure 5. A View of the Loading System

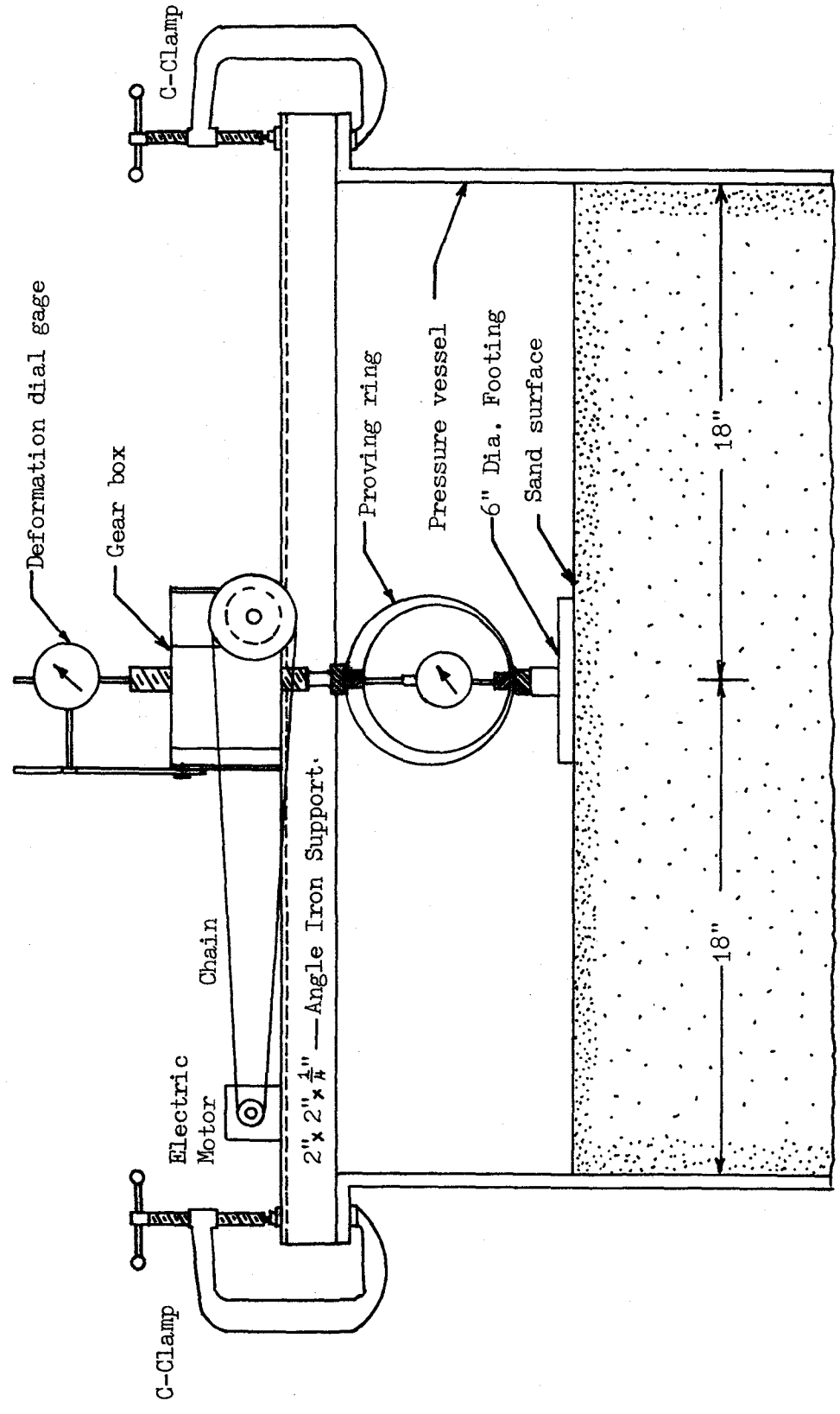


Figure 6. Apparatus for Statically Loaded Footing

a proving ring dial gage, and the penetration was measured by a deformation dial gage.

Embedded Stress Gages

Stress-time measurements were recorded by using the piezoresistive gages developed at IIT Research Institute⁶². This gage is schematically shown in Fig. 7. The overall dimensions of this gage are 1.5 in. in dia. by 0.255 in. thick and with a frequency response of 60 KHz. The gage consists of a disk-shaped aluminum case with stiff walls and a thin diaphragm machined in the bottom surface. The gage operates on the deflected diaphragm principle and the deflection of the diaphragm is sensed by a piezoresistive strain gage. These gages were constructed with four active arms forming a complete Wheatstone Bridge and a balance unit to provide an initial balancing of the bridge circuits. This balance unit was also provided with four different calibration resistors to allow for variations in excitation voltages. The excitation voltage used throughout the experimental program was 5.0 volts d.c. These stress gages were calibrated both under hydrostatic conditions as well as in confined specimens of sand.

Calibration of Stress Gages. The schematic diagram of the device used for hydrostatic calibrations is shown in Fig. 8. The device consisted of two steel cups filled with water, each covered by a thin rubber membrane. These cups were then clamped together face-to-face with the gage between them. A known air pressure was applied to the water

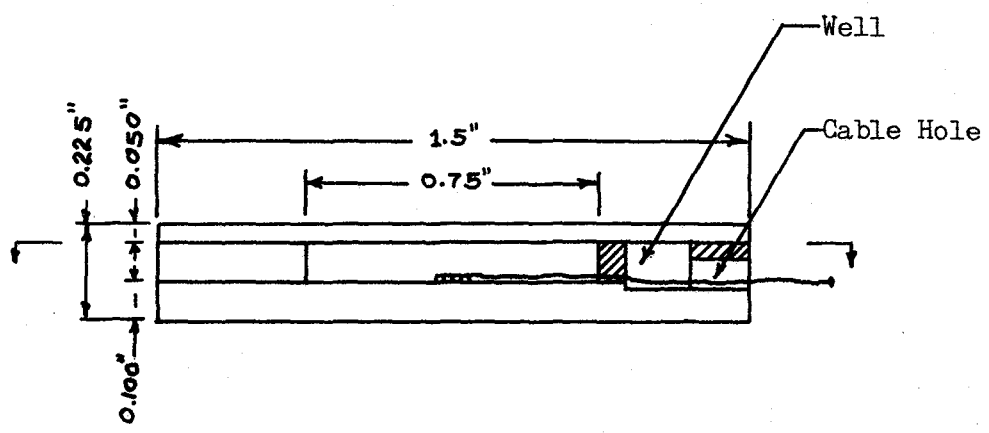
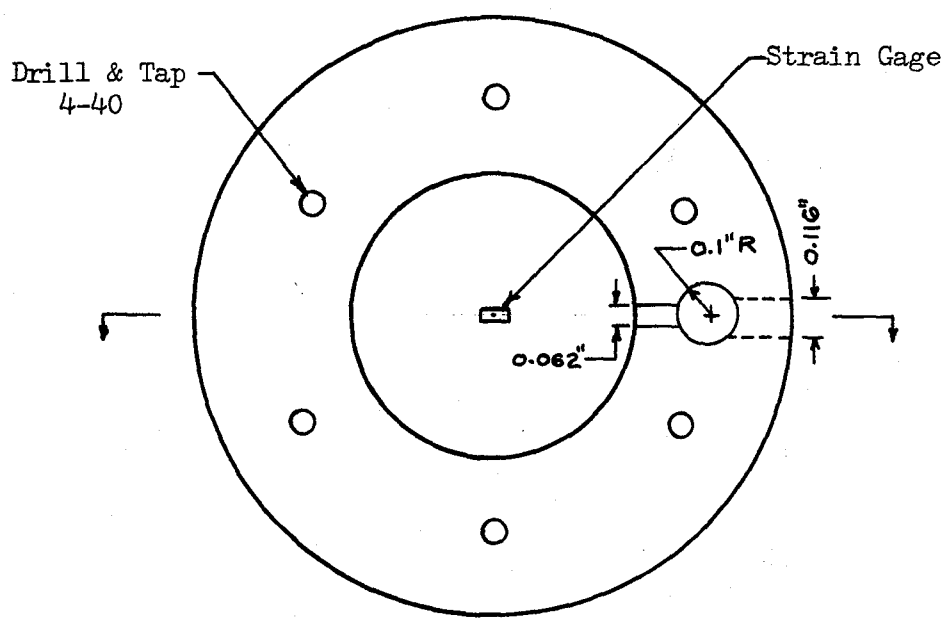


Figure 7. Piezoresistive Soil Stress Gage

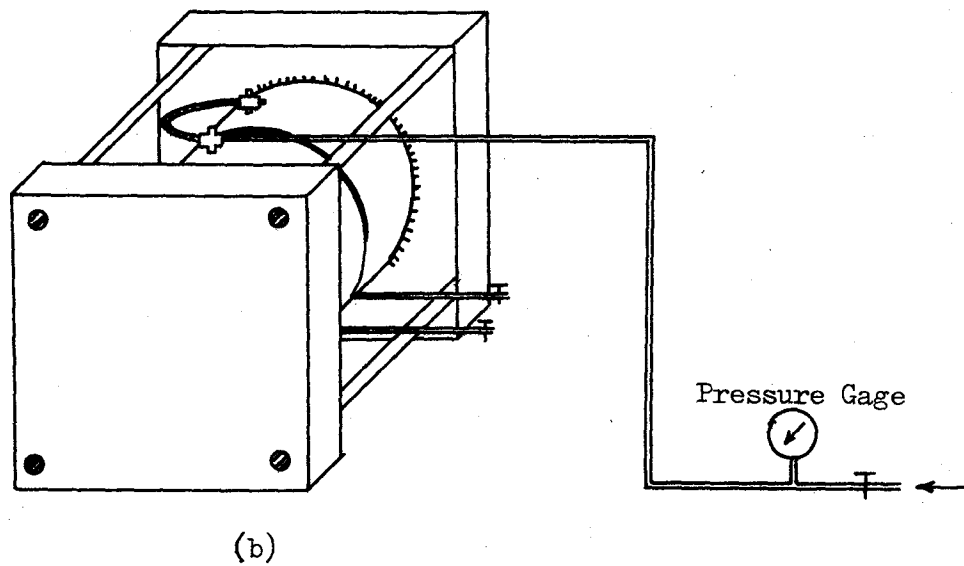
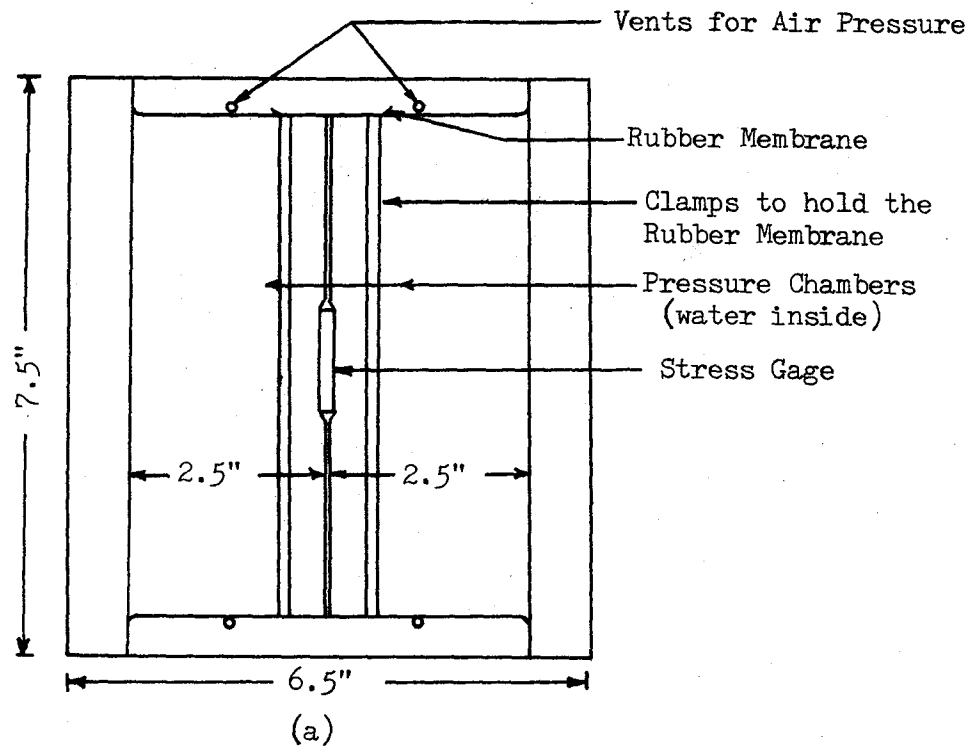


Figure 8. Schematic Diagram of Water Chamber for Gage Calibration

in both the cups and hence to both sides of the gage uniformly. This pressure was increased in increments of 10 psi to a maximum of 80 psi, while the gage output was being recorded for each increment on an X-Y plotter. The pressure was then decreased to zero in 10 psi decrements with the gage output again being recorded. This procedure was repeated several times to check reproducibility. A typical calibration curve under hydrostatic conditions is shown in Fig. 9. For all gages the curves obtained for the ambient normal pressure calibrations were straight lines passing through the origin. The sensitivity values of these gages under hydrostatic conditions are tabulated in Table 1.

Table 1. Sensitivity Values of Piezoresistive Stress Gages Under Hydrostatic Conditions

Stress Gage Number	:	2	3	4
Sensitivity (mv/v/psi)	:	0.0648	0.0603	0.0441

These stress gages were also calibrated in confined specimens to determine the effect of confinement on soil calibration. These gages were placed at 1/3, 2/3 and mid-depth of a 7 in. long by 5 in. diameter confined specimens of the same soil used in the test vessel. The calibration results of the gages placed at mid-depth were used in the analysis, because the stress and strain at mid-depth of the sample are least effected by the end plates. The experiments

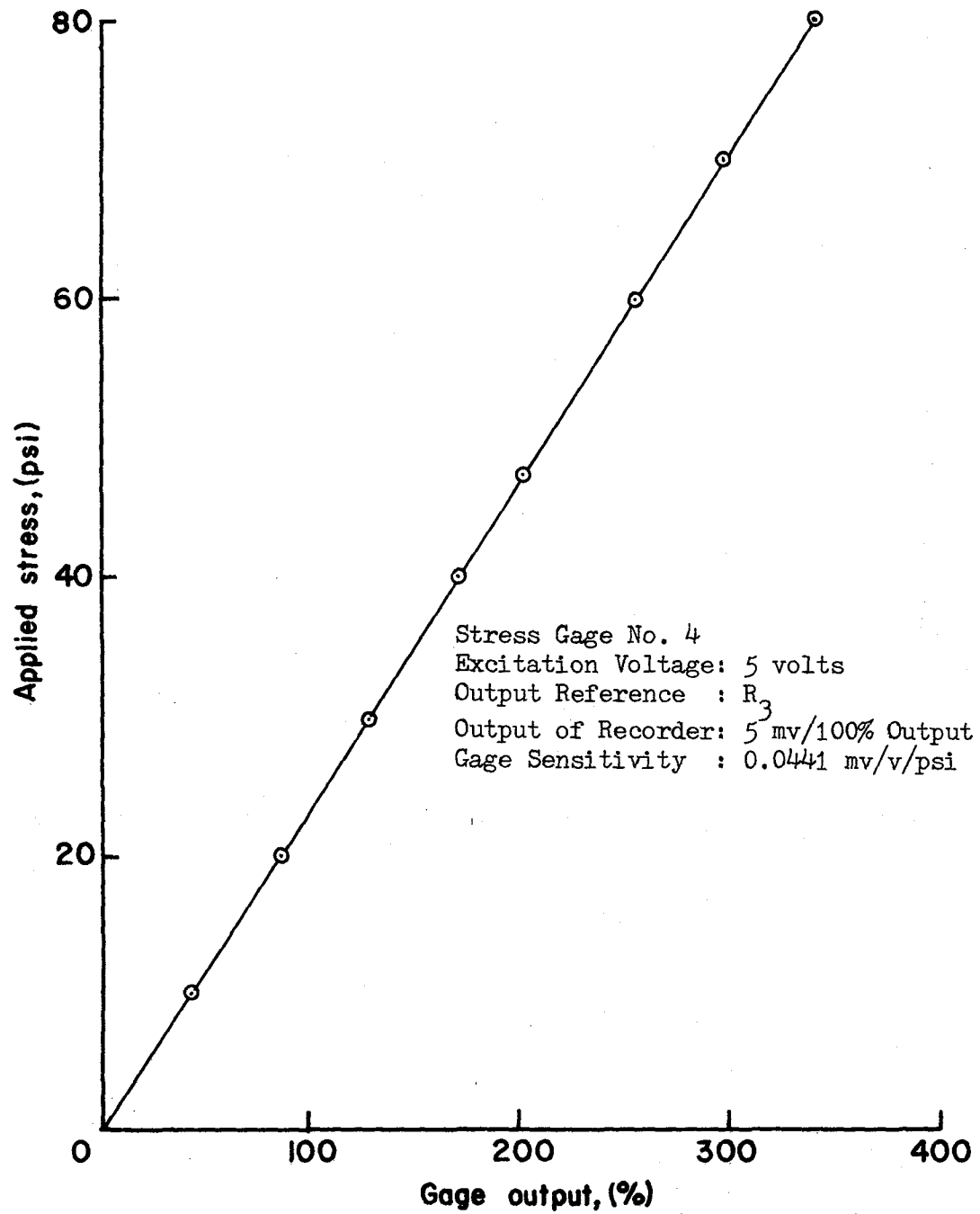


Figure 9. Typical Calibration Curve for Piezoresistive Gage Under Hydrostatic Conditions

conducted by Januskevicius and Vey³¹ have shown that the measurement of stresses at this depth are true representation of the actual stresses. Thus it was assumed that the vertical stress acting at these gage locations was equal to the applied pressure. The sensitivity values of these gages in confined specimens of the soil used in this program are tabulated in Table 2., and a typical calibration curve for these piezoresistive stress gages is shown in Fig. 10.

Table 2. Sensitivity Values of Piezoresistive Stress Gages in Confined Specimens of the Soil

Stress Gage Number	2	3	4
Sensitivity (mv/v/psi):	0.0747	0.0728	0.0558

Embedded Strain Gages. Strain-time measurements were recorded by using the mechanically uncoupled strain sensing elements operating on the transformer principle. These gages were developed at IITRI and have been extensively evaluated in the laboratory^{68,69,27,33}. These gages consist of two identical sets, each set with two coils. Some strain gage units consisted of 3/4 in. dia. by 1/16 in. thick coils and the other units consisted of 1 in. dia. by 1/8 in. thick (Bison Instruments) coils. Each set of soils represents primary and secondary windings of a transformer. Soil deformations are measured by the resulting changes in the

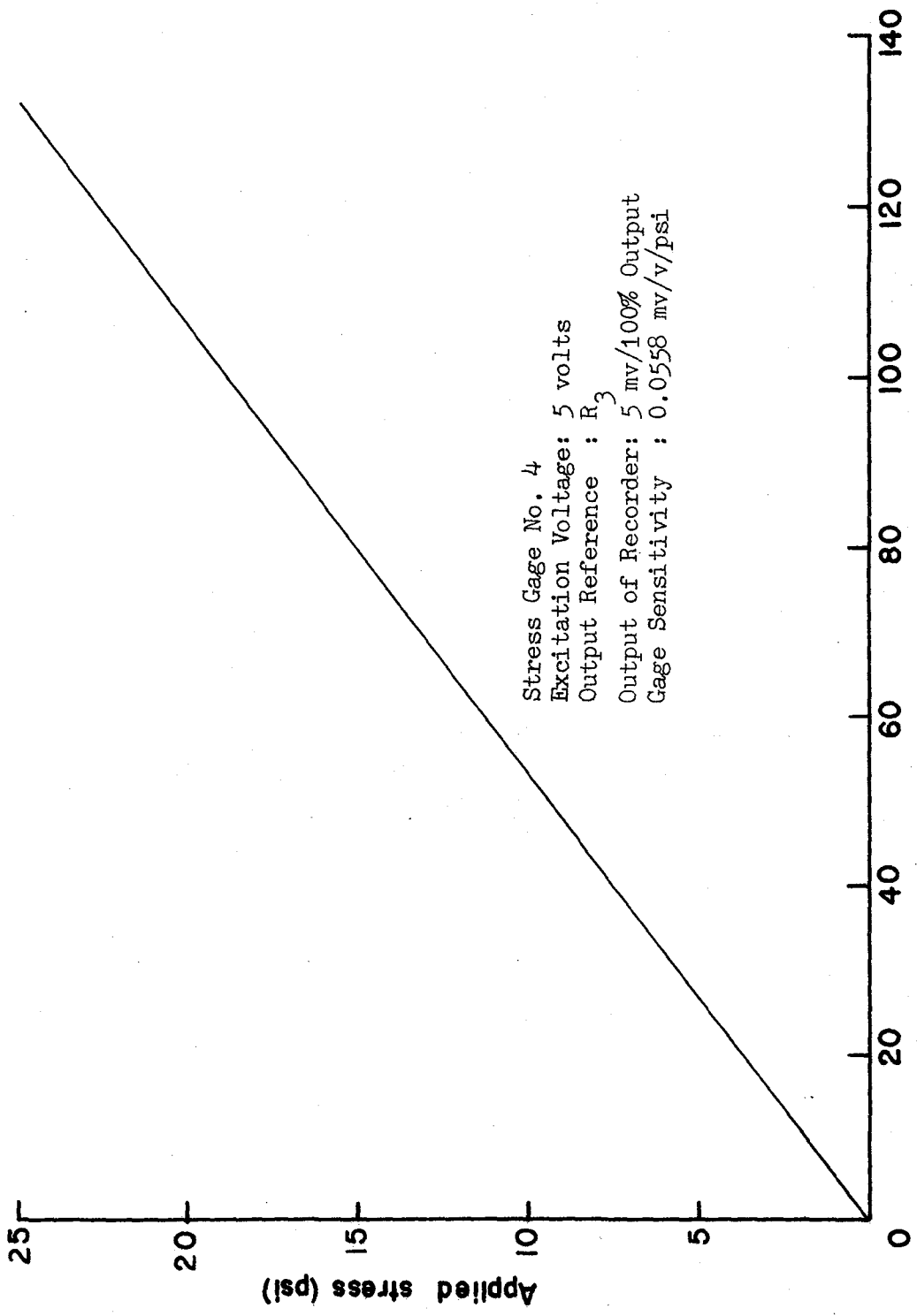
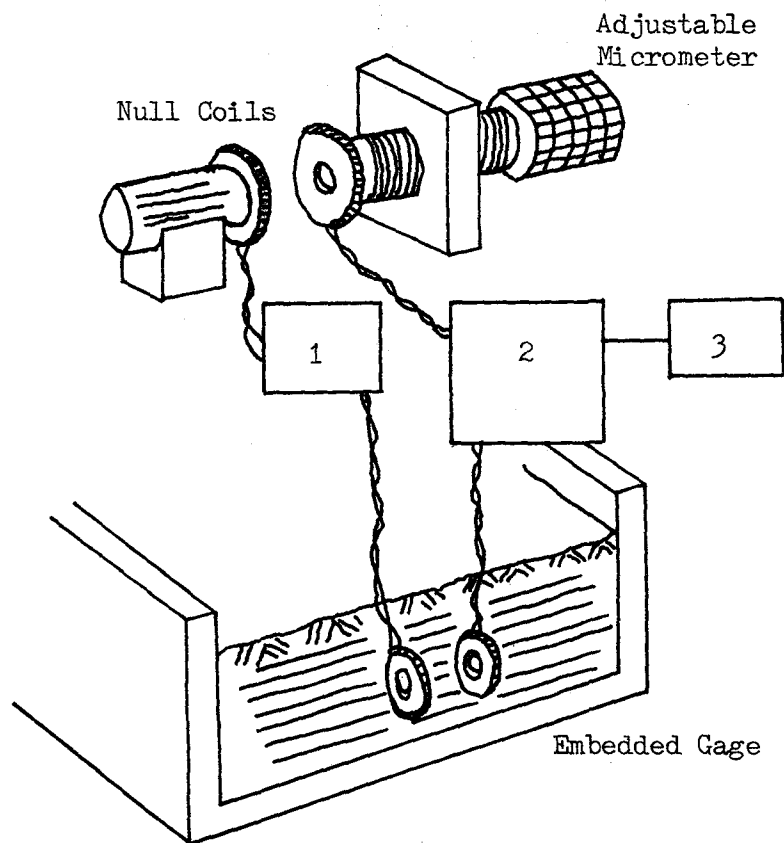


Figure 10. Typical Calibration Curve for Piezoresistive Gage Embedded in Sand

mutual inductance of the coils which are directly proportional to the changes in spacing of the embedded coils. Based on the evaluation of past investigations^{31,68,69}, these gages can be reliably used up to 6% compressive strains. The reliable limit of strain measurements in case of tensile strains is 3%, and the frequency response is 10 KHz.

Calibration of Strain Gages. In operation, one set of coils (in-situ coils) is embedded in the soil, and the other set (reference coils) is mounted on an adjustable micrometer mount as shown in Fig. 11. For calibration purposes the in-situ coils set is mounted on another adjustable micrometer mount. This calibration test consisted of applying known displacements in 0.005 in. increments to one set of coils, while the other set of coils is at a certain fixed spacing, and recording each instrumentation-system response. A typical calibration curve for one soil strain gage is shown in Fig. 12. The gage output values are again plotted against the compressional and tensional strains as shown in Fig. 13. This calibration procedure was repeated for coil spacings of 0.4 in., 0.5 in. and 0.6 in. and the gage output values versus coil movements are plotted in Fig. 14 for compressional strains.

In operation, the actual spacing of these in-situ coils in sand, however, was not the same as they were initially placed, due to the displacement of the coils as the sand was being poured. The actual spacing of the in-situ coils is determined by adjusting the reference coils until a null



1. Driver Coils Circuit
2. Tuned Amplifier and Detector Circuit
3. Output Device

Figure 11. IITRI Coil Strain Gage

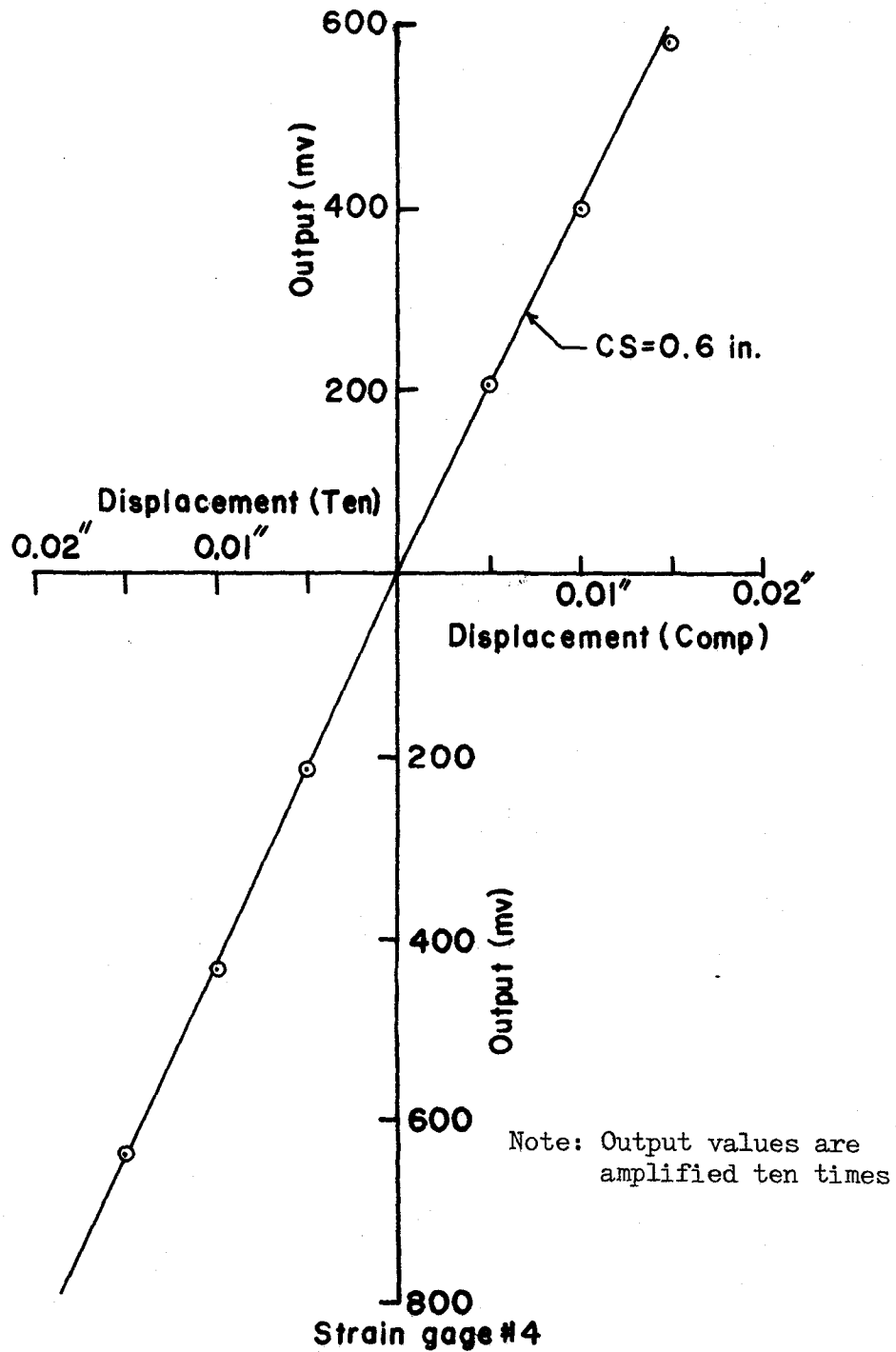


Figure 12. Calibration of Strain Gage (1 in. dia. coils)
(Displacement vs Gage Output)

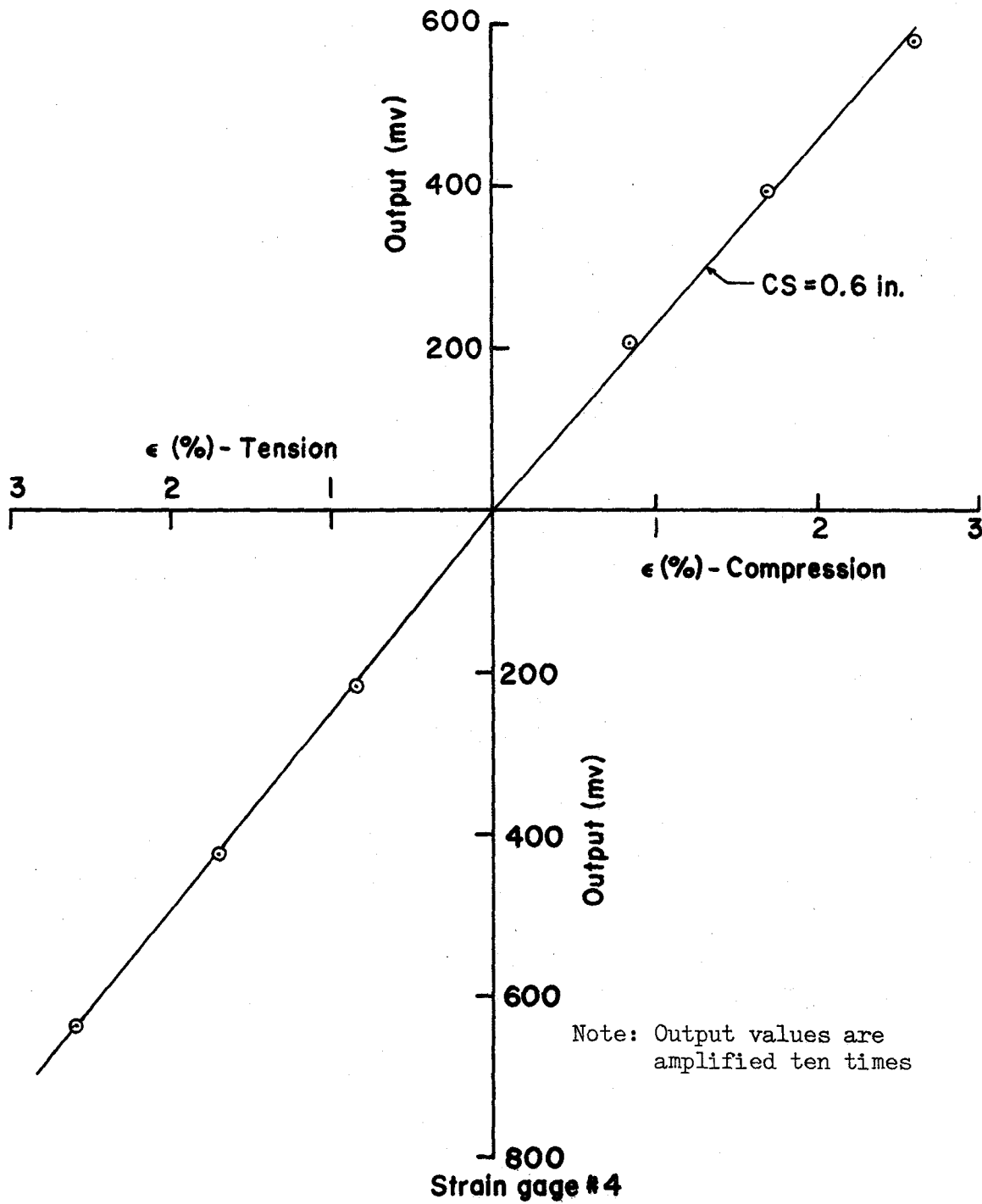


Figure 13. Calibration of Strain Gage (1 in. dia. coils)
(Strain vs Gage Output)

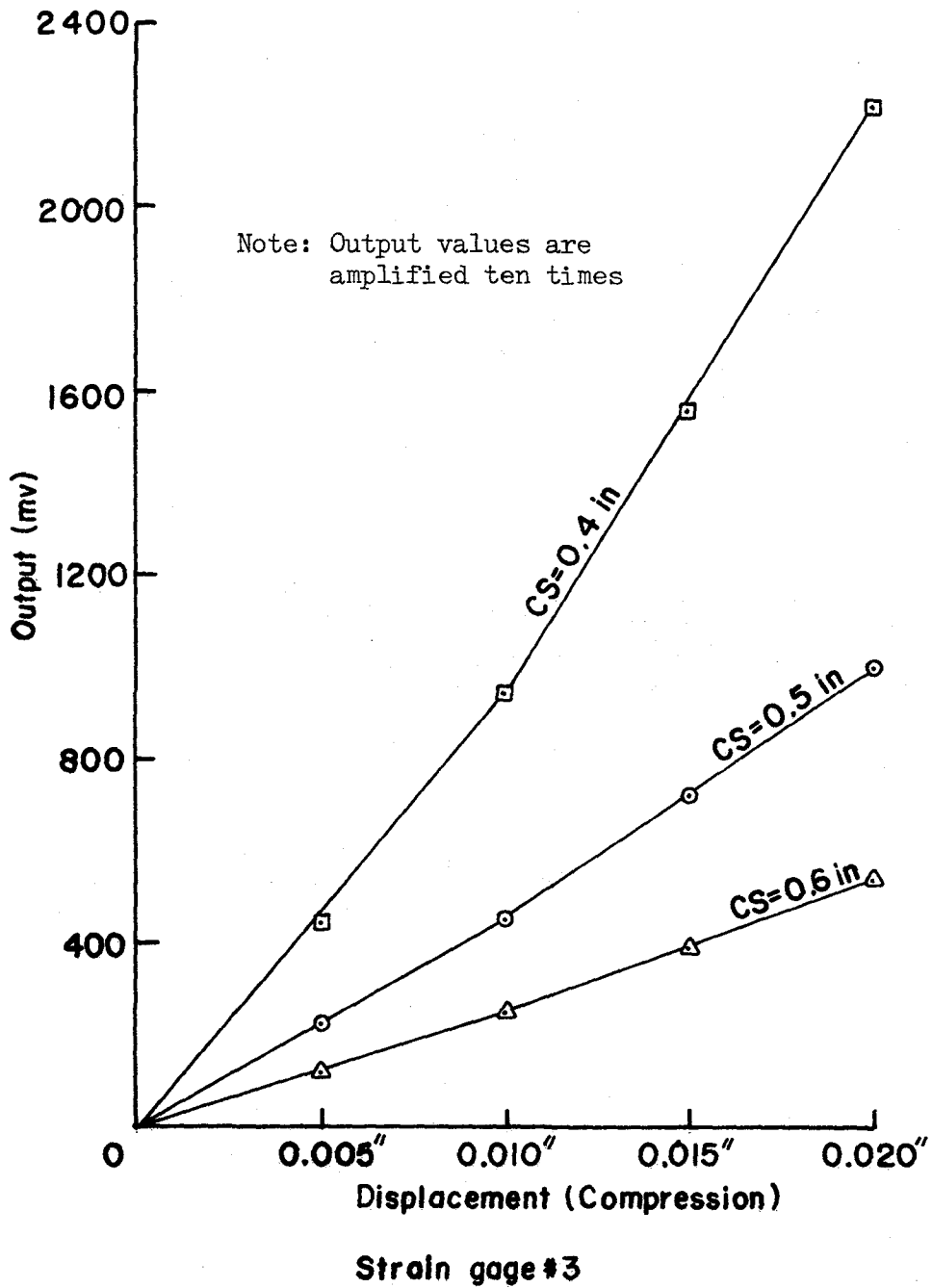


Figure 14. Calibration of Strain Gage (3/4 in. dia. coils)
(Displacement vs Gage Output)

balance is obtained.

Instrumentation

A view of the instrumentation system is shown in Fig. 15. The acceleration-time records of the bottom movable steel plate in the vessel and the footing were recorded by means of accelerometers. For this purpose two high-resonance frequency (80 KHz) shock accelerometers (The ENDEVCO, Model 2225 Accelerometer) were used. The model 2225 incorporates Piezite Element Type P-8 in a shear design that is capable of measurements to 20,000 g and is not affected by transverse components of acceleration. These accelerometers were of piezoelectric-type transducers which generated an electric charge. This output charge from the accelerometers was carried to the electrostatic charge amplifiers (Charge amplifier Model 566, Kistler Instrument Corp.) by means of low noise cables, and was converted to a voltage signal. This converted voltage signal was then recorded on a recording equipment.

Stress-time relations were recorded by using piezo-resistive gages. These gages as described earlier were constructed with two active arms having a nominal resistance of 350 ohms, and two dummy resistors forming a complete bridge. Only a strain gage element was mounted in the gage body at its center. This system provided the gage with only one active diaphragm. These gages were then connected to a bridge balance unit which provided initial balancing of the bridge circuits and an excitation voltage of 5 volts d.c.

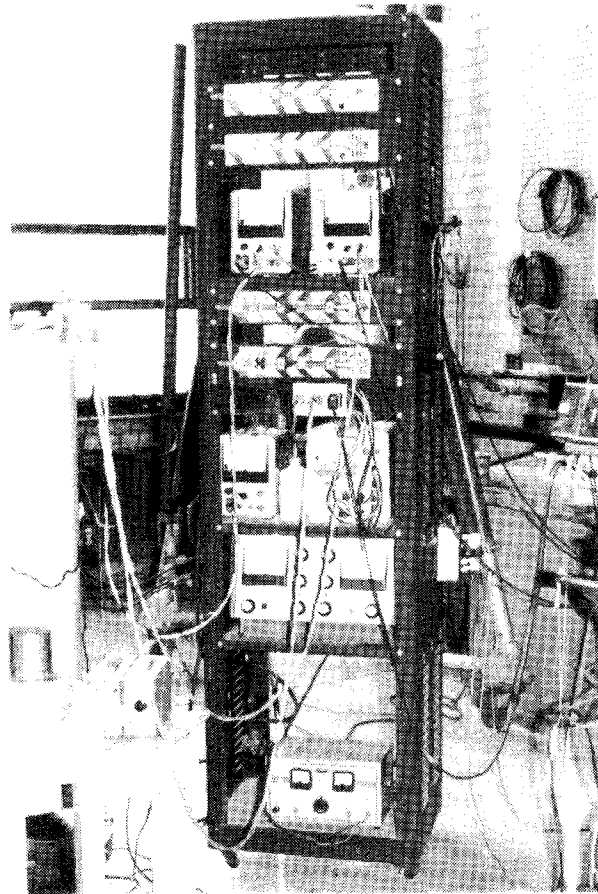


Figure 15. Instrumentation Setup

Strain-time relations were recorded by using the mechanically uncoupled strain sensing elements operating on the transformer principle. In this, air-core true differential transformer was used instead of a conventional linear variable differential transformer with iron core. Fig. 16 is a block diagram of the basic components of this differential transformer for application as a soil strain sensor. As shown in Fig. 11, only one driver- and one sensor-coil are embedded in the soil. The other driver and sensor coils are mounted on an adjustable micrometer mount external to the soil sample under test. The driver coils (connected in series) are excited with an a.c. current. The pick-up coils are also connected in series with the phase of the individually induced signals in opposition so that the total resulting signal is the difference of the outputs of the two pick-up coils. When the coils in each set are equally spaced, the resulting differential output is zero or nulled.

Acceleration-time, stress-time and strain-time responses were recorded and stored on a 14-channel magnetic tape recorder (Magnetic Tape Recorder Model 5600B, Honeywell). This model magnetic tape system is a full 14-channel instrumentation grade recorder which handles virtually any tape recording requirement, and is capable of recording/reproducing up to 14-channels of data at seven servo controlled tape speeds. A view of the data recording system is shown in Fig. 17. The frequency response of direct electronics is up to 300 KHz and F.M. electronics to 40 KHz. The entire experimental data was

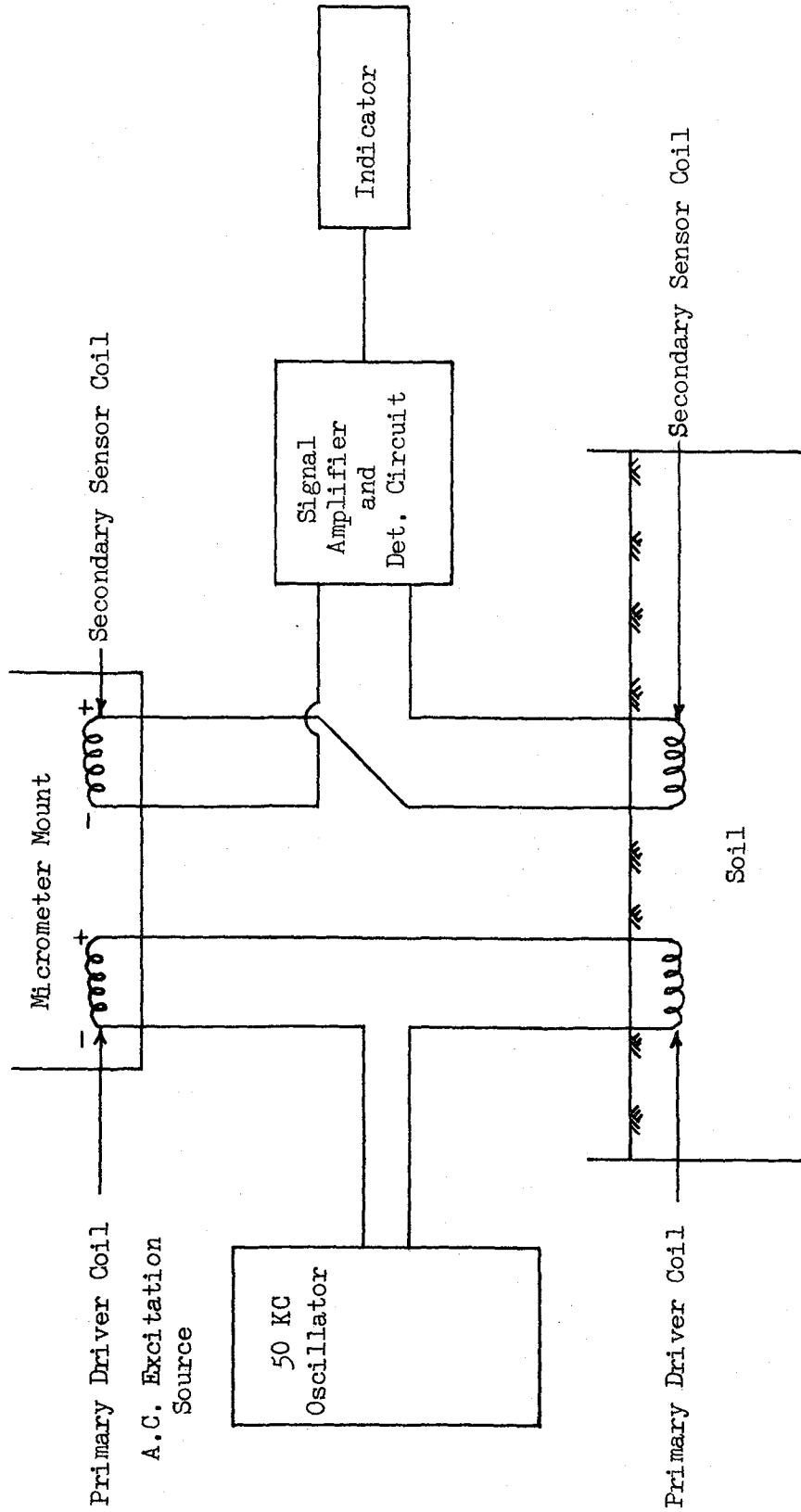


Figure 16. Schematic Diagram of Electrical Circuit for the Soil-Strain Gage Unit

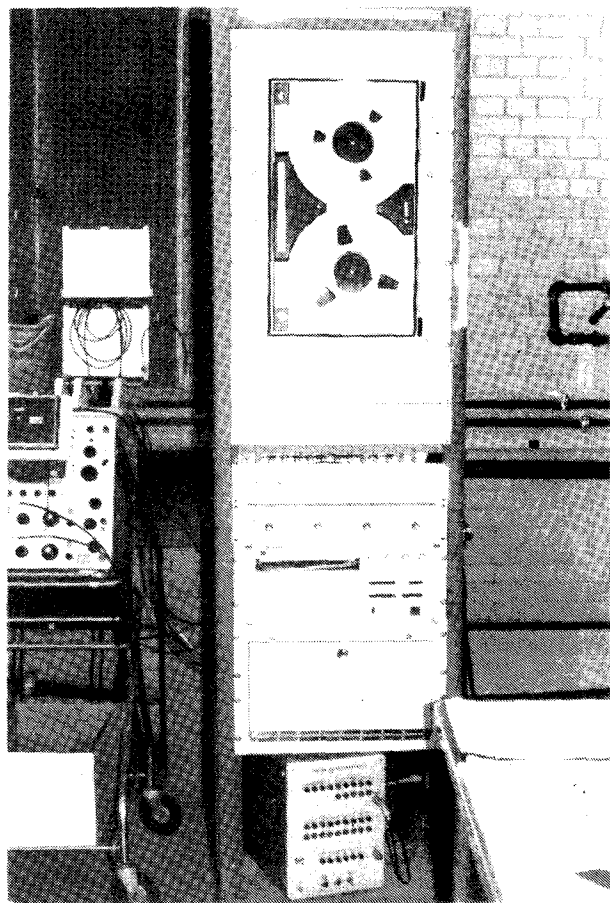


Figure 17. Data Recording System (Magnetic Tape Recorder Model 5600B, Honeywell)

recorded at a high speed of 60 ips (inch per second) and was reproduced at a low speed 7-1/2 ips. The output data from the tape recorder was amplified in a multi-channel d.c. amplifier (Multi-Channel DC Amplifier, Model Accudata 117, Honeywell) and was printed on a sensitive paper. A visicorder oscillograph (Visicorder Oscillograph Model 1508B, Honeywell) was used to print this data from the multi-channel d.c. amplifier. A view of this data printing equipment is shown in Fig. 18. A bank of four oscilloscopes (Dual Beam Oscilloscopes, Type 502, Tektronix Inc.) was also used to check the response of the accelerometers and the embedded gages, before it was recorded by the magnetic tape recording system. The oscilloscopes were also used for calibration purposes and to record the response on a polaroid film. An internal triggering system was provided in the first oscilloscope of the bank, and the remaining oscilloscopes were simultaneously triggered by connecting them in series.

Experimental Procedures

In the preparation of the sand bed in the vessel, the most uniform placement was obtained by a slow rain of sand³⁴ (termed here Pluvial Compaction). This was the method used at IITRI and later by Wetzel at IIT⁷⁷. This "raining technique" was also used by the Waterways Experiment Station⁷ (WES), where they employed three devices. In their paper, Bieganousky and Marcuson⁷ have referred to other experimentors who have also used this raining technique. A schematic diagram of the equipment used for this purpose is shown in Fig. 19.

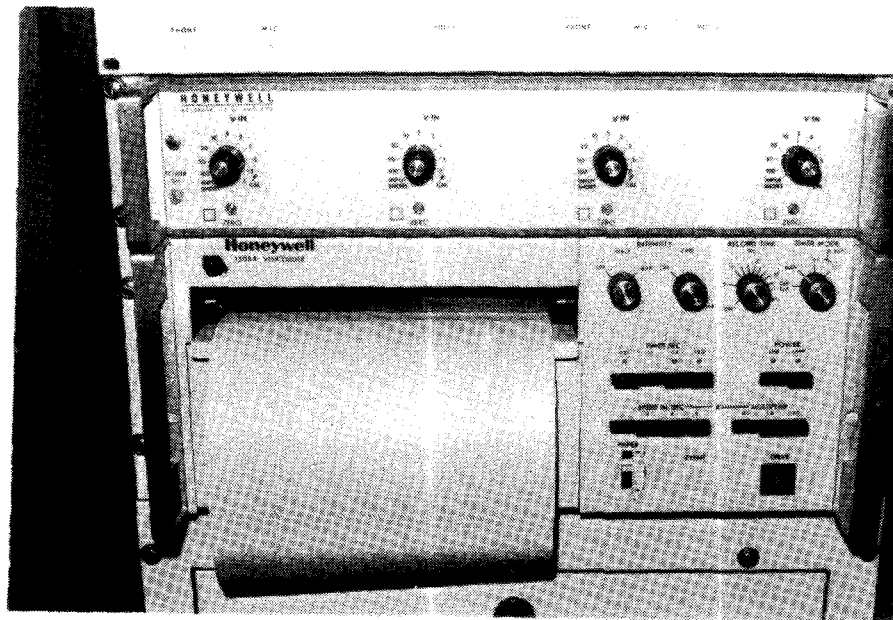


Figure 18. Data Printing Equipment (Visicorder Oscillograph Model 1508B, Honeywell)

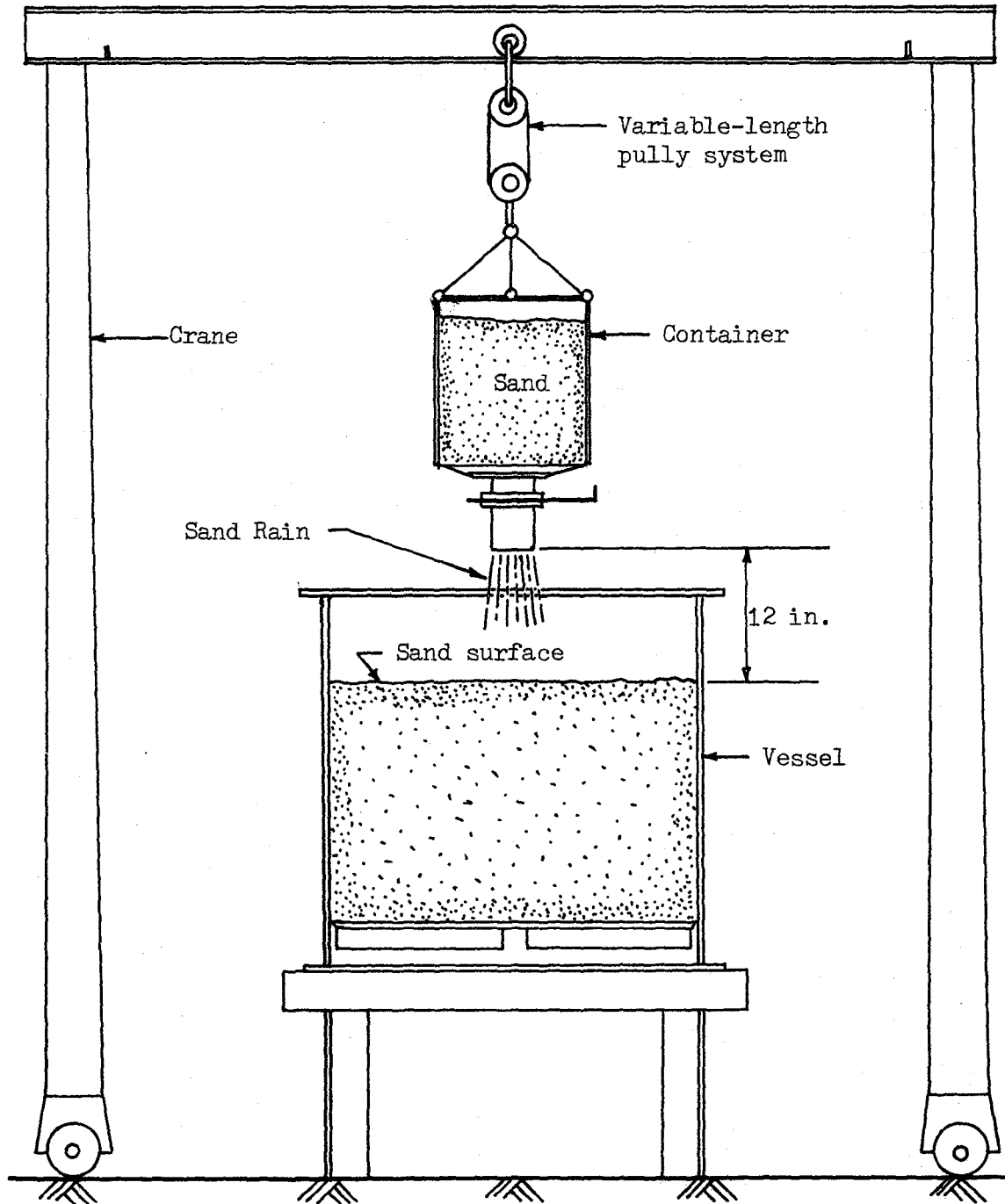


Figure 19. Raining Device for Placement of 20-40 Ottawa Sand

As shown in this figure, a free fall distance of 12 in. produced medium densities of the order $104.5 \pm 1.0\%$ pcf. The properties of the sand used in this experimental program are given in Appendix A. Stress gages and strain gages were oriented at desired locations as shown in Fig. 20, while placing the sand in the vessel. A typical gage array of these stress gages and strain gages is shown in Fig. 21.

The stress gages were placed by the set-on-surface method. Hadala²⁵ in his conclusions suggested that this set-on-surface method was the best gage placement method for sands. Ingram^{28,29} also reported that the tests in his experimental program have indicated a minimum mean registration by the set-on-surface method. The procedures for placing the stress gages consisted of the following steps:

1. The sand surface was levelled,
2. The stress gage was placed on the levelled surface with its active face perpendicular to the direction of loading,
3. The gage was slightly pressed into the surface of the soil,
4. Sand filling was resumed by placing sand on top and around the gage.

For strain gages to sense vertical strains, the gage placing method is shown in Fig. 22. The procedure was as follows:

1. The sand surface was levelled and a coil of one set (in-situ coil set) was placed on the

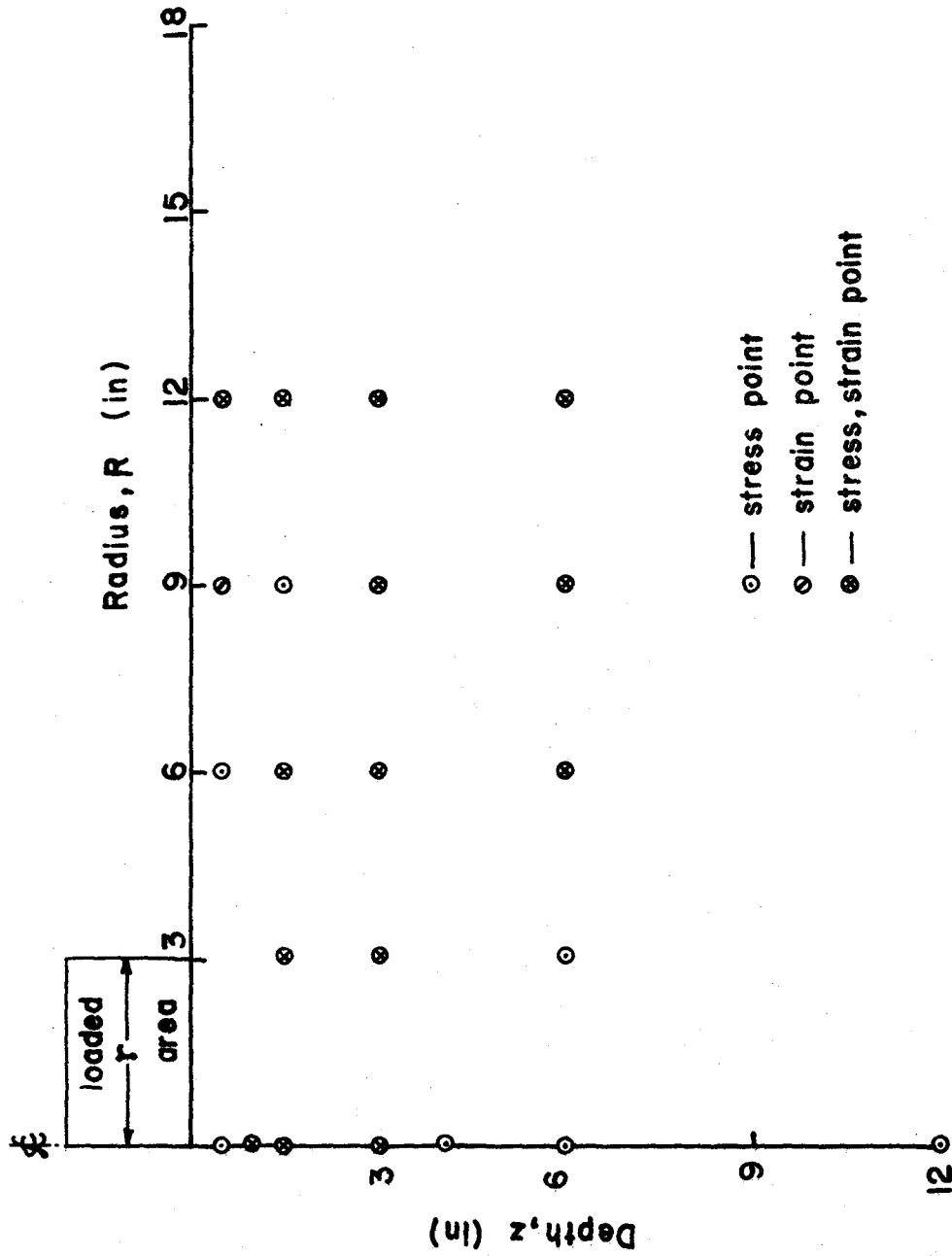


Figure 20. Location of Stress and Strain Measurements

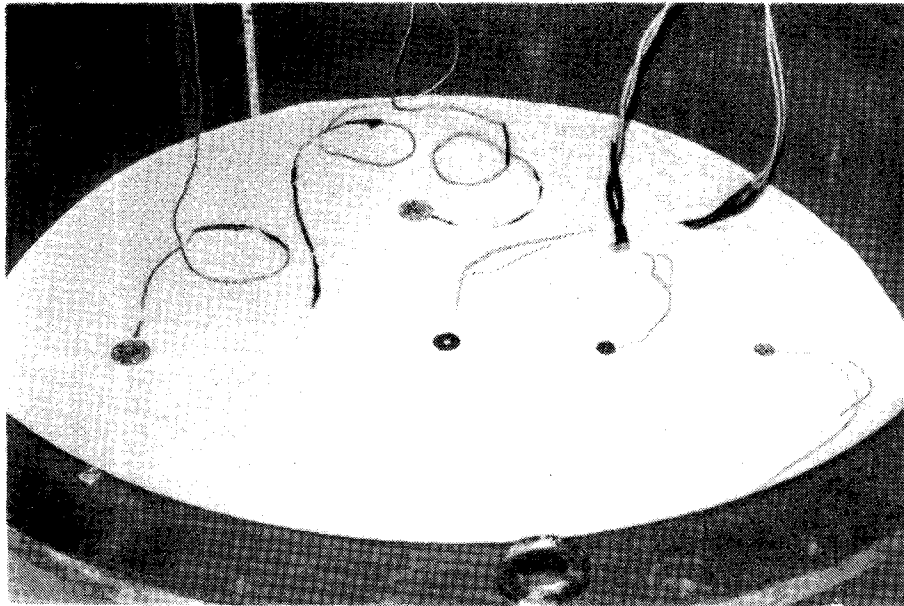
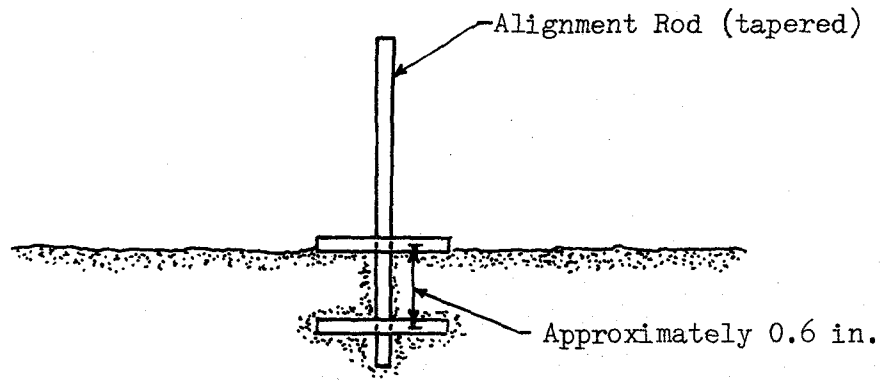
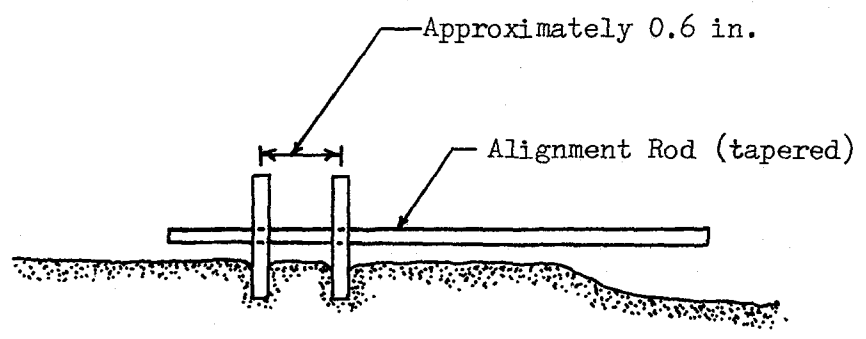


Figure 21. A Typical Gage Array of the Embedded Gages



a) Vertical Strain



b) Radial and Tangential Strain

Figure 22. Schematic Diagram of Placement Methods for Strain Gages

levelled surface,

2. A tapered rod was placed through a hole in the center of the coil. The taper of the rod served to hold the coil flat on the surface as the sand was being placed above it. Additional soil was then compacted around the rod to obtain the cover necessary to give the desired gage spacing,
3. The second coil was slid over the rod and placed on the soil surface,
4. Additional soil was compacted to a height of 2 to 3 in. above the top of the coil and the alignment rod carefully removed,
5. The second set of coils (reference coils) was positioned on a micrometer mount which served as the reference.

After the vessel was filled with sand to the desired height, the surface was levelled and the footing was placed on the surface at the center as shown in Fig. 23. Transient loads were then applied to the bottom movable steel plate inside the vessel which transmitted the ground motions through the underlying soil. A schematic diagram and a view of the loading apparatus is shown in Fig. 4 and Fig. 5, respectively. The procedure in applying the transient loads consisted of the following steps (see Fig. 4):

1. The nitrogen gas (N_2 -gas) under pressure was supplied to the accumulator from the nitrogen

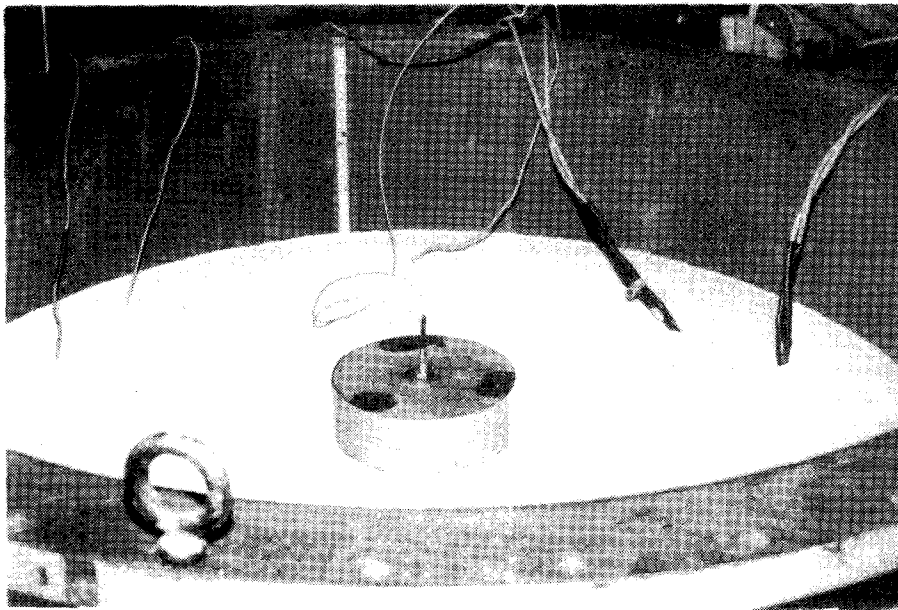


Figure 23. Footing Before Being Subjected to Transient Load

cylinder,

2. The accumulator consisted of a rubber bladder inside, separating N_2 -gas from the hydraulic oil. The nitrogen gas under pressure was compressed by using a hand pump. Therefore, by Newtons Third Law (For every action, there is an equal but opposite reaction), the N_2 -gas and the hydraulic oil were under pressure up to a certain location in the pipeline system, where the solenoid dump valve is located. Under normal conditions this solenoid valve will be closed, and will be open when the electrical circuit is closed by pressing the switch,
3. When the switch was pressed, the hydraulic oil under pressure was delivered through a flow control valve to the distribution chamber, which finally distributed an equal quantity of oil to each of the three hydro-line cylinders. The piston rods of these hydro-line cylinders were connected to the bottom of the movable steel plate at 120° apart, which supported the soil-footing system inside the vessel. Therefore, the sudden release of pressure to the hydro-line cylinders caused a dynamic movement of the bottom movable steel plate along with the soil and the footing inside the vessel, hence

transmitting the ground motions through
underlying soil.

CHAPTER V
PRESENTATION AND ANALYSIS OF RESULTS

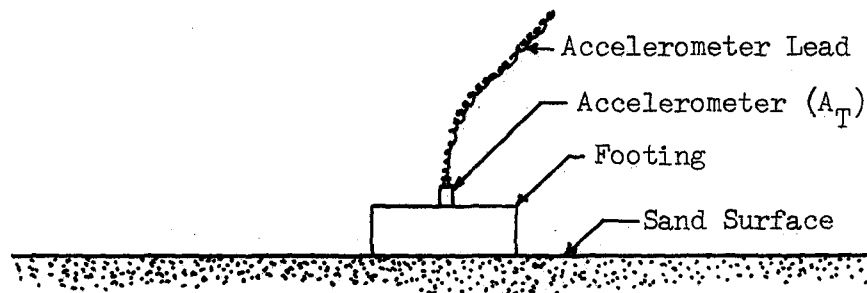
The experimental program consisted of three test series. Each test series represented a set of tests on various size and shape of rigid footings having different contact pressures. The test series on a 6 in. dia. circular footing having a contact pressure $\sigma_c = 0.55$ psi was designated as TA-No. A total of 130 dynamic tests were conducted on this footing. Similarly, TB-No. represented a test series with 46 tests conducted on 3 in. dia. circular footing with a contact pressure $\sigma_c = 0.88$ psi. The third series, TD-No., represented a set of experiments (a total of 48 tests) conducted using 3 in. by 3 in. square footing having a contact pressure $\sigma_c = 0.20$ psi. Test series TA also included some static bearing capacity and dynamic response tests with a compressible material (6 in. dia. circular) beneath the surface footing (6 in. dia. circular), at a depth one radius below the footing.

The test data was analyzed with respect to: (1) the footing response; (2) the characteristics of the one-dimensional stress-wave propagated upwards towards the bottom of the footing through the sand mass; (3) the effect of depth of burial on the footing response and stress distribution beneath the footing; and, (4) the footing isolation.

Footing Response

Transient loads were transmitted to the bottom of the footing through the underlying soil mass. The acceleration-

time response of the bottom movable steel plate (A_B) and the footing (A_T) were recorded by means of accelerometers mounted as shown in Fig. 24. As shown in this figure, the accelerometer mounted on top of the footing is identified as A_T and the one mounted upside-down on bottom of the movable steel plate as A_B . Therefore, the acceleration-time traces corresponding to the footing and the bottom movable steel plate are identified as A_T and A_B , respectively, throughout this experimental program. A typical record of the acceleration-time traces for the bottom movable steel plate and a footing is shown in Fig. 25. As shown in this figure, the first trace on the top identified as A_B , corresponds to the input source, that is the bottom movable steel plate. The second trace on the bottom is identified by A_T , corresponds to the response of the footing, resting on the surface of a sand layer 24 in. thick, inside the vessel (3 ft. diameter). As shown in Fig. 24, the accelerometer on the bottom movable steel plate is mounted upside down. Therefore, the acceleration-time trace identified as A_B throughout this thesis, is upside down. In other words, the trace is opposite to that of the trace corresponding to the footing (A_T). In this trace A_T , the portion of the curve above the zero line corresponds to deceleration of the footing, whereas in trace A_B the portion of trace below the zero line represents deceleration of the bottom movable steel plate. Similarly, the portion of the trace A_T below zero line corresponds to acceleration towards gravity of the footing;



Sand Layer
(24 in. thick)

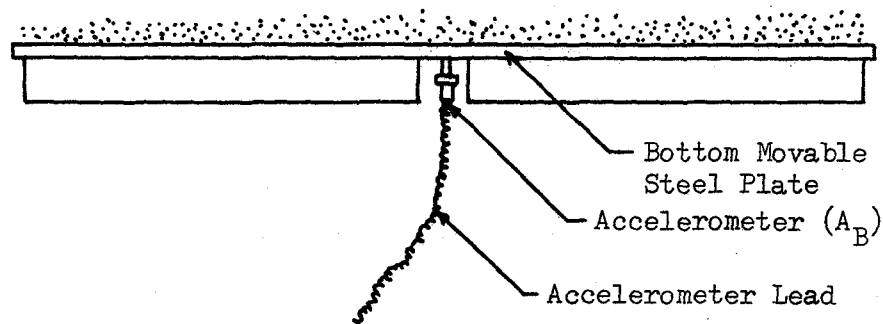


Figure 24. Schematic Diagram of Footing Apparatus

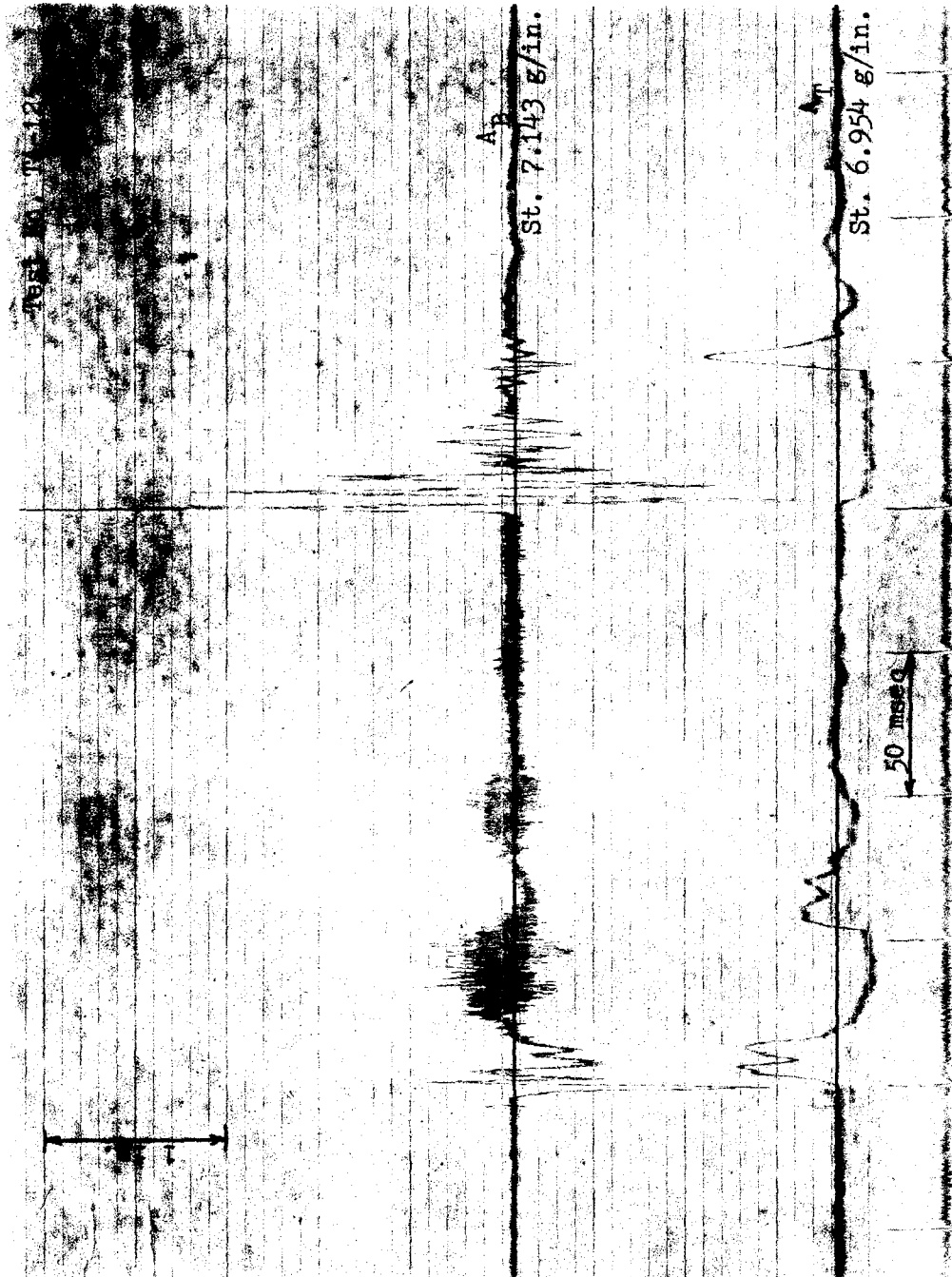


Figure 25. Acceleration-Time Traces for the Bottom Movable Steel Plate and a Footing
(6 in. dia. circular)

and, in trace A_P , the portion above the zero line represents acceleration towards gravity of the bottom movable steel plate. As shown in Fig. 25, the input response spectra consisted of two peaks. The first peak occurred in 3.5 msec and attenuated in less than 40 msec. This corresponds to the response of the input source. The second peak, which has a higher amplitude than the first peak, occurred in about 200 msec. This peak attenuated in about 65 msec and is attributed to the bouncing and ringing effect of the bottom movable steel plate. Even though the amplitude of this peak is much higher than the first peak, the time in which it attenuates (65 msec) is much less than the time in which it occurs (200 msec). The footing acceleration-time response (A_T), shown in Fig. 25, also consisted of two peaks corresponding to the input response trace. The first pair of peaks attenuated in about 40 msec. After 200 msec, the footing started moving in the direction of gravity with an acceleration $1g$ and continued to move for 50 msec, then it decelerated. The average value of peak deceleration amplitude for a 6 in. dia. footing ($\sigma_c = 0.55$ psi), measured from zero line is $4.87g$. This peak attenuated in about 12.5 msec to 50 msec. The pattern of the latter portion of the footing response trace is almost similar to the response traces of the actual structures under explosion-induced ground motions⁴⁷. They differ only in their amplitudes and time.

The footing response (acceleration-time) trace (A_T), shown in Fig. 25, is integrated once to obtain the velocity-

time relationship as shown in Fig. 26, which is again integrated to obtain displacement-time relationship for the footing as shown in Fig. 27. The acceleration-time trace from the same test (TA-125) was also recorded on a polaroid film, as shown in Fig. 28. A direct current differential transformer (DCDT) was also used to record the displacement-time response of the footing. The displacement versus time relationship, shown in Fig. 27, is exactly the same as the trace shown in Fig. 28 recorded directly by using a DCDT.

As shown in Fig. 27, the maximum displacement of the footing is 0.158 ft. (1.89 in.). A sudden release of pressure to three hydro-line cylinders causes displacement of the bottom movable steel plate, the sand bed and the footing with a momentum. After the piston rods travel to the maximum stroke length, the sand bed with the footing (which is in a state of motion), is stopped suddenly. This sudden restriction provided to a body in motion causes it to move backwards with a negative velocity as shown in Fig. 26. The footing then moves forward and finally comes to a complete rest, as shown by the displacement-time curve in Fig. 27 and 28. A typical acceleration-time trace for a 3 in. dia. circular footing ($\sigma_c = 0.88$ psi) is shown in Fig. 29. The average value of peak deceleration amplitude for this footing is 4.20g. The average value of peak deceleration amplitude for a 3 in. by 3 in. square footing ($\sigma_c = 0.20$ psi) is 7.84g, and the acceleration-time trace for this footing is shown in Fig. 30. In all these experiments the same input pressure was maintained. These peak deceleration values were

Test No. TA-125
Photo No. PA-86

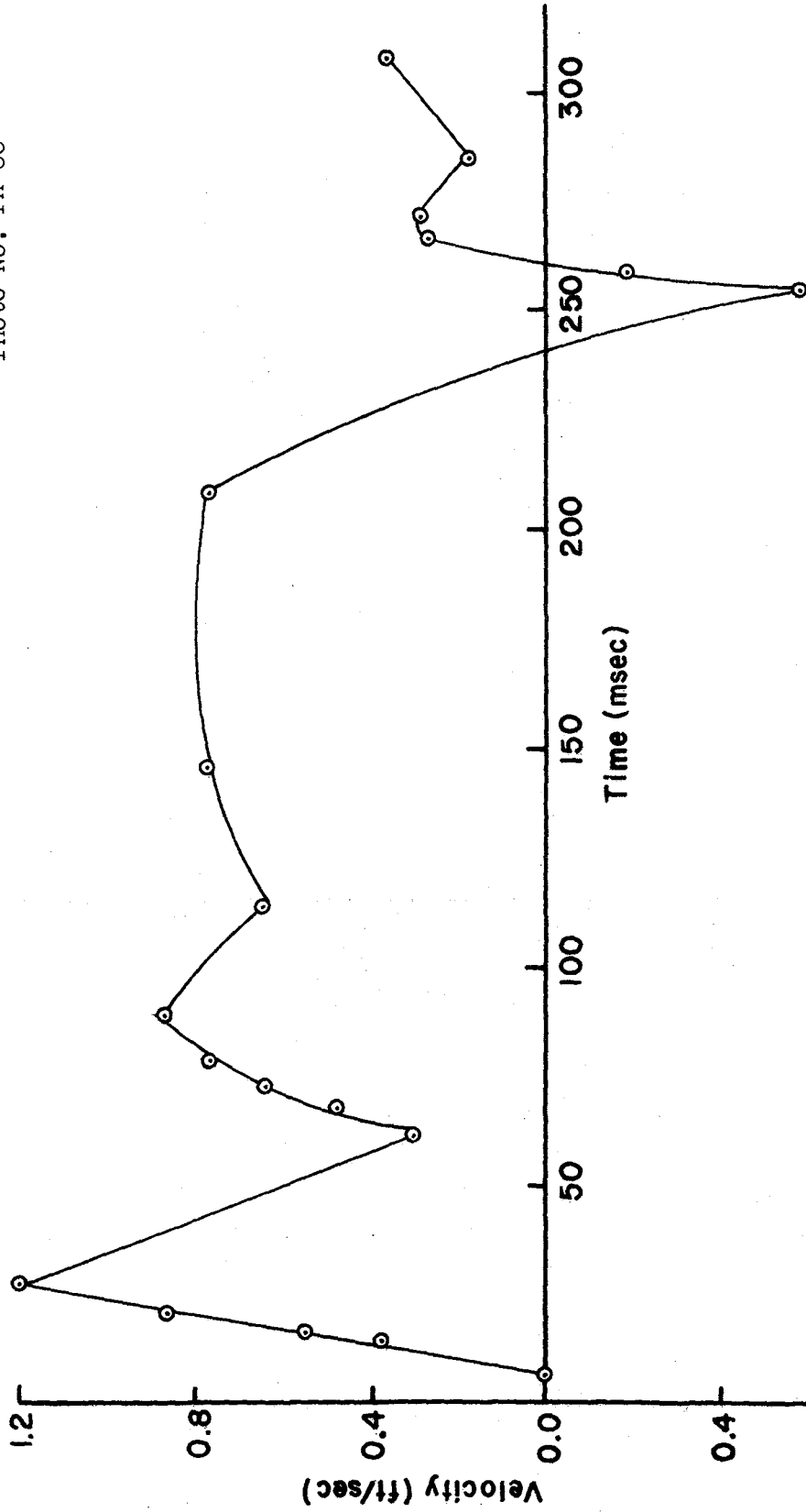


Figure 26. Velocity vs Time Relationship for a Surface Footing (6 in. dia. circular)

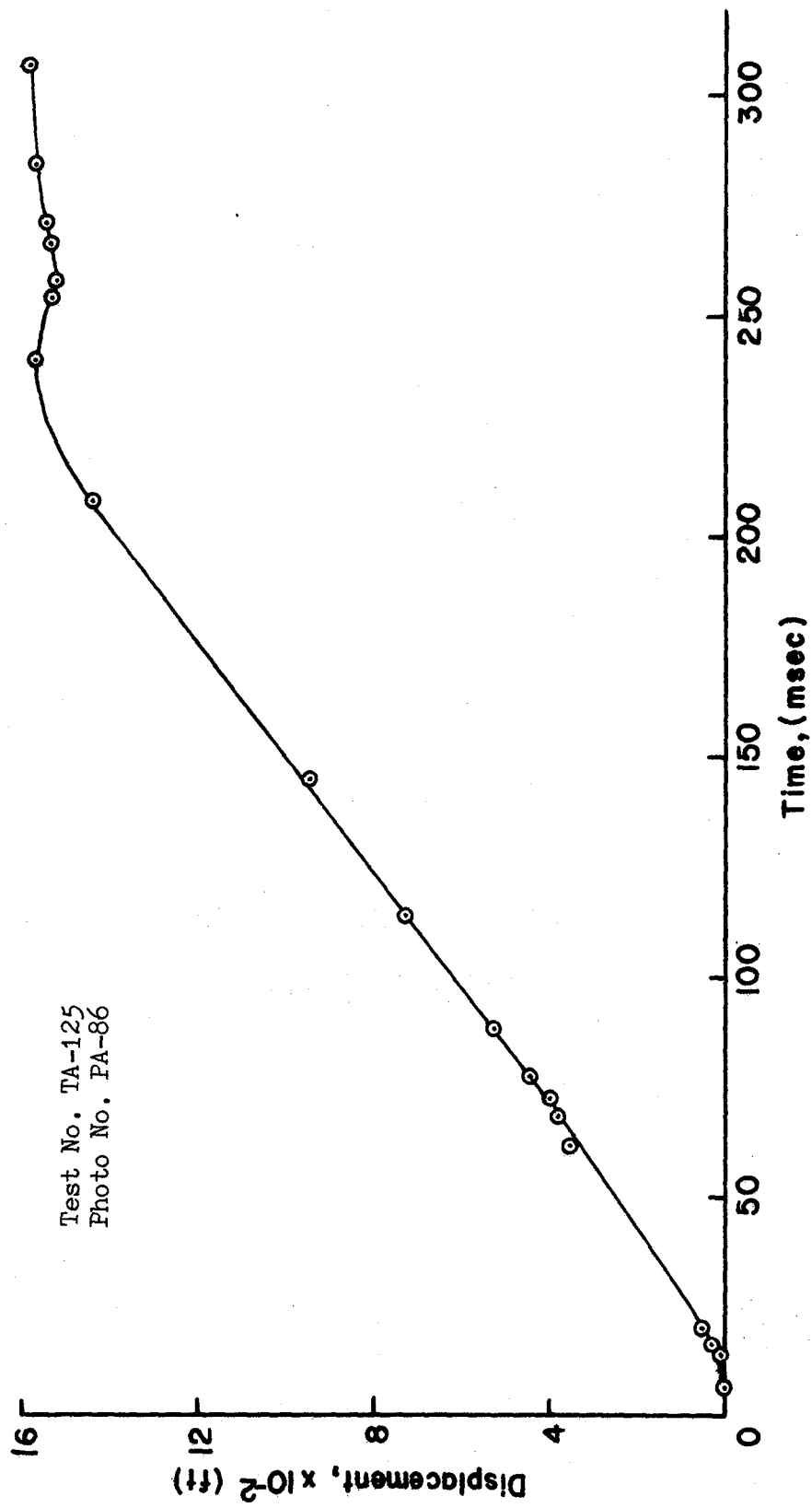


Figure 27. Displacement vs Time Relationship for a Surface Footing (6 in. dia. circular)

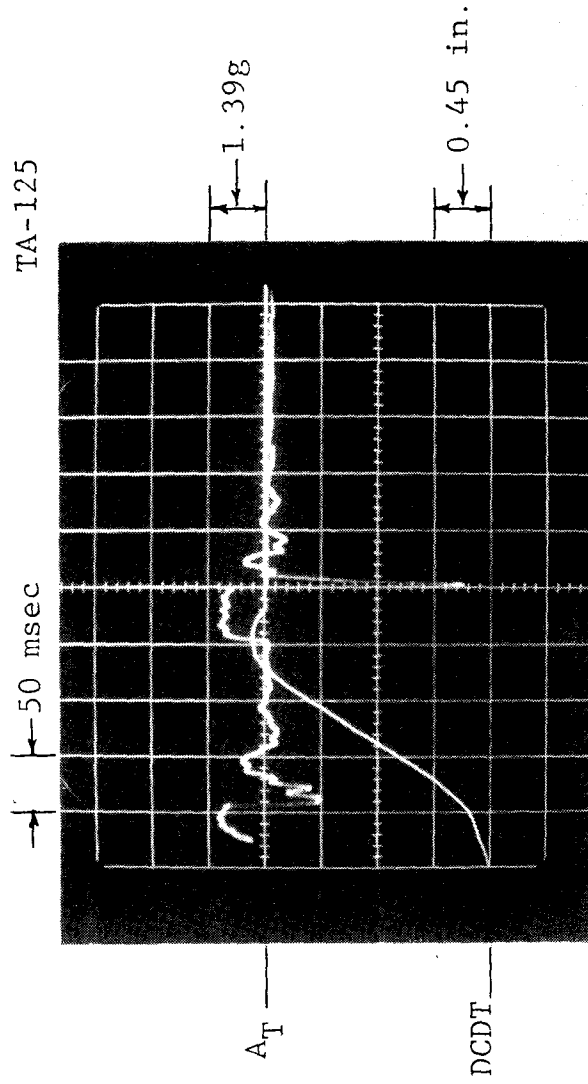


Figure 28. Acceleration, Displacement-Time Traces for a Surface Footing (6 in. dia. circular)

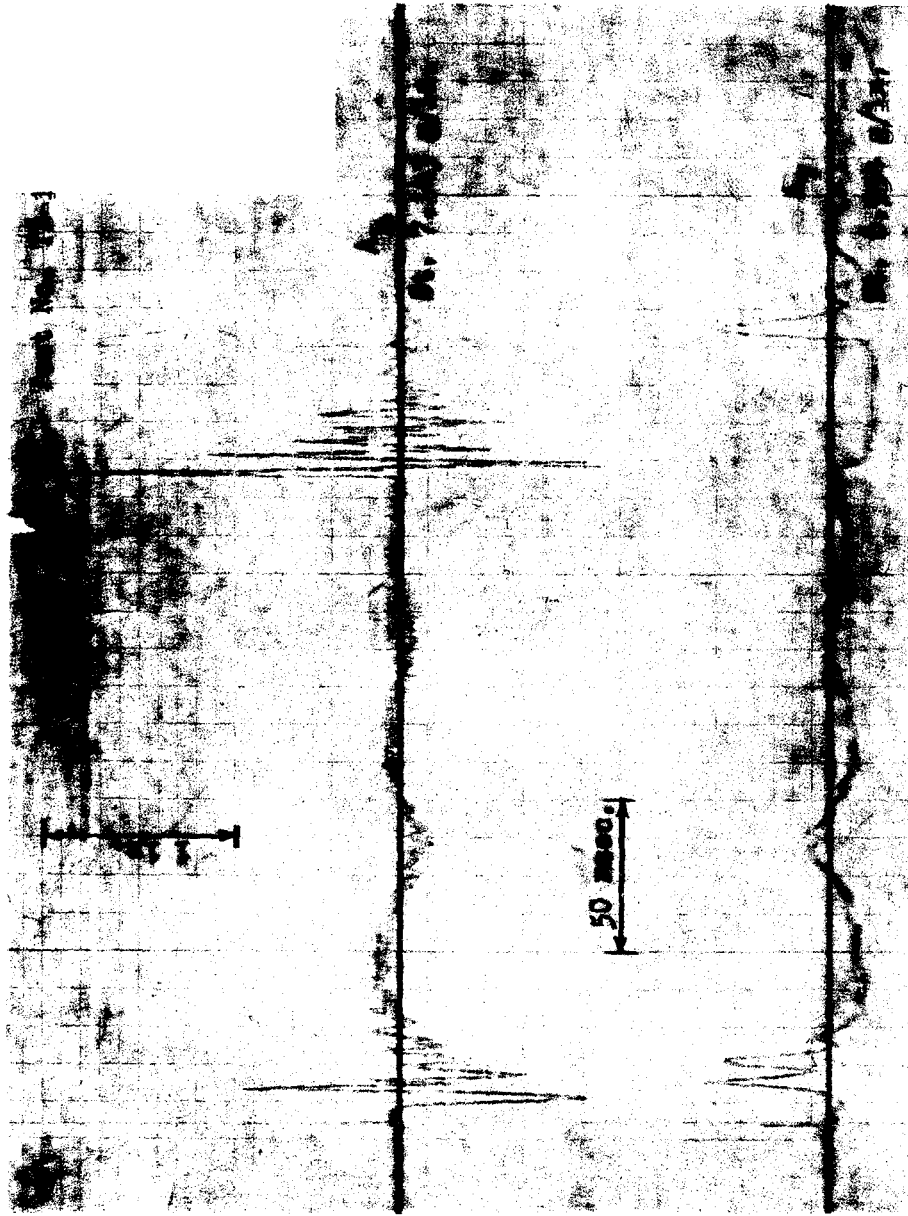


Figure 29. Acceleration-Time Traces for the Bottom Movable Steel Plate and a Footing (3 in. dia. circular)

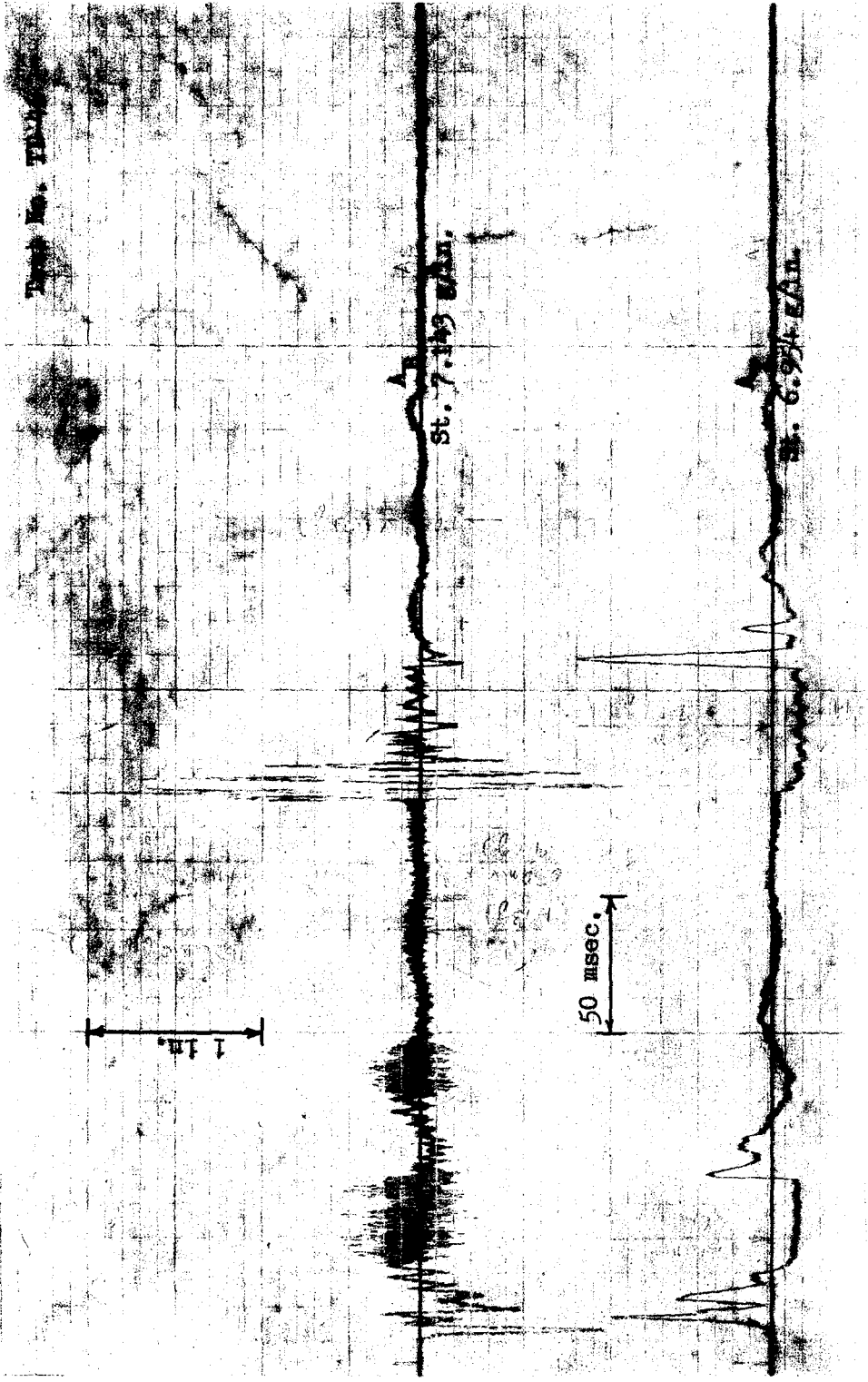


Figure 30. Acceleration-Time Traces for the Bottom Movable Steel Plate and a Footing (3 in. by 3 in. square)

plotted against their weights and a linear relationship is obtained as shown in Fig. 31. This linear relationship between deceleration of the footing and weight of the footing is justified because the deceleration of a body is inversely proportional to its mass.

Stress-Wave Propagation

In the experiments transient load was applied to the bottom of the footing through the underlying soil mass. When the hydraulic oil under pressure in the loading apparatus was released to the hydro-line cylinders, the bottom movable steel plate attached to the piston rods was moved upwards. This generates a stress-wave which propagated up towards the bottom of the footing through the sand mass. To study the characteristics of this one-dimensional stress-wave propagated up towards the bottom of the footing through the sand mass, embedded stress gages and strain gages were placed at various locations in the sand. Stress-time and strain-time histories, at the respective gage stations as shown in Fig. 20, were recorded as the stress wave passed. Wave propagation velocities and sand moduli are given in Appendix B.

Stress Measurements. Stress-time histories at various gage locations were recorded using embedded stress gages. The location of the stress measurements is shown in Fig. 20. The description of the gages, calibration procedures and recording instrumentation are described in Chapter IV. Three to four measurements were made at each gage location and

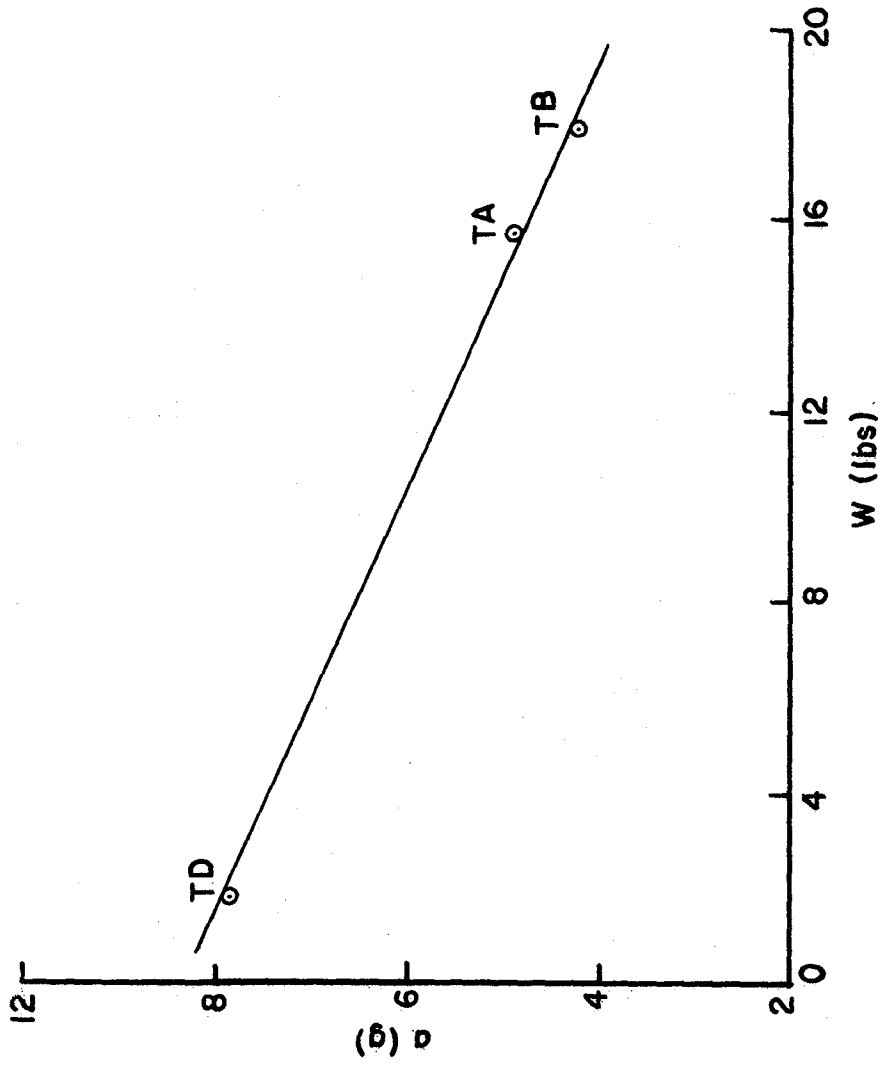


Figure 31. Deceleration of Surface Footing vs Weight of Footing

average values were used to determine the stress-distribution in the soil under the various size footings. Attenuation of peak vertical stress on the axis of symmetry and offset from the axis of symmetry for each footing were determined. The general form of stress-time traces recorded in the vicinity of the footing followed the same pattern as the acceleration-time trace.

Typical stress-time histories recorded at different depths on the axis of symmetry for a 6 in. dia. footing resting on the surface of sand are shown in Fig. 32 through 35. A total of three stress gages were used, each having a different sensitivity. To obtain data at different depths, tests were repeated under identical test conditions. This data was used to obtain peak vertical stress values at various depths on the axis of symmetry. The distribution of peak vertical stress, with depth on the axis of symmetry for a 6 in. dia. circular footing resting on the surface, is shown in Fig. 36. Based on a recent study by Rao and Höeg⁵¹ wherein the effect of footing rigidity was examined, a uniform stress distribution on the base of the footing is considered. Therefore, assuming a uniform distribution, a static contact pressure of 0.55 psi for this footing was obtained. From Fig. 36, the peak vertical stress on the bottom of the footing under dynamic loading conditions is 10.9 times its static contact pressure ($\sigma_c = 0.55$ psi).

A similar type of dynamic tests were also conducted with a surface footing 3 in. dia. ($\sigma_c = 0.88$ psi). Again,

Test No. TA-81

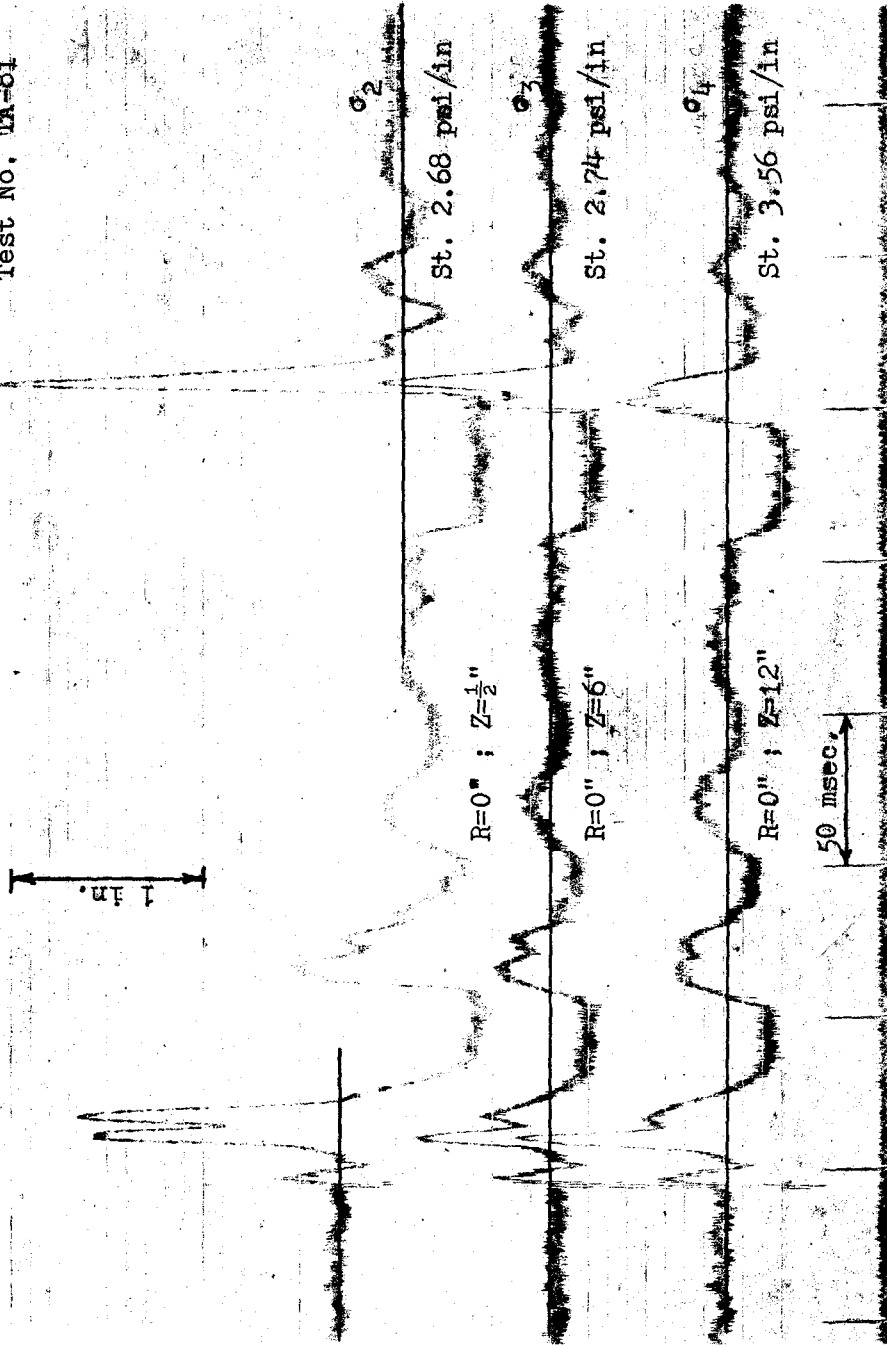


Figure 32. Vertical Stress-Time Traces on Axis of Symmetry at $Z = 1/2$ in; 6 in.; 12 in. (6 in. dia. circular footing)

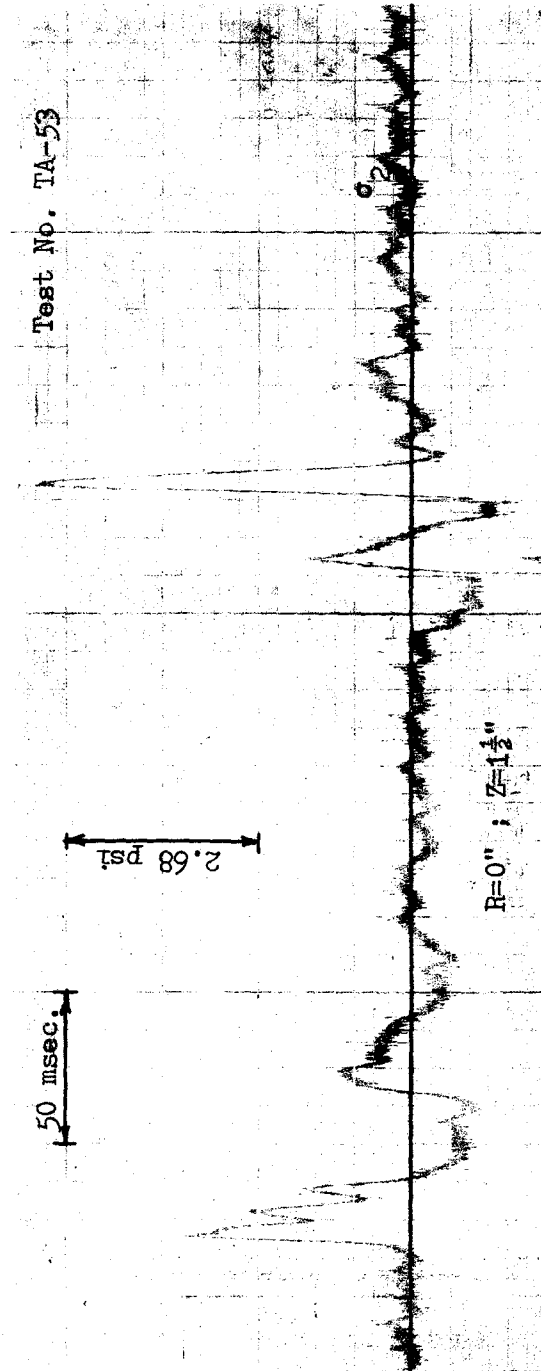


Figure 33. Vertical Stress-Time Trace at R = 0 in.; Z = 1-1/2 in. (6 in. dia. circular footing)

Test No. TA-10

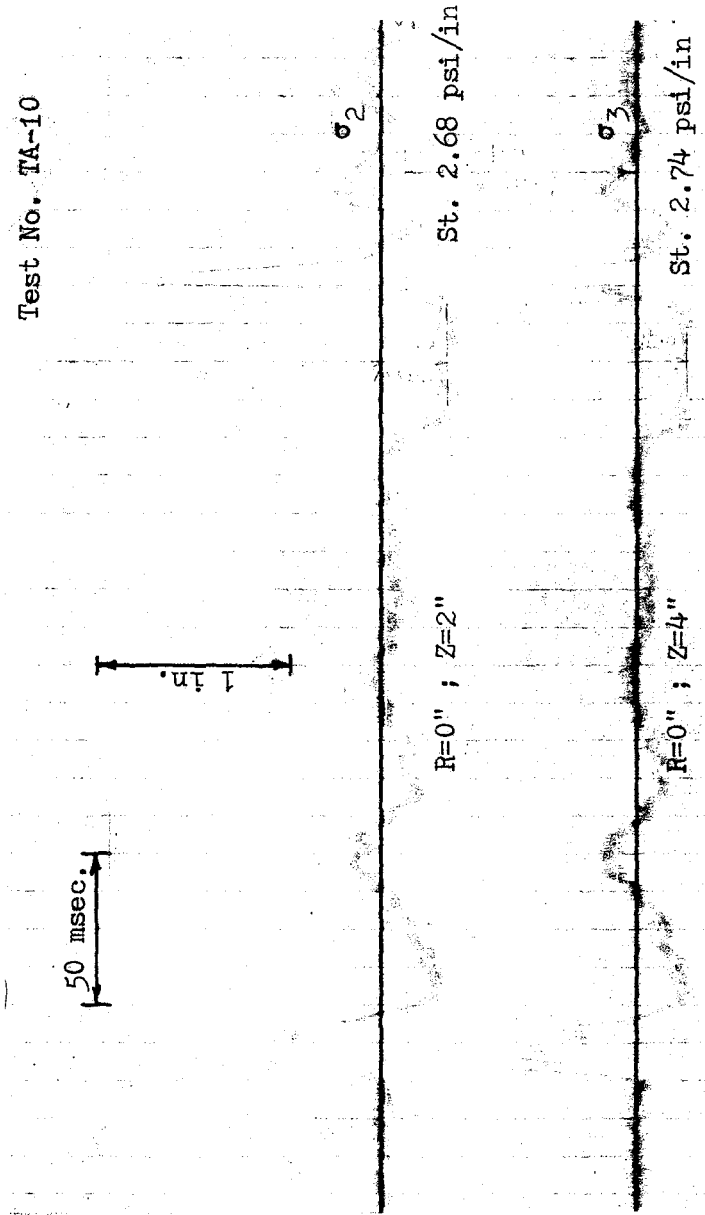


Figure 34. Vertical Stress-Time Traces on Axis of Symmetry at $Z = 2$ in.; $\frac{1}{4}$ in. (6 in. dia. circular footing)

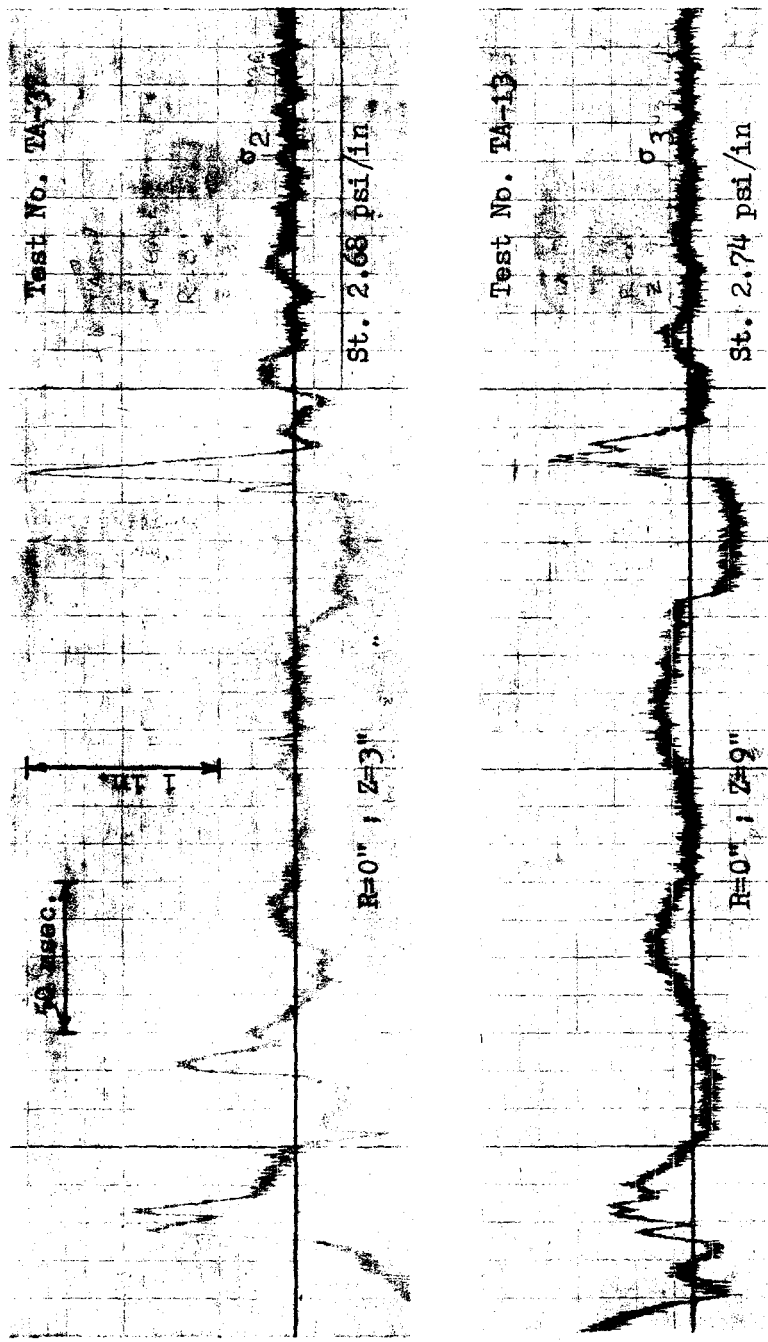


Figure 35. Vertical Stress-Time Traces on Axis of Symmetry at Z = 3 in.; 9 in. (6 in. dia. circular footing)

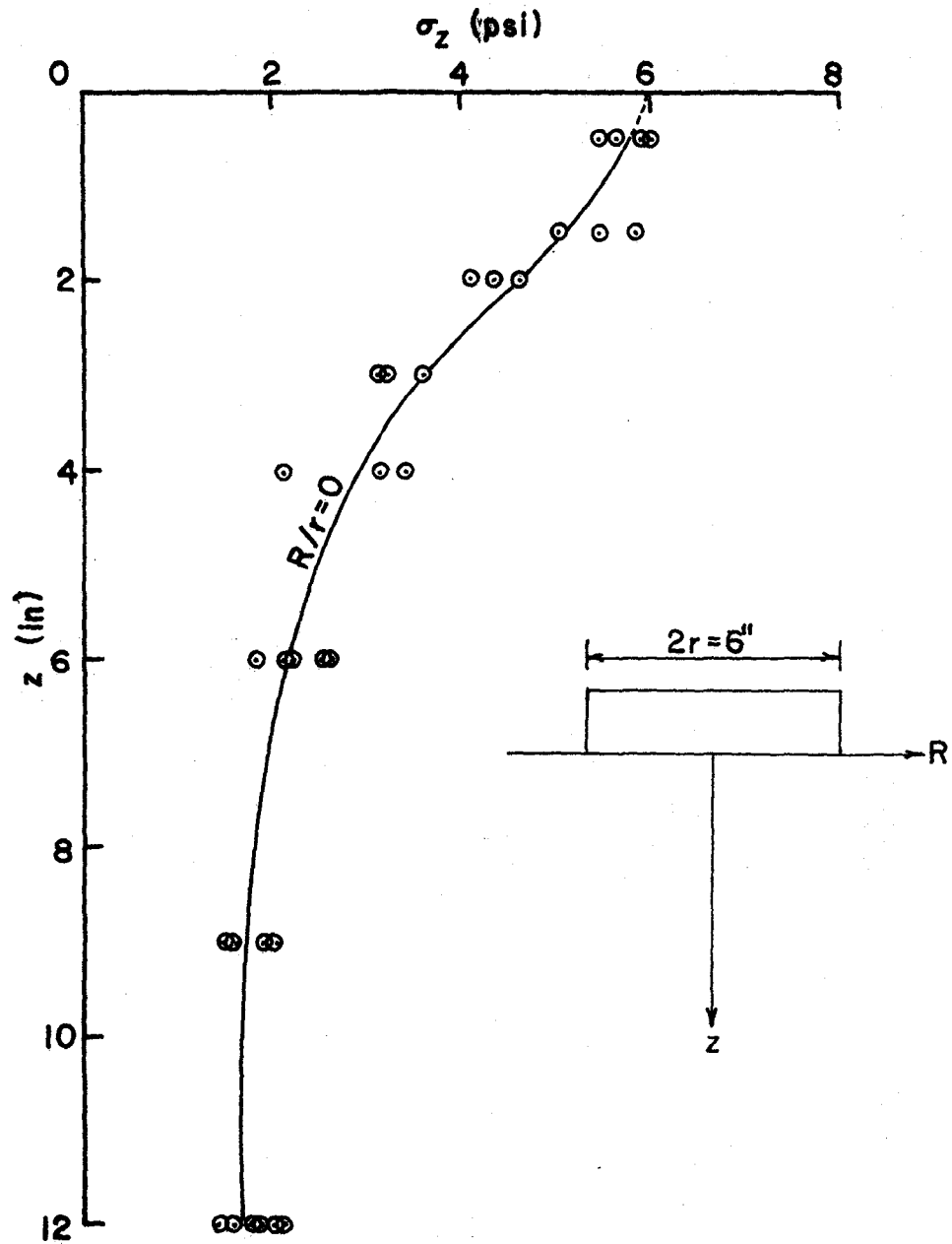


Figure 36. Attenuation of Peak Vertical Stress on Axis of Symmetry for a 6 in. dia. Circular Footing ($\sigma_c = 0.55$ psi)

three to four tests were conducted to obtain representative values at each gage station and the average value was used to plot the stress distribution. Typical stress-time traces, recorded at various depths on the axis of symmetry, for this footing are shown in Figs. 37 through 41. The response of these traces is compatible to that of the acceleration-time response of the footing. Data from other tests conducted under identical test conditions was used to obtain peak vertical stress values at various depths on the axis of symmetry. Attenuation of peak vertical stress on the axis of symmetry, for a 3 in. dia. circular footing resting on the surface, is shown in Fig. 42. As shown in this Fig. 42, the peak vertical stress on the bottom of the footing under dynamic loading conditions is 10.7 times its contact pressure ($\sigma_c = 0.88$ psi).

A set of experiments similar to those conducted on 6 in. dia. and 3 in. dia. circular footings were also conducted on a 3 in. by 3 in. square footing having a very low contact pressure ($\sigma_c = 0.20$ psi). Again, in this case, three to four tests were conducted at each gage station and data from different tests conducted under identical test conditions was used to obtain peak vertical stress values at various depths on the axis of symmetry. Typical stress-time traces are shown in Figs. 43 and 44. From average values of these test data, a stress distribution curve with depth on the axis of symmetry is plotted as shown in Fig. 45. In this case, the peak vertical stress on the bottom of the footing is 22 times

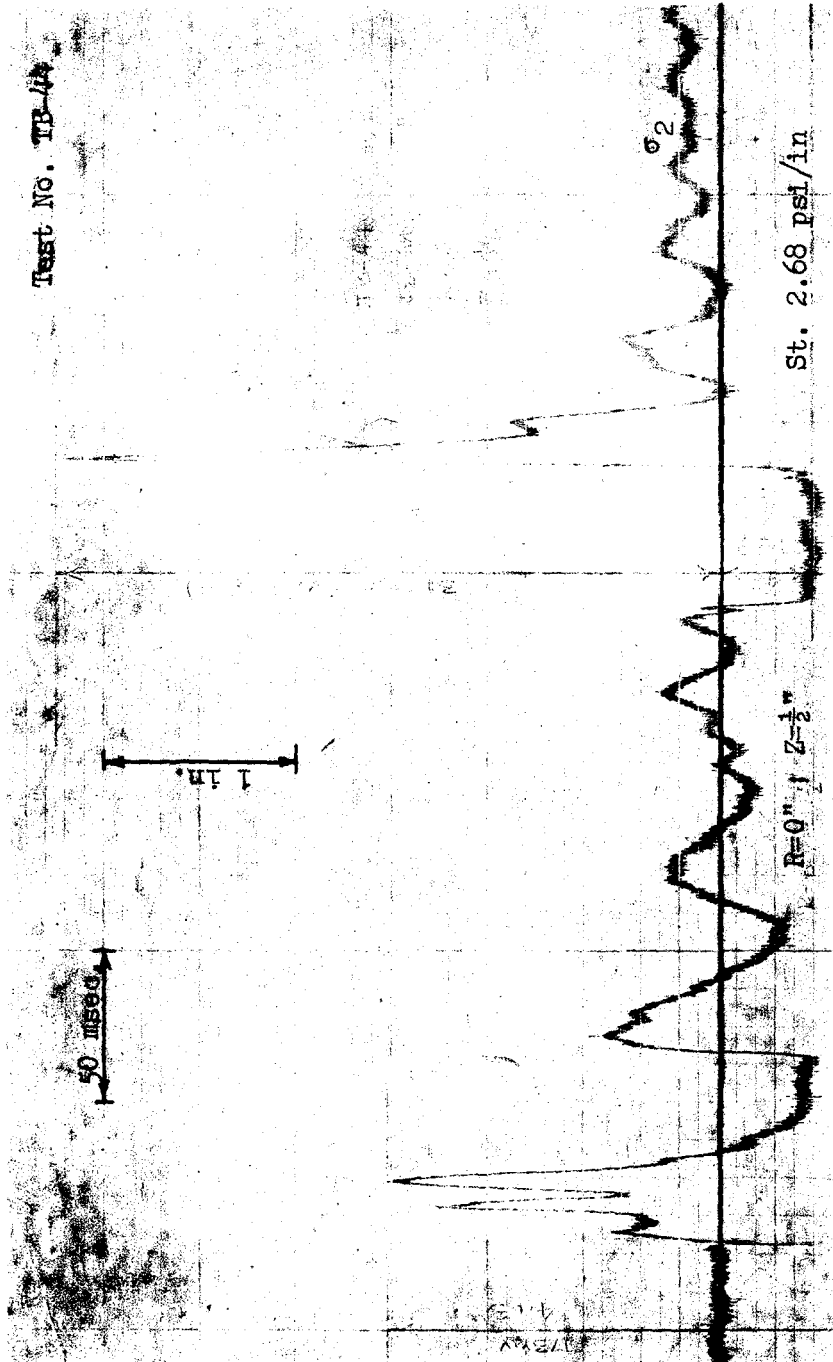


Figure 37. Vertical Stress-Time Trace at R = 0 in.; Z = 1/2 in. (3 in. dia. circular footing)

Test No. TB-12

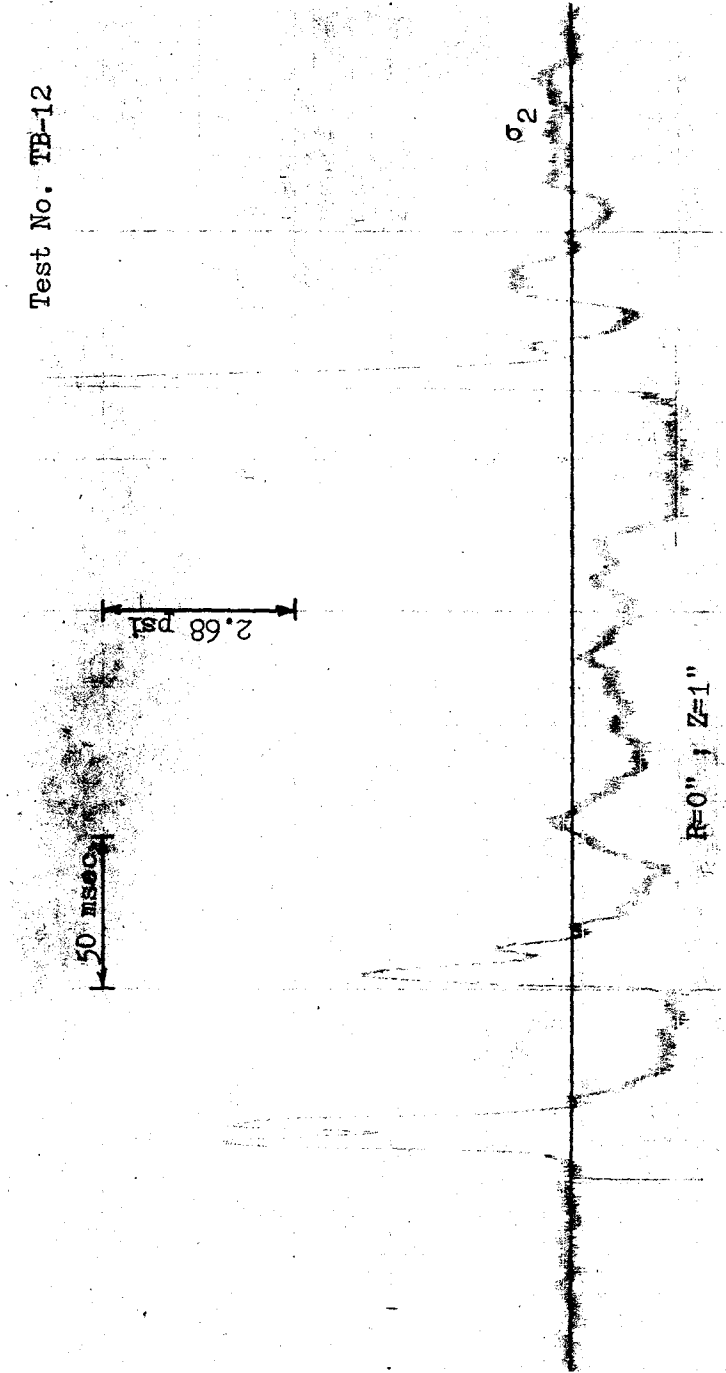


Figure 38. Vertical Stress-Time Trace at $R = 0$ in.; $Z = 1$ in. (3 in. dia. circular footing)

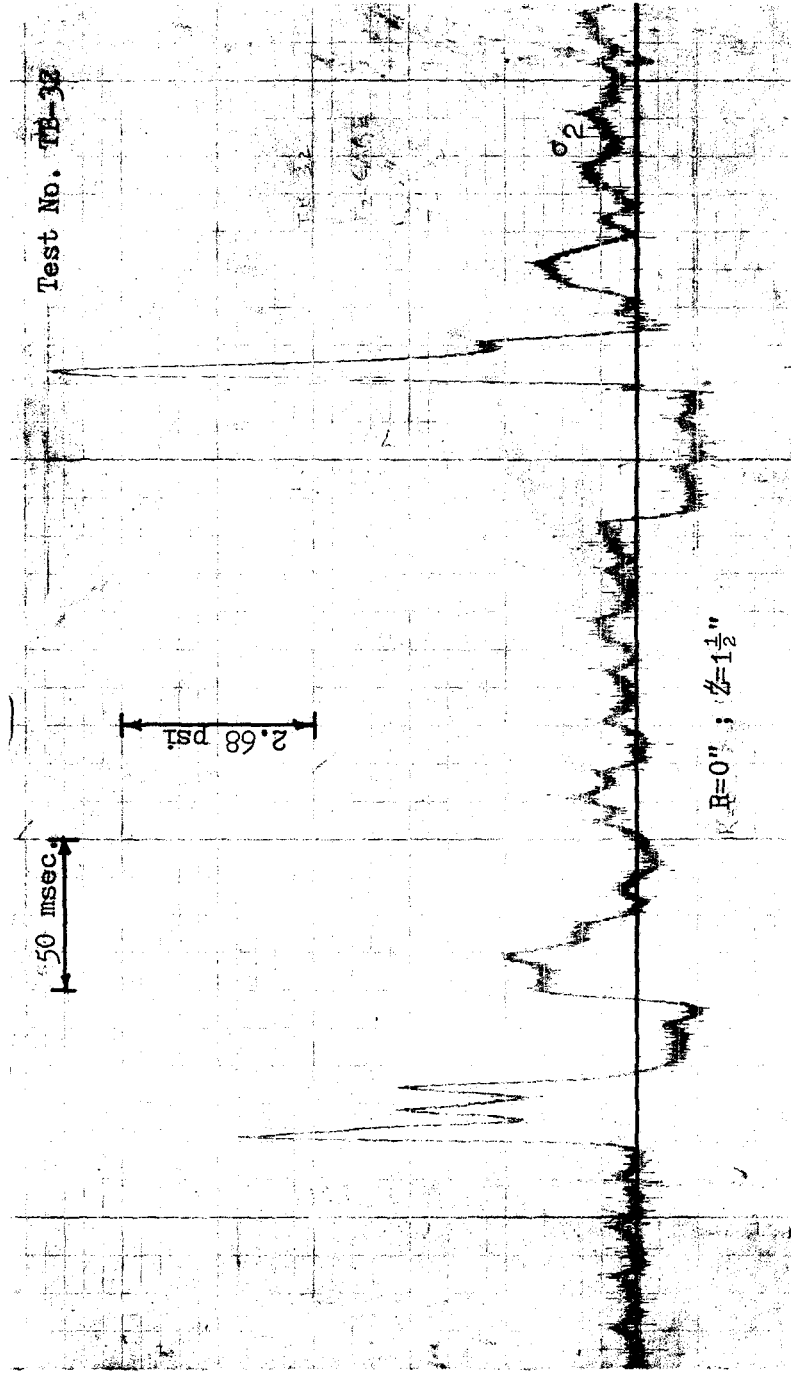


Figure 39. Vertical Stress-Time Trace at $R = 0$ in.; $Z = 1-1/2$ in. (3 in. dia. circular footing)

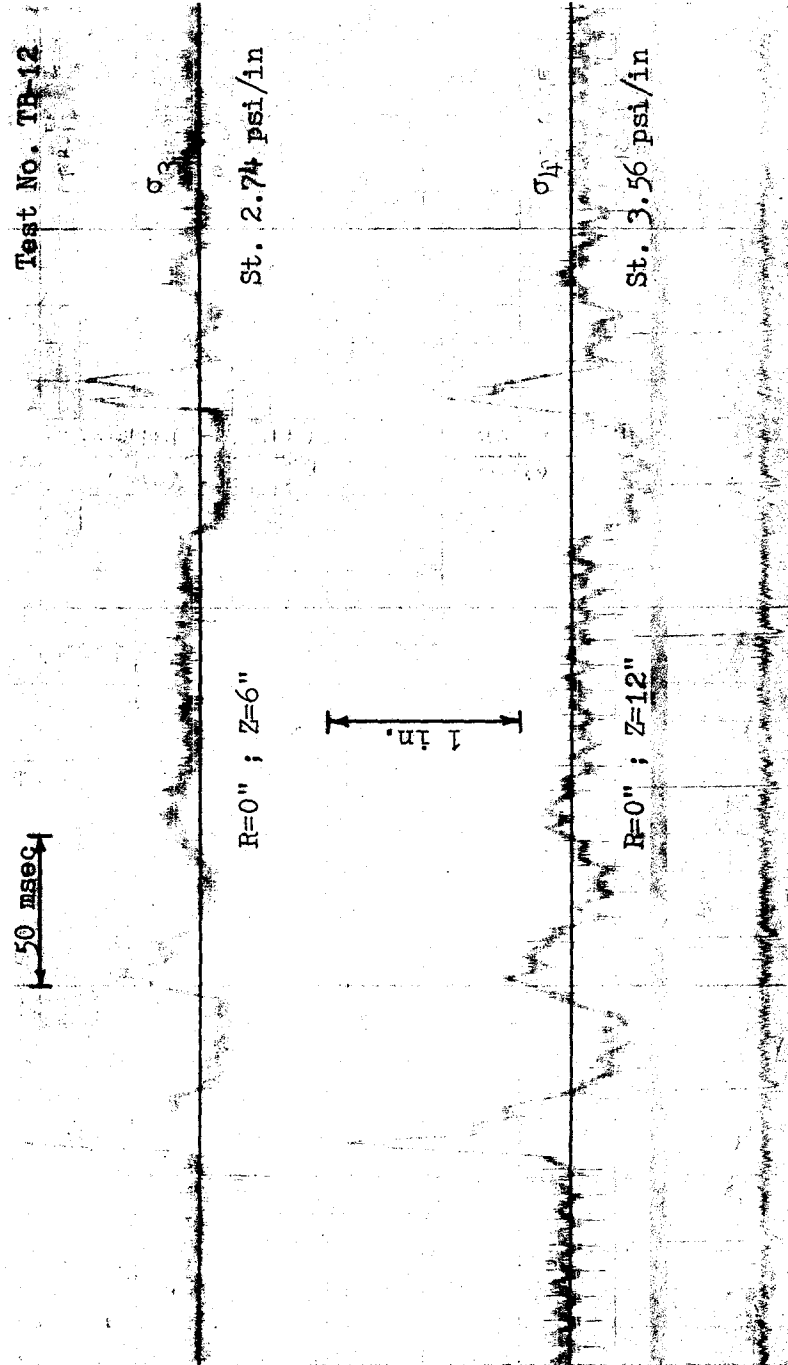


Figure 40. Vertical Stress-Time Traces on Axis of Symmetry at Z = 6 in.; 12 in. (3 in. dia. circular footing)

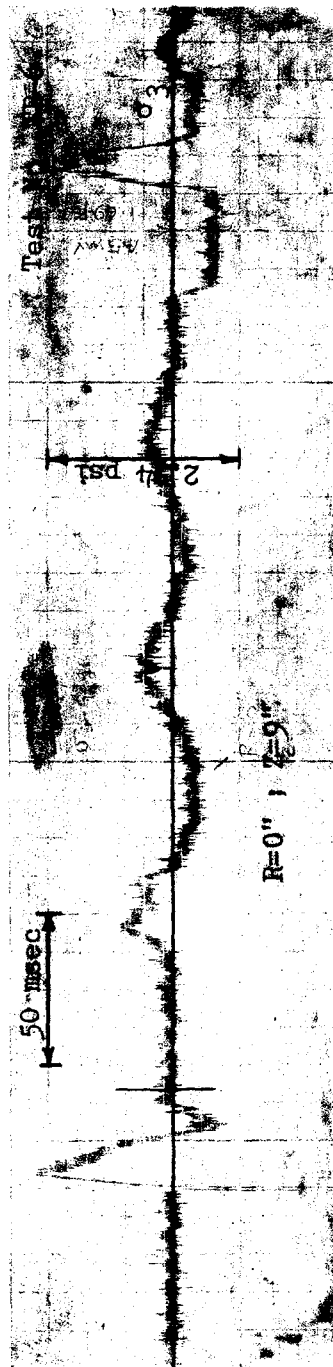


Figure 41. Vertical Stress-Time Trace at $R = 0$ in., $Z = 9$ in. (3 in. dia. circular footing)

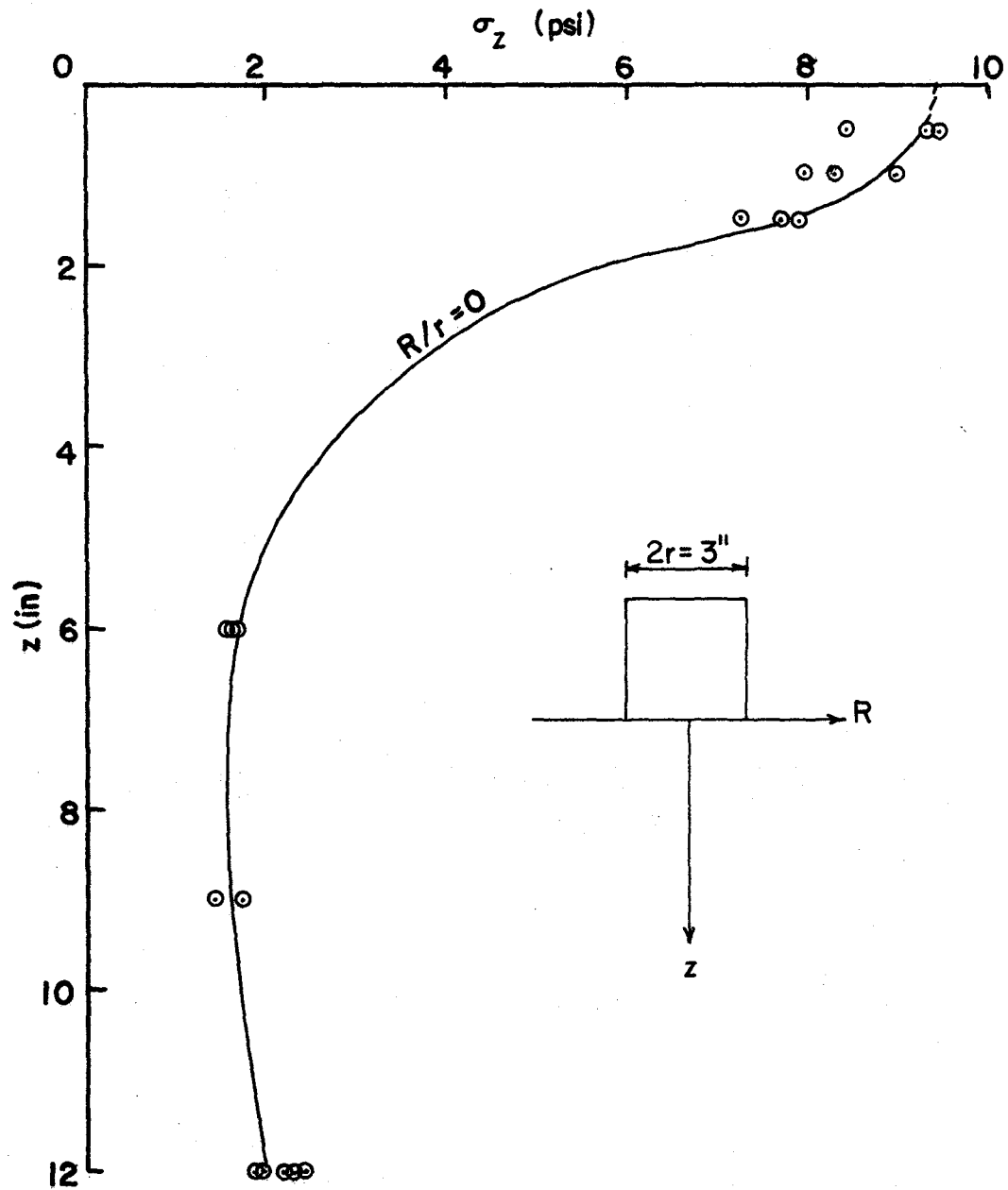


Figure 42. Attenuation of Peak Vertical Stress on Axis of Symmetry for a 3 in. dia. Circular Footing ($\sigma_c = 0.83$ psi)



Figure 43. Vertical Stress-Time Traces on Axis of Symmetry at $Z = 1/2$ in.; $1-1/2$ in. (3 in. by 3 in. square footing)



Figure 4.4. Vertical Stress-Time Traces on Axis of Symmetry at Z = 1 in.; 6 in.; 12 in. (3 in. by 3 in. square footing)

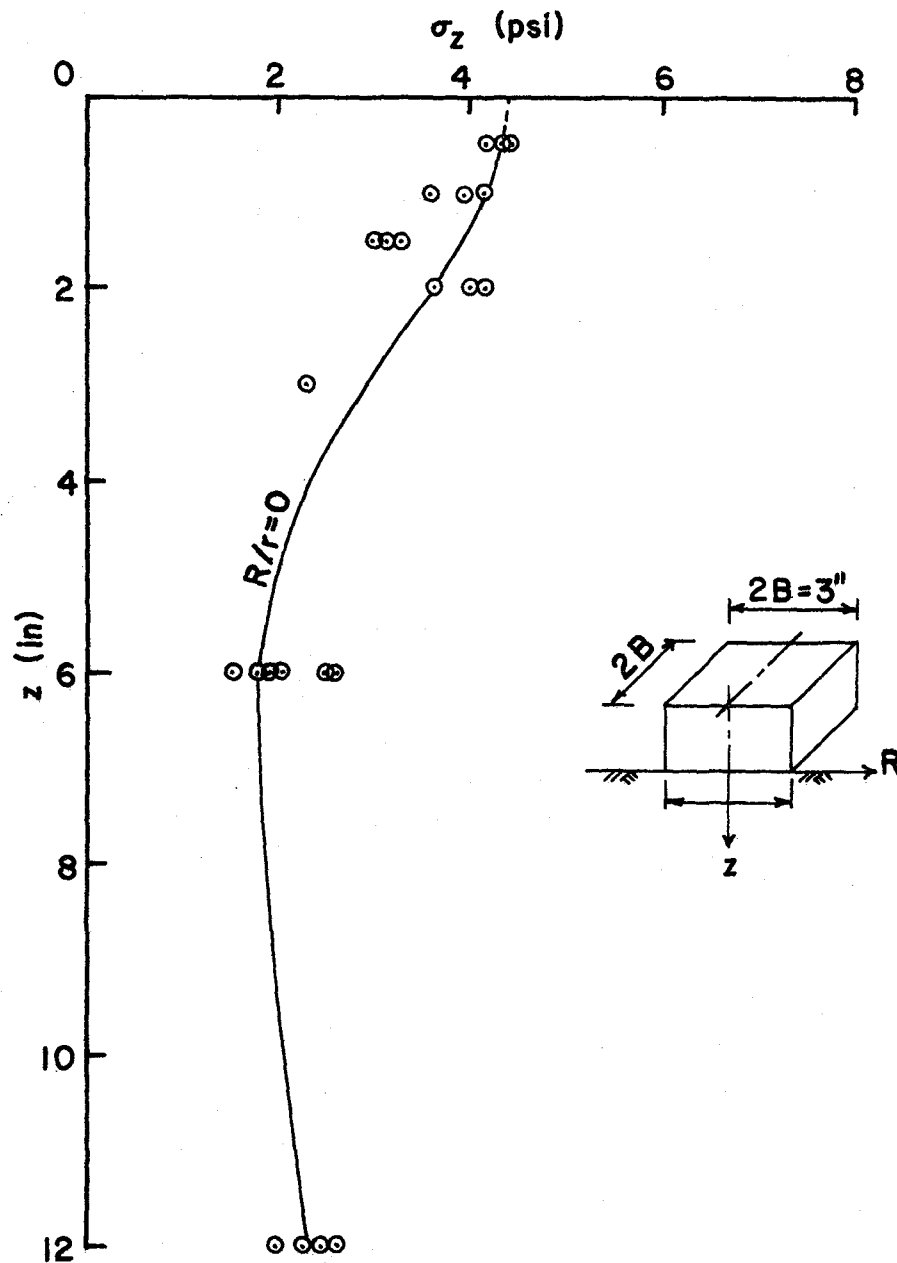


Figure 45. Attenuation of Peak Vertical Stress on Axis of Symmetry for a 3 in. by 3 in. Square Footing ($\sigma_c = 0.20$ psi)

its static contact pressure ($\sigma_c = 0.20$ psi). From the above results, it appears that the magnification of the vertical dynamic stress on the bottom of the footing is related to the deceleration of the footing.

To compare the pattern of these stress distribution curves, shown in Figs. 36, 42 and 45, with the theoretical stress distribution curves under static loading conditions, a set of curves for three footings were drawn using^{32,1}, Boussinesque's stress distribution theory, as shown in Fig. 46.

Tests were also conducted on the same soil mass inside the vessel under identical test conditions, but without any footing on the surface. To obtain a representative stress value at various depths on the axis of symmetry, three to four tests (sometimes even five tests) were conducted at each gage position. Using these representative values, a stress distribution curve in the soil mass under dynamic loading conditions was drawn, as shown in Fig. 47. On the same graph, overburden pressure at various depths is plotted for comparison purposes. The data indicated that the stress distribution under dynamic loading conditions almost follows the same pattern as the overburden pressure, except for a sudden decrease near the surface. This may be due to the fact that the soil particles near the surface will not have any confinement and when a transient load is transmitted from the bottom through the soil, the soil particles near the surface will be in a state of near liquefaction.

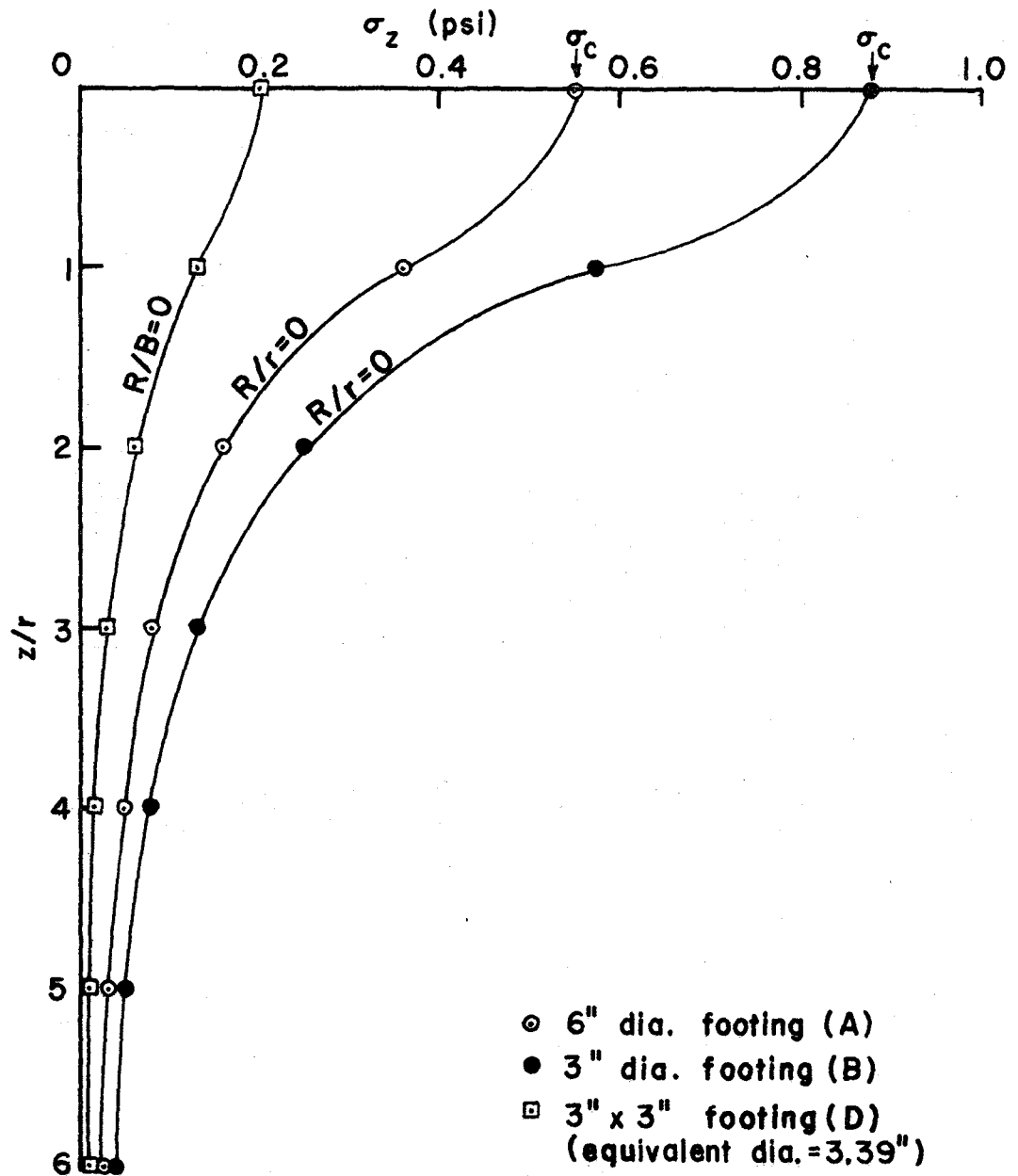


Figure 46. Stress at Any Point from Circular Bearing Area
 (Boussinesque's Stress Distribution Theory)

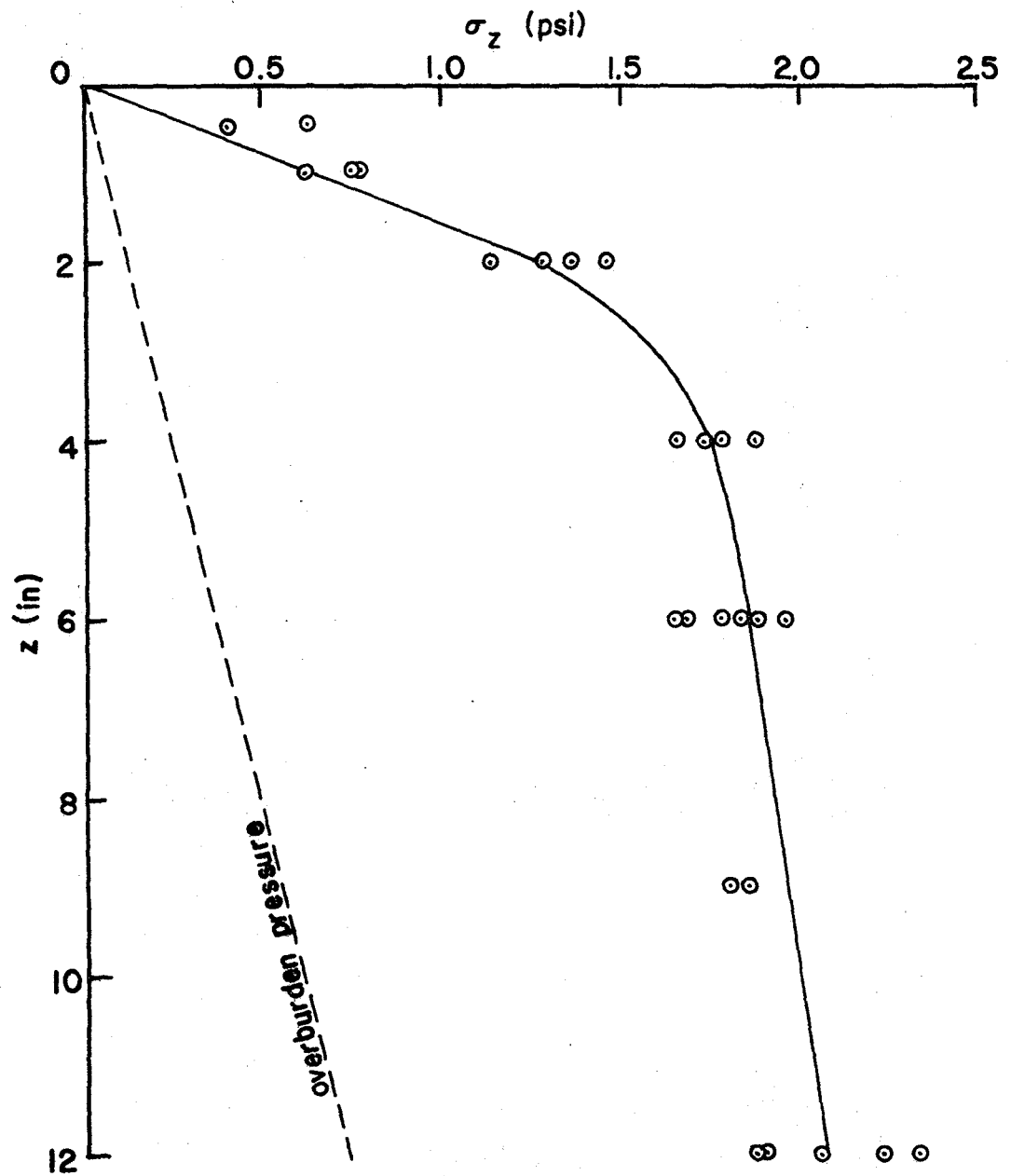


Figure 47. Peak Vertical Stress Distribution With Depth Under Transient Loads (without any footing on the surface)

The stress distribution shown in Fig. 47 was plotted also, to compare with the stress distribution curves (with a footing on the surface) shown in Figs. 36, 42 and 45, and thus to investigate the influence of the mass of the footing, on the vertical stress distribution in the soil. In all the three cases of surface footings subjected to transient load, it was noticed that the influence of the mass of the footing on the vertical stress distribution is negligible at a depth of two footing diameters below the footing. This is reasonably in agreement with Orrje's conclusion⁴⁹. Orrje conducted both laboratory and field tests on four different soils. The behavior of these soils was investigated by measuring the retardation of free falling weight when it strikes the soil surface. One of his conclusions was that the depth to which the loading tests affected the underlying soil corresponded to approximately 1.5 plate diameters. Landsman³⁷ conducted dynamic tests on Kaoline clay. Behavior of this soil was investigated by measuring the deceleration of a free falling weight when it strikes the soil surface. He also used embedded stress gages at various depths in the soil to study the stress distribution. From the stress distribution relationships it was noticed that, at a depth equal to twice the footing diameter, the stress had reduced to 10 percent of the applied value.

Tests were also conducted with a surface footing and with stress gages embedded in the soil at various offset distances from the axis of symmetry, to determine the stress

distribution along the gage locations. These stress distributions were also investigated at various depths. A typical set of stress-time traces for a 6 in. dia. circular footing are shown in Figs. 48 through 50. These traces followed the same pattern as the acceleration-time traces of the footing. Attenuation of peak vertical stress versus offset from the axis of symmetry for this footing is shown in Fig. 51.

A similar set of stress-time traces in the case of a 3 in. dia. circular footing on the surface are shown in Figs. 52 through 58. These traces also responded accordingly as the acceleration-time response of the footing. Attenuation of peak vertical stress versus offset from the axis of symmetry for this footing is shown in Fig. 59.

Stress-time histories were also recorded at various offset distances from the axis of symmetry and at various depths with a 3 in. by 3 in. square footing on the surface. A typical set of these traces are shown in Figs. 60 through 63. The data was used to obtain peak vertical stress distribution with offset from the axis of symmetry as shown in Fig. 64.

Comparing the stress distribution curves of the three footings, it was noticed that the pattern of stress distribution, with offset distance for a 6 in. dia. circular footing on the surface differed from that of the 3 in. dia. circular and 3 in. by 3 in. square footing on the surface. The pattern of stress distribution shown in Figs. 59 and 64 for



Figure 48. Vertical Stress-Time Traces at 6 in. Depth and at $R = 0$ in.; 6 in.; 12 in.
(6 in. dia. circular footing)

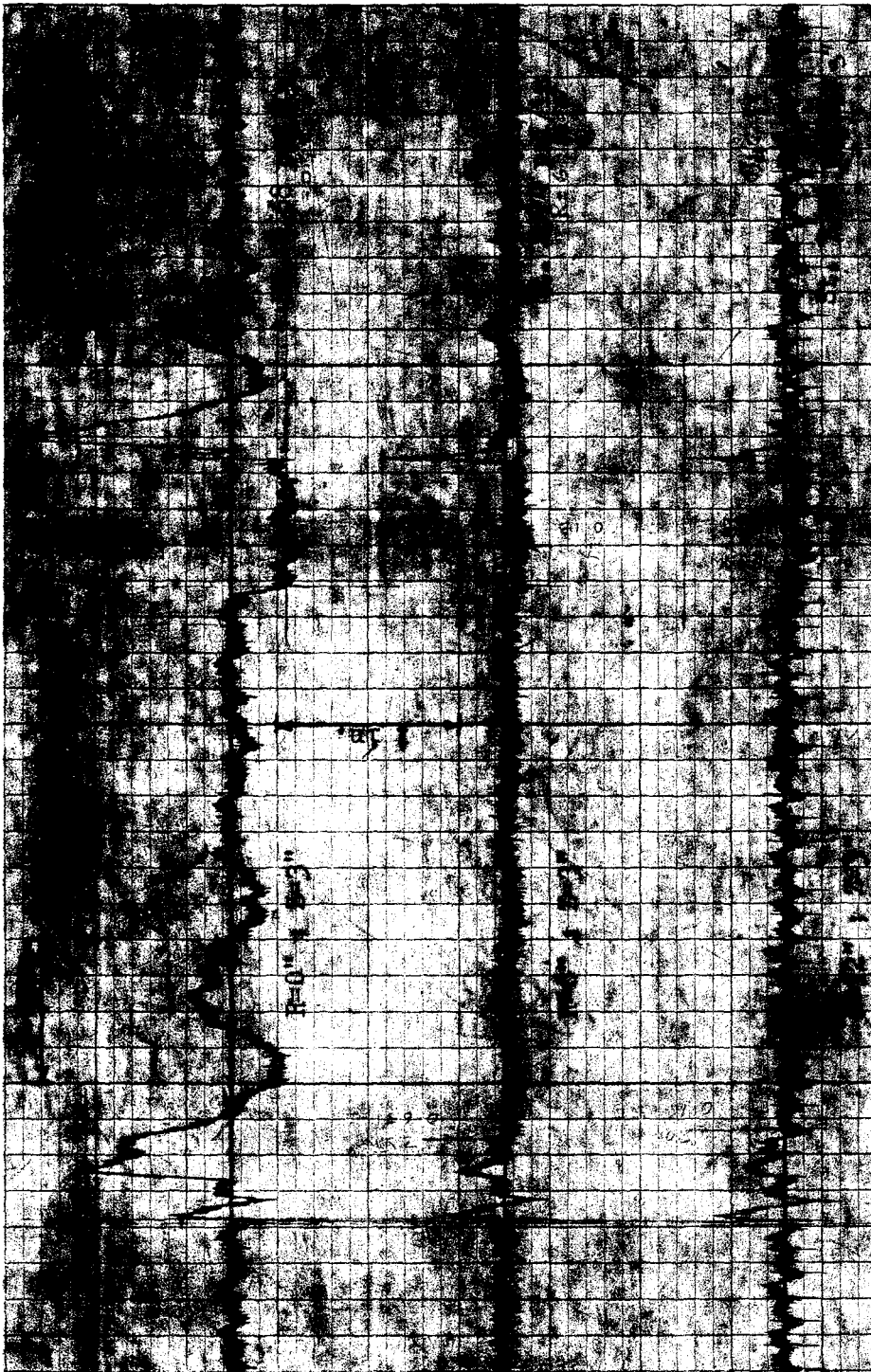


Figure 49. Vertical Stress-Time Traces at 3 in. Depth and at $R = 0$ in.; 6 in.; 12 in. (6 in. dia. circular footing)




Reproduced from
best available copy. 

Figure 50. Vertical Stress-Time Traces at 1-1/2 in. Depth and at $R = 0$ in.; 6 in.; 12 in.
(6 in. dia. circular footing)

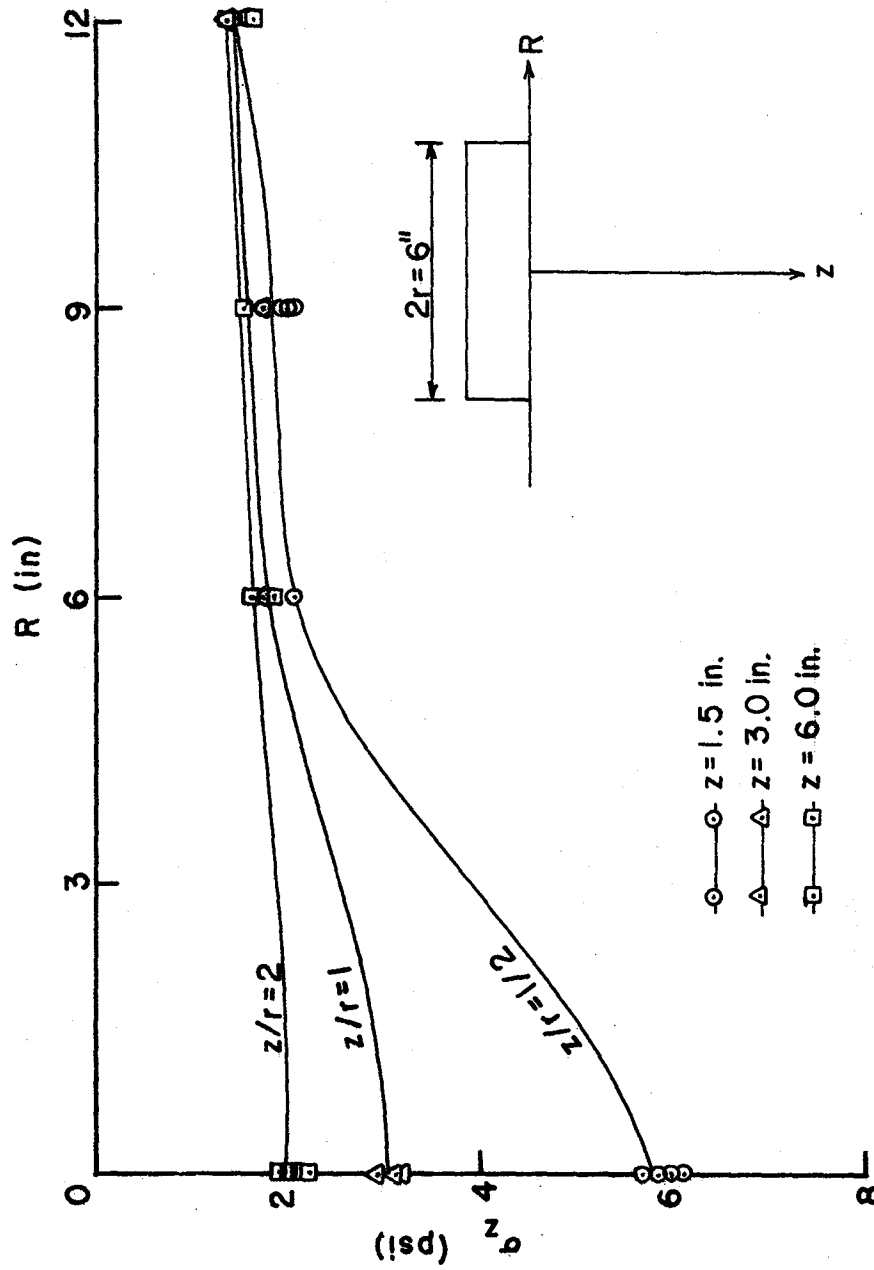


Figure 51. Attenuation of Peak Vertical Stress vs Offset from Axis of Symmetry for a 6 in. dia. Circular Footing ($\sigma_c = 0.55$ psi)

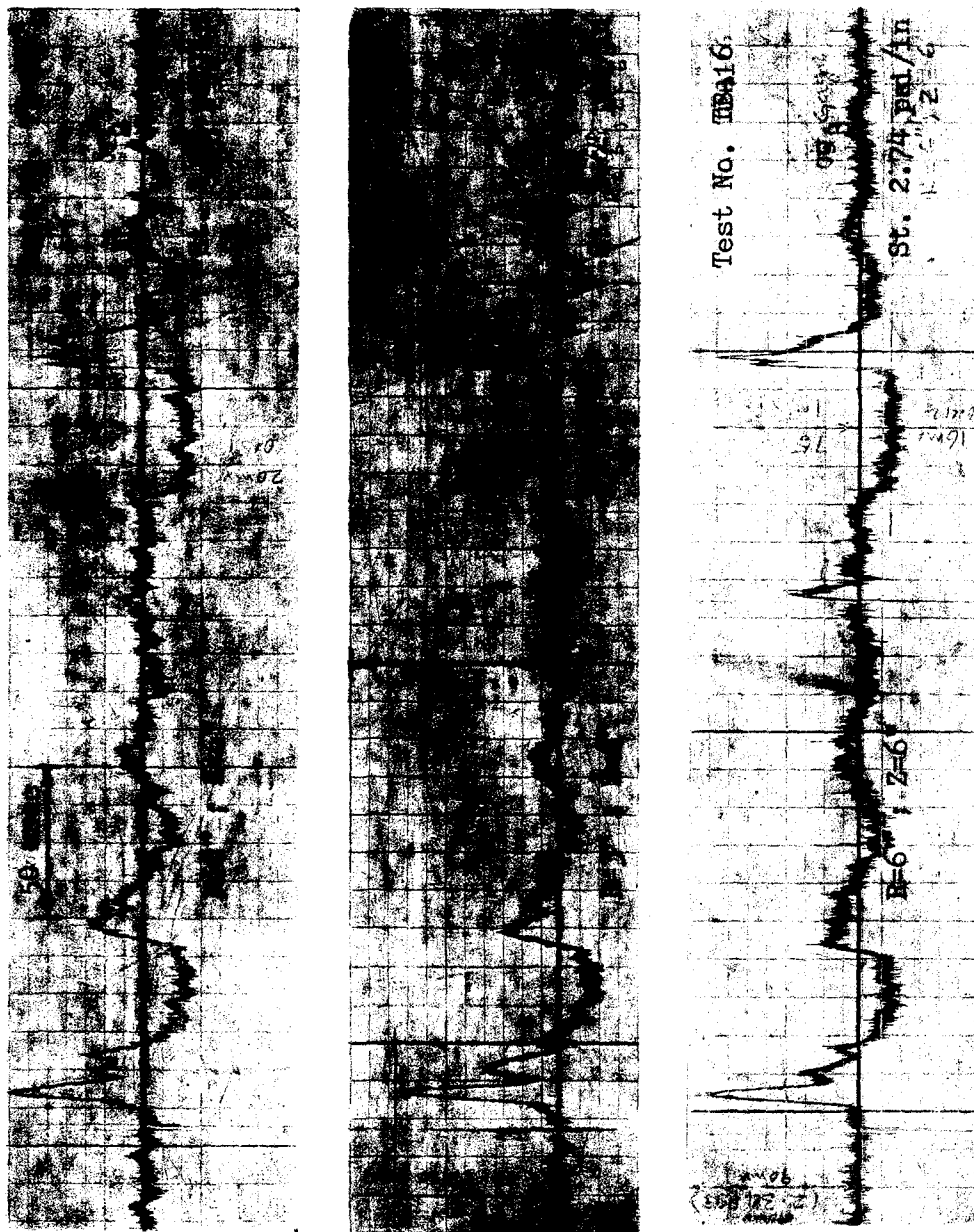


Figure 52. Vertical Stress-Time Traces at 6 in. Depth and at P = 0 in.; 3 in.; 6 in. (3 in. dia. circular footing)

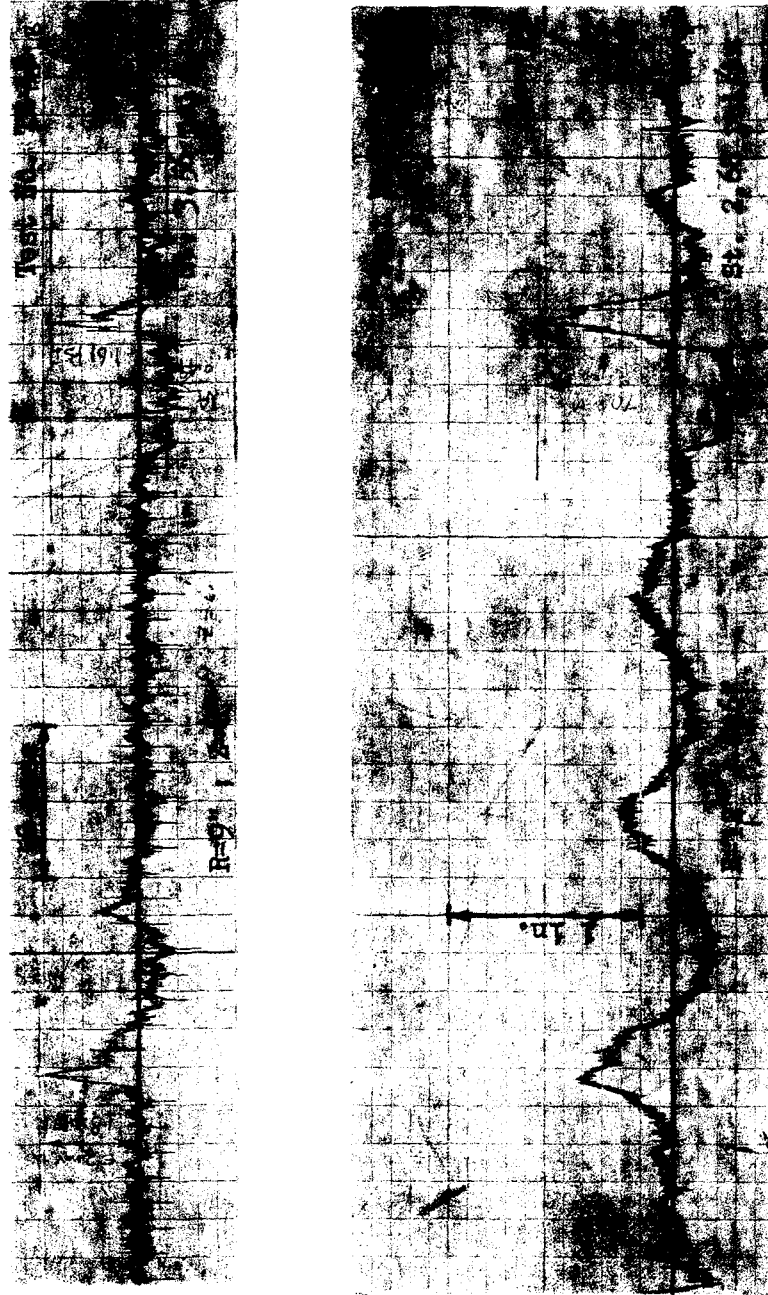


Figure 53. Vertical Stress-Time Traces at 6 in. Depth and at R = 9 in.; 12 in. (3 in. dia. circular footing)



Figure 54. Vertical Stress-Time Traces at 3 in. Depth and at $R = 0$ in.; 6 in.; 12 in. (3 in. dia. circular footing)



Figure 55. Vertical Stress-Time Traces at 1-1/2 in. Depth and at R = 0 in.; 6 in. (3 in. dia. circular footing)

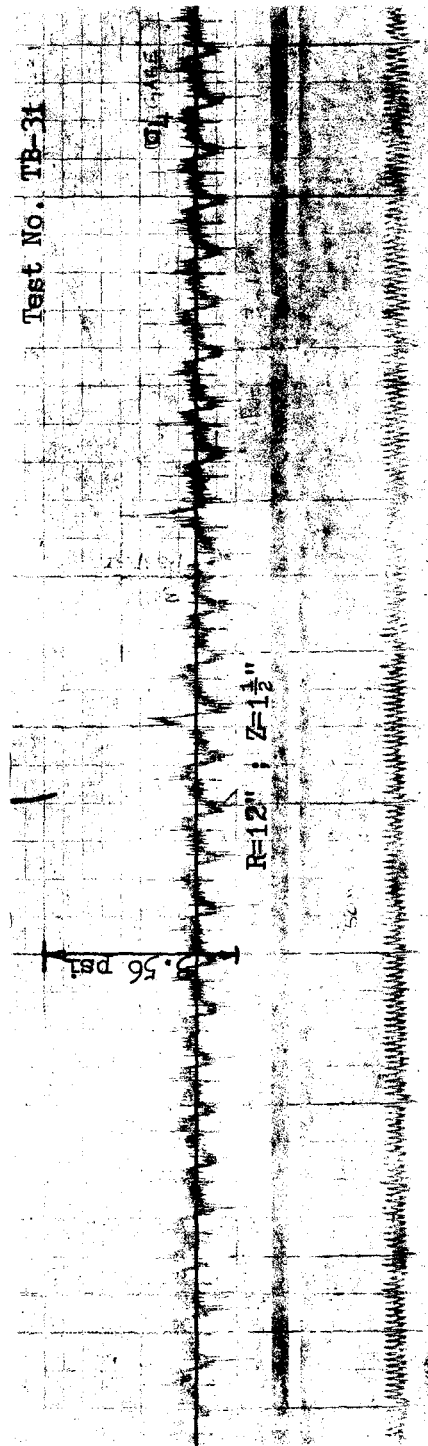


Figure 56. Vertical Stress-Time Trace at $R = 12$ in.; $Z = 1-1/2$ in. (3 in. dia. circular footing)

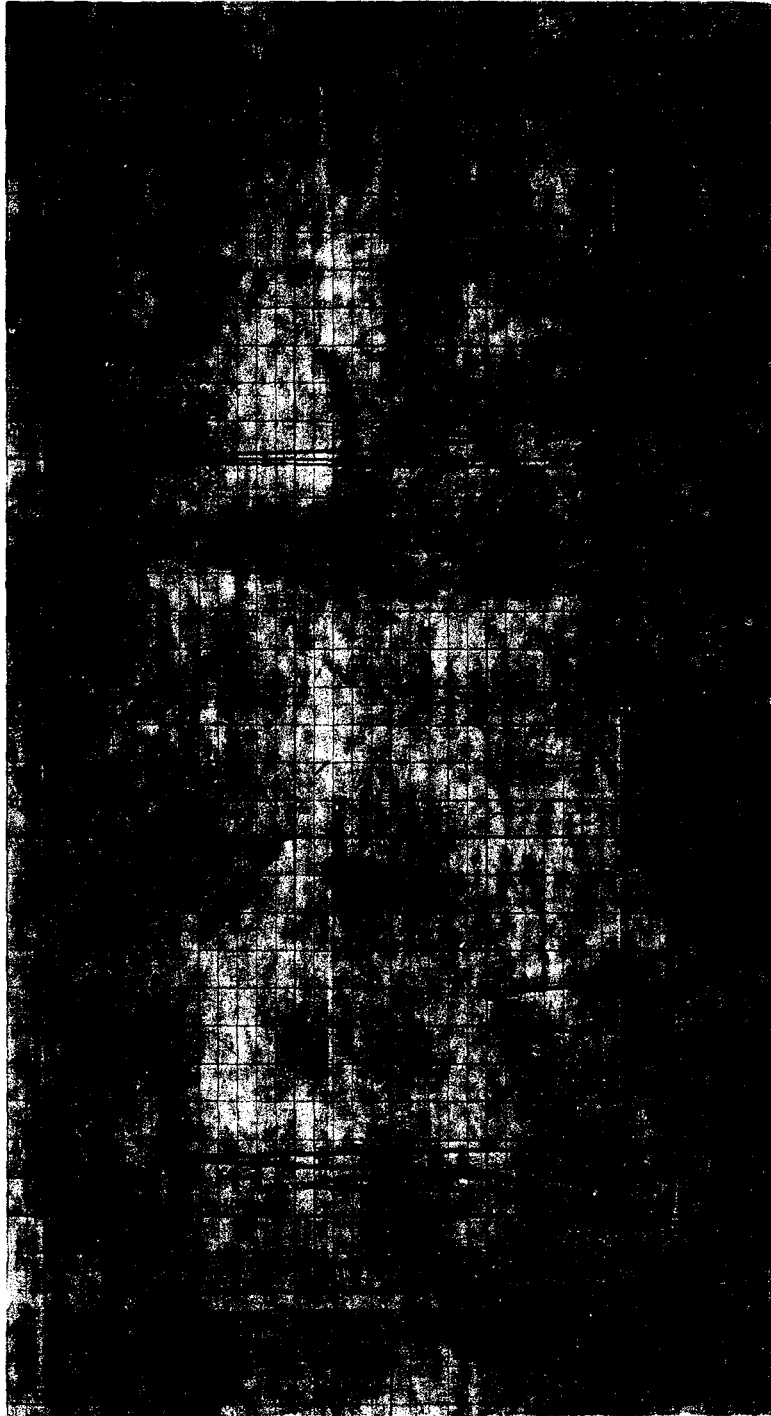


Figure 57. Vertical Stress-Time Trace at $R = 0$ in.; $Z = 1/2$ in. (3 in. dia. circular footing)

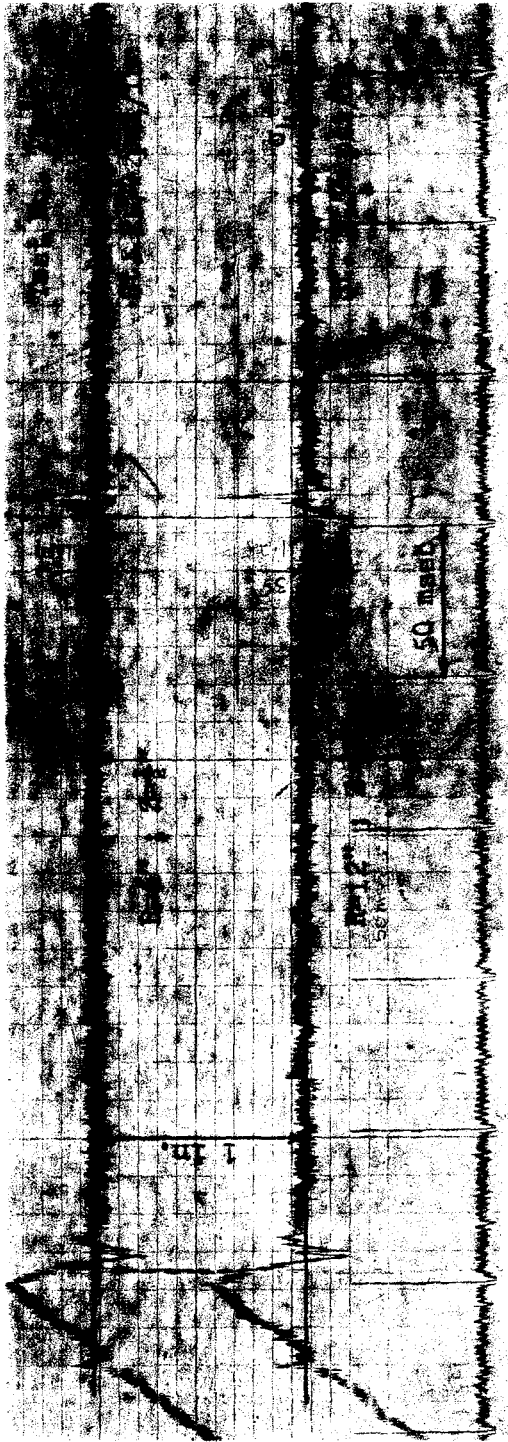


Figure 58. Vertical Stress-Time Traces at 1/2 in. Depth and at $R = 6$ in.; 12 in. (3 in. dia. circular footing)

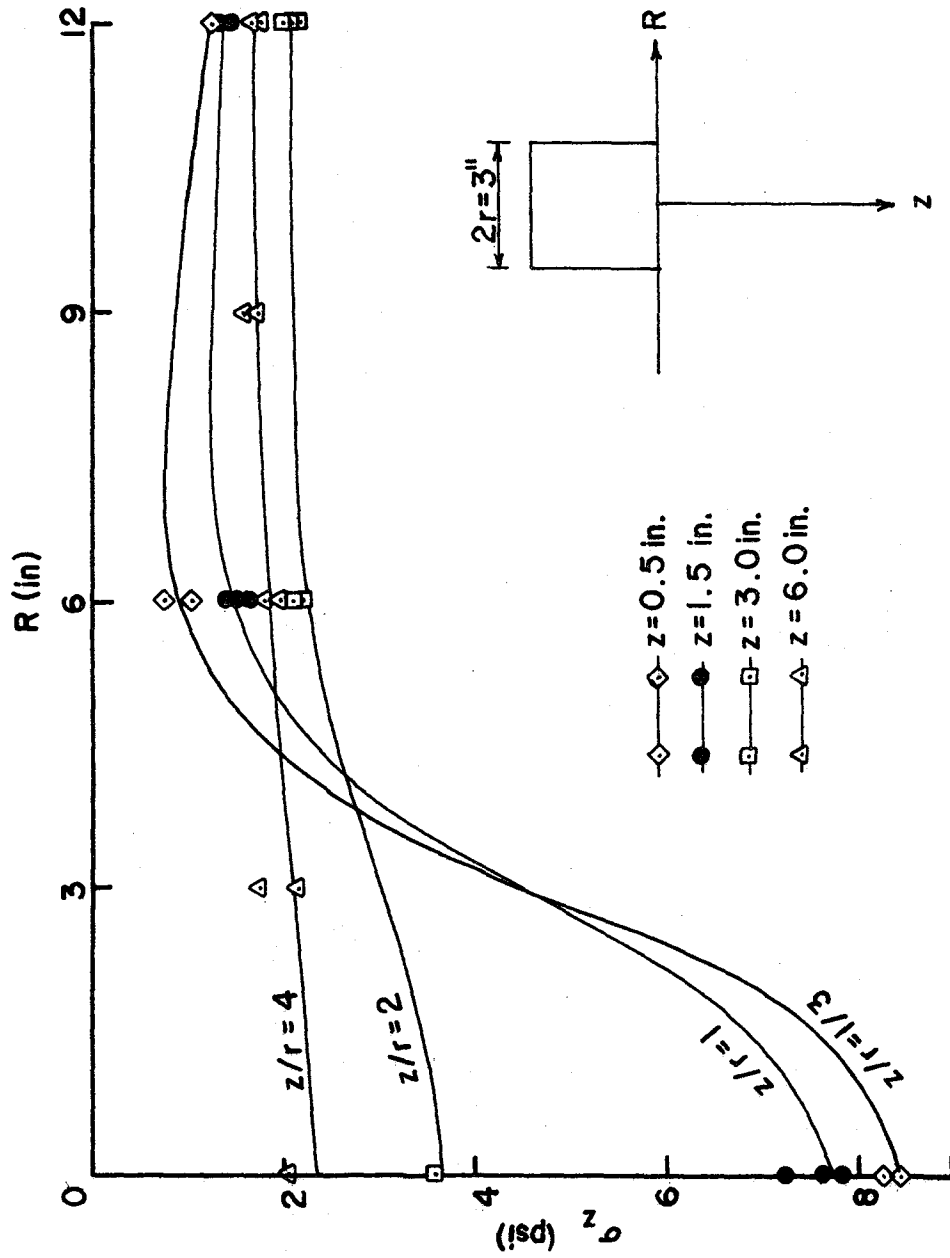


Figure 59. Attenuation of Peak Vertical Stress vs Offset from Axis of Symmetry for a 3 in. dia. Circular Footing ($\sigma_c = 0.33$ psi)

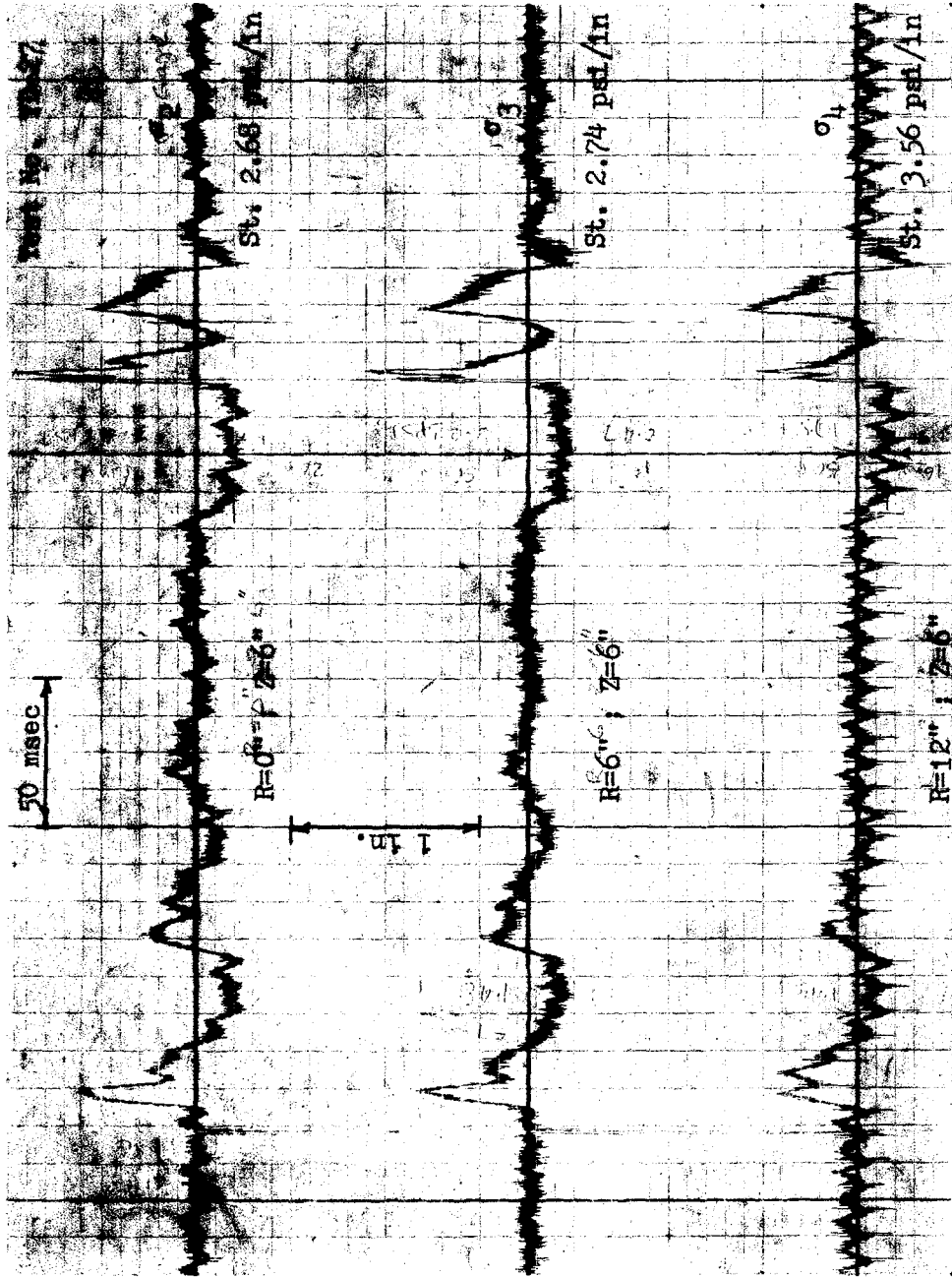


Figure 60. Vertical Stress-Time Traces at 6 in. Depth and at $R = 0$ in.; 6 in.; 12 in. (3 in. by 3 in. square footing)

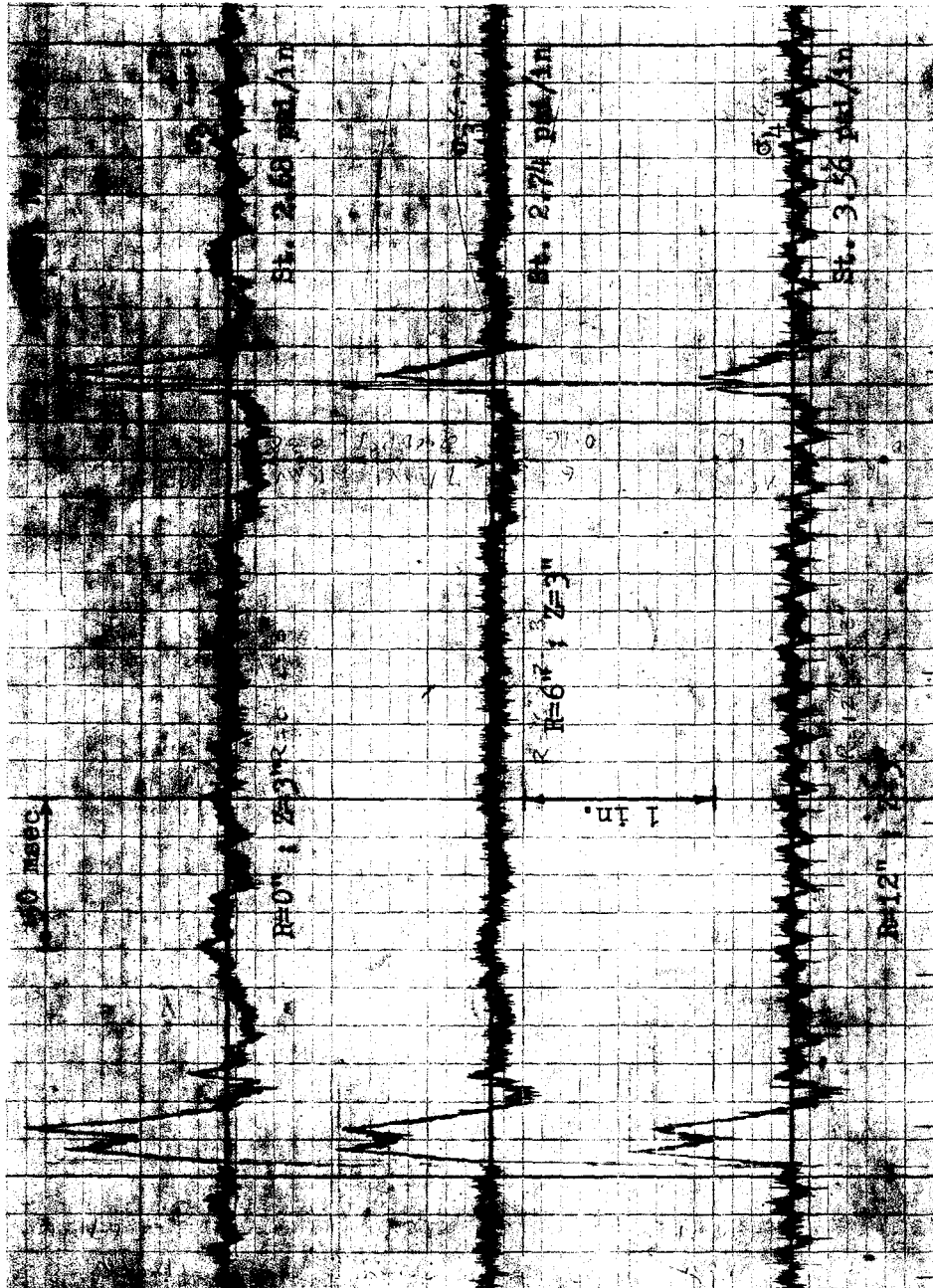


Figure 61. Vertical Stress-Time Traces at 3 in. Depth and at R = 0 in., 6 in.; 12 in. (3 in. by 3 in. square footing)

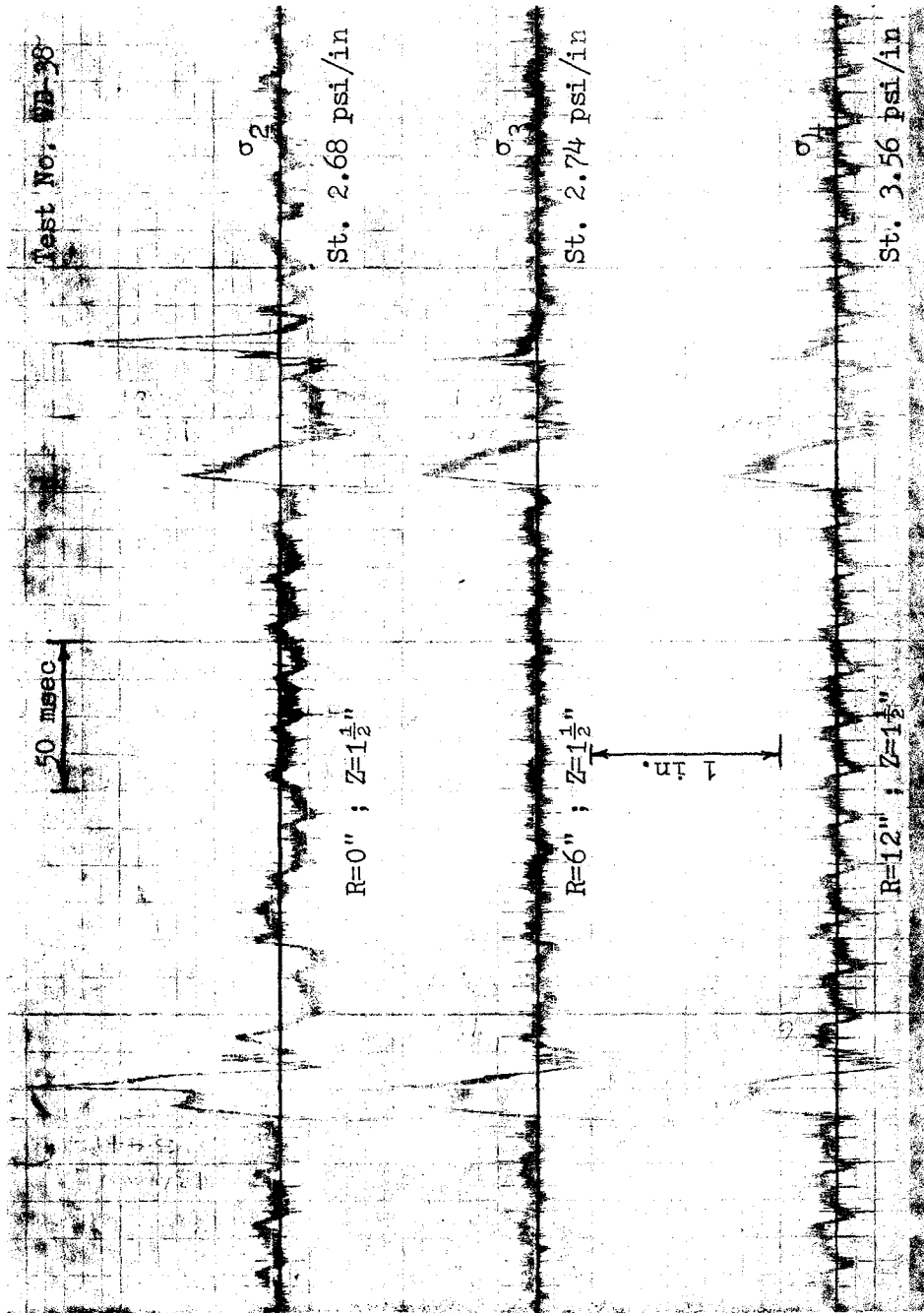


Figure 62. Vertical Stress-Time Traces at 1-1/2 in. Depth and at R = 0 in.; 6 in.; 12 in. (3 in. by 3 in. square footing)

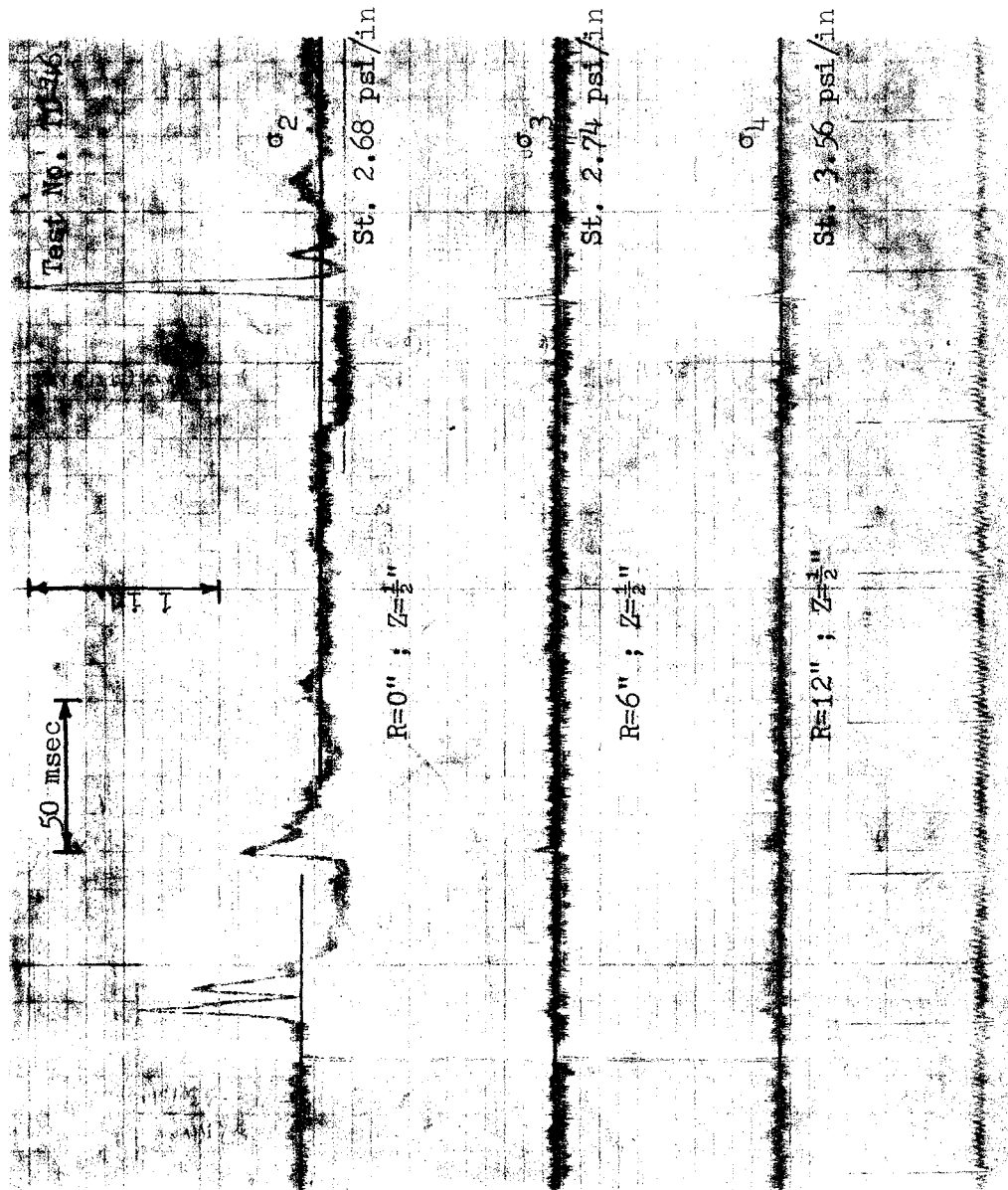


Figure 63. Vertical Stress-Time Traces at 1/2 in. Depth and at $R = 0$ in.; 6 in.; 12 in. (3 in. by 3 in. square footing)

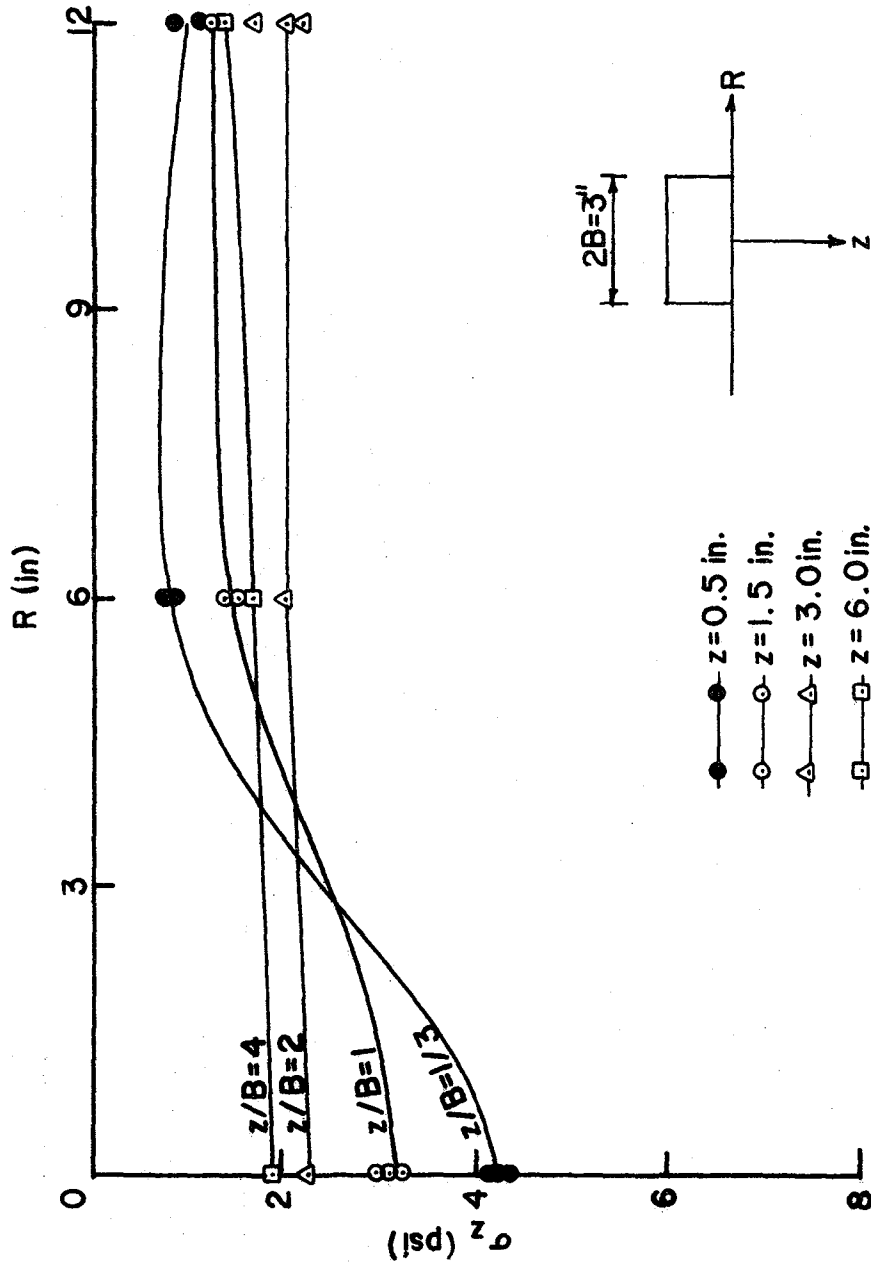


Figure 64. Attenuation of Peak Vertical Stress vs Offset from Axis of Symmetry for a 3 in. by 3 in. Square Footing ($\sigma_c = 0.20$ psi)

a 3 in. dia. circular and 3 in. by 3 in. square footings respectively, agreed well except for their stress intensity values on the axis of symmetry. The data shown in Figs. 51, 59 and 64 indicated that the size of the footing affects the stress distribution in the soil. Attenuation was very rapid in a distance equal to the diameter of the footing. At a distance equal to 1.5 times the diameter of the footing from the axis of symmetry, the effect of footing on the vertical stress distribution is negligible.

Strain Measurements. Strain-time histories at various gage locations were recorded by using the embedded strain gages. Location of these strain measurements is shown in Fig. 20. Details of these strain gages, the calibration procedures and the method of placement in the soil are described in Chapter IV. Typical visicorder traces of the output from the embedded strain gages at various positions on the axis of symmetry with a 6 in. dia. circular footing on the surface are shown in Figs. 65 and 66. As shown in these figures, strain-time trace consisted of positive (trace above zero line) or compressive strain, and negative (trace below zero line) or tensile strain. These strain-time records are consistent with the acceleration-time and stress-time records. Initial compressional strain is followed by a tensile strain, which occurs in about 200 msec, followed by a compressional strain. Data from these strain-time records was used to plot vertical strain distribution with depth on the axis of symmetry for a 6 in. dia. circular footing on the surface,

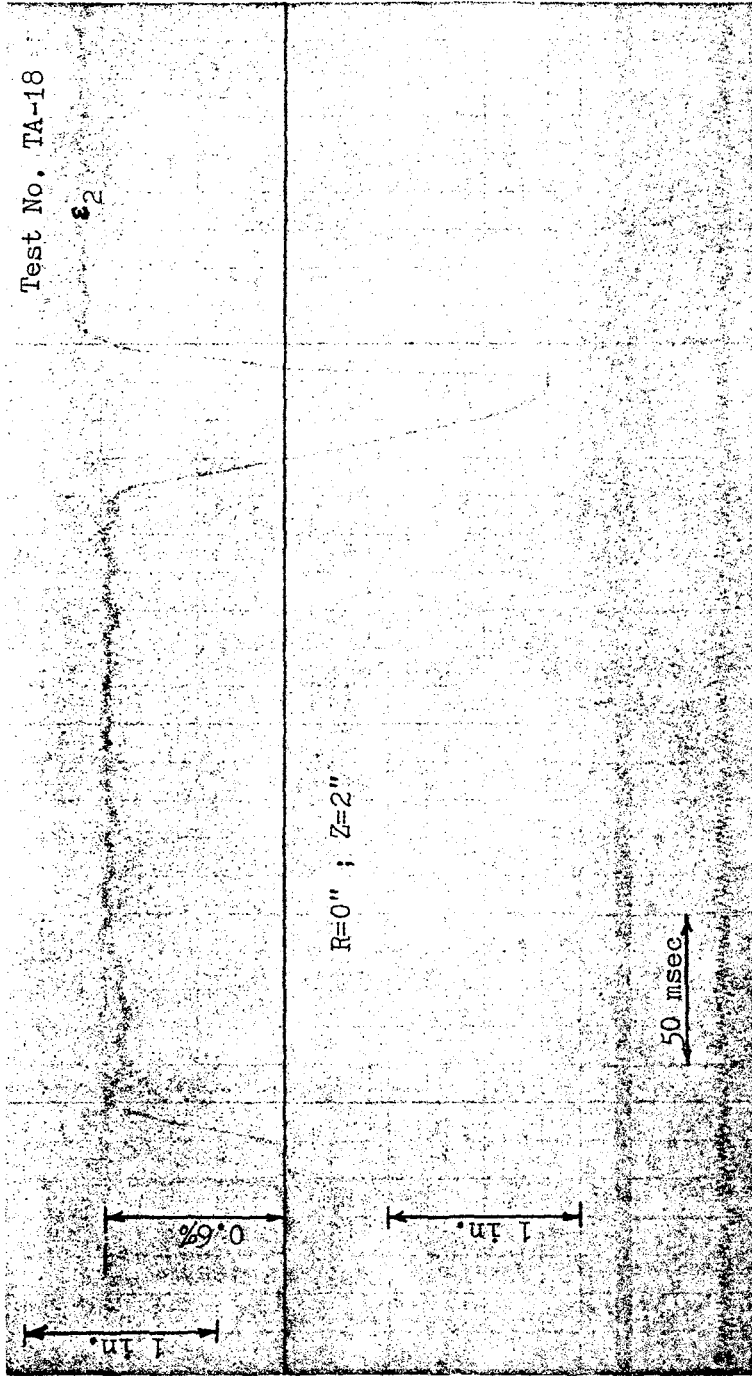


Figure 65. Strain-Time Trace at $R = 0$ in.; $Z = 2$ in.; (6 in. dia. circular footing)

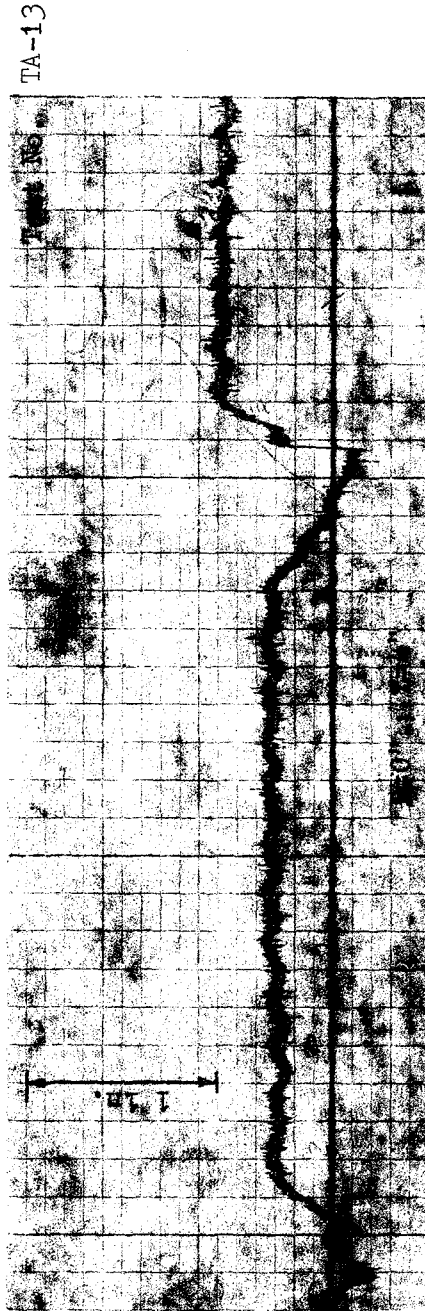
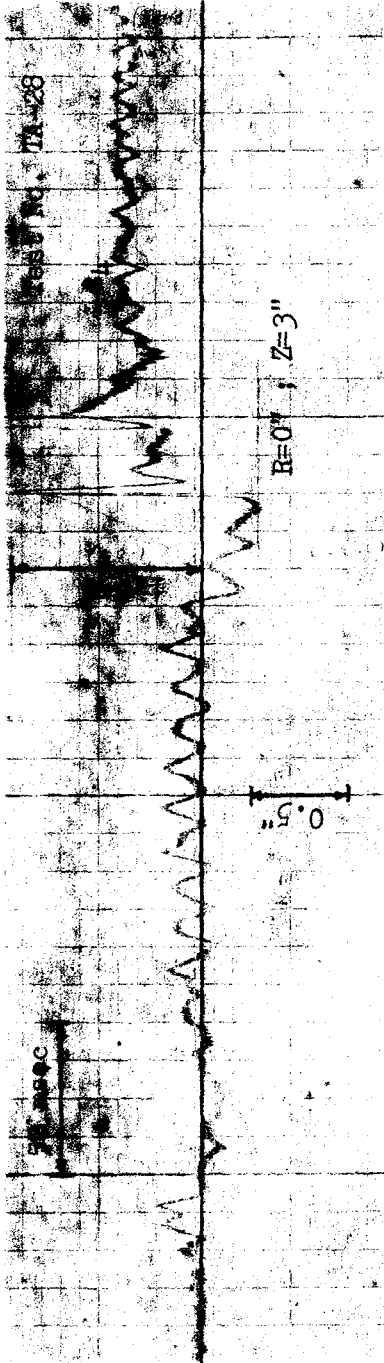


Figure 66. Strain-Time Traces on Axis of Symmetry at $Z = 3$ in.; 4 in.; (6 in. dia. circular footing)

and is shown in Fig. 67. Vertical strain distribution versus offset from the axis of symmetry for this footing was also drawn at various depths as shown in Fig. 68.

Stress-Strain Relations. Data was obtained by the stress and strain gages embedded at the same depth and same offset distance from the axis of the footing, but on opposite sides of the footing. Typical stress-strain and modulus-strain relationships constructed at two locations are shown in Figs. 69 and 70. These relationships corresponded to the peak values of the stress-time and strain-time traces which generally occurred in about 250 msec. It should be noted that these curves represent a one-dimensional stress-strain relationship. General characteristics of stress-time traces indicate that the time in which peak vertical stress occurs is very small, and in these experiments was found to be about 1 msec to 1.5 msec. During this period the stresses increased very rapidly from zero to their maximum values. Strains were relatively small with little yielding of the soil and there was no evidence of failure zones and volume contraction. Based on these observations, the soil behavior during this phase may be approximated as one-dimensional. The constrained modulus of the soil at various strain levels and at various locations can be computed by constructing similar graphs, as shown in Figs. 69 and 70. Methods for constructing these stress-strain relationships is well described by Landsman in his work³⁷.

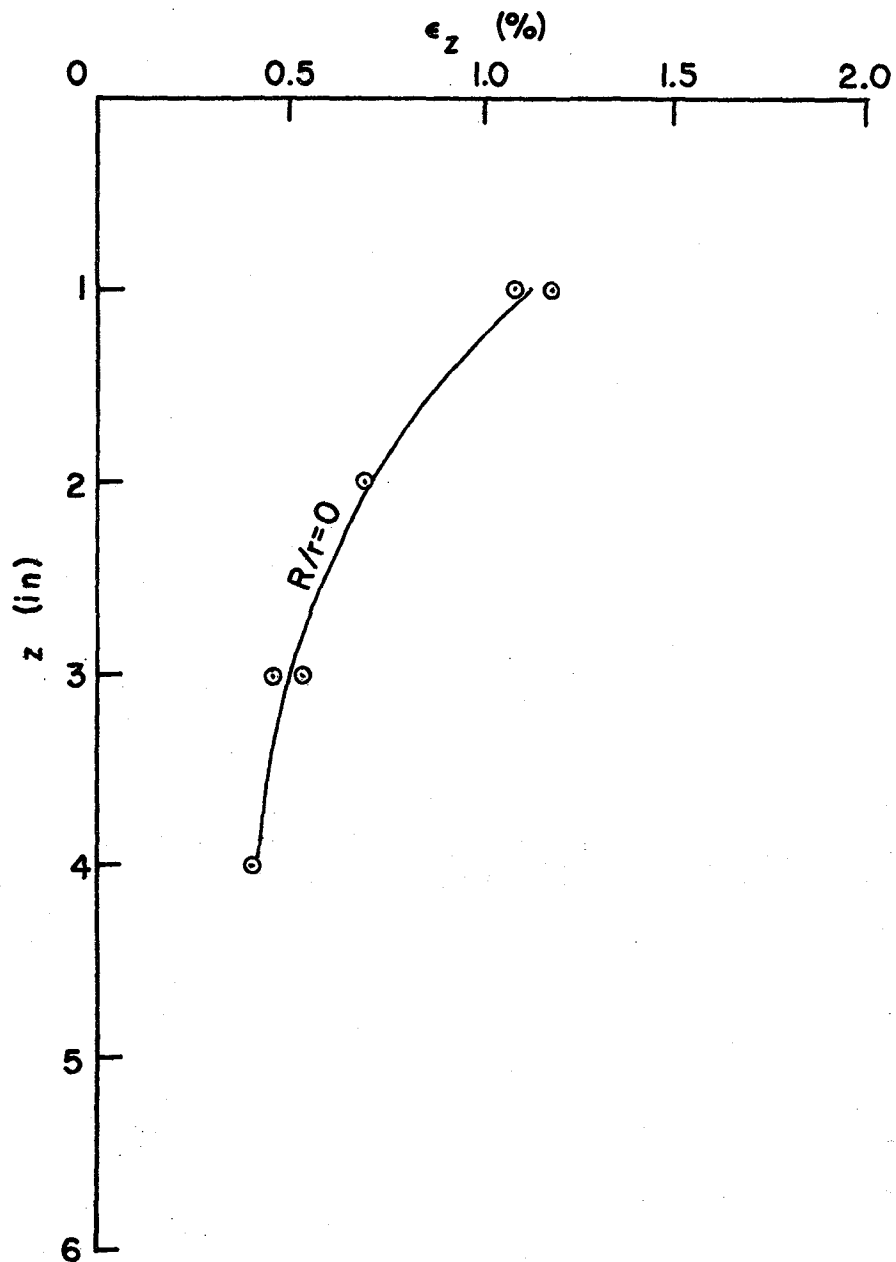


Figure 67. Vertical Strain Distribution With Depth on Axis of Symmetry for a 6 in. dia. Circular Footing

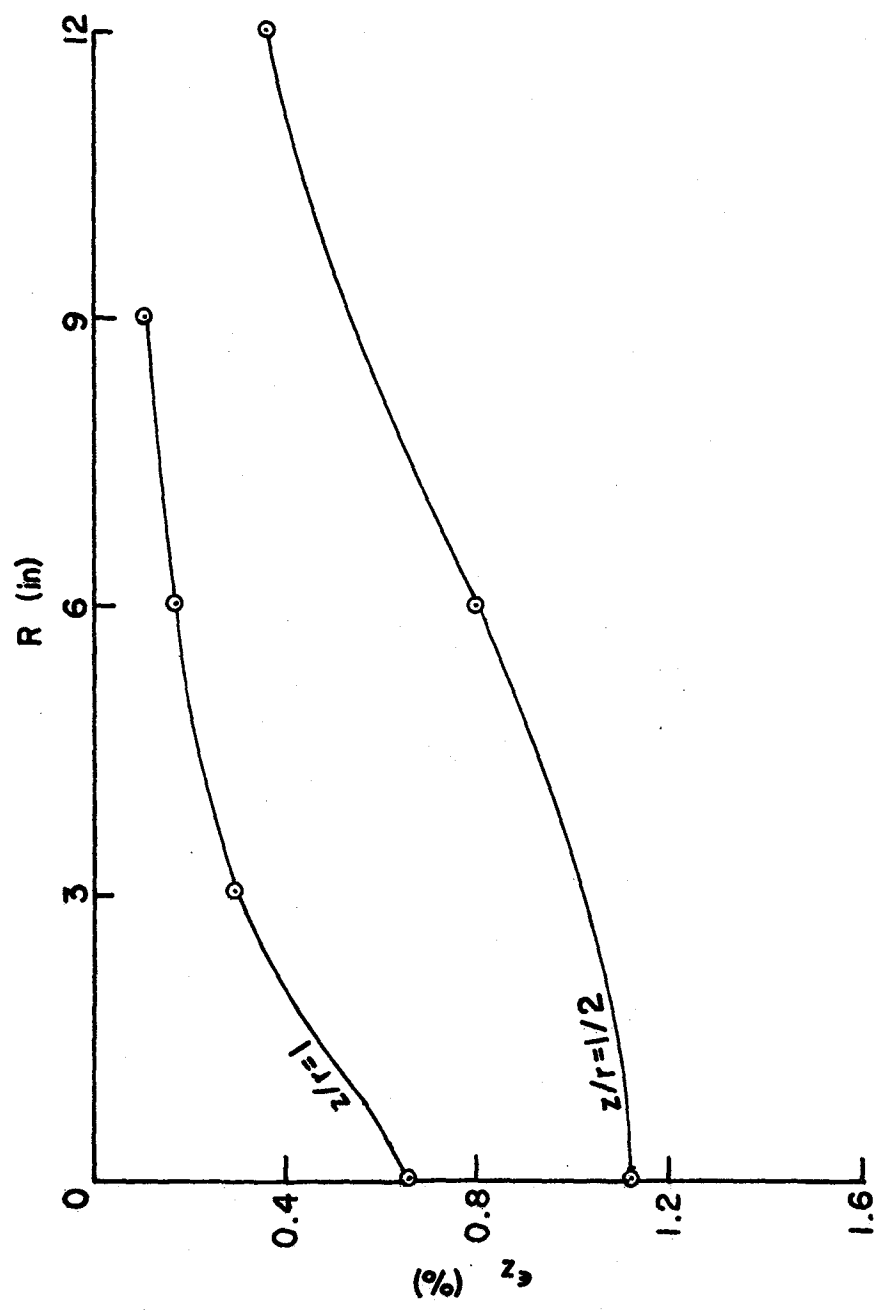


Figure 68. Vertical Strain Distribution vs Offset from Axis of Symmetry for a 6 in. dia. Circular Footing

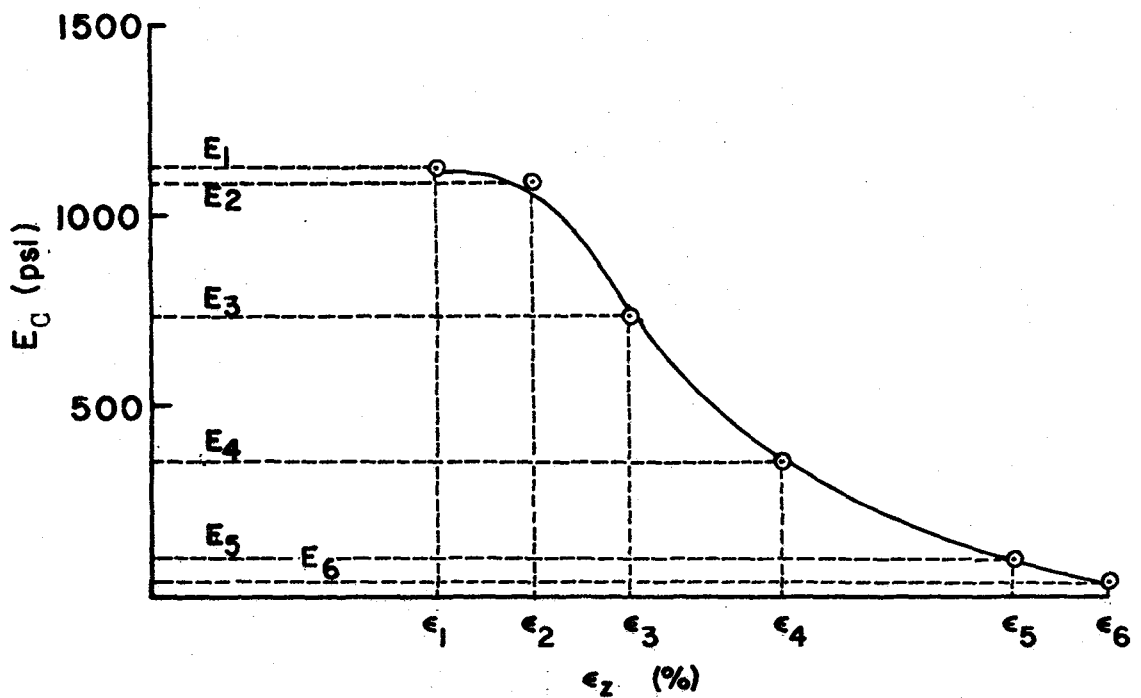
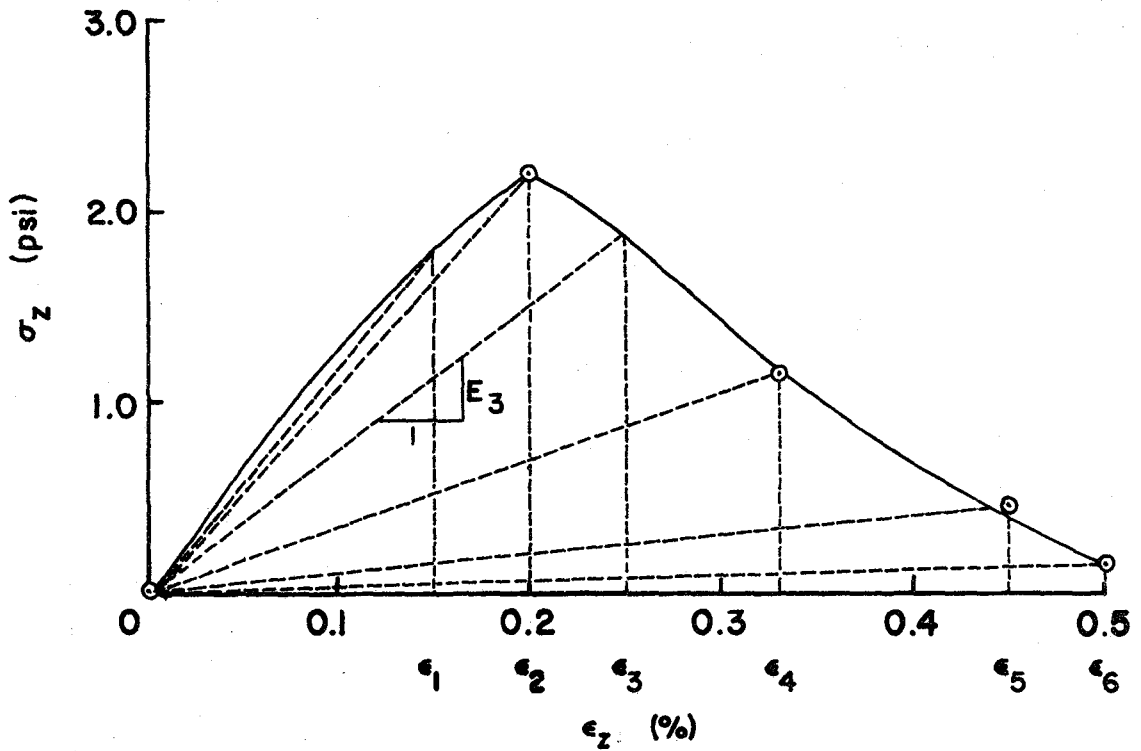


Figure 69. Modulus vs Strain Relationship at $Z/r = 1/2$;
 $R/r = 2$ (Test No. TA-61)

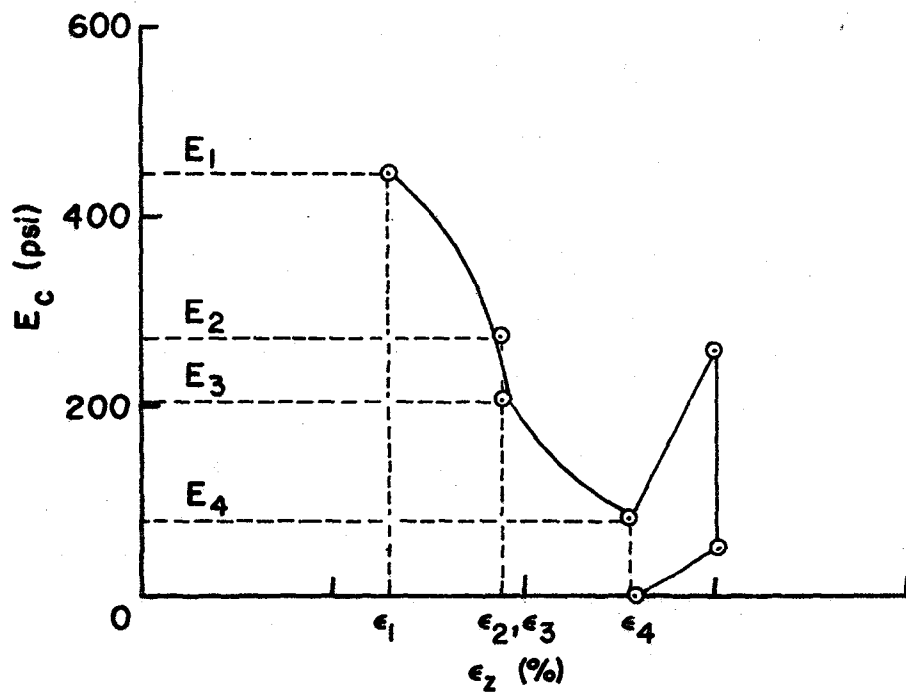
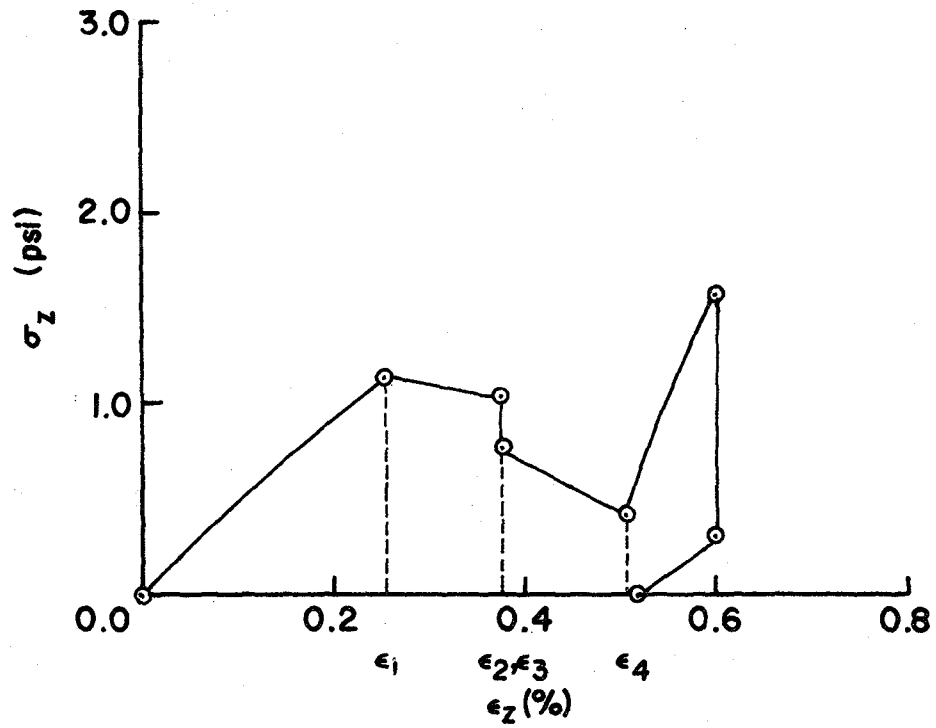


Figure 70. Modulus vs Strain Relationship at $Z/r = 1$; $R/r = 1$ (Test No. TA-111)

Depth of Burial

Stress-time measurements were made at various depths beneath the footing on the axis of symmetry, with the footing buried at various depths. Measurements were also made with a surcharge equivalent to the height of the footing. Tests were conducted with a 6 in. dia. circular footing ($\sigma_c = 0.55$ psi); and, other size footings were not included in this investigation. Typical stress-time traces on the axis of symmetry at various depths beneath the footing with a 2 in. thick surcharge around it are shown in Fig. 71. A similar set of stress-time traces for a surface footing are shown in Fig. 72. The traces, when the footing was buried at 2 in. depth, are shown in Fig. 73. Similarly Fig. 74 shows stress-time traces at various depths beneath the footing buried 4 in. from the surface. In the case of a footing buried at 6 in. depth, stress-time measurements were made at only two locations on the axis of symmetry as shown by the two traces in Fig. 75. General behavior of all these stress-time traces were similar to that of the acceleration-time traces of the footing. The data from these traces, shown in Figs. 71 through 75, was used to draw vertical stress distribution with depth on the axis of symmetry beneath the footing at various depth of burial. This relationship is shown in Fig. 76. From the data it was noticed that the vertical stress intensities in the vicinity of the footing increase as the depth of burial (depth of embedment) increases (as the distance from the transient load source decreases).



Reproduced from
best available copy.

Figure 71. Vertical Stress-Time Traces on Axis of Symmetry at Various Depths for a 6 in. dia. Circular Footing With 2 in. Surcharge

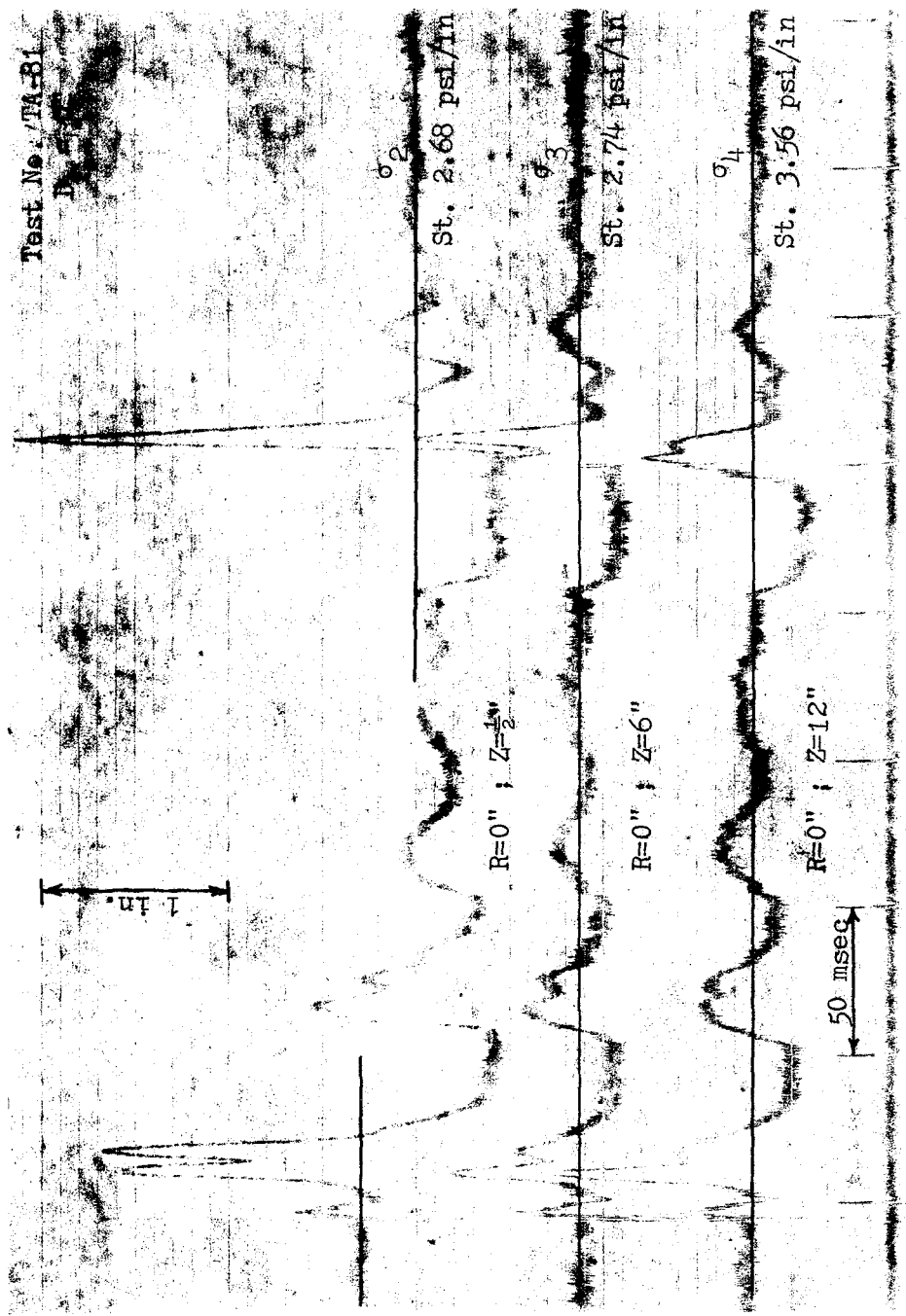


Figure 72. Vertical Stress-Time Traces on Axis of Symmetry at Various Depths for a 6 in. dia. Circular Footing on the Surface of a Soil Media

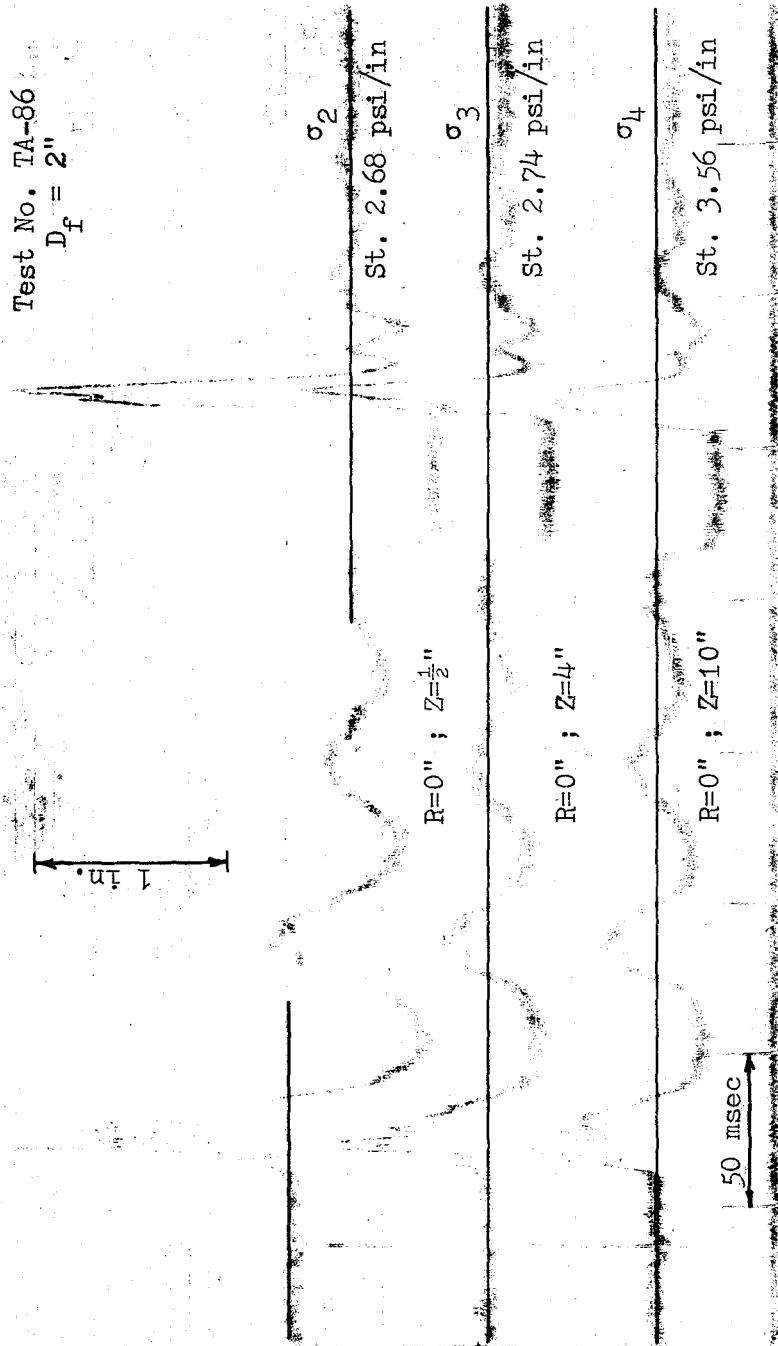


Figure 73. Vertical Stress-Time Traces on Axis of Symmetry at Various Depths for a 6 in. dia. Circular Footing Buried at 2 in. Depth

Test No. TA-91

$D_f = 4''$

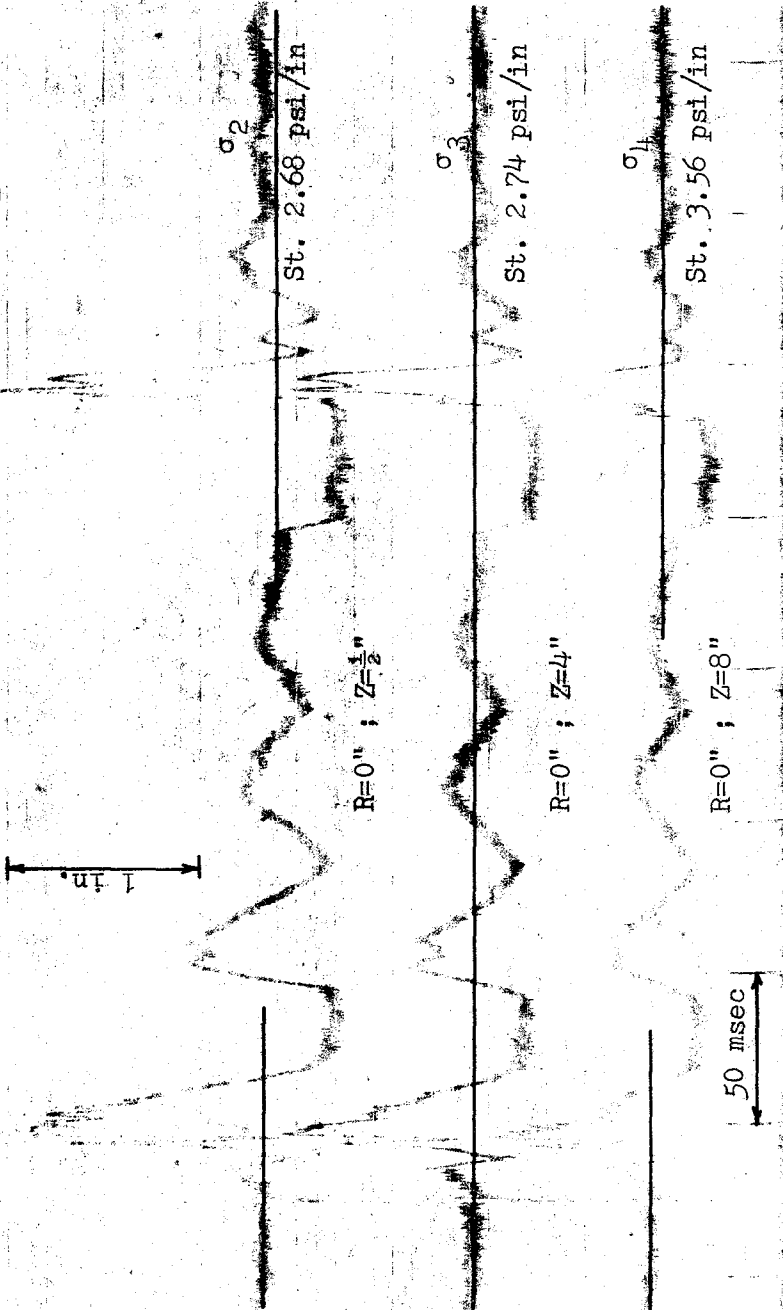


Figure 74. Vertical Stress-Time Traces on Axis of Symmetry at Various Depths for a 6 in. dia. Circular Footing Buried at 4 in. Depth

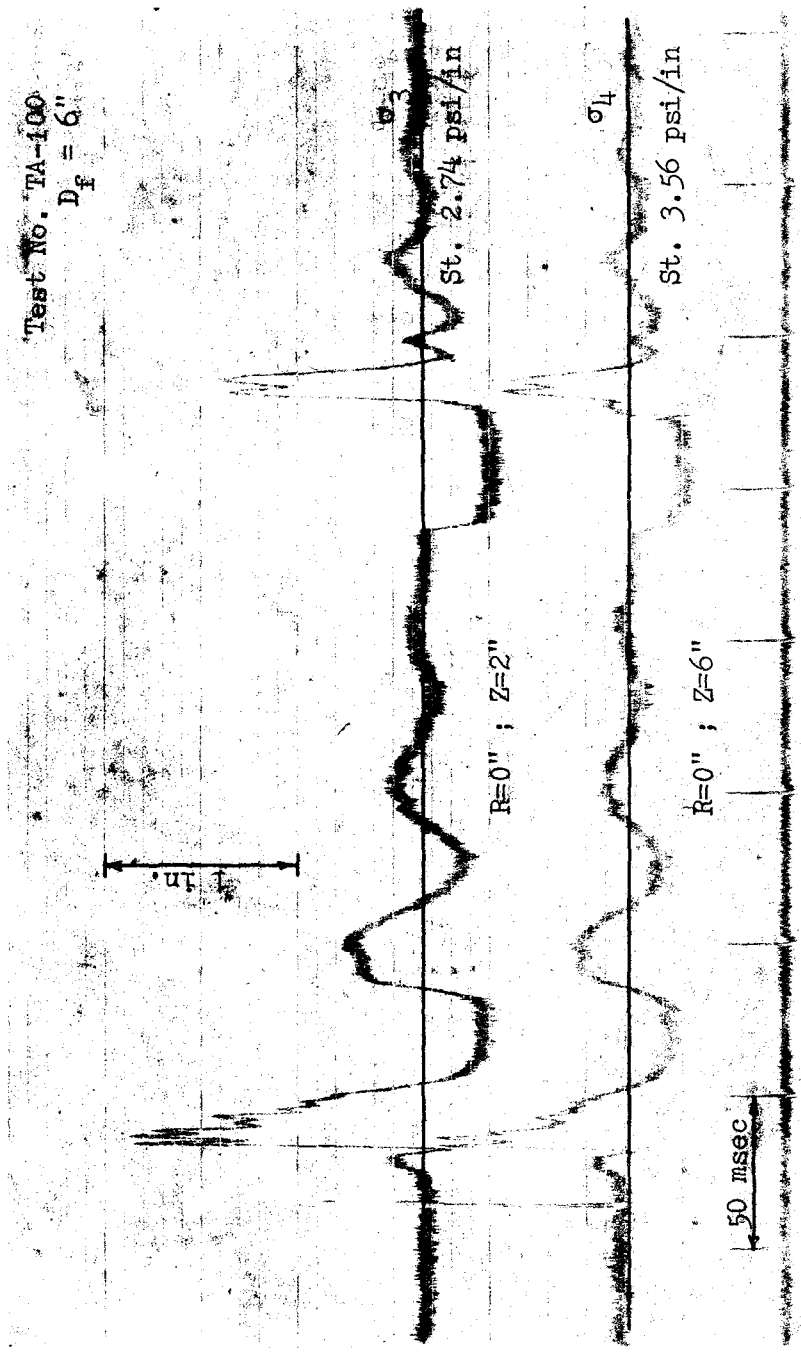


Figure 75. Vertical Stress-Time Traces on Axis of Symmetry at Various Depths for a 6 in. dia. Circular Footing Buried at 6 in. Depth

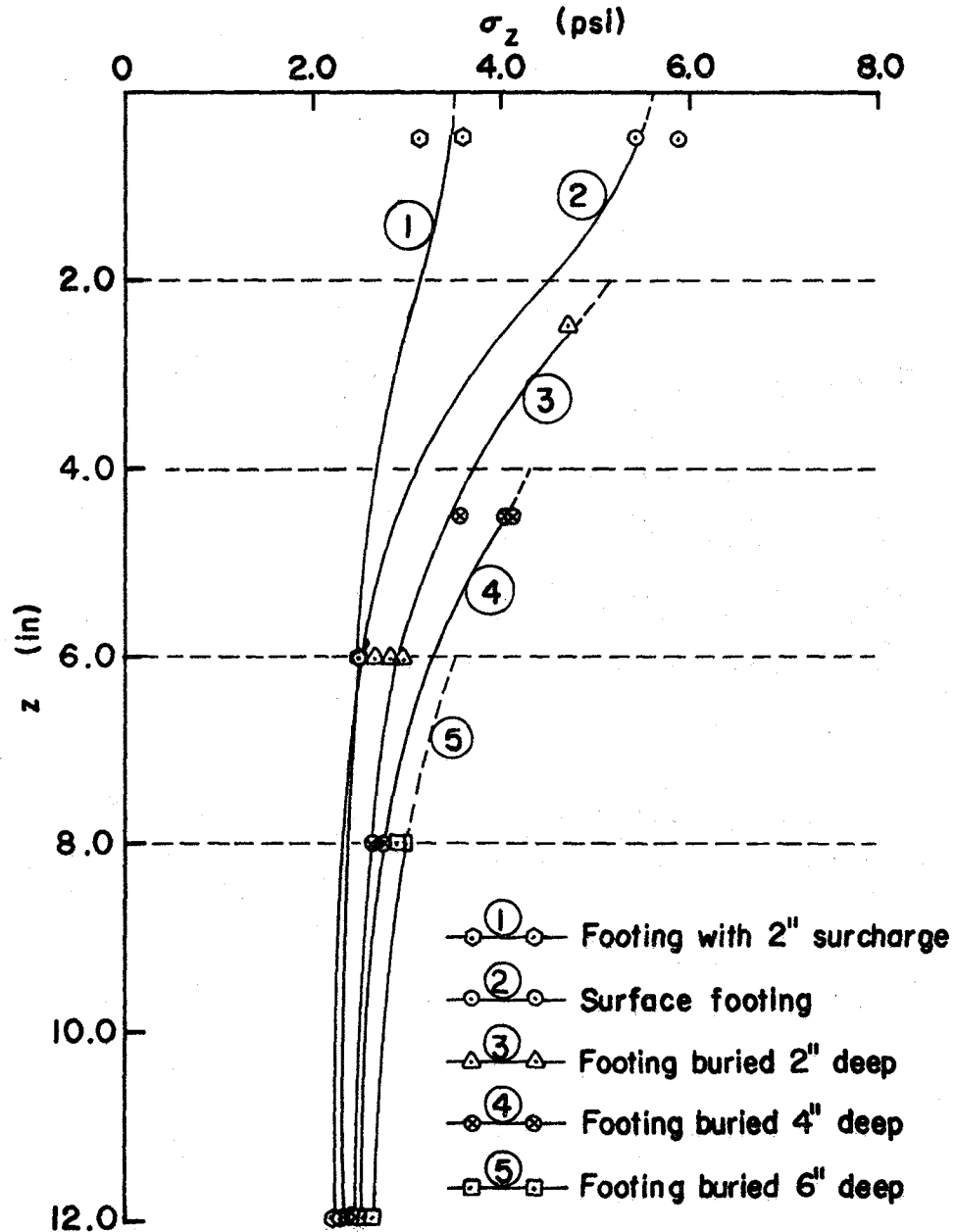


Figure 76. Attenuation of Peak Vertical Stress With Depth on Axis of Symmetry for a 6 in. dia. Circular Footing at Different Depths of Burial

Acceleration-time traces for the footing were also recorded at the same time as the stress-time traces were recorded, in the tests described in the preceding paragraph. Typical acceleration-time traces for this footing at various depths of burial (embedment) are shown in Figs. 77 through 80. The data from these figures was combined to obtain a relationship between the deceleration of the footing and depth of burial (embedment). This relationship is shown in Fig. 81. As shown in Fig. 81, deceleration amplitude of the footing decreased linearly with depth of burial (embedment) of the footing, thus indicating greater damping. This is in agreement with other investigations. Whitman and Richart⁷⁹ have included some references on tests of footings partially embedded as well as for footings at the surface. They stated that the partial embedment reduces the magnitude of motions at the resonant peaks.

The relationship shown in Fig. 81 is also justified by the fact that embedment increases the stiffness of the system. The increase in stiffness comes from three sources⁴⁶: (1) resistance to deformation due to the embedment; (2) side friction between the soil and the foundation; and, (3) increased soil stiffness due to the confinement (overburden).

Lysmer and Kuhlemeyer⁴³ used a finite element technique to study the effect of embedment of a circular footing on the dynamic soil response. Their results indicated that the effect of embedment is to increase the resonant frequency and to decrease the dynamic amplification at resonance.

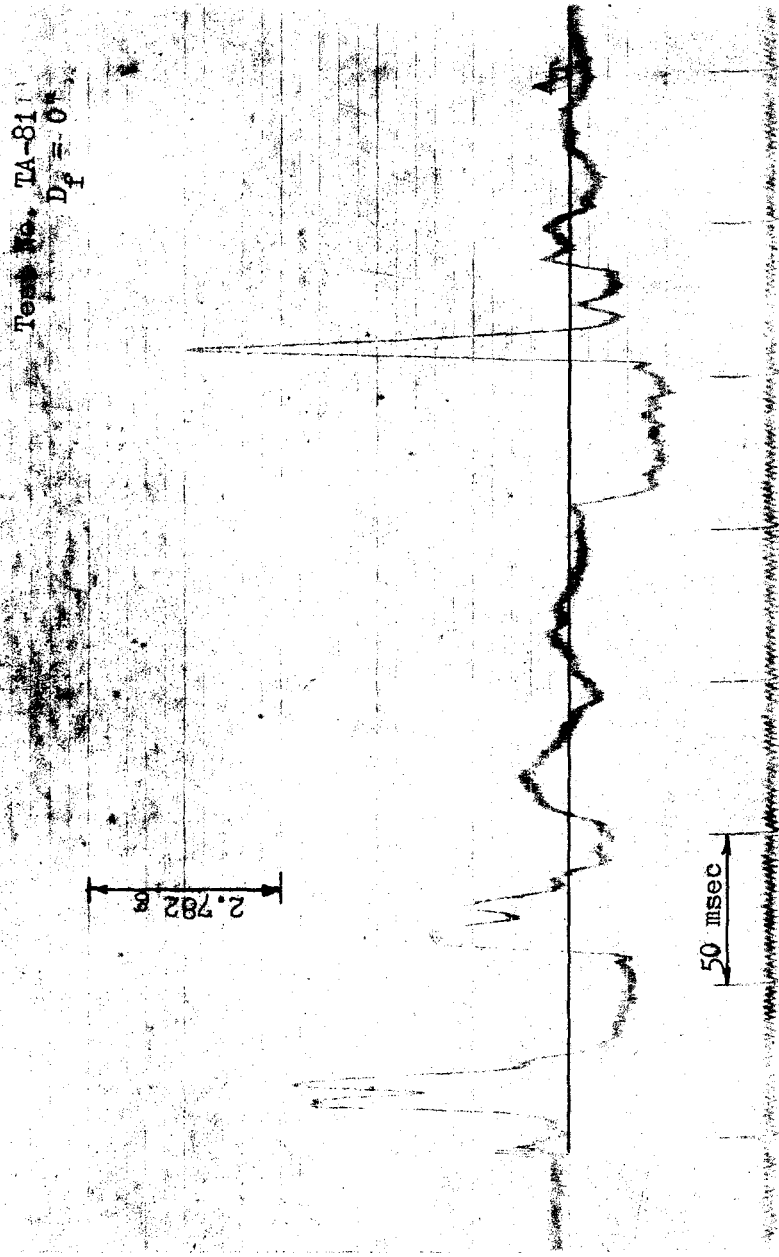
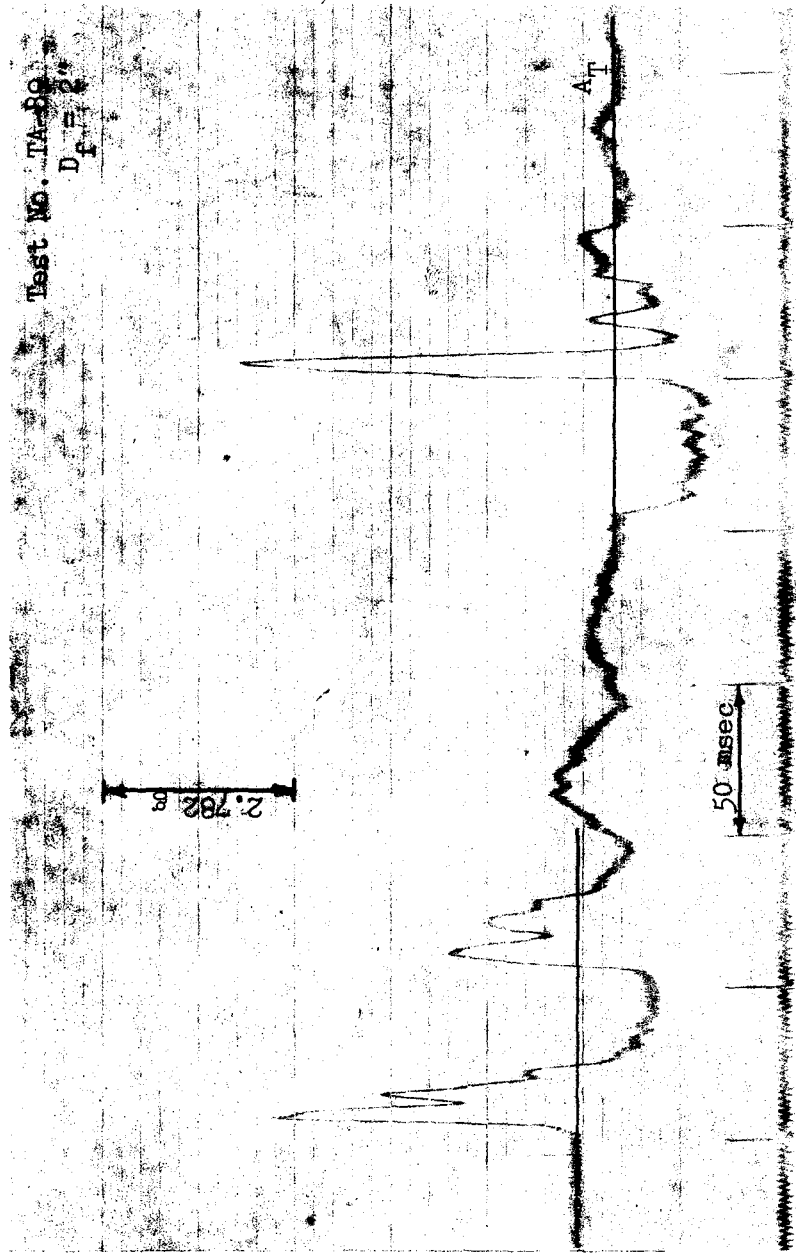


Figure 77. Acceleration-Time Trace for a 6 in. dia. Circular Footing on the Surface of a Soil Media in the Vessel



Reproduced from
best available copy.



Figure 78. Acceleration-Time Trace for a 6 in. dia. Circular Footing Buried at 2 in. Depth

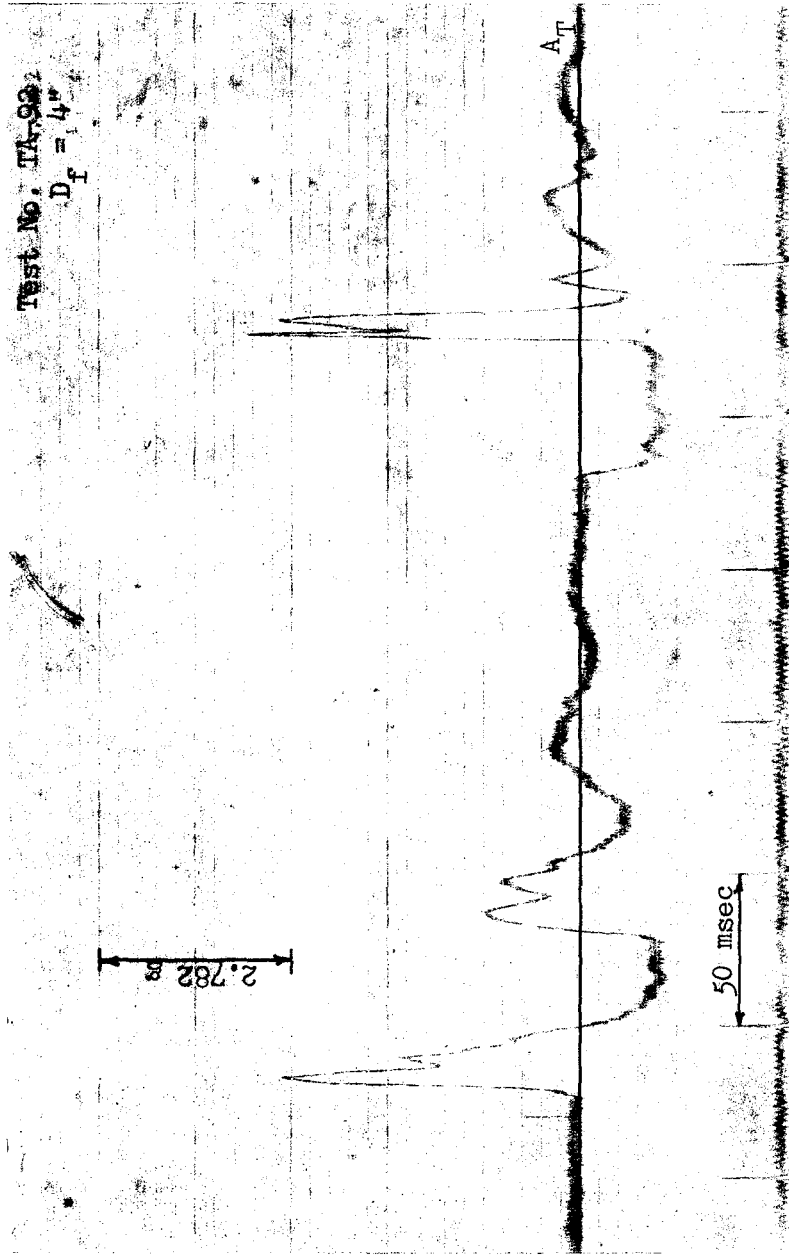


Figure 79. Acceleration-Time Trace for a 6 in. dia. Circular Footing Buried at 4 in. Depth

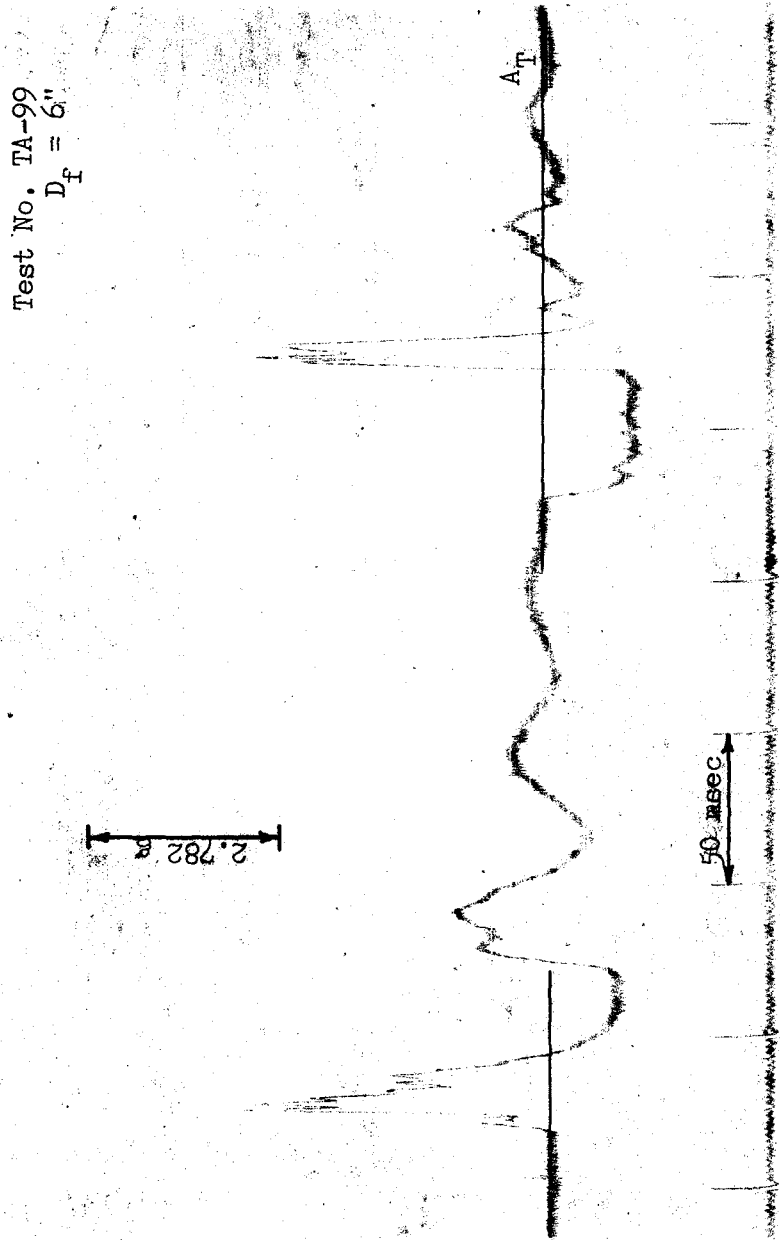


Figure 80. Acceleration-Time Trace for a 6 in. dia. Circular Footing Buried at 6 in. Depth

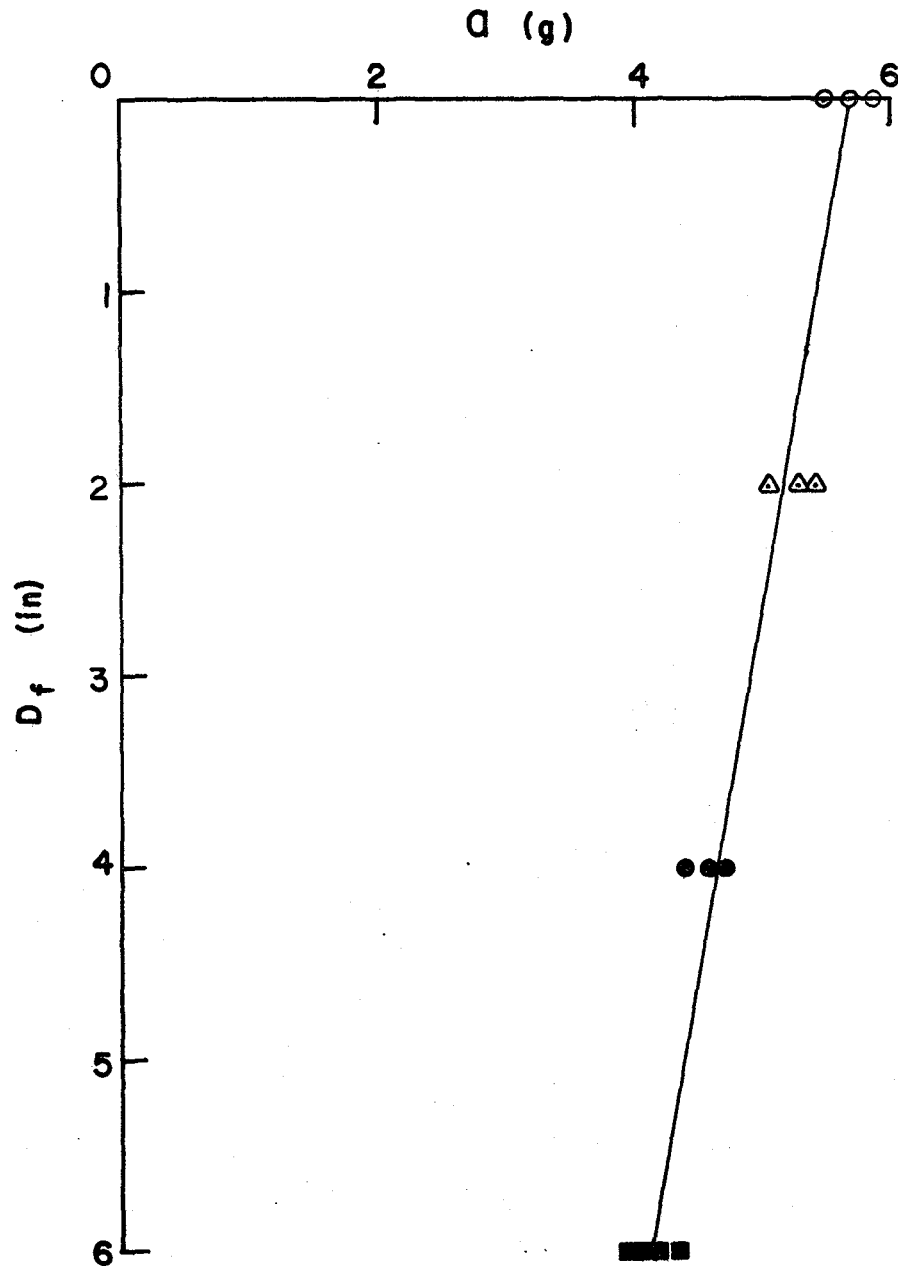


Figure 81. Deceleration of Footing vs Footing Depth from the Surface of the Soil Media for a 6 in. dia. Circular Footing

Valliappan, Favaloro and White⁷⁰ considered a rigid strip footing resting on an isotropic and homogeneous soil mass vertically excited by a harmonic force in the axis of symmetry. They used a finite element mesh for this model. They concluded that, for increasing embedment of footing, there is a reduction in the vibration amplitude because of the apparent increase in soil stiffness, and not the damping characteristics of the system.

Footing Isolation

In the past, various isolation techniques have been used for the earthquake problem to reduce the effect of transient loadings on the structure. Review of related studies on this subject is presented in Chapter II. A passive isolation technique was used in this investigation. For this purpose four sponge materials and a rubber material having different compressible characteristics were used. These compressible materials were of the same size as the footing (6 in. dia. circular) and their thicknesses varied from 1/4 in. to 1/2 in. Static compression tests were conducted on these materials, and stress versus deformation relationships were obtained, as shown in Figs. 82 and 83. The same relationships under loading and unloading conditions are shown in Figs. 114 through 118 (see Appendix C). Using these relationships, subgrade modulus (K_c) of each compressible material at static contact stress ($\sigma_c = 0.55$ psi) level was computed. For example:

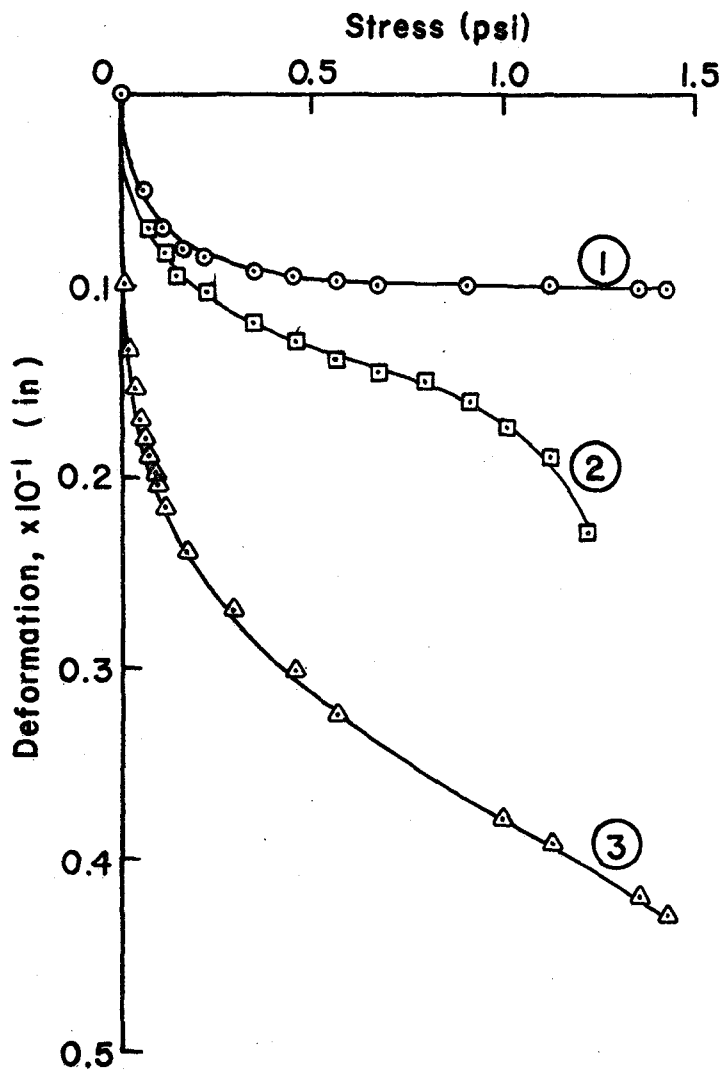


Figure 82. Stress vs Deformation for Compressible Materials M_1, M_2, M_3

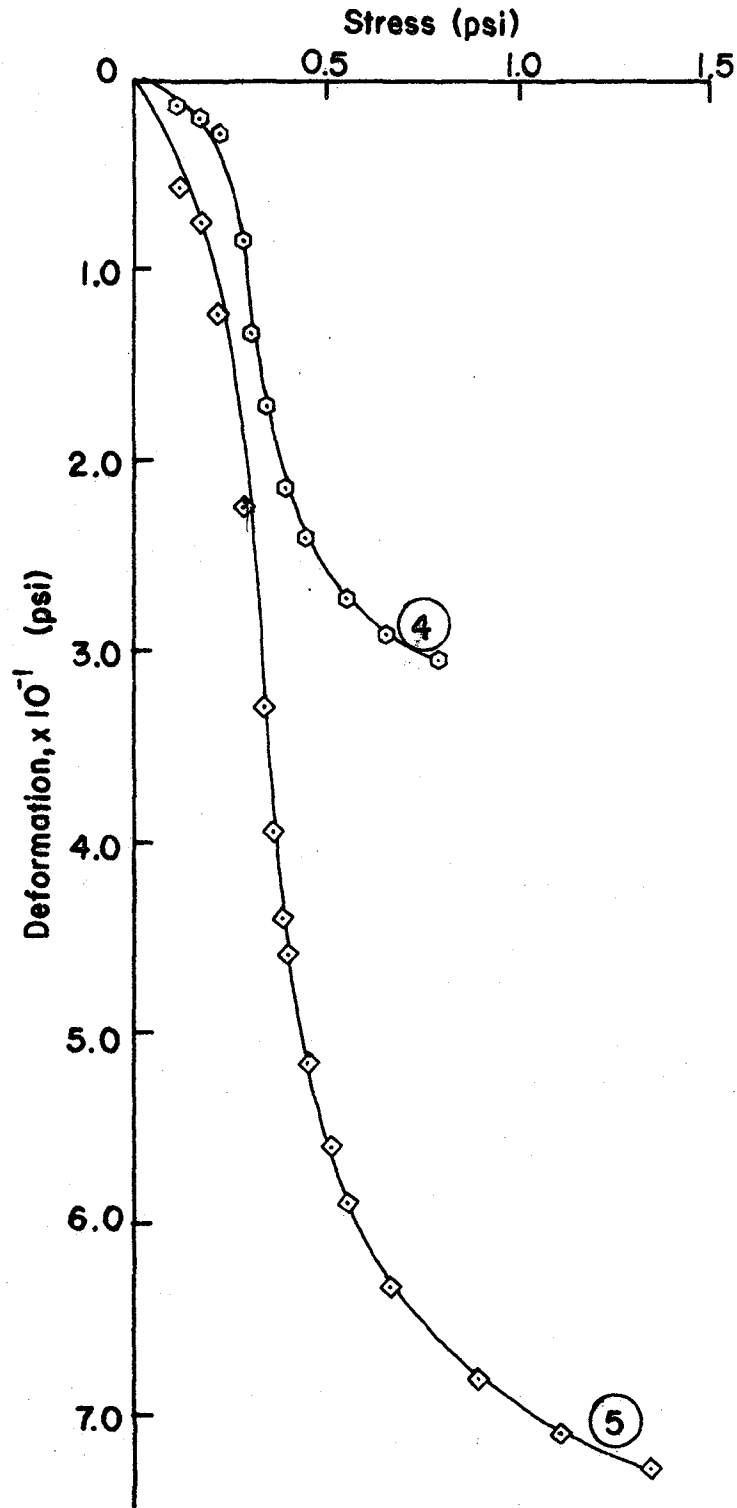


Figure 83. Stress vs Deformation for Compressible Materials
 M_4, M_5

K_c = [static contact stress/deformation corresponding to the static contact stress], (psi/in).

Acceleration-time response of the footing was recorded with a footing (6 in. dia. circular) on the surface, but without any compressible material buried in the soil. The acceleration-time trace corresponding to this is shown in Fig. 84, and, is used as a reference for the other tests conducted under identical test conditions, but with a compressible material buried at one radius depth. A series of dynamic tests were conducted with a compressible material buried beneath the footing at a depth of one radius. A compressible material M_1 placed in position at this depth is shown in Fig. 85. Acceleration-time traces corresponding to the five compressible materials are shown in Figs. 86 through 90. Percentage reduction in deceleration (R_a) of the footing was computed for each case. For example:

$$R_a = 100 \left[\frac{\text{deceleration of the footing without any compressible material buried in the soil} - \text{deceleration of the footing with a compressible material buried in the soil}}{\text{deceleration of the footing without any compressible material buried in the soil}} \right]$$

These R_a values were plotted against the K_c values and a relationship was obtained as shown in Fig. 91. These values were again used to draw R_a versus $\log K_c$ plot and a straight line relationship was obtained, as shown in Fig. 92.

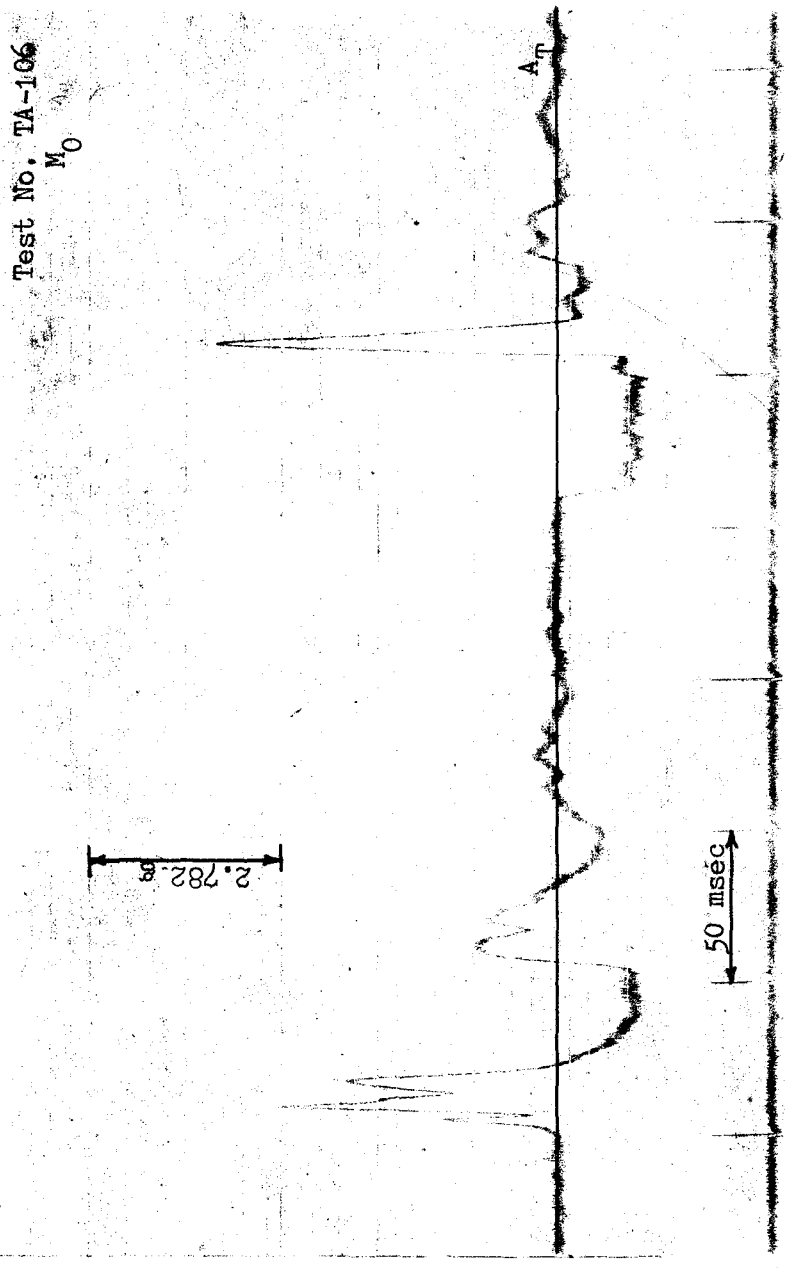


Figure 84. Acceleration-Time Trace for a 6 in. dia. Circular Footing on the Surface Without Any Compressible Material in the Soil Media

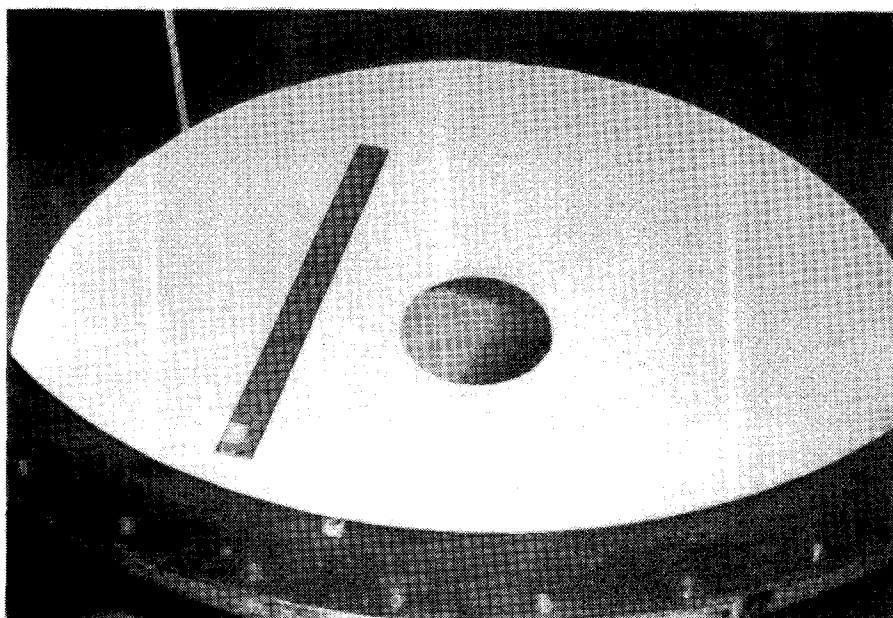


Figure 85. A Compressible Material M_1 Placed in Position at a Depth $Z/r = 1$ Before Being Buried in the Sand

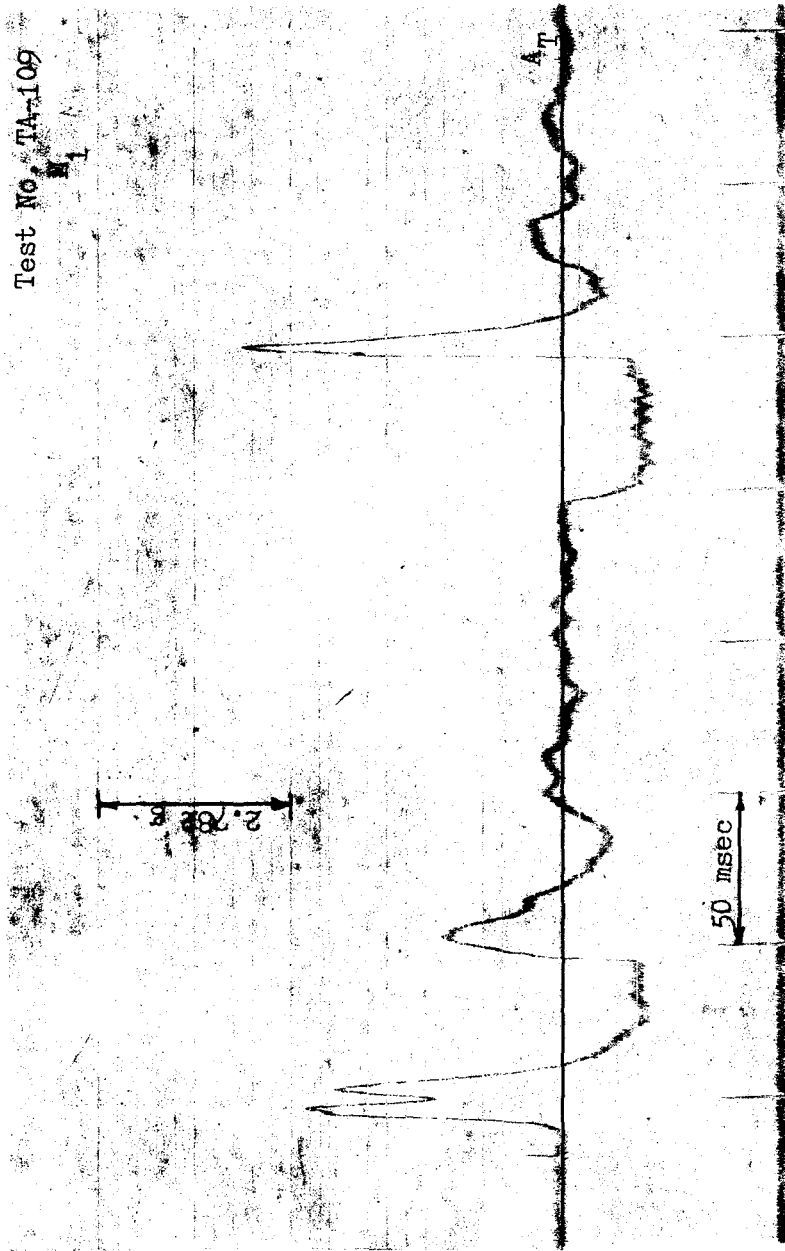


Figure 86. Acceleration-Time Trace for a 6 in. dia. Circular Footing With a Compressible Material M_1 Buried at $R/r = 0$; $Z/r = 1$

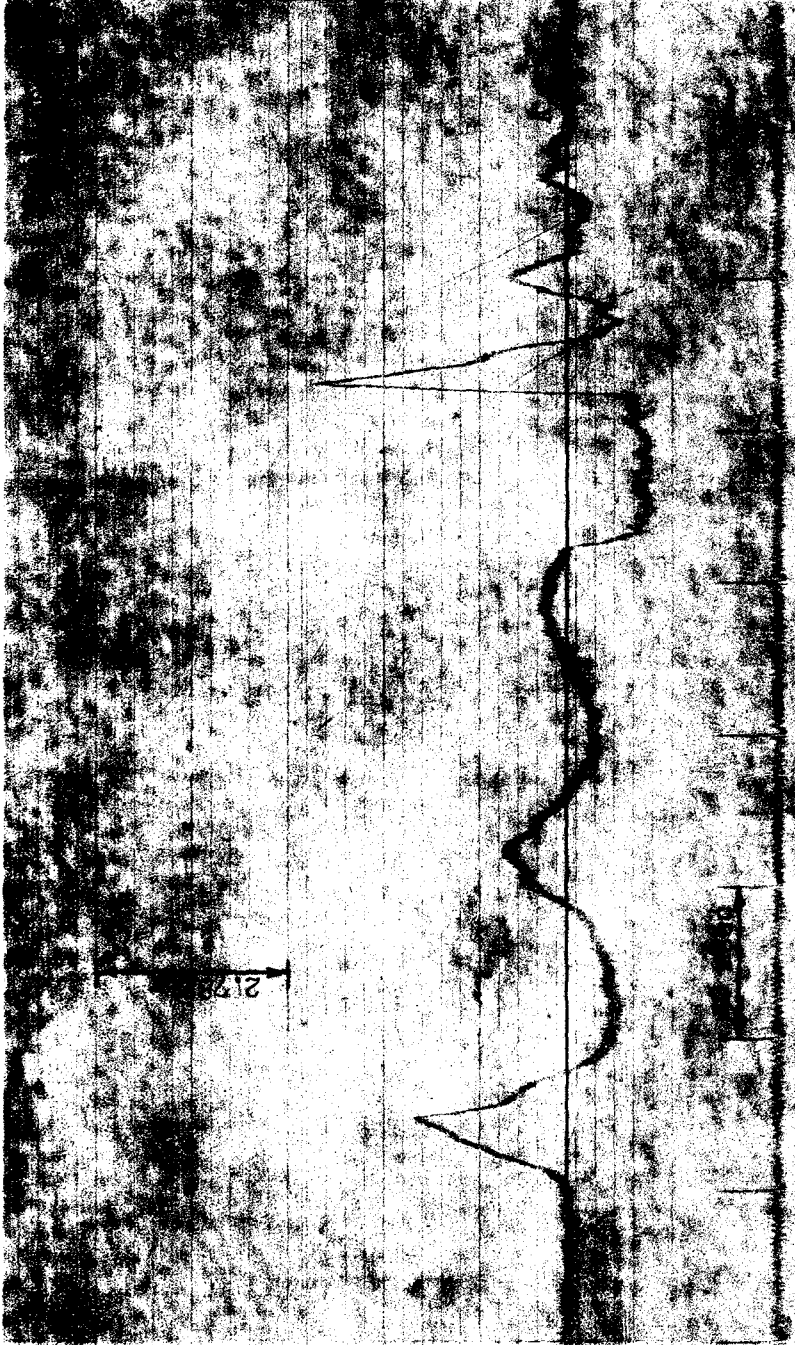


Figure 37. Acceleration-Time Trace for a 6 in. dia. Circular Footing With a Compressible Material M_2 Buried at $R/r = 0$; $Z/r = 1$

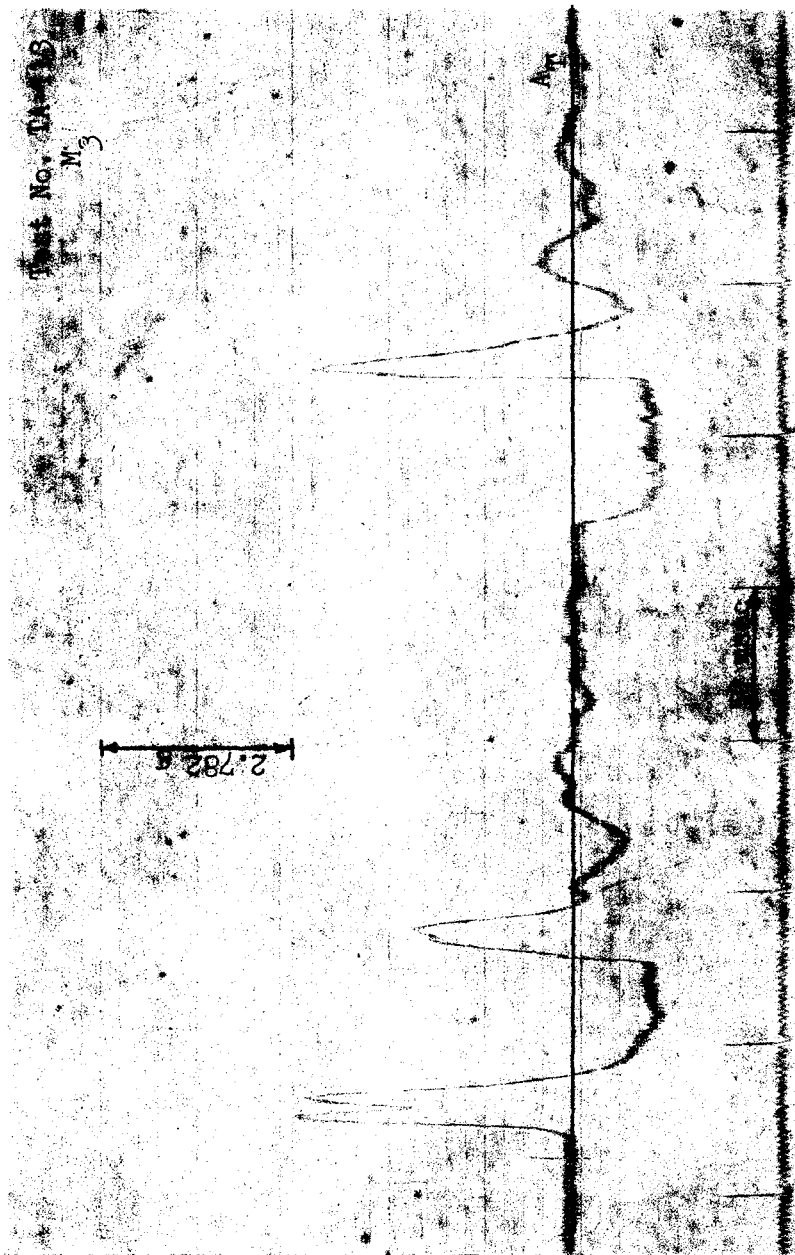


Figure 88. Acceleration-Time Trace for a 6 in. dia. Circular Footing With a Compressible Material M₃ Buried at R/r = 0; Z/r = 1

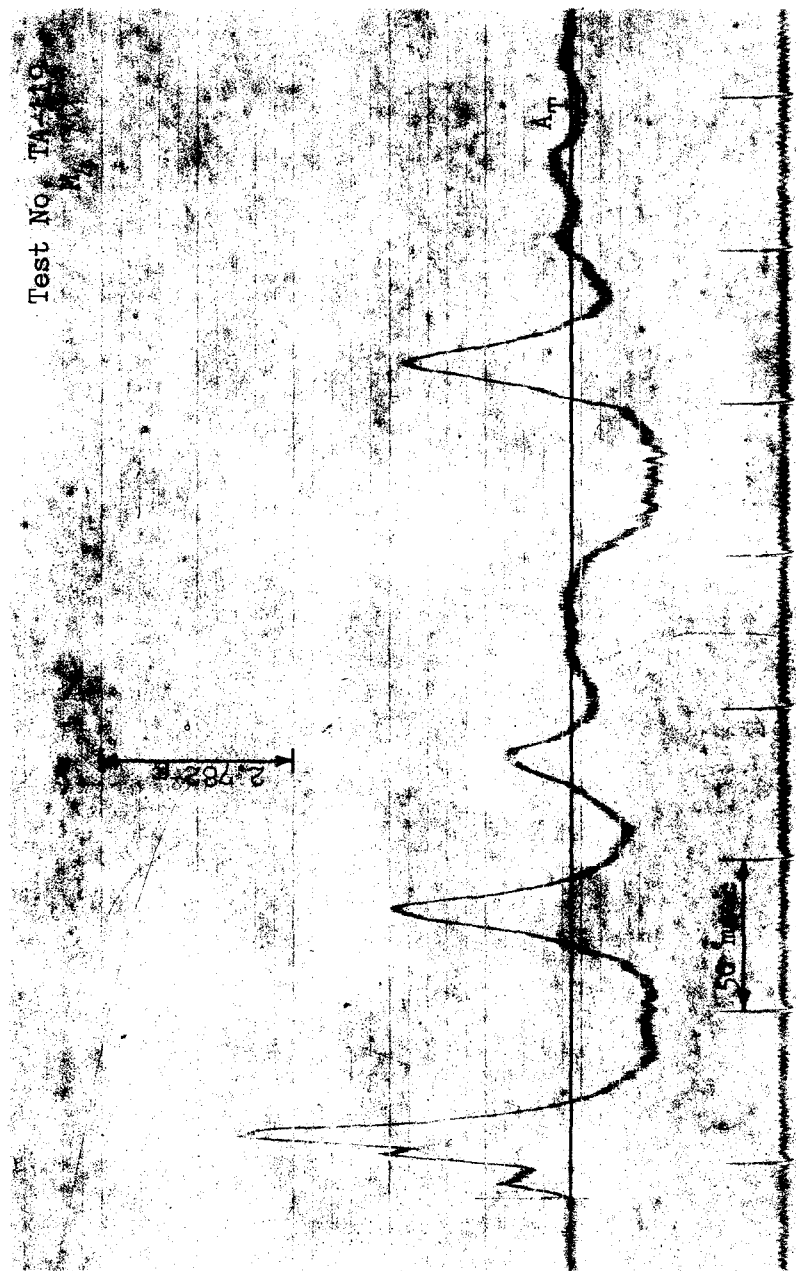


Figure 39. Acceleration-Time Trace for a 6 in. dia. Circular Footing With a Compressible Material M_4 Buried at $R/r = 0$; $Z/r = 1$

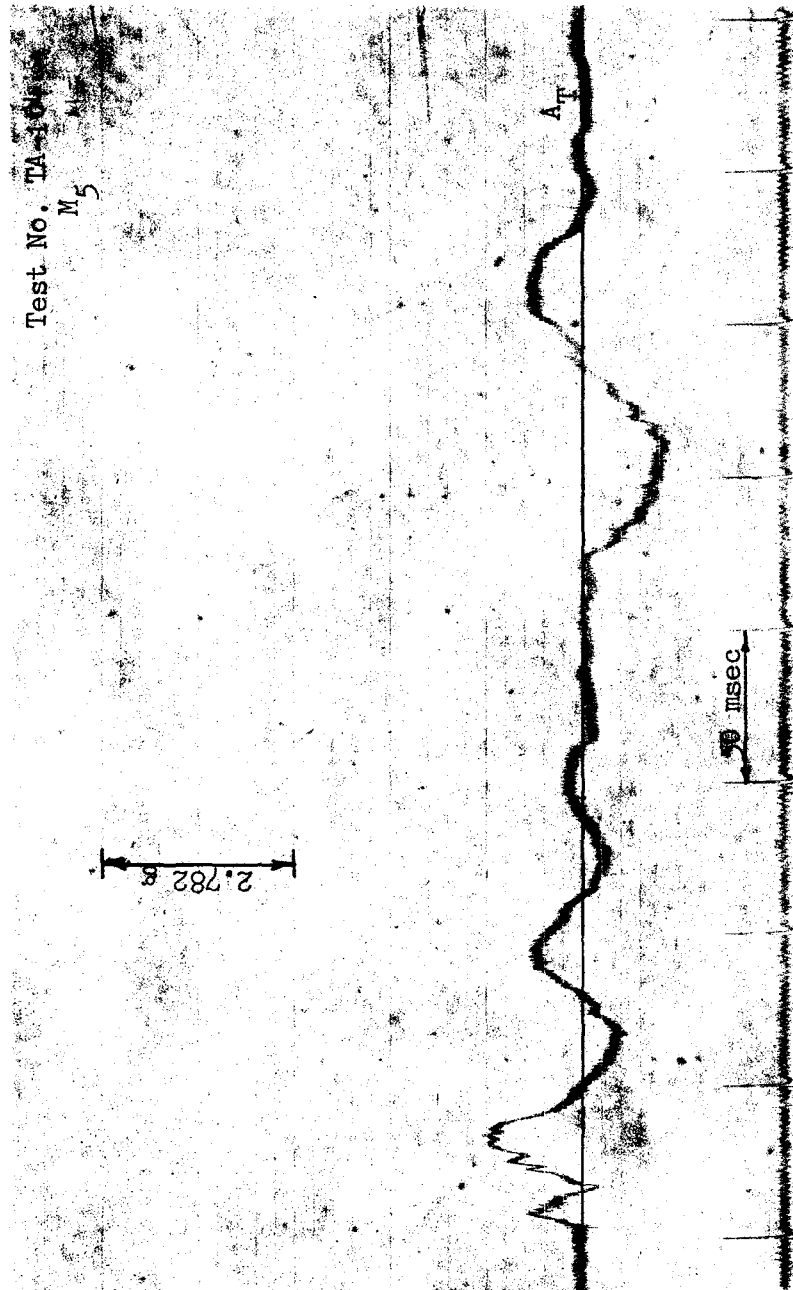


Figure 90. Acceleration-Time Trace for a 6 in. dia. Circular Footing With a Compressible Material M₅ Buried at R/r = 0; Z/r = 1

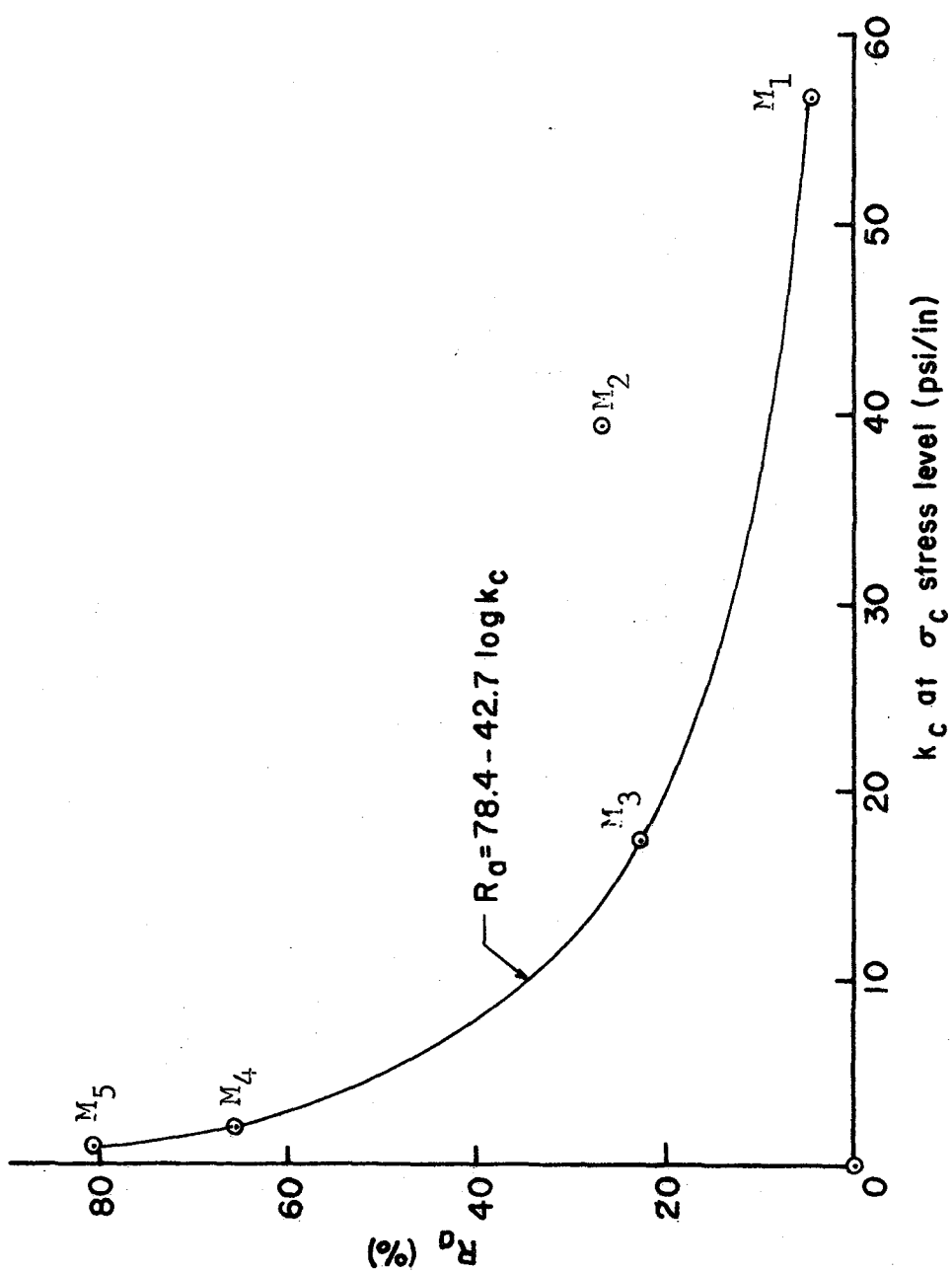


Figure 91. Deceleration Reduction vs Subgrade Modulus of Compressible Material

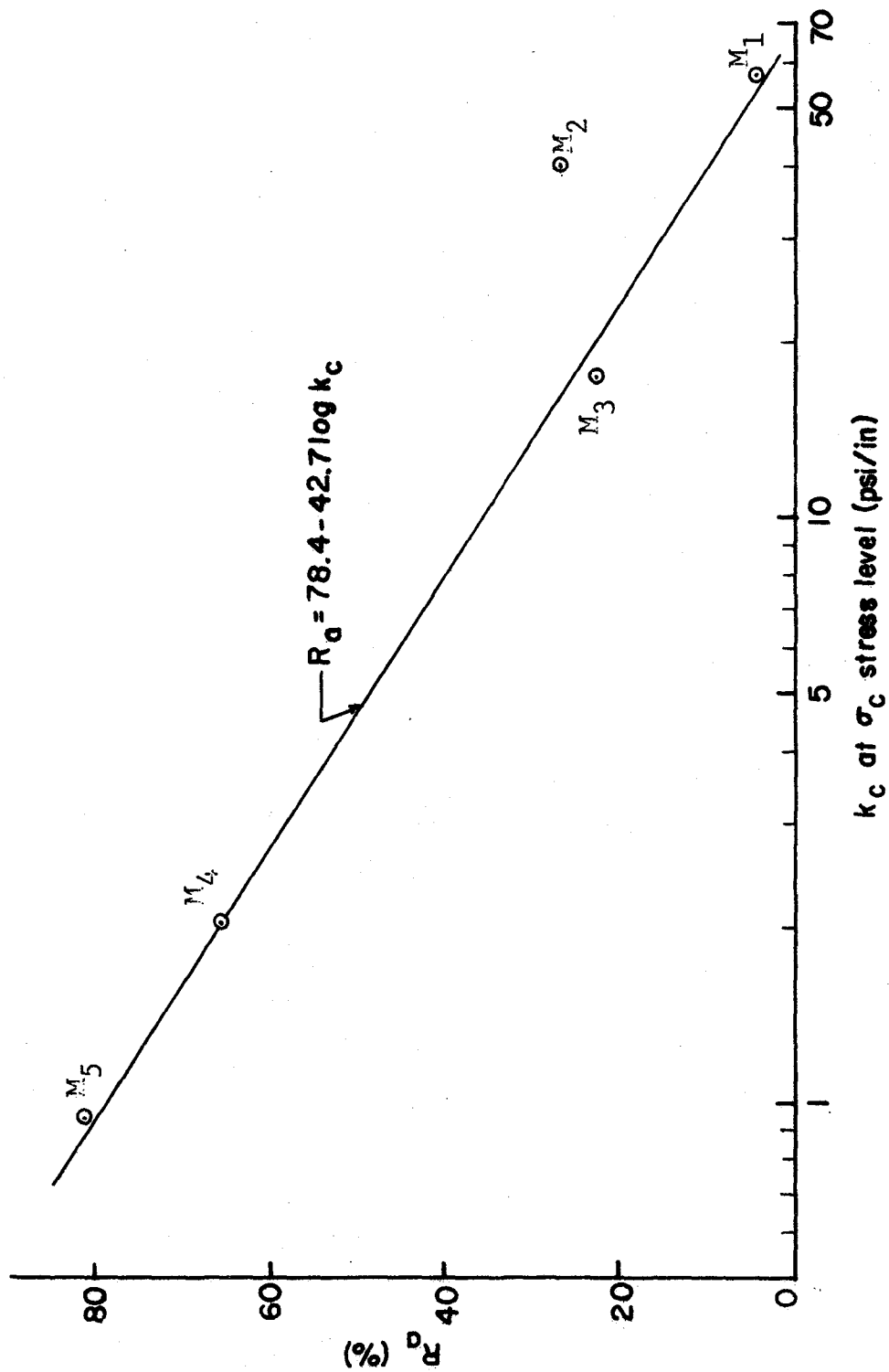


Figure 92. Deceleration Reduction vs Log of Subgrade Modulus of Compressible Material

This straight line relationship is also represented by the equation $R_a = 78.4 - 42.7 \log K_c$. In a generalized form this can be expressed as $R_a = A_1 - A_2 \log K_c$, where A_1 and A_2 are constants.

As shown in Figs. 91 and 92 there is a slight deviation of a value corresponding to the compressible material designated as M_2 . This may be due to the fact that the size of voids in this sponge material M_2 were slightly bigger than the size of the sand particles. Therefore, when a transient load was applied, a stress wave was generated and travelled in a direction perpendicular to the plane of the compressible material buried in the sand. Some sand particles were penetrated into the voids of the sponge material. Thus the actual compressible characteristics of this material were not fully mobilized.

Stress-time trace of a stress gage embedded at $R/r = 0$; $Z/r = 1/2$ and without any compressible material buried in the soil is shown in Fig. 93. Stress-time measurements were also made with the stress gage embedded in the soil at mid-depth between the bottom of the footing and the compressible material (i.e., at $R/r = 0$; $Z/r = 1/2$). Stress-time traces were recorded each time a test was run with a compressible material buried in the soil. These stress-time traces are shown in Figs. 94 through 98. The stress-time histories indicated that there is a considerable amount of peak vertical stress reduction by the presence of a compressible material buried in the soil, which damped out some of the



Figure 93. Stress-Time Trace at $R = 0$ in.; $Z = 1-1/2$ in (6 in. dia. circular footing on the surface)

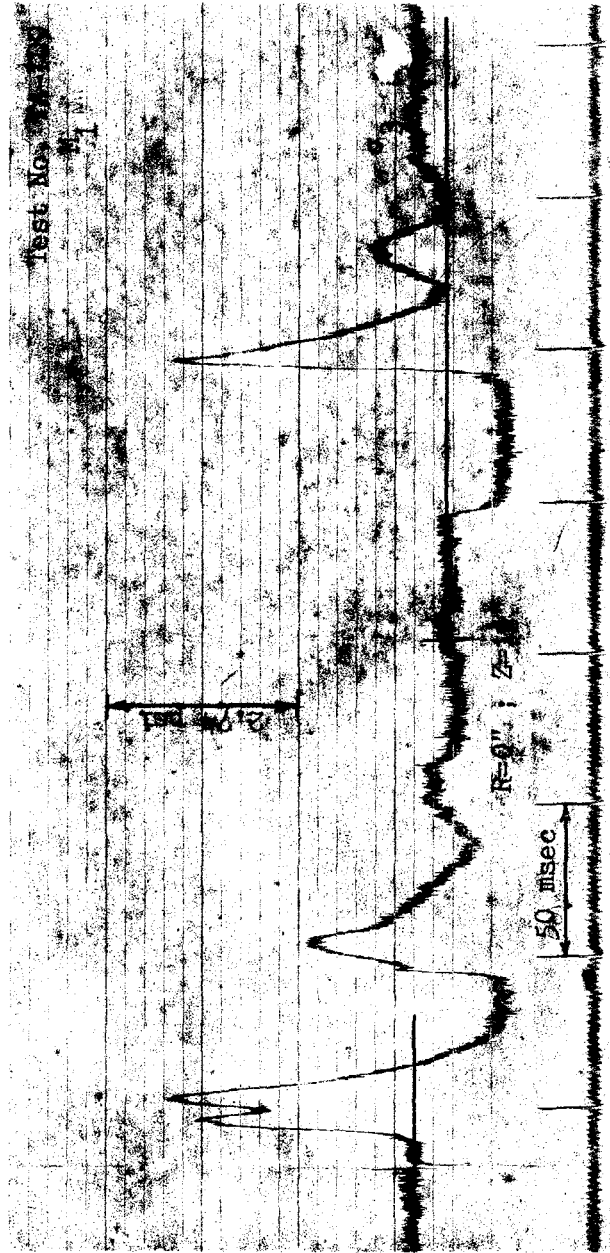


Figure 94. Stress-Time Trace at $R/r = 0$; $Z/r = 1/2$ With a Compressible Material M_1 Buried at $R/r = 0$; $Z/r = 1$ (6 in. dia. circular footing on the surface)

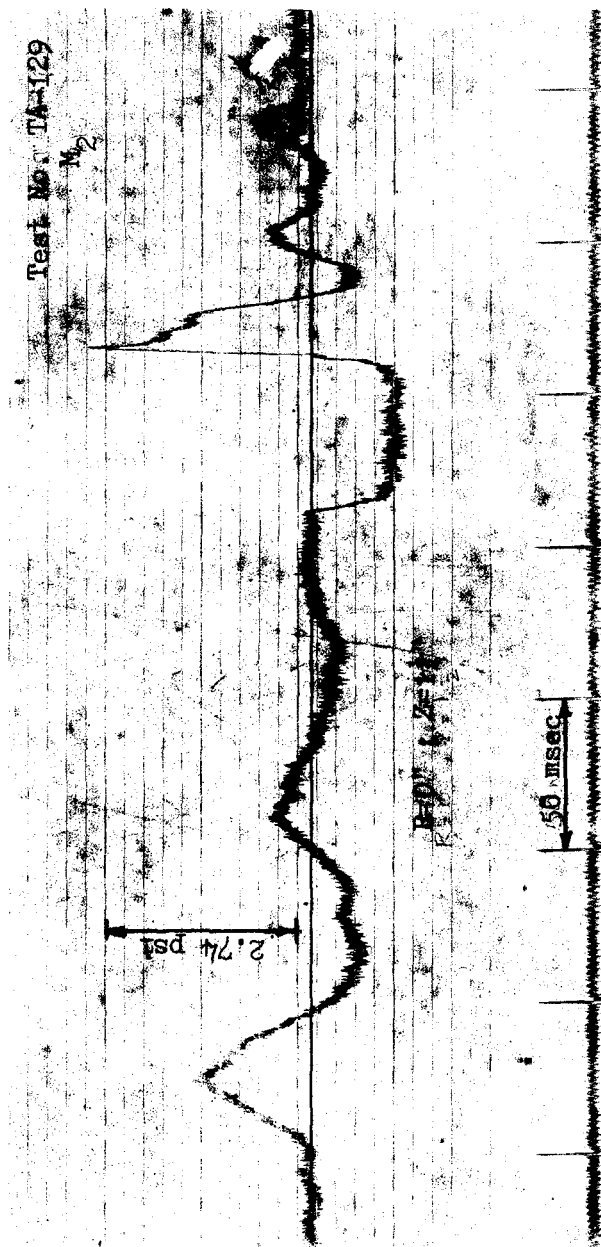


Figure 95. Stress-Time Trace at $R/r = 0$; $Z/r = 1/2$ With a Compressible Material M_2 Buried at $R/r = 0$; $Z/r = 1$ (6 in. dia. circular footing on the surface)



Figure 96. Stress-Time Trace at $R/r = 0$; $Z/r = 1/2$ With a Compressible Material M_3 Buried at $R/r = 0$; $Z/r = 1$ (6 in. dia. circular footing on the surface)

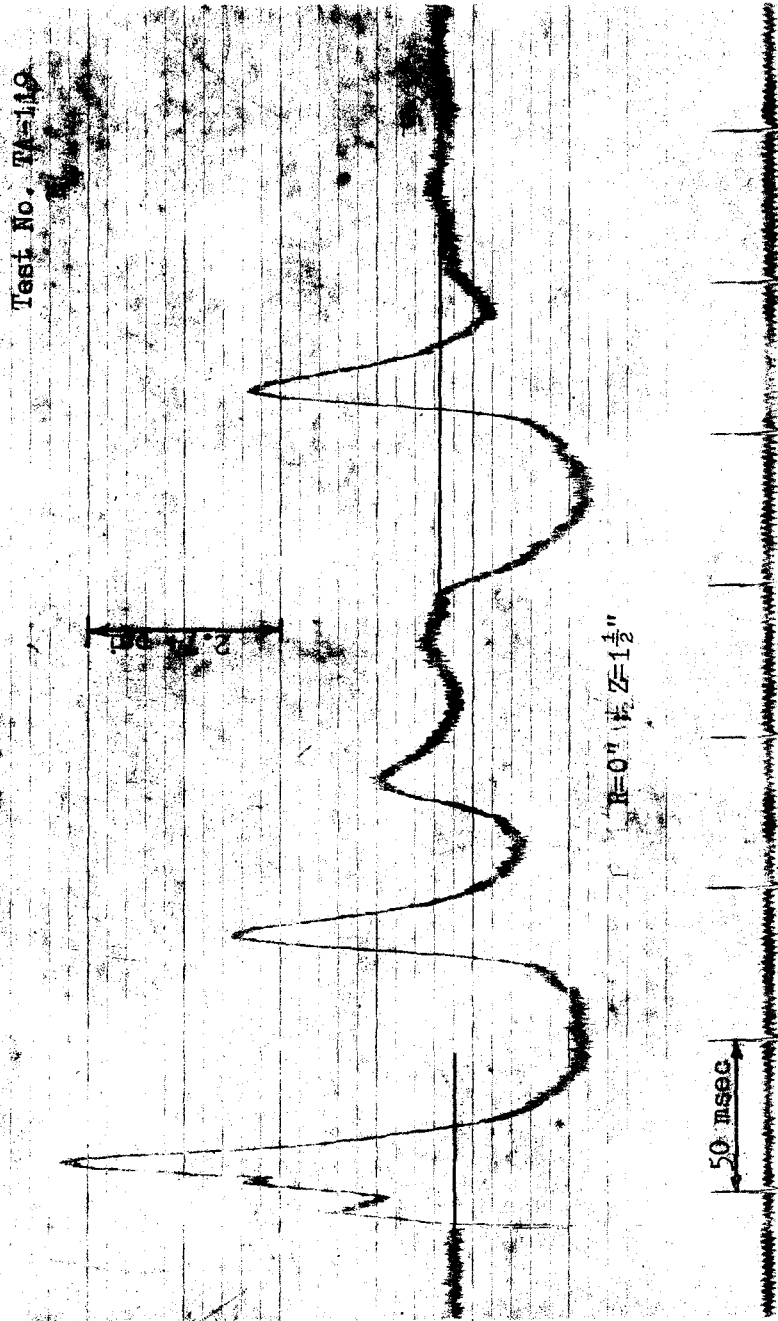


Figure 97. Stress-Time Trace at $R/r = 0$; $Z/r = 1/2$ With a Compressible Material M_4 Buried at $R/r = 0$; $Z/r = 1$ (6 in. dia. circular footing on the surface)



Figure 98. Stress-Time Trace at $R/r = 0$; $Z/r = 1/2$ With a Compressible Material M₅ Buried at $R/r = 0$; $Z/r = 1$ (6 in. dia. circular footing on the surface)

stress waves. Peak vertical stress values from Figs. 94 through 98 were compared with that of Fig. 93, and percentage reduction of the peak vertical stress (R_s) at $R/r = 0$; $Z/r = 1/2$ corresponding to each compressible material were computed. For example:

$$R_s = 100 \left[\frac{\text{peak vertical stress without any compressible material buried in the soil} - \text{peak vertical stress with a compressible material buried in the soil}}{\text{peak vertical stress without any compressible material buried in the soil}} \right]$$

These R_s values were plotted against the K_c values and a relationship shown in Fig. 99 was obtained. These R_s values were again plotted against $\log K_c$ values and a straight line relationship (similar to that shown in Fig. 92) was obtained, and is shown in Fig. 100. This straight line relationship is represented by the equation $R_s = 89.3 - 30.7 \log K_c$. This equation is also expressed in a generalized form as $R_s = A_3 - A_4 \log K_c$, where A_3 and A_4 are constants. The relationship as derived above may prove to be very useful in the design of earthquake resistant structures.

A series of static load-displacement tests were also conducted for a 6 in. dia. surface footing with and without a compressible material buried at a depth equal to the radius of the footing. These tests were conducted under identical test conditions in the same vessel as the dynamic tests. A schematic diagram of the loading apparatus is shown in Fig. 6,

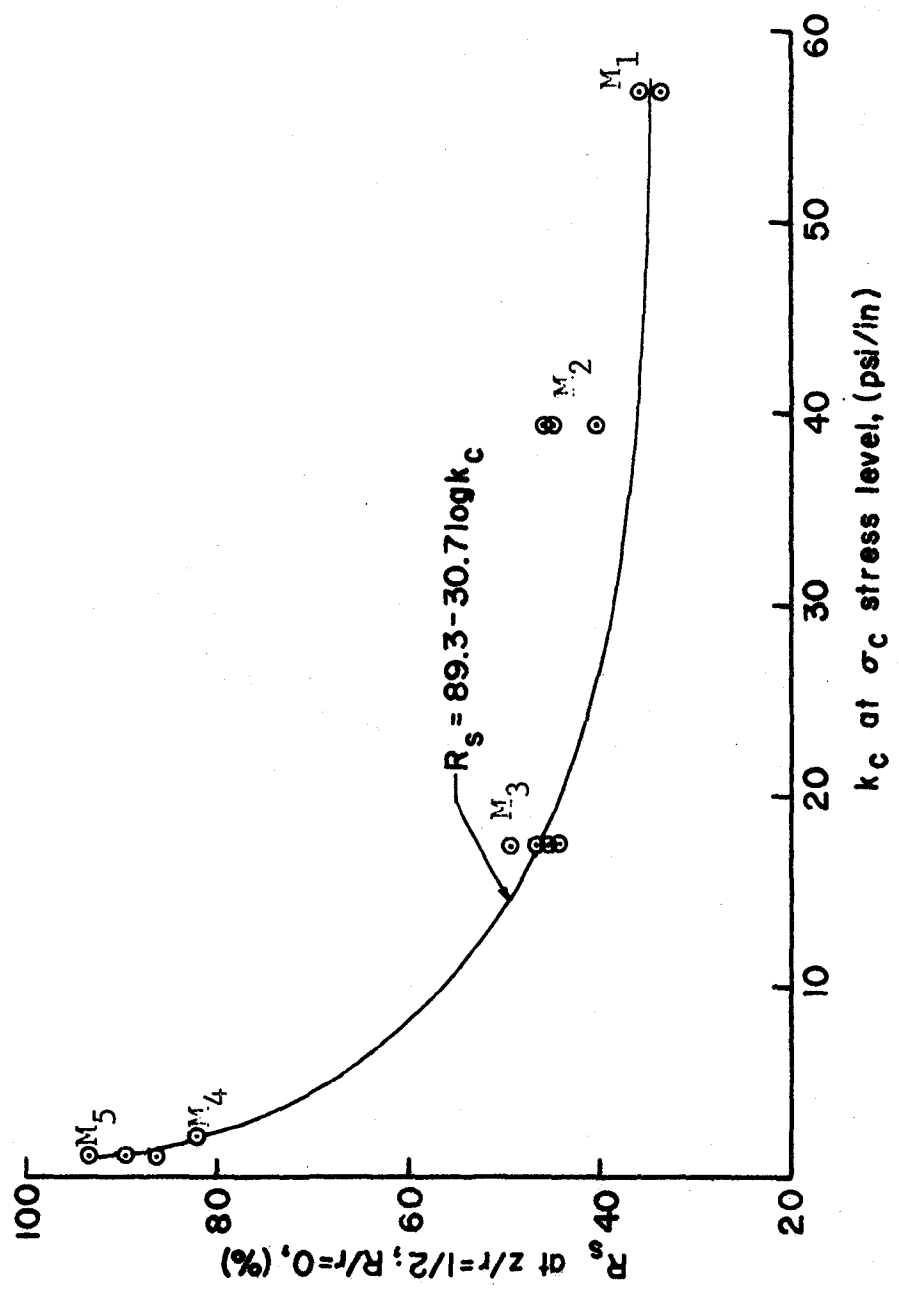


Figure 99. Peak Vertical Stress Reduction vs Subgrade Modulus of Compressible Material

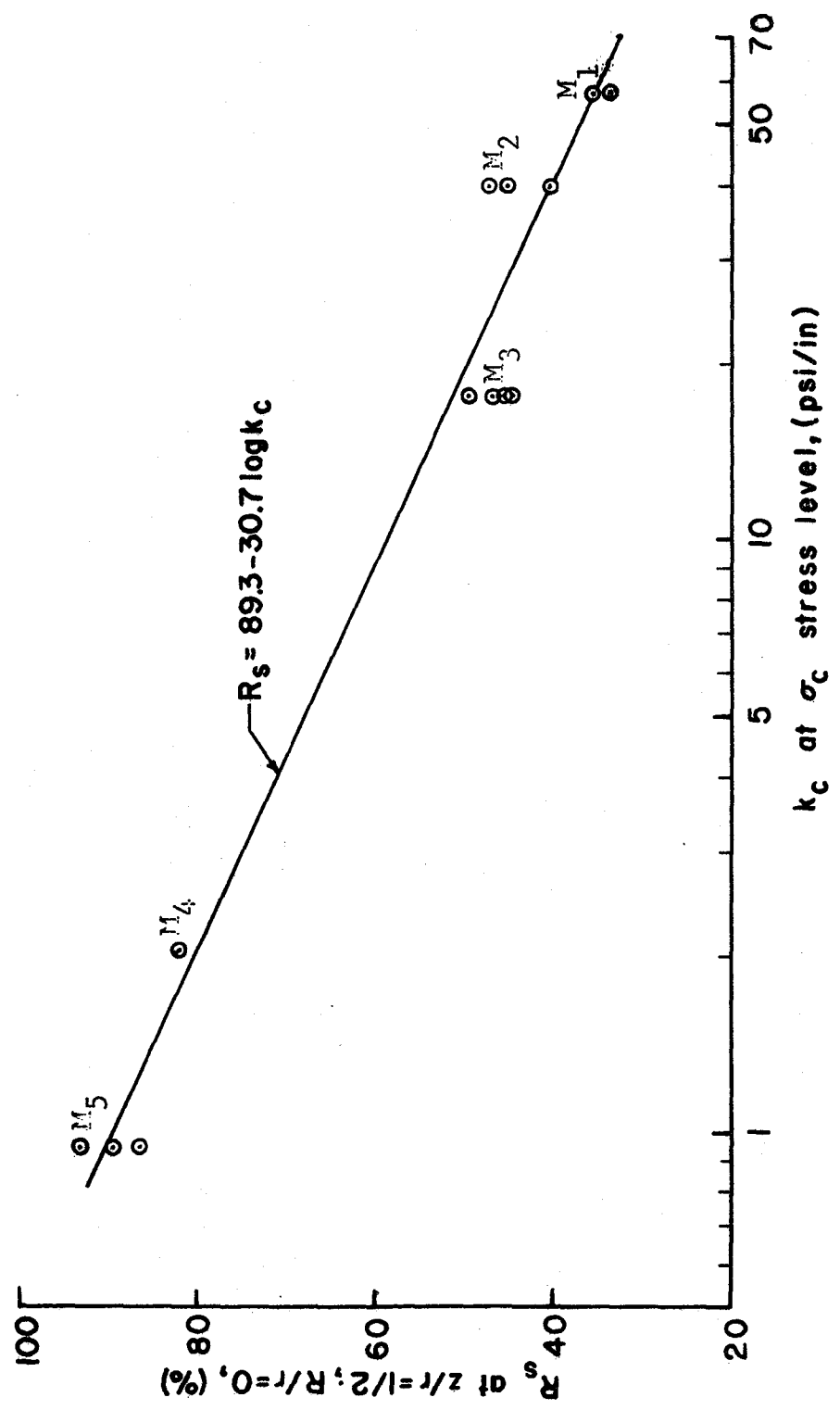


Figure 100. Peak Vertical Stress Reduction vs Log of Subgrade Modulus of Compressible Material

and, a view of this apparatus is shown in Fig. 101. As shown in these figures, load was applied to the soil through the footing at a constant strain rate through a gear box arrangement. The footing pressure and penetration measurements were made using a proving ring dial gage, to measure pressure, and a deformation dial gage, to measure penetration (settlement) of the footing.

Ultimate Load Criterion. Several ultimate load criteria were evaluated for use in this study. The first versatile ultimate load criterion, recommended by Vesic^{72,73}, defines the ultimate load as the point at which the slope of the load-displacement curve first reaches zero or a steady, minimum value. Another (De Beer's) criterion¹⁴ defines the ultimate load at the point of break of the load-settlement curve in a log-log plot. Both criteria require that the loading test be carried to very large displacements. Therefore, from the practical point of view, another criterion must be selected based on critical settlement (allowable settlement). One criterion used in practice⁷³, where a peak load cannot be established, is to adopt a limit of critical settlement as 5% to 15% of the footing width. Critical settlement (allowable settlement) criterion was adopted in this study. Considering 0.5 in. settlement of the load area (1 ft. square) under a given load q per unit area, the allowable settlement at the same load per unit area of a 6 in. dia. circular footing (using its equivalent width) was computed using the formula suggested by Terzaghi and

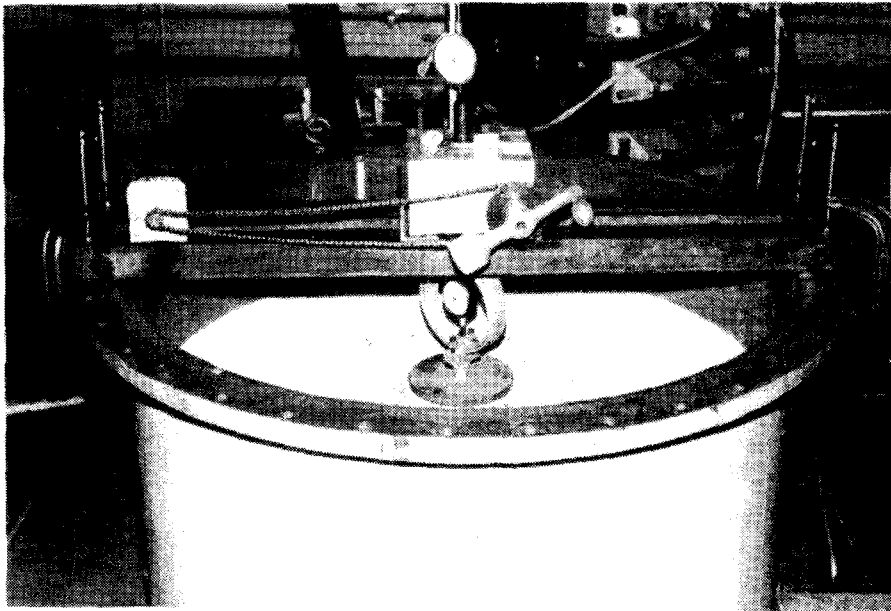


Figure 101. A View of the Apparatus for Statically Loaded Footing

Peck⁶⁶. Thus a critical settlement of 0.18 in. was obtained for a 6 in. dia. footing.

A footing pressure versus settlement relationship, for a 6 in. dia. circular footing on the surface (without any compressible material buried in the sand) is shown in Fig. 102. These values, footing pressure and settlement were again plotted on a log-log plot as shown in Fig. 103. Using De Beer's¹⁴ method, ultimate load was obtained from this log-log plot. Surprisingly, this ultimate load corresponded to a critical settlement of 0.18 in. (3% of the footing diameter).

Factor of Safety (F.S.). Factor of safety against bearing capacity failure, based on allowable settlement, was computed for a 6 in. diameter surface footing, with and without any compressible material buried in the sand. For this purpose two levels of allowable settlement were considered. Therefore, factor of safety values based on 0.18 in. and 0.10 in. allowable settlements were computed from the footing pressure versus settlement relationships. Footing pressure versus settlement relationships for this footing, with a different compressible material buried each time in the soil at $Z/r = 1$, are shown in Figs. 104 through 108. These relationships were used to compute the factor of safety. Percentage reduction, in the factor of safety values (R_F) with respect to the factor of safety computed from Fig. 102, was calculated. For example, for material M_1 (F.S. values based on 0.18 in. settlement):

$$R_F = 100 \frac{[\text{F.S. from Fig. 102} - \text{F.S. from Fig. 104}]}{[\text{F.S. from Fig. 102}]}$$

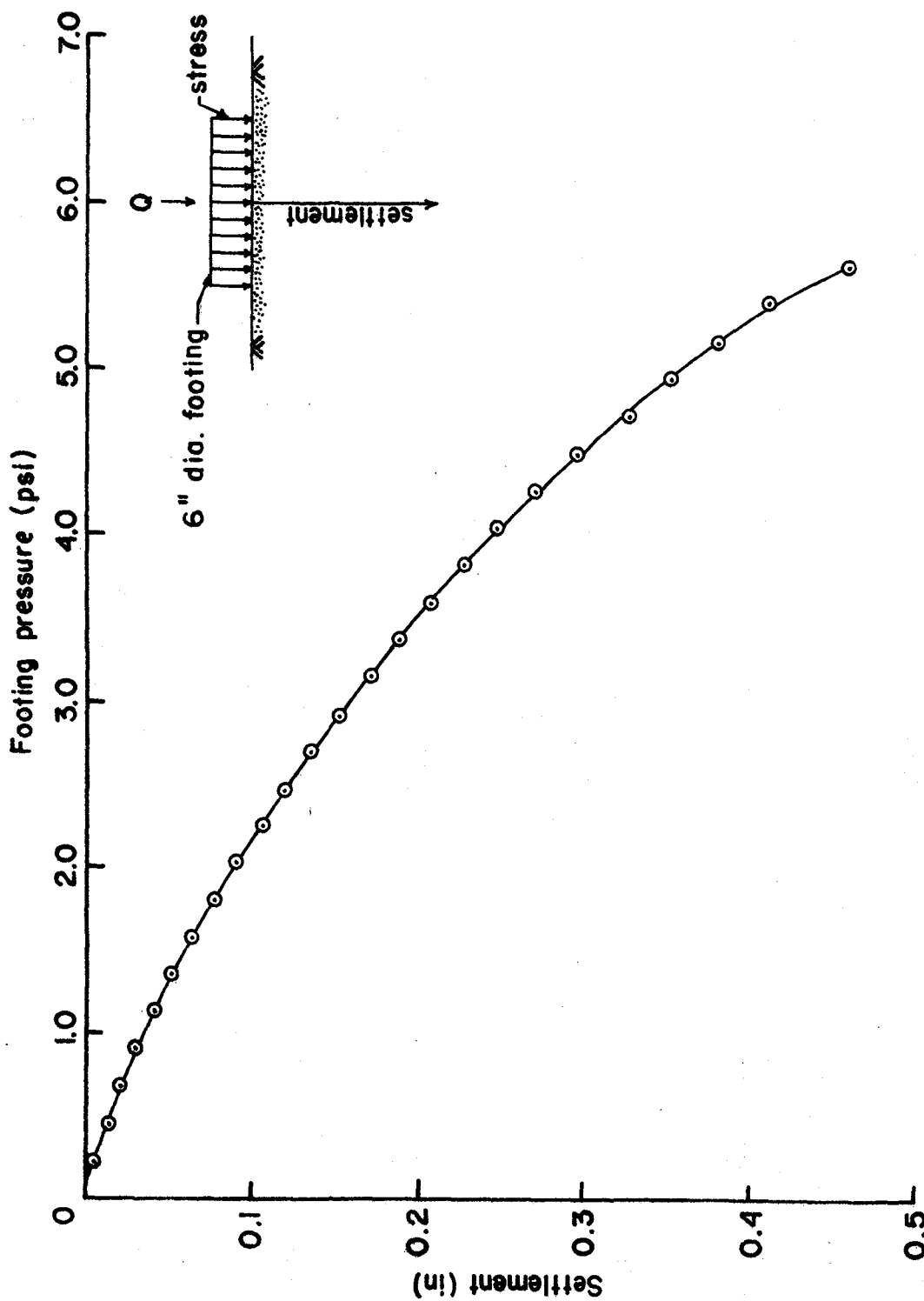


Figure 102. Footing Pressure vs Settlement (under static conditions)

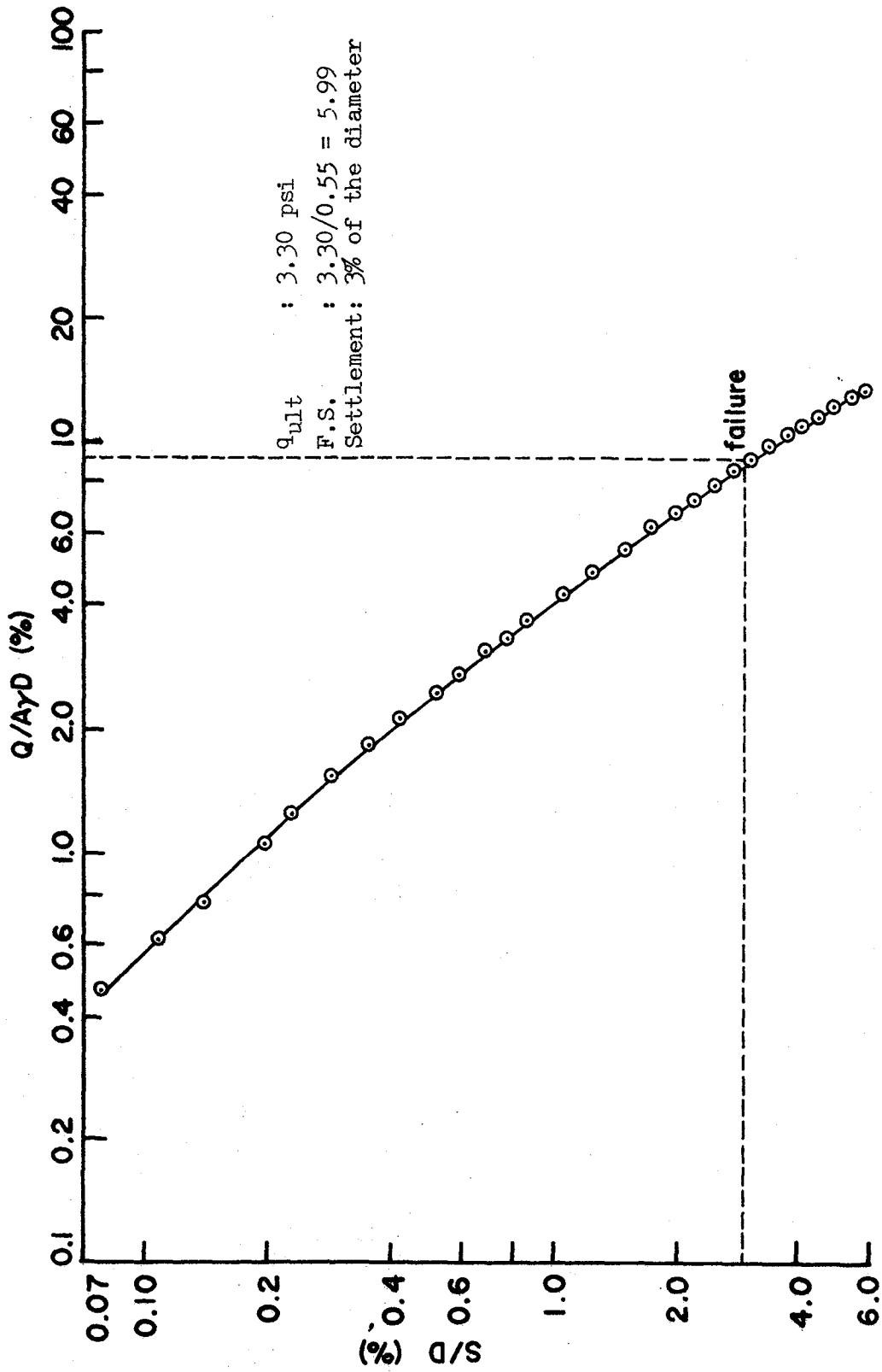


Figure 103. Ultimate Load Criterion Based on Log Load-Log Settlement Plot (De Beer's Method)

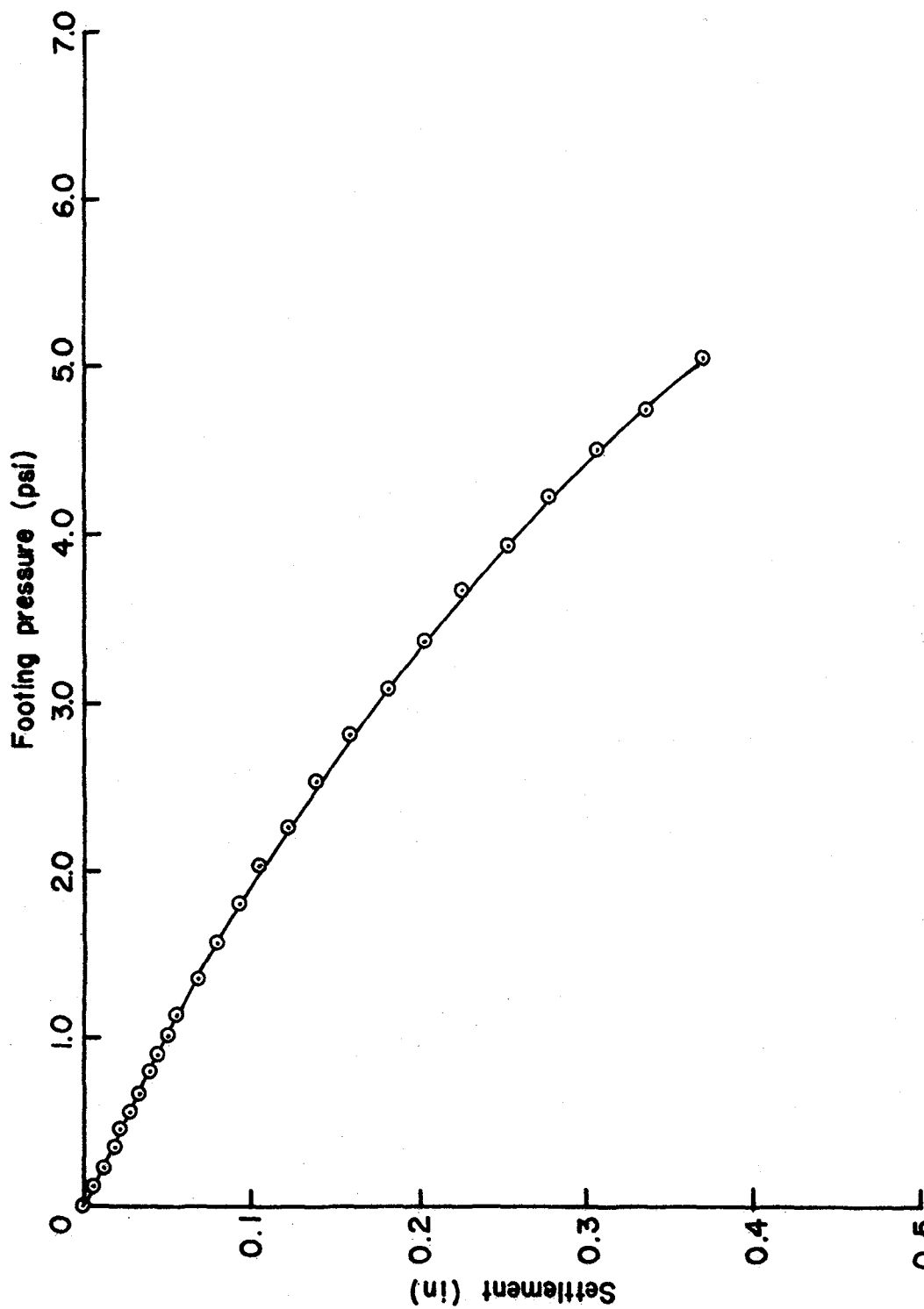


Figure 104. Footing Pressure vs Settlement With a Compressible Material M_1 Buried at $R/r = 0$; $z/r = 1$

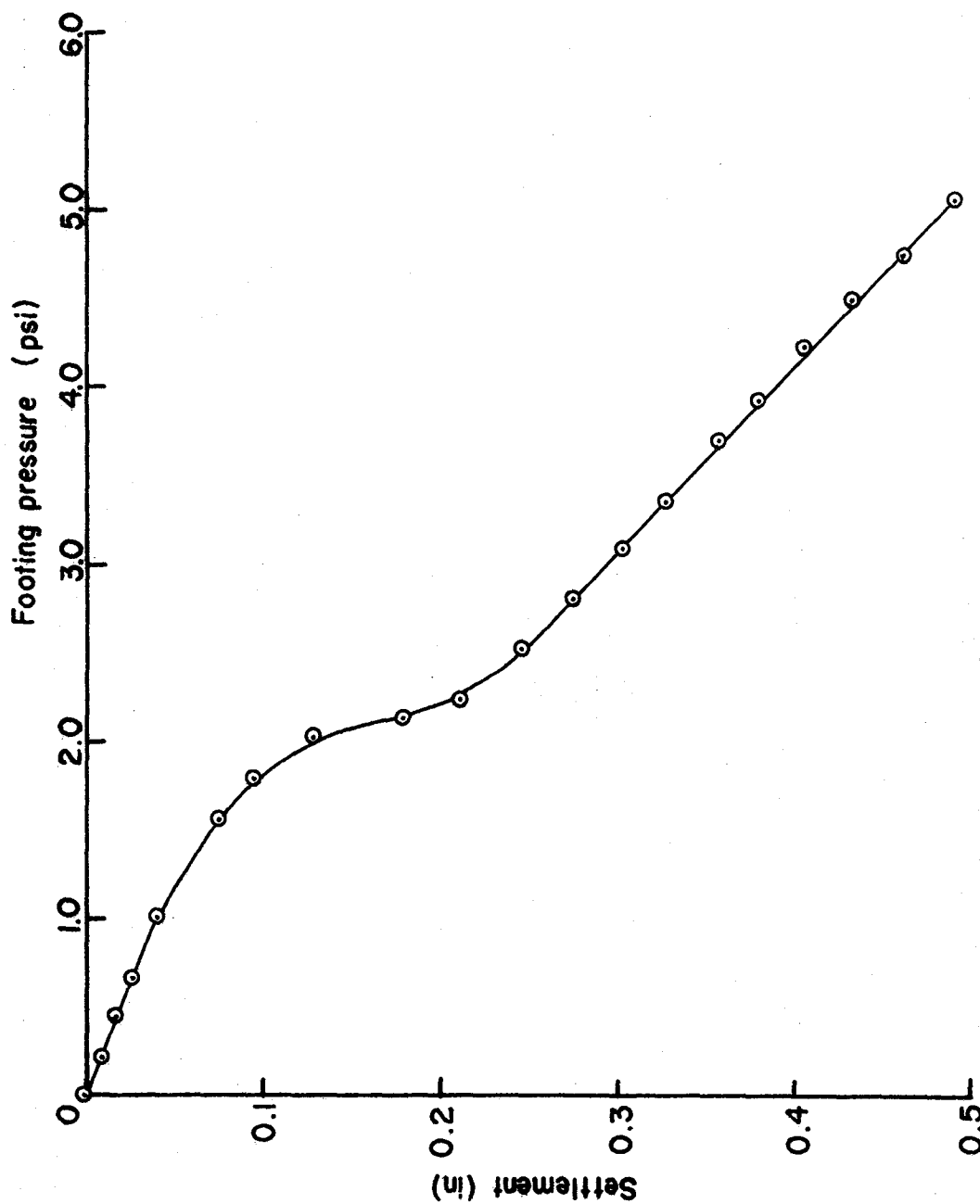


Figure 105. Footing Pressure vs Settlement With a Compressible Material M_2 Buried at $R/r = 0$; $z/r = 1$

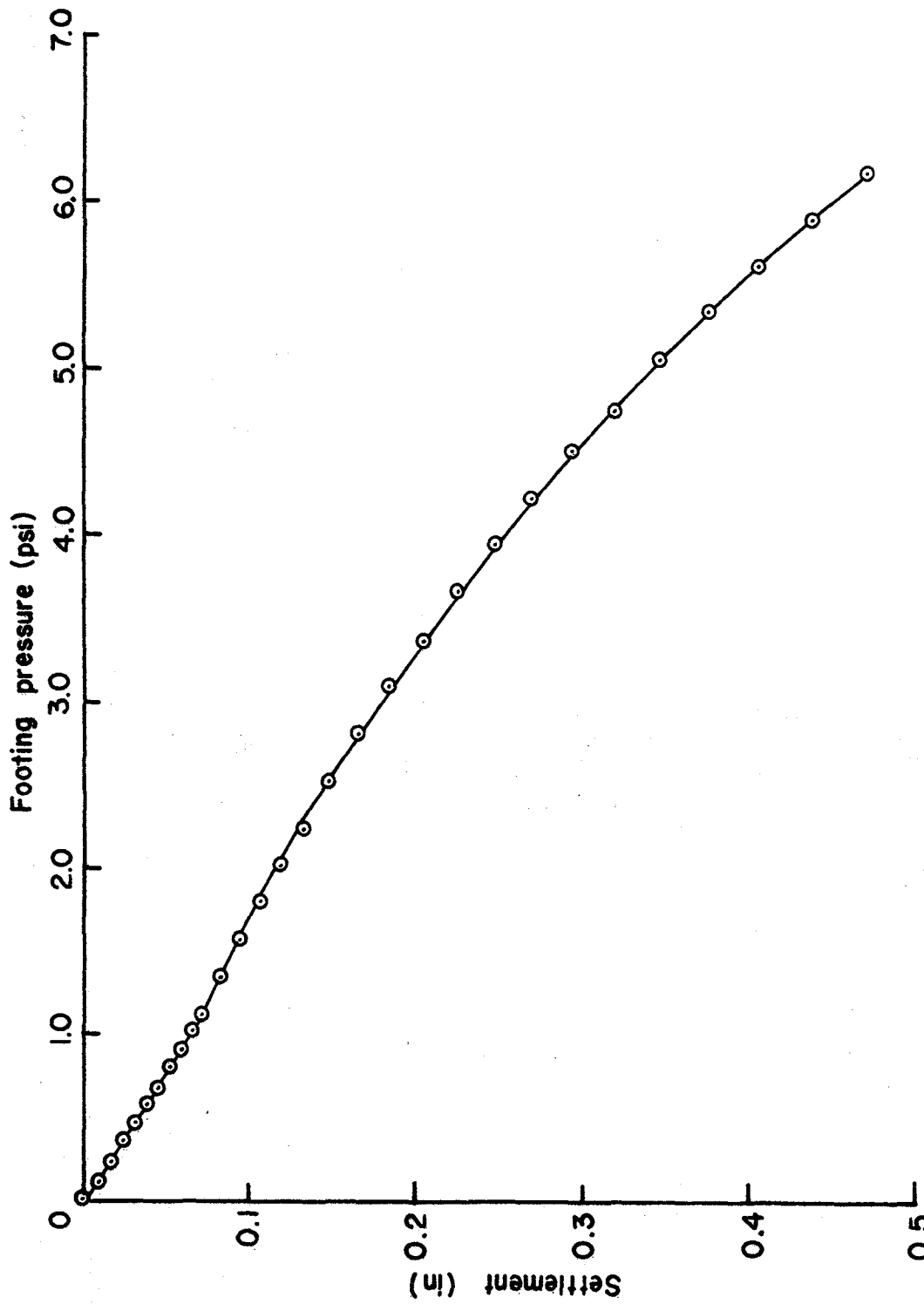


Figure 106. Footing Pressure vs Settlement With a Compressible Material M_3 Buried at $R/r = 0$; $Z/r = 1$

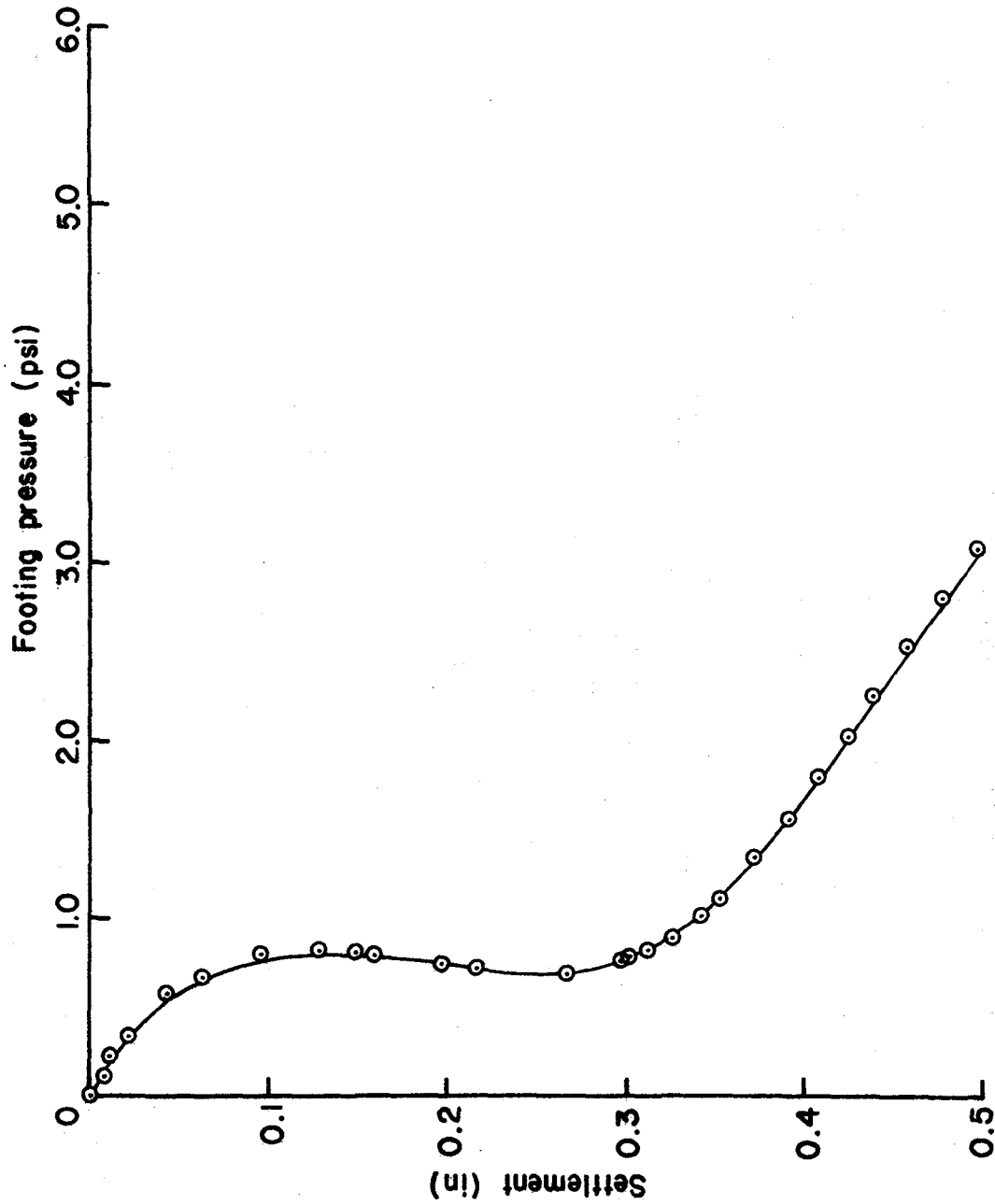


Figure 107. Footing Pressure vs Settlement With a Compressible Material M_4 Buried at $R/r = 0$; $Z/r = 1$

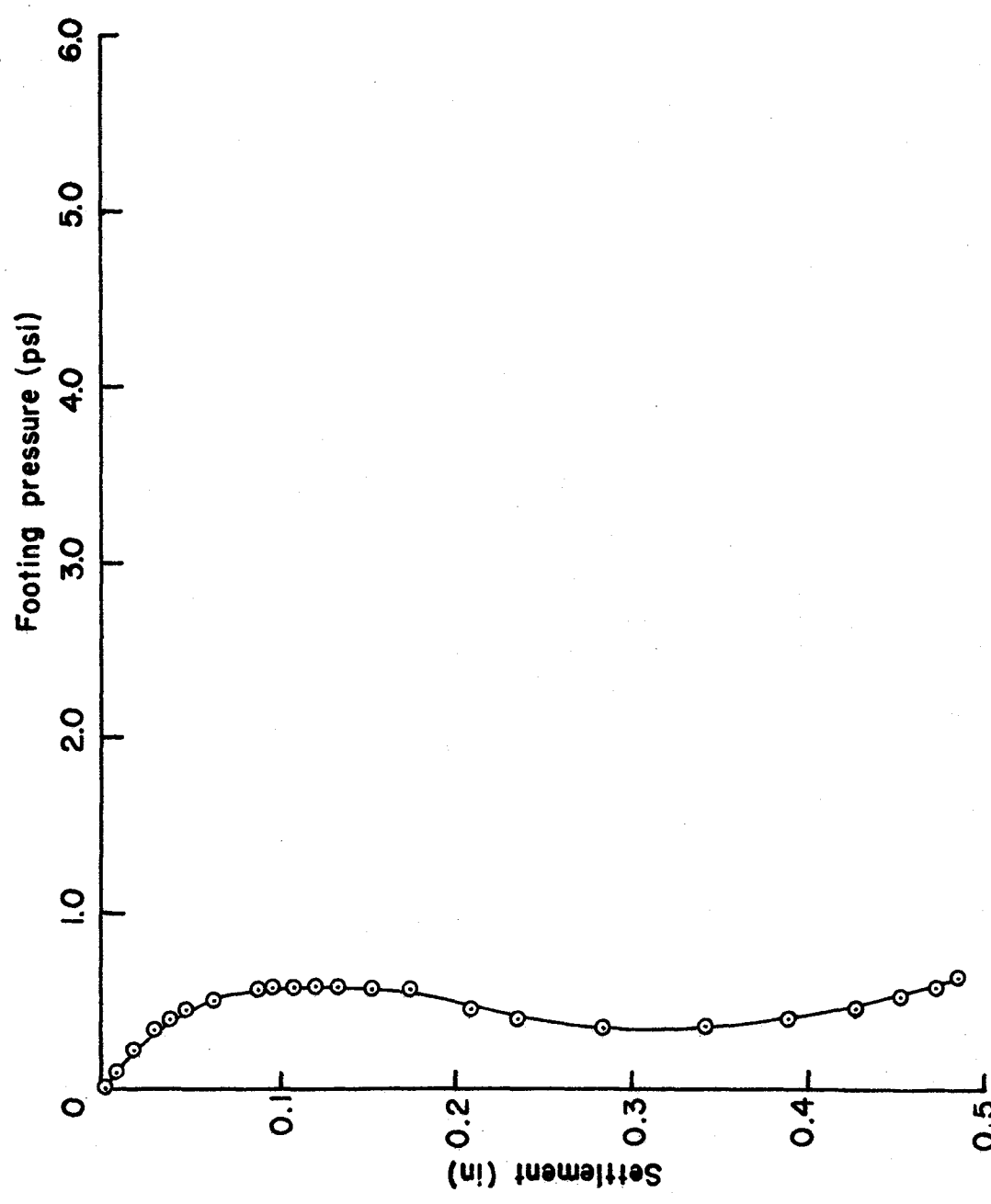


Figure 108. Footing Pressure vs Settlement With a Compressible Material M₅ Buried at R/r = 0; z/r = 1

These R_F values were plotted against R_a values (from Fig. 92) and a straight line relationship was obtained, as shown in Fig. 109. Similarly R_F values computed with F.S. values based on 0.10 in. allowable settlement were also plotted against the same R_a values, as before, and again a straight line relationship was obtained. This relationship is shown in Fig. 110. The relationships as derived above may prove to be very useful in design of earthquake resistant structures. These relationships are applicable to a selected criterion of settlement. For any other criterion a new relationship has to be established. However, these types of relationships provide a useful mechanism for reducing the foundation deceleration based on the settlement criterion.

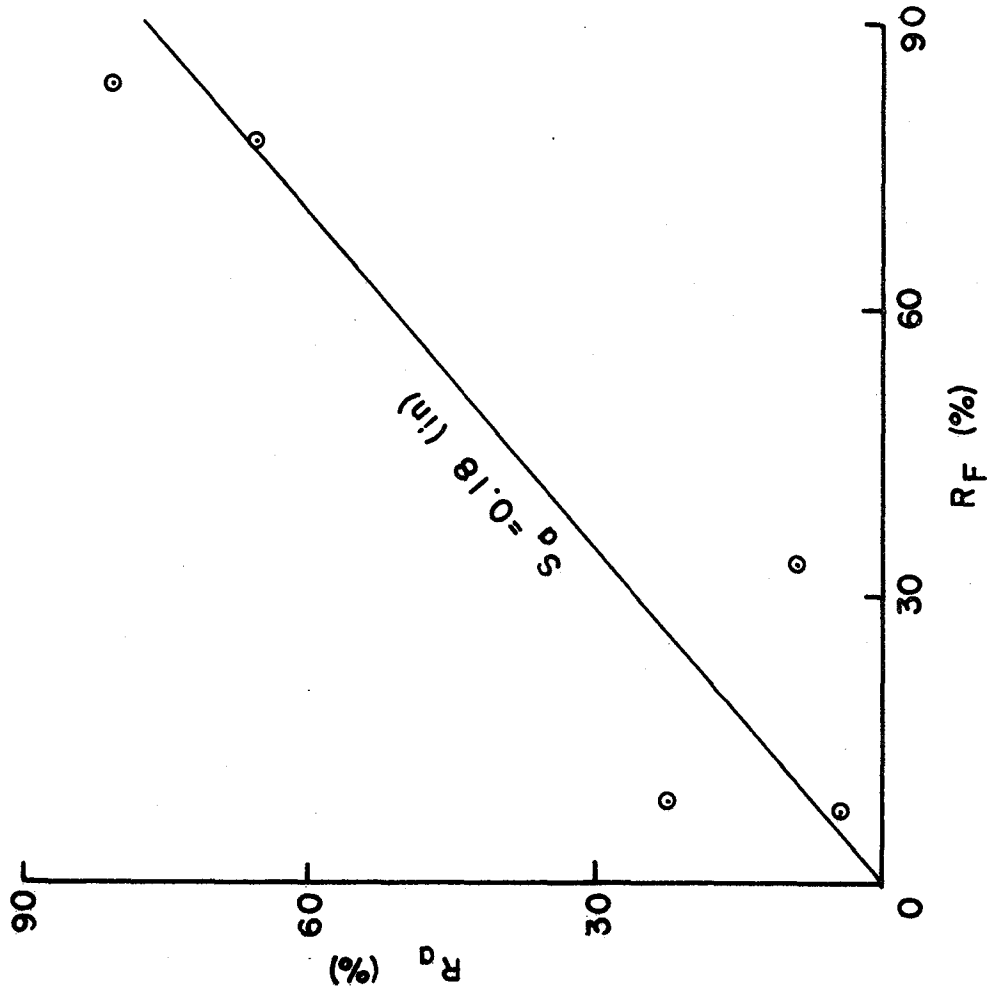


Figure 109. Deceleration Reduction vs Factor of Safety Reduction (factor of safety based on 0.18 in. allowable settlement)

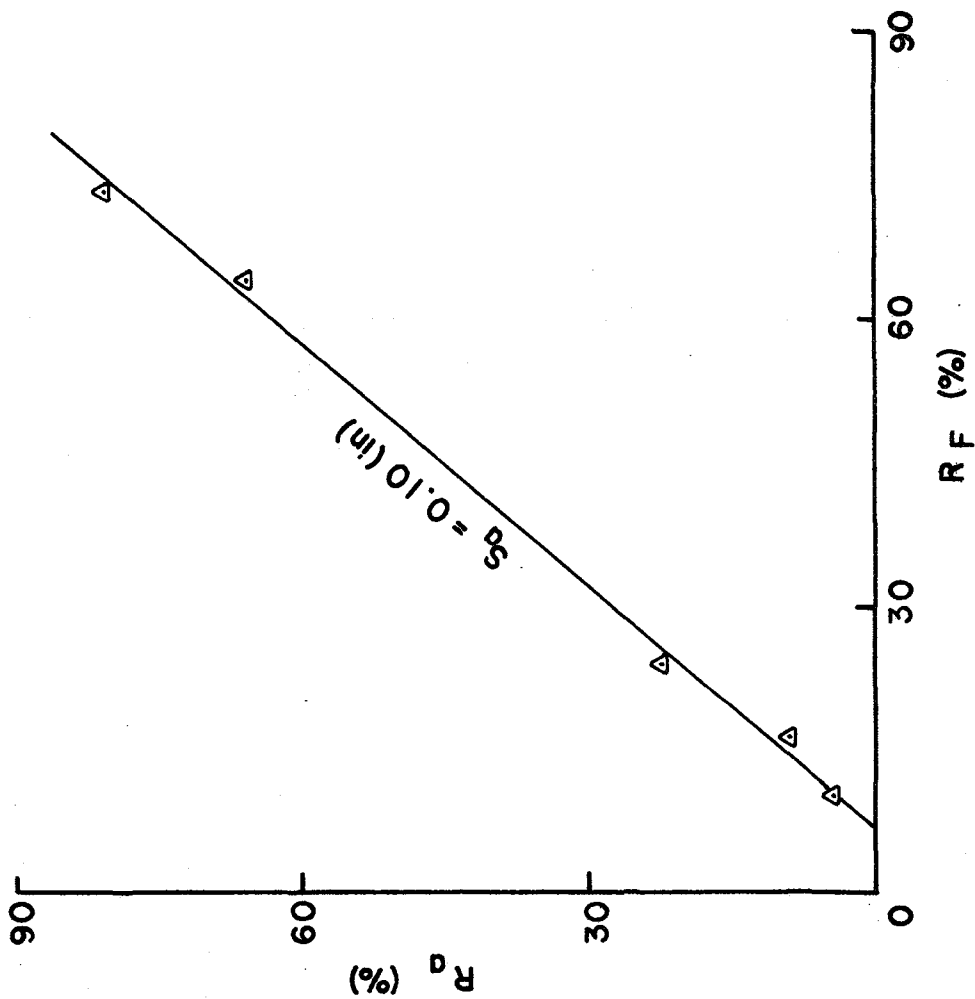


Figure 110. Deceleration Reduction vs Factor of Safety Reduction (factor of safety based on 0.1 in. allowable settlement)

CHAPTER VI
CONCLUSIONS

Based on the results of the experimental stress-wave propagation investigation the following conclusions were drawn:

1. The general stress-time response in the vicinity of the footing followed the same pattern as the acceleration-time response. The peak vertical stress intensities near the surface on the axis of symmetry were in the order of 11 times the static contact pressure of the footing with an exception of lighter footings, in which case these intensities were much higher.
2. The data indicates that the size of the footing affected the stress distribution in the soil. In all the three cases investigated, the attenuation of peak vertical stress was very rapid in a distance equal to the diameter of the footing. The data also indicates that at a distance equal to 1.5 times the diameter of the footing from the axis of symmetry, the effect of footing on the vertical stress distribution is negligible.
3. In all the three cases of surface footings

subjected to transient load, it was noticed that, at a depth equal to twice the footing diameter, the influence of footing mass on the vertical stress distribution is negligible.

4. Stress intensities in the vicinity of the footing increased with depth of burial (depth of embedment) of the footing (as the distance from the transient load source decreased).

According to the results of the footing response experiments it was concluded that:

1. There exists a linear relationship between deceleration of the footing and weight of the footing. Deceleration of the footing was inversely proportional to its weight.
2. Deceleration amplitude of the footing decreased with the depth of burial (embedment) of the footing, thus indicating a greater damping and increased stiffness (since the maximum depth of burial was only one footing diameter, the soil above the footing had a negligible contribution to the weight of the footing).

Based on the analyses of results from the footing isolation experiments it was concluded that:

1. A linear relationship can be generated between the percentage reduction in

deceleration amplitude of the footing (R_a) and log of subgrade modulus (K_c) of the compressible material computed at (σ_c) stress level. This straight line equation is represented by the equation $R_a = 78.4 - 42.7 \log K_c$. In a generalized form this can be expressed as $R_a = A_1 - A_2 \log K_c$, where A_1 and A_2 are constants.

2. Similar linear relationship can be established between the percentage reduction of the vertical stress (R_s) in the vicinity of the footing and log of subgrade modulus (K_c) of the compressible material at (σ_c) stress level. This linear plot, on semi-log graph can be represented by the equation $R_s = 89.3 - 30.7 \log K_c$, and in a generalized form, $R_s = A_3 - A_4 \log K_c$, where A_3 and A_4 are constants.
3. The data from static load-displacement tests (with and without a compressible material buried in the soil) indicated that a linear relationship can be generated between the percentage reduction in the factor of safety (based on allowable settlement) of a surface footing (R_F) and percentage reduction in deceleration of the footing (R_a). For an allowable settlement of 3% of the footing diameter (0.18 in.), the deceleration

amplitude of the footing is reduced by 30%, however, the factor of safety reduced to 65%. Similarly, for an allowable settlement of 1.67% of the footing diameter (0.10 in.), the factor of safety reduced to 68% for the same reduction in deceleration.

The above conclusions were drawn based on small scale model tests. A comparison of small scale model test results with large size prototype structures may prove helpful in developing some similitude criterion and may also provide better understanding of the influence of the vertical component of earthquake induced forces. It must be recognized that information from large size structures in a meaningful form may not be available now and obtaining the information may involve considerable time. Furthermore, it may not be possible to establish one-to-one scale factor between the small scale models and prototype structures, but relationships similar to those presented in this investigation can be developed and established.

Future research should include:

- (a) Extensive analysis of the experiments conducted, perhaps by the finite element technique to provide a better understanding of the foundation response, and also to predict the stress intensities in the

vicinity of the foundation for a given input spectra.

- (b) Use of cohesive material (clay) as a soil media beneath the footing to transmit transient loads to the bottom of the footing.
- (c) More number of compressible materials in footing isolation studies.
- (d) Evaluation of the constants A_1 , A_2 , A_3 and A_4 in various soil types.

APPENDIX A
SOIL PROPERTIES

APPENDIX A
SOIL PROPERTIES

In the experimental program of this thesis, the soil used was dry, 20-40 Ottawa sand. The sand was uniformly graded, and consisted of subrounded particles. This soil is classified as (SP) according to the Unified Soil Classification System (USCS). The grain size distribution of this soil is shown in Fig. 111. The specific gravity test was conducted for this soil material, and a value of 2.66 is obtained.

Maximum and minimum dry density tests were conducted for this soil, according to the ASTM standards. The maximum and minimum dry densities obtained are 110 pcf and 92 pcf, respectively. A graph, as shown in Fig. 112, is drawn using the maximum and minimum dry densities, in order to obtain the relative density at any known initial dry density.

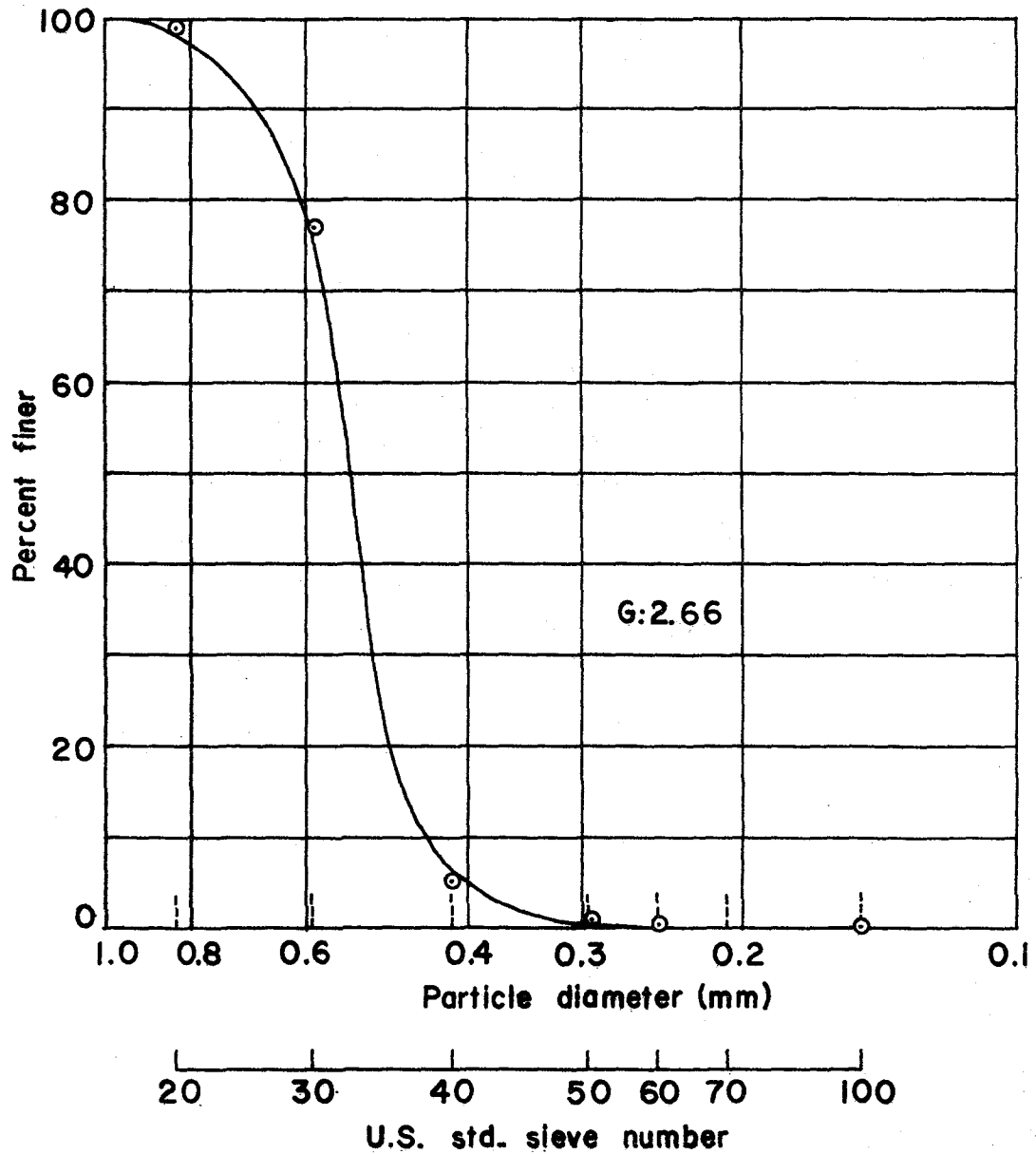


Figure 111. Grain Size Distribution of Ottawa Sand

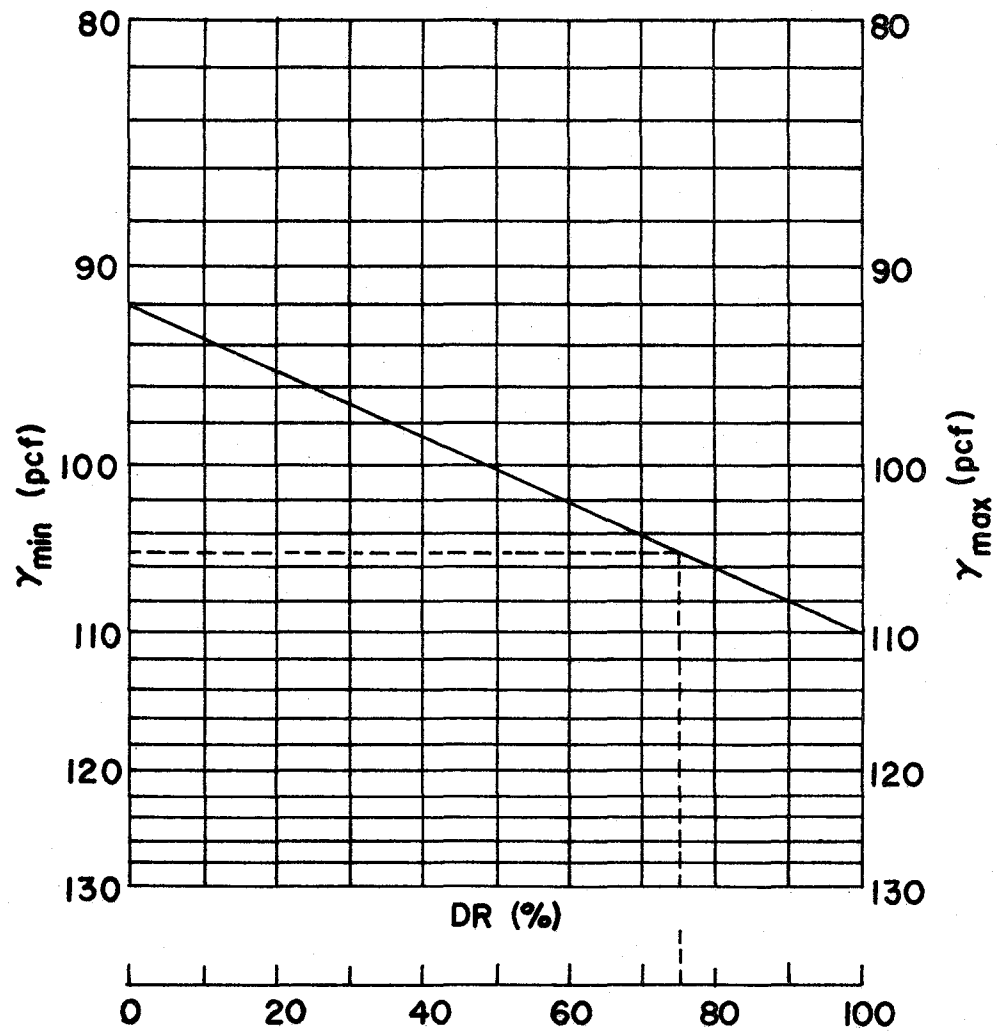


Figure 112. Relative Density vs Specimen Density for Dry Ottawa Sand (20-40 Mesh)

APPENDIX B
WAVE PROPAGATION VELOCITIES AND SOIL MODULI

APPENDIX B

WAVE PROPAGATION VELOCITIES AND SOIL MODULI

According to the elastic half-space theory, there are two basic types of waves, body waves and surface waves. Again the body waves are subdivided into two important waves, the compression or dilatational-also called P-wave, and the shear wave or S-wave. The only surface wave is the Rayleigh wave-also called R-wave. Lord Rayleigh⁵² was first to study the motion of a wave confined to a zone near the boundary of the half-space. Lamb³⁶ described in detail the surface motion that occurs at distances far away from the point source, at the surface of the half-space. These Rayleigh waves propagate radially outward on a cylindrical wave front. The particle motion, associated with this wave at the surface, is a retrograde ellipse.

The body waves propagate radially outward from the source along hemispherical wave fronts. The particle motion associated with the compression wave is a push-pull motion in the direction of the wave front; and, the particle motion associated with the shear wave is a transverse displacement normal to the direction of the wave front. The distribution of displacement waves from a circular footing on a homogeneous, isotropic, elastic half-space is schematically shown by Woods⁸², in his work. There is also a considerable amount of information relative to the propagation of seismic waves in homogeneous, isotropic, elastic half-space^{35,19,20}.

In the experimental work of this thesis, compressional

waves were transmitted to the bottom of the footing, through the soil media. Stress-time relationships were recorded at each gage station along the vertical axis of symmetry. From these records the arrival times of the compressional wave were computed at each gage station. These arrival times were plotted against the distance of the gage from the loading source, as shown in Fig. 113, to represent the average dilatational (compressional) wave velocity. The average dilatational wave velocity observed in these experiments was 557 ft./sec.

This dilatational wave velocity varies from soil to soil. It is primarily a function of the constrained modulus (E_c) and the mass density (ρ), and is represented by the equation:

$$C_D = \sqrt{\frac{E_c}{\rho}}$$

where, E_c is defined as the modulus of deformation for tests in which no lateral movement of the material is allowed, and is given by the equation:

$$E_c = \frac{E (1 - \nu)}{(1 + \nu)(1 - 2\nu)}$$

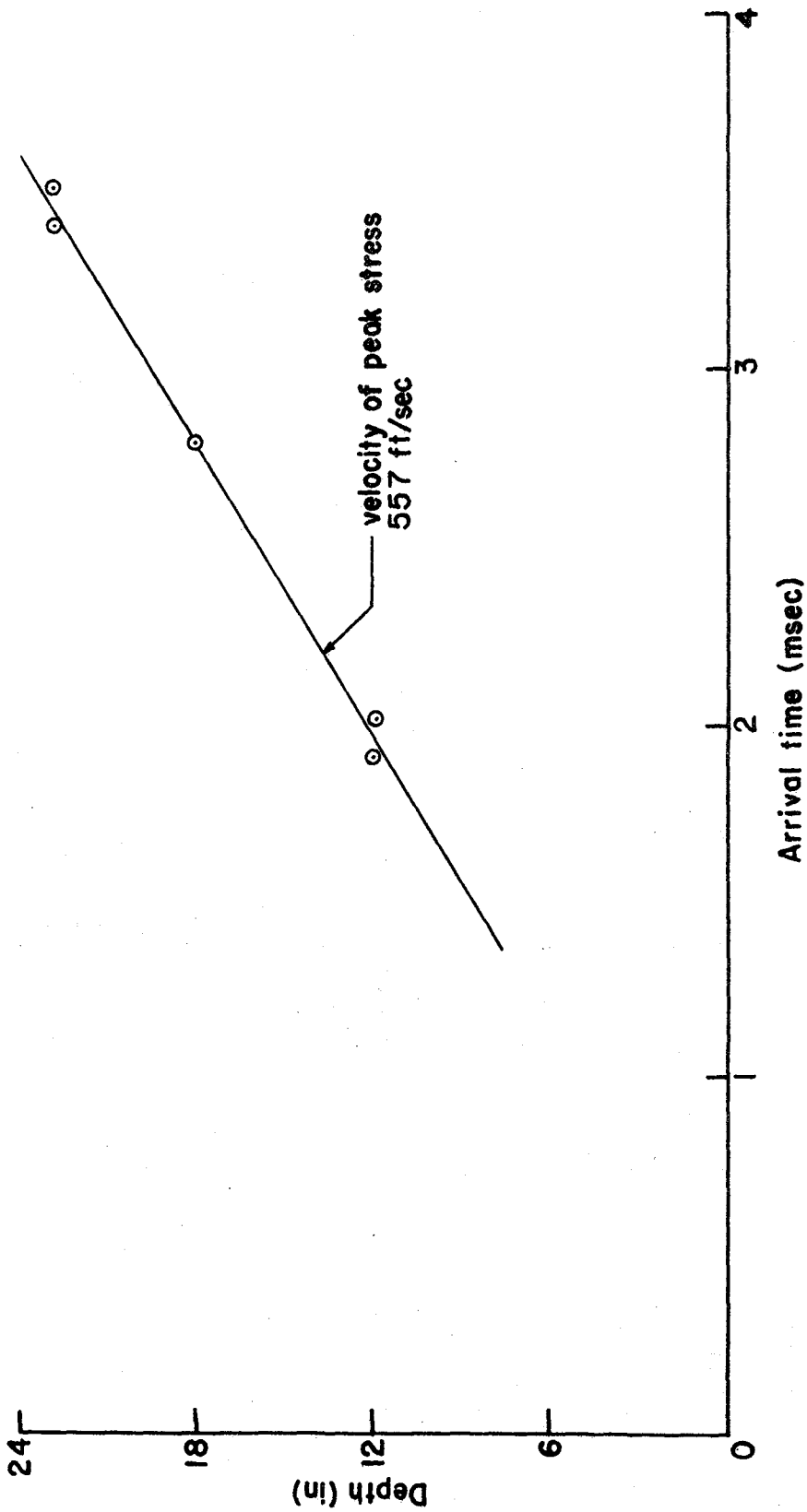


Figure 113. Vertical Stress Arrival Time vs Depth

APPENDIX C
STRESS-DEFORMATION RELATIONSHIP FOR COMPRESSIBLE MATERIALS

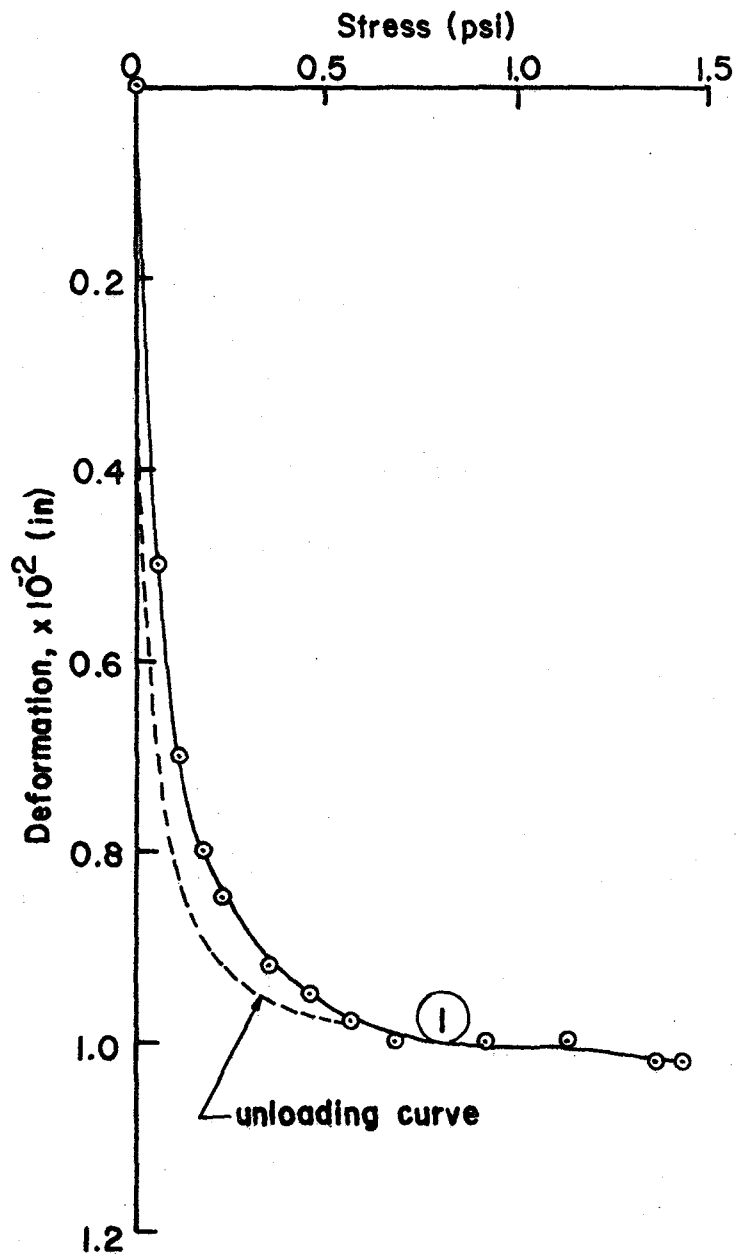


Figure 114. Stress vs Deformation Relationship for Compressible Material No. 1 (loading and unloading conditions)

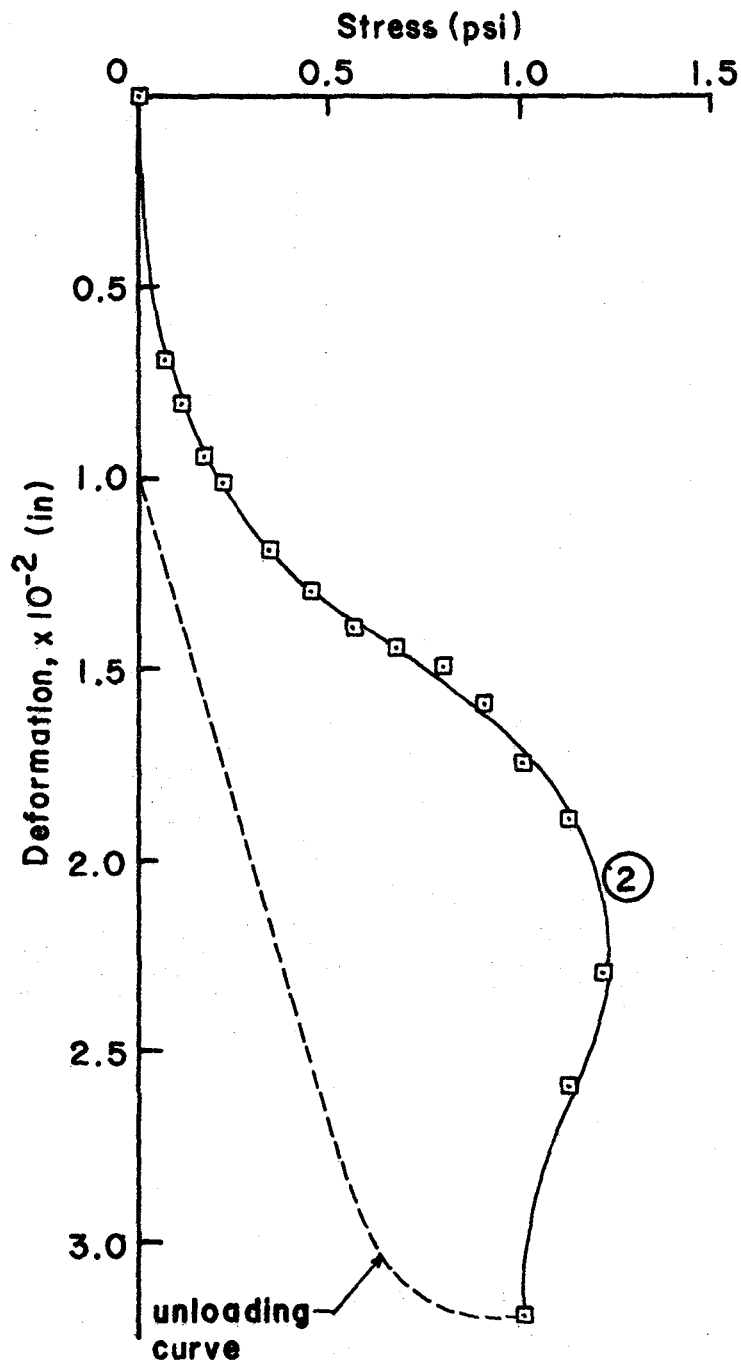


Figure 115. Stress vs Deformation Relationship for Compressible Material No. 2 (loading and unloading conditions)

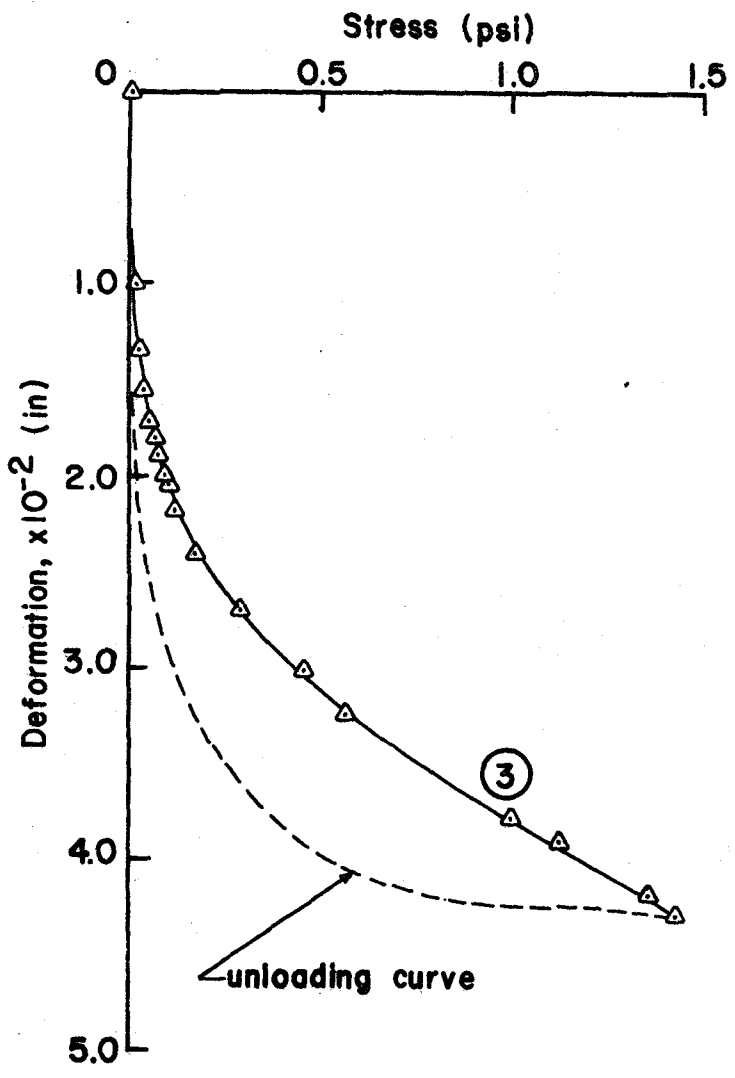


Figure 116. Stress vs Deformation Relationship for Compressible Material No. 3 (loading and unloading conditions)

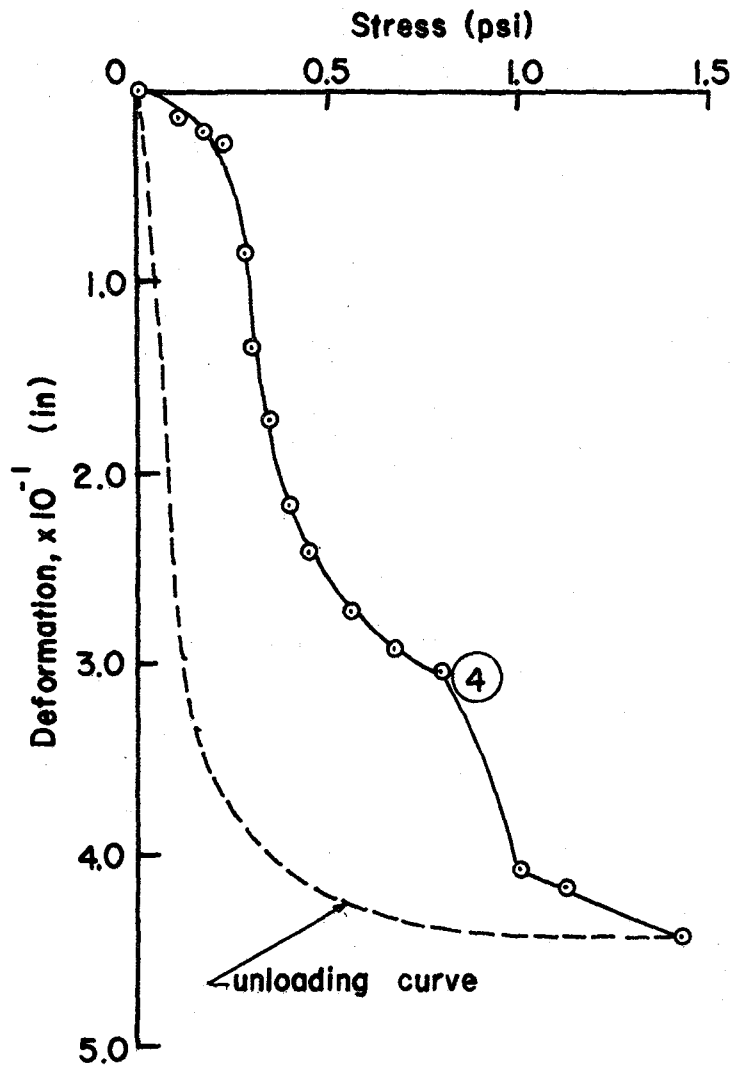


Figure 117. Stress vs Deformation Relationship for Compressible Material No. 4 (loading and unloading conditions)

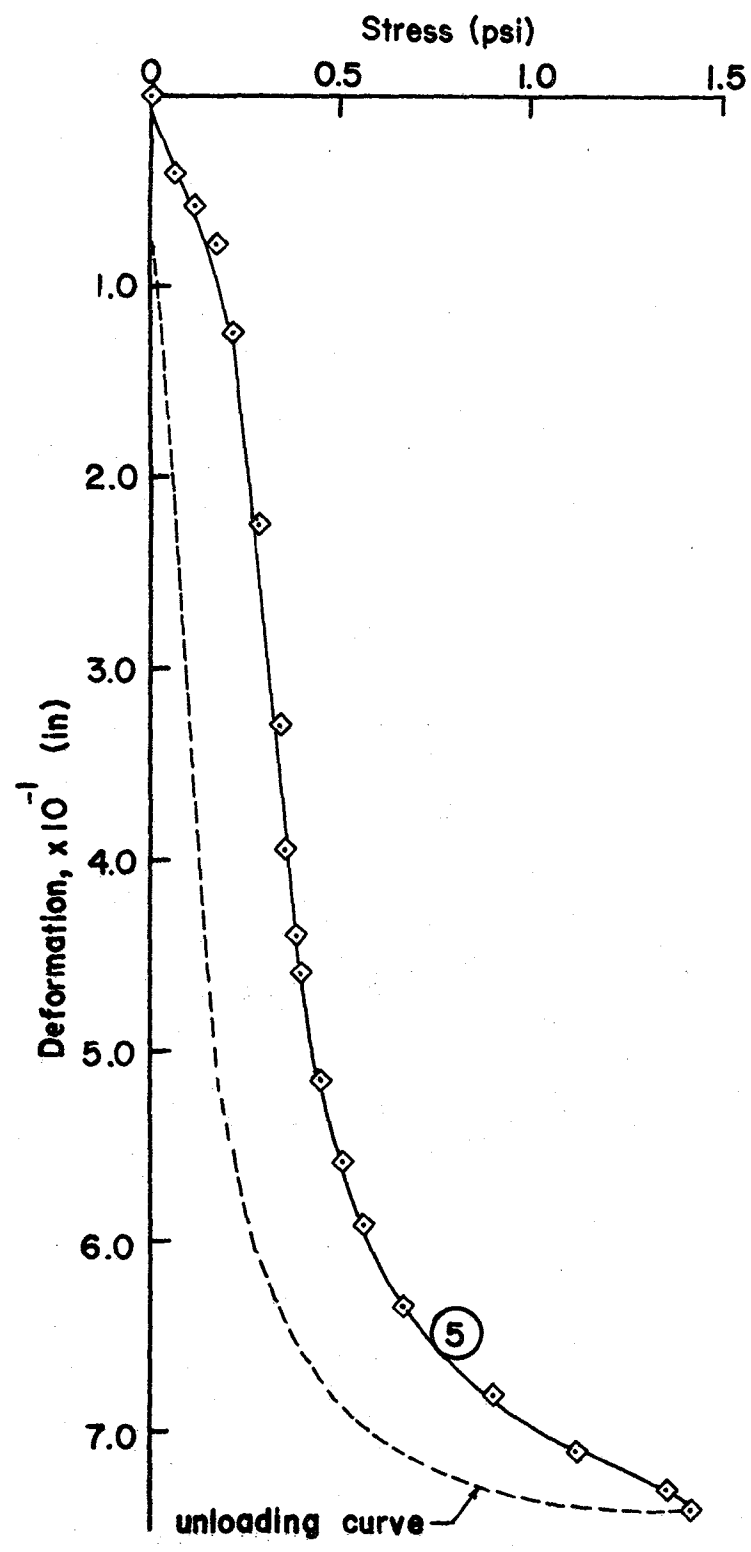


Figure 118. Stress vs Deformation Relationship for Compressible Material No. 5 (loading and unloading conditions)

BIBLIOGRAPHY

1. Ahlvin, R.G., and Ulery, H.H., "Tabulated Values for Determining the Complete Pattern of Stresses, Strains, and Deflections Beneath a Uniform Circular Load on a Homogeneous Half Space", Highway Research Board Bulletin 342, Jan., 1962, pp. 1-13.
2. Arnold, R.N., Bycroft, G.N., and Warburton, G.B., "Forced Vibrations of a Body on an Infinite Elastic Solid", Journal of Applied Mechanics, September, 1955, pp. 391-400.
3. Barkan, D.D., "Field Investigation of the Theory of Vibration of Massive Foundations Under Machines", Proceedings, First International Conference on Soil Mechanics and Foundation Engineering, Vol. II, 1936.
4. Barkan, D.D., "Experimental Study of Vibrations of Mat Foundations Resting on Cohesive Saturated Soils", Transactions, Institute for Engineering Foundation Research (VIOS); Moscow, U.S.S.R., 1934.
5. Barkan, D.D., Dynamics of Bases and Foundations, McGraw-Hill Book Co., Inc., New York, New York, 1962.
6. Bassol, Jean Luc., "Numerical Analysis of Stress Wave Propagation in an Elastic-Plastic Medium", Unpublished M.S. Thesis, Illinois Institute of Technology, May, 1971.
7. Bieganousky, Wayne A., and Marcuson, William F., III, "Uniform Placement of Sand", Journal of the Geotechnical Engineering Div., ASCE, Vol. 102, No. GT3, March 1976, pp. 229-233.
8. Carroll, W.F., "Dynamic Bearing Capacity of Soils, Report No. 5, Vertical Displacements of Spread Footings on Clay: Static and Impulsive Loadings", U.S. Army Engineer Waterways Experiment Station Technical Report No. 3-599, Vicksburg, Mississippi, September, 1963, pp. 1-154.
9. Converse, F.J., Housner, G.W., Hausman, D.A., Quinlan, R.M., and Paul, A., "An Investigation of the Compaction of Soils by Vibration", California Institute of Technology, Research Project, U.S. Army Engineering and Development Labs., The Engineer Center, Fort Belvoir, Virginia, March, 1950.

BIBLIOGRAPHY (Cont'd.)

10. Cortright, Clifford J., "A New Look at California Dams and Earthquakes", Meeting Preprint 2011, ASCE National Structural Engineering Meeting, San Francisco, California, April, 1973, pp. 1-10.
11. Cox, A.D., Eason, G., and Hopkins, H.G., "Axially Symmetric Plastic Deformations in Soils", Philosophical Transactions, The Royal Society of London, Series A, No. 1036, Vol. 254, London, England, August, 1961, pp. 1-45.
12. Crockett, J.H.A., and Hammond, R.E.R., "The Natural Oscillation of Ground and Industrial Foundation", Proceedings, Second International Conference on Soil Mechanics and Foundation Engineering, Vol. III, June, 1948, pp. 88-93.
13. Crockett, J.H.A., and Hammond, R.E.R., "Dynamic Principles of Machine Foundations and Ground", Proceedings, Institution of Mechanical Engineers, Vol. 160, pp. 512-523, discussion, 1949, pp. 523-553.
14. De Beer, E.E., "Experimental Determination of the Shape Factors and the Bearing Capacity Factors of Sand", Geotechnique 20, No. 4, 1970, pp. 387-411.
15. Drnevich, Vincent, P., and Hall, J.R., Jr., "Transient Loading Tests on a Circular Footing", Journal of the Soil Mechanics and Foundations Division, ASCE, Vol. 92, No. SM6, Nov., 1966, pp. 153-167.
16. Duns, C.S., "Vertical Response of a Rigid Base to Dynamic Loading", Civil Engineering and Public Works Rev. 64, No. 760, 1969, pp. 1081-1095.
17. Eastwood, W., "The Factors which Affect the Natural Frequency of Foundations and the Effect of Vibrations on the Bearing Power and Settlement of Foundations on Sand", Structural Engineering, Vol. 31, March, 1953, pp. 82-98.
18. Elliot, A.L., "Lessons from a Major Earthquake", American Highways, Vol. 50, No. 2, April, 1971.
19. Ewing, W.M., Jardetzky, W.S., and Press, F., Elastic Waves in Layered Media. McGraw-Hill Book Co., Inc., New York, 1957.
20. Grant, F.S., and West, G.F., Interpretation Theory in

BIBLIOGRAPHY (Cont'd.)

Applied Geophysics. International Series in The Earth Sciences, McGraw-Hill Book Co., Inc., New York, 1965.

21. Green, N.B., "Flexible First Story Construction for Earthquake Resistance", Transactions, ASCE, Vol. 100, 1935, pp. 645-674.
22. Gupta, Y.P., and Chandrasekaran, A.R., "Absorber System for Earthquake Excitations", 4WCEE, Vol. II, Santiago De Chile, January, 1969, pp. 139-148.
23. Hadala, P.F., "Dynamic Bearing Capacity of Soils, Report No. 4, Investigation of a Dimensionless Load Displacement Relation for Footings on Clay", U.S. Army Engineer Waterways Experiment Station Technical Report No. 3-599, Vicksburg, Mississippi, June, 1965.
24. Hadala, P.F., and Jackson, J.G. Jr., "A Model Study of the Small Boy Footing Behavior", U.S. Army Engineer Waterways Experiment Station Technical Report No. 3-793, Vicksburg, Mississippi, August, 1967, pp. 1-266.
25. Hadala, P.F., "The Effect of Placement Method on the Response of Soil Stress Gages", Proceedings, International Symposium on Wave Propagation and Dynamic Properties of Earth Materials, Albuquerque, New Mexico, Aug., 1967, pp. 255-263.
26. Hampton, D., and Wetzel, R.A., "Stress Wave Propagation in Confined Soils", Proceedings, Symposium on Wave Propagation and Dynamic Properties of Earth Materials, Albuquerque, New Mexico, August, 1967, pp. 433-442.
27. Hicks, C.W., Janza, F.J., and Reid, W.G., "Evaluation of Soil Strain Gage Instrumentation", Air Force Weapons Laboratory Technical Report No. AFWL-TR-67-50, Kirtland AFB, New Mexico, Aug., 1967, pp. 1-280.
28. Ingram, J.K., "The Development of a Free-Field Soil Stress Gage for Static and Dynamic Measurements", Instruments and Apparatus for Soil and Rock Mechanics, American Society for Testing of Materials Special Publication, ASTM STP 392, Washington, D.C., 1965, pp. 20-36.

BIBLIOGRAPHY (Cont'd.)

29. Ingram, J.K., "Development of a Free-Field Soil Stress Gage for Static and Dynamic Measurements", U.S. Army Engineer Waterways Experiment Station Technical Report No. 1-184, Vicksburg, Mississippi, Feb., 1968, pp. 1-112.
30. Jackson, J.G. Jr., and Hadala, P., "Dynamic Bearing Capacity of Soils, Report No. 3, The Application of Similitude to Small-Scale Footing Tests", U.S. Army Engineer Waterways Experiment Station Technical Report No. 3-599, Vicksburg, Mississippi, December, 1964.
31. Januskevicius, C.K., and Vey, E., "Stresses and Strains in Triaxial Specimens Using Embedded Gages", American Society for Testing of Materials, STP No. 392, Instrumentation and Apparatus for Soil and Rock Mechanics, 1965, pp. 37-54.
32. Jumikis, A.R., "Vertical Stress Tables for Uniformly Distributed Loads on Soil", Engineering Research Publication No. 52, College of Engineering, Bureau of Engineering Research, Rutgers University, New Brunswick, New Jersey, 1971.
33. Keller, R.W., and Anderson, M.E., "Development of a Soil Strain Gage for Laboratory Dynamic Test", Air Force Weapons Laboratory Technical Report No. AFWL-TDR-64-7, Kirtland AFB, New Mexico, 1964.
34. Kolbuszewski, J., and Jones, R.H., "The Preparation of Sand Samples for Laboratory Testing", Proceedings, Midland Soil Mechanics and Foundations Engineering Society, Vol. 4, 1961, p. 107.
35. Kolsky, H., Stress Waves in Solids. Dover Publications, New York, 1963, pp. 4-98; also Clarendon Press, Oxford, 1953.
36. Lamb, H., "On the Propagation of Tremors over the Surface of an Elastic Solid", Philosophical Transactions of the Royal Society of London, Series A., Vol. 203, 1904, pp. 1-42.
37. Landsman, R.B., "Stress Wave Propagation in a Clay Soil Under an Impulsively Loaded Circular Footing", Unpublished Ph.D. Dissertation, Illinois Institute of Technology, May, 1973.

BIBLIOGRAPHY (Cont'd.)

38. Larkin, L.A., "Theoretical Bearing Capacity of Very Shallow Footings", Journal of the Soil Mechanics and Foundations Division, ASCE, Vol. 94, No. SM6, November, 1968, pp. 1347-1347.
39. Lorenz, H., Hertwig, A., and Frusk, G., "Die Ermittlung der für das Bauwesen wichtigsten Eigenschaften durch erzwungene Schwingungen", Veröffentlichungen des Instituts der deutschen Forschungsgesellschaft für Bodenmechanik (DEGEB0) an der Technischen Hochschule Berlin, Heft I, Berlin, Deutschland, Verlag von Julius Springer, 1933.
40. Lorenz, H., "Neue Ergebnisse der dynamischen Baugrunduntersuchung", Zeitschrift des Vereins deutscher Ingenieure, Band 78, Nr. 12, 1934 S. 379-385.
41. Lorenz, H., "Zeichnerische Auswertung von Resonanzkurven", Ingenieur - Archiv, Band 5, 1934, S. 376-394.
42. Lysmer, J., and Richart, F.E., Jr., "Dynamic Response of Footings to Vertical Loading", Journal of the Soil Mechanics and Foundations Division, ASCE, Vol. 92, No. SM1, January, 1966, pp. 65-91.
43. Lysmer, J., and Kuhlemeyer, R.L., "Finite Dynamic Model for Infinite Media", Journal of the Engineering Mechanics Division, ASCE, Vol. 95, No. EM4, August, 1969, pp. 859-877.
44. Matsushita, K., and Izumi, M., "Some Analysis on Mechanisms to Decrease Seismic Force Applied to Buildings", 3WCEE, Vol. III, February, 1965, pp. 342-359.
45. Matsushita, K., and Izumi, M., "Studies on Mechanisms to Decrease Earthquake Forces Applied to Buildings", 4WCEE, Vol. II, Santiago De Chile, January, 1969, pp. 117-125.
46. McNeill, R.L., "Machine Foundations-The State-of-the-Art", Soil Dynamics Speciality Conference, Mexico City, Mexico, August, 1969.
47. Medearis, K.G., "A Comparative Study of" "Structural Response to Explosion-Induced Ground Motions", A Report Prepared for the ASCE Research Council on Performance of Structures, ASCE Project

BIBLIOGRAPHY (Cont'd.)

- 210.03/17-2.72-3, American Society of Civil Engineers, New York, 1975, pp. 1-138.
48. Naik, T.R., "Analysis of Foundations on a Semi-Infinite Elastic Mass Under Dynamic Loads", Unpublished Ph.D. Thesis, University of Wisconsin, January, 1972.
 49. Orrje, O., "Dynamic Loading Tests on Cohesionless Soils With Free Falling Weights, Compared With Static Plate Loading Tests", Division of Soil Mechanics, Royal Institute of Technology, Stockholm, 1968, pp. 1-42.
 50. Quinlan, P.M., "The Elastic Theory of Soil Dynamics", Symposium on Dynamic Testing of Soils, ASTM Special Technical Publication No. 156, July, 1953, pp. 3-34.
 51. Rao, H.A.B., and Hoeg, K., "Two-Dimensional Analysis of Stress and Strain in Soils, Report No. 4, Dynamic Response of Strip Footing on Elastic-Plastic Soils", U.S. Army Engineer Waterways Experiment Station Technical Report No. 3-129, Vicksburg, Mississippi, November, 1967, pp. 1-72.
 52. Rayleigh, Lord, "On Waves Propagated Along the Plane Surface of an Elastic Solid", London Mathematical Society Proc., 17, pp. 4-11.
 53. Reissner, E., "Stationare, axialsymmetrische, durch eine schüttelnde Masse erregte Schwingungen eines homogenen elastischen Halbraumes", Ingenieur-Archiv, Band 7, 1936, S. 381-396.
 54. Rhines, W.J., "Elastic Plastic Foundation Model for Punch-Shear Failure", Journal of the Soil Mechanics and Foundations Division, ASCE, Vol. 95, No. SM3, May, 1969, pp. 819-828.
 55. Richart, F.E., "Foundation Vibrations", Journal of the Soil Mechanics and Foundations Division, ASCE, Vol. 86, No. SM4, August, 1960, pp. 1-34.
 56. Richart, F.E., and Whitman, R.V., "Comparison of Footing Vibration Tests with Theory", Journal of the Soil Mechanics and Foundations Division, ASCE, Vol. 93, No. SM11, November, 1967, pp. 143-168.
 57. Seed, H.B., "Some Lessons from Recent Earthquakes in Relation to Seismic Design in North Carolina Adjacent

BIBLIOGRAPHY (Cont'd.)

- States", Sixth Annual H.M. Show Lecture Series in Civil Engineering, North Carolina State University, Raleigh, North Carolina, November 1970.
58. Selig, E.T., "Response of Foundations to Dynamic Loads", Unpublished M.S. Thesis, Illinois Institute of Technology, January, 1960.
59. Selig, E.T., "A Review of Stress and Strain Measurement in Soil", Proceedings, Soil-Structure Interaction Symposium, Tucson, Arizona, September, 1964, pp. 172-186.
60. Selig, E.T., and Wetzel, R.A., "A Miniature Piezo-electric Gage for Static and Dynamic Soil Stress Measurement", Contract Report No. 1-105, U.S. Army Engineer Waterways Experiment Station, Vicksburg, Mississippi, November, 1964.
61. Selig, E.T., and Vey, Eben, "Shock-Induced Stress Wave Propagation in Sand", Journal of the Soil Mechanics and Foundations Division, ASCE, Vol. 91, No. SM3, May, 1965, pp. 19-49.
62. Selig, E.T., and Tobin, H., "Piezoresistive Soil Stress Gages", Air Force Weapons Laboratory Report No. AFWL-TR-66-51, IIT Research Institute, May, 1966.
63. Skormin, G.A., and Malysev, M.B., "Investigation of Stress Distribution in Sand Under a Circular Footing During Loading Increase", Osnov. Fund. Mech. Grunt. 12, No. 5, 1970.
64. Slade, J.J., "A Discontinuous Model for the Problems of Soil Dynamics", Symposium on Dynamic Testing of Soils, ASTM Special Technical Publication No. 156, July, 1953, pp. 69-76.
65. Sung, Tse Yung, "Vibrations in Semi-Infinite Solids Due to Periodic Surface Loading", Symposium on Dynamic Testing of Soils, ASTM Special Technical Publication No. 156, July, 1953, pp. 35-68.
66. Terzaghi, K., and Peck, R.B., Soil Mechanics in Engineering Practice. New York, John Wiley & Sons, Inc., New York, 1967.
67. Triandafilidis, G.E., "Analytical Study of Dynamic Bearing Capacity of Foundations", Defense Atomic Support Agency Technical Report No. 1189,

BIBLIOGRAPHY (Cont'd.)

Washington, D.C., January, 1961.

68. Truesdale, W.B., "Development of a Small Strain Gage", Air Force Weapons Laboratory Technical Report No. AFWL-TDR-63-3, Kirtland AFB, New Mexico, 1963.
69. Truesdale, W.B., and Schwab, R.B., "Soil Strain Gage Instrumentation", Air Force Weapons Laboratory Technical Report No. AFWL-TDR-65-207, Kirtland AFB, New Mexico, 1965, pp. 1-92.
70. Valliappan, S., Favaloro, J.J., and White, W., "Dynamic Analysis of Embedded Footings", Technical notes, Journal of the Geotechnical Engineering Division, ASCE, Vol. 103, No. GT2, February, 1977, pp. 129-133.
71. Varadhi, S.N., "Foundation Response Due to Disturbances In Underlying Soil", Unpublished M.S. Thesis, Illinois Institute of Technology, Chicago, Illinois, December, 1972.
72. Vesic, A.S., "Bearing Capacity of Deep Foundation in Sand", National Academy of Sciences, National Research Council, Highway Research Record, No. 39, 1963, pp. 112-153.
73. Vesic, A.S., "Analysis of Ultimate Loads of Shallow Foundations", Journal of the Soil Mechanics and Foundations Division, ASCE, Vol. 99, No. SM1, January, 1973, pp. 45-73.
74. Vey, E., and Strauss, L., "Stress-Strain Relationships in Clay Due to Propagating Stress Waves", Proceedings, Symposium on Wave Propagation and Dynamic Properties of Earth Materials, Albuquerque, New Mexico, August 1967, pp. 575-586.
75. Wetzel, R.A., "Shock Induced Stress Wave Propagation in a Cohesive Soil", Unpublished M.S. Thesis, Illinois Institute of Technology, Chicago, Illinois, January, 1965.
76. Wetzel, R.A., "Axisymmetric Stress Wave Propagation in Sand", Unpublished Ph.D. Dissertation, Illinois Institute of Technology, June, 1969.
77. Wetzel, R.A., and Vey, E., "Axisymmetric Stress Wave Propagation in Sand", Journal of the Soil Mechanics and Foundations Division, ASCE, Vol. 96, No. SM5, September, 1970, pp. 1763-1786.

BIBLIOGRAPHY (Cont'd.)

78. Whitman, R.V., "Analysis of Foundation Vibrations", Presented to Symposium on Man-made Vibrations in Civil Engineering, British National Section, International Association for Earthquake Engineering, London, April, 1965.
79. Whitman, R.V., and Richart, F.E., "Design Procedures for Dynamically Loaded Foundations", Journal of the Soil Mechanics and Foundations Division, ASCE, Vol. 93, No. SM6, November, 1967, pp. 169-193.
80. Winterkorn, H.F., "Macromeritic Liquids", Symposium on Dynamic Testing of Soils, ASTM Special Technical Publication No. 156, July, 1953, pp. 77-89.
81. Wirsching, Paul H., and Yao, James, T.P., "A Statistical Study of Some Design Concepts in Earthquake Engineering", Bureau of Engineering Research, The University of New Mexico Technical Report CE-21(70) NSF-065, Albuquerque, New Mexico, May, 1970, pp. 1-169.
82. Woods, R.D., "Screening of Surface Waves in Soils", Journal of the Soil Mechanics and Foundations Division, ASCE, Vol. 94, No. SM4, July, 1968, pp. 951-979.